UNIVERSITÀ DEGLI STUDI DI MILANO

Dottorato di Ricerca in Scienze della Terra
Ciclo XXXI

The microstructure of modern and fossil brachiopod archives

Ph.D. Thesis

Facheng Ye
Matricola R11389

Tutor	**Academic Year**	*Coordinator*
Prof. ssa Lucia Angiolini	**2017-2018**	**Prof. ssa Elisabetta Erba**

Co- Tutors

Prof. Uwe Brand
Prof. Shuzhong Shen

INDEX

Abstract

Due to their high biodiversity and widespread distribution in the Phanerozoic oceans, brachiopods are very important tools for research in palaeontology and related fields in Earth Sciences to investigate the past and present global change. Their biominerals have been considered the best carbonate archives of proxies for extending climate and environmental records on a broad geographical scale over long periods of time. Their fidelity as archives is supported by the following: 1) they record the physical and chemical composition of the seawater in which they live without, or with very limited, vital effects; 2) they precipitate a low-Mg calcite shell, which withstands post-depositional alteration; and 3) they are low metabolic and physiologically unbuffered animals sensitive to change in the physicochemical composition of the ambient seawater. However, there is still insufficient knowledge of the microstructures of these biomineral archives and their biomineralization processes during the evolutionary history of the phylum. The aims of the present thesis, focused on solving these issues, are to: 1) examine the micro- and morpho- structural diversity of modern and fossil brachiopods, 2) assess the microstructure variation in different environmental conditions; and 3) reconstruct the evolutionary changes and fabric differentiation of the main brachiopod classes through geological time.

A multidisciplinary approach was used for the microstructural analyses: 1) a comprehensive dataset was established based on detailed microstructural observations of modern and fossil brachiopods analysed by Scanning Electron Microscopy (SEM); 2) new measurement methods were developed based on SEM observations to quantitatively describe the morphology and size of the structural units (fibres) of the shell secondary layer, the thickness of the primary layer, and the density and size of endopunctae of modern brachiopod shells; 3) new measurement methods were developed to describe the structural units (laminae and fibres) of fossil brachiopod shells; 4) statistical analyses of the acquired data were performed, i.e. independent-sample *t*-tests, frequency distribution plots, principal component analysis, and symmetric and asymmetric variants analyses; 5) stable isotope compositions ($\delta^{13}C$ and $\delta^{18}O$) were tested from the secondary shell layer along shell ontogenetic increments in both dorsal and ventral valves of modern brachiopod shells; and 6) Transmission Electron Microscope (TEM) and Electron Backscatter Diffraction (EBSD) were performed in collaboration with other researchers to investigate the micro- and nanoscale features of modern brachiopod shells.

Through these approaches, details of microstructural patterns were described and compared of twenty-nine specimens of six recent brachiopod species [*Notosaria nigricans* (Sowerby, 1846), *Liothyrella neozelanica* (Thomson, 1918), *Liothyrella uva* (Broderip, 1833), *Magasella sanguinea* (Leach, 1814), *Gryphus vitreus* (Born, 1778), *Calloria inconspicua* (Sowerby, 1846)] from different environmental conditions. Based on the morphology and size of the shell secondary layer fibres, the following conclusions were reached:

1) There was no significant difference in the shape and size of the fibres between ventral and dorsal valves of the same specimen;

2) An ontogenetic trend in the morphology of the fibres was found, as they become larger, wider, and flatter with increasing age. This change in size and shape indicated that the animal produced a fibrous layer with a different organic content during the ontogeny.
3) The relationship between size and shape of fibres and environmental conditions was clear when comparing two species of the same genus (*L. neozelanica*, *L. uva*) living in seawater with different carbonate saturation state and temperature, i.e. the fibres of *L. uva* are narrower and rounder than those of *L. neozelanica.* This in turn indicated a higher shell organic content in *L. uva*.

Additional investigations were performed on the species *Magellania venosa* (Dixon, 1789), grown in the natural environment and in controlled culturing experiments in different pH conditions (7.35 to 8.15 ±0.05), and led to following conclusions:
1) Under low pH conditions, *M. venosa* produced a more organic-rich shell with larger and higher density endopunctae, and smaller secondary layer fibres, when subjected to about one year of culturing.
2) Increasingly negative $\delta^{13}C$ and $\delta^{18}O$ values were recorded by the shell produced during culturing and are related to the CO_2–source in the culture setup.
3) Both the microstructural changes and the stable isotope results supported the value of brachiopods as robust archives of proxies for studying ocean acidification events in the geologic past.

Finally, the measurements made on the size of structural units (laminae/fibres) of Cambrian to Devonian fossil brachiopod shells coupled with very detailed qualitative micro-scale observations, allowed the following conclusion:
1) The fossil organocarbonate brachiopod shells produced two main secondary layer fabrics: a laminar fabric in the Strophomenata, and a fibrous fabric in the Rhynchonellata. The Strophomenata laminar fabric shells appeared to be more variable and complex in their structural organization, but the thickness of the laminae was rather uniform and much thinner than that of the fibres. The Rhynchonellata fibrous fabric was more simple and uniform in its organization, but the size of the fibres was much more variable and comparable to the fabric of modern brachiopods.
2) Brachiopods with a fibrous secondary layer were mostly associated with biconvex shells, whereas brachiopods with a laminar secondary layer are associated with a variety of shell shapes.
3) Detailed microstructural studies were shown to be a very useful tool to construct the phylogenetic tree of the Phylum Brachiopoda. For example, the recorded gradual change in thickness of laminae from Billingselloidea to Productida could be important evidence to support the hypothesis that taxa with laminar microstructure diverged from the Billingsellida. Microstructural observation on the Chonetidina suggested that their shells had already evolved a laminar fabric during the Devonian.

In summary, this new multidisciplinary and quantitative approach to describe the microstructure of brachiopod shells is a powerful tool to interpret microstructural variations of brachiopod shells in different ontogenetic stages and environmental conditions. Moreover, using the microstructure of brachiopod shells as a biomineral archive is a very promising tool for studying climate and environmental change and reconstructing the state of the oceans over the long history of geological time, and may be used to constrain the evolutionary history of the Phylum Brachiopoda.

Chapter 1
Introduction and aims

Understanding the past, and forecasting the future is the eternal mission of scientists. Biominerals, the hard parts produced by organisms for support and protection, are one of the best tools to understand climate change in the past, present and future, as they are high-resolution archives of proxies recording the environmental conditions prevailing during their life.

In the marine realm, brachiopod and mollusc shells are considered excellent archives for reconstructing the state and composition of the oceans in recent and past times, and predict their evolution in the near future (e.g., Popp et al., 1986; Grossman et al., 1991; Parkinson et al., 2005; Angiolini et al., 2007, 2009; Brand et al., 2011; Cusack and Huerta, 2012; Schöne and Surge, 2012; Brocas et al., 2013; Crippa et al., 2016; Garbelli et al., 2017). Brachiopod shells have been extensively used for extending climate and environmental records on a broad geographical scale and over long periods of time, because: 1) they record the physical and chemical composition of the seawater in which they live with no or limited vital effects (e.g., Parkinson et al., 2005; Brand et al., 2013, 2015; Milner et al., 2018); 2) they precipitate a low-Mg calcite shell, which is generally resistant to diagenetic alteration (e.g., Brand et al., 2011; Brand, 2018); 3) they are very common in the Phanerozoic, especially during the Palaeozoic (Curry and Brunton, 2007); 4) they are low metabolic and physiologically unbuffered organisms sensitive to change in the physicochemical composition of the ambient seawater (Peck et al., 1997; Peck, 2007).

However, the interpretation of the brachiopod archive records is limited due to uncertainties regarding chemical alteration and determining primary seawater compositions, and analytical restrictions measuring certain geochemical data. To solve these issues, the H2020-MSCA-ITN-2014 BASE-LiNE Earth (Brachiopods As SEnsitive tracers of gLobal marINe Environment: Insights from alkaline, alkaline Earth metal, and metalloid trace element ratios and isotope systems) program has been undertaken. Lead by GEOMAR Helmholtz Centre for Ocean Research (Kiel, Germany), the program involved 13 European academic institutions, two large companies and one museum and trained 15 ESRs to perform a multi-disciplinary approach considering ecological, geological, mineralogical and physical studies to closely determine original trace element and isotope time series of the Phanerozoic Ocean from brachiopod shells.

The present thesis is part of the BASE-LiNE Earth program, performed at the Dipartimento di Scienze della Terra “A. Desio”, Università degli Studi di Milano with the objective of examining the micro-, morpho- and chemico-structural diversity of modern and fossil brachiopods, to assess the microstructure variation in different environmental conditions and to reconstruct the evolutionary

changes and fabric differentiation of the main brachiopod classes through time. Individual tasks include:

1) To examine the micro-and chemico-structure of modern and Palaeozoic brachiopod shells;

2) To reconstruct evolutionary changes and fabric differentiation of the main brachiopod classes during the Palaeozoic.

To reach these goals, I have followed three steps in my three years Ph.D. research:

Step 1 (corresponding to chapter 3): Examining the morphology and size of the basic structural units (the fibres within the secondary layer) of several modern brachiopod species. Understanding how their morphostructure responds to climate changes, environmental pressure or even ontogenetic/species-specific variation. The investigated modern specimens come from collections already available at Dipartimento di Scienze della Terra "A. Desio".

Step 2 (corresponding to chapter 4): Investigating the microstructure and stable isotope geochemistry investigation of nine adult brachiopod specimens of *Magellania venosa* (Dixon, 1789), grown in the natural environment as well as in controlled culturing experiments at different pH conditions over different time intervals. The investigated specimens have been provided by GEOMAR, Kiel.

Step 3 (corresponding to chapter 5): Examining the microstructure of Palaeozoic brachiopod shells, trying to reconstruct evolutionary changes and fabric differentiation of the main brachiopod classes during the Phanerozoic, focusing on the comparison between laminar and fibrous fabrics of the secondary layer. The investigated fossil specimens come in part from collections already available at Dipartimento di Scienze della Terra "A. Desio" and in part have been collected during field work in Iran.

References

Angiolini, L., Darbyshire, D.P.F., Stephenson, M.H., Leng, M.J., Brewer, T.S., Berra, F., Jadoul, F., 2007. Lower Permian brachiopods from Oman: their potential as climatic proxies. Earth and Environmental Science Transactions of the Royal Society of Edinburgh 98, 327–344.

Angiolini, L., Jadoul, F., Leng, M.J., Stephenson, M.H., Rushton, J., Chenery, S., Crippa, G., 2009. How cold were the Early Permian glacial tropics? Testing sea-surface temperature using the oxygen isotope composition of rigorously screened brachiopod shells. Journal of the Geological Society 166, 933–945.

Brand, U., 2018. Modern and fossil brachiopods: superheroes of archives. 8th International Brachiopod Congress Milan, 11–14 September 2018, Permophiles 66, 29.

Brand, U., Logan, A., Bitner, M.A., Griesshaber, E., Azmy, K., Buhl, D., 2011. What is the ideal proxy of Palaeozoic seawater chemistry? Memoirs of the Association of Australasian Palaeontologists 41, 9–24.

Brand, U., Azmy, K., Bitner M.A., Logan, A., Zuschin, M., Came, R., Ruggiero, E., 2013. Oxygen isotopes and $MgCO_3$ in brachiopod calcite and a new paleotemperature equation. Chemical Geology 359, 23–31.

Brand, U., Azmy, K., Griesshaber, E., Bitner, M.A., Logan, A., Zuschin, M., Ruggiero, E., Colin, P.L., 2015. Carbon isotope composition in modern brachiopod calcite: A case of equilibrium with seawater? Chemical Geology 411, 81–96.

Brocas, W.M., Reynolds, D.J., Butler, P.G., Richardson, C.A., Scourse, J.D., Ridgway, I.D., Ramsay, K., 2013. The dog cockle, *Glycymeris glycymeris* (L.), a new annually-resolved sclerochronological archive for the Irish Sea. Palaeogeography, Palaeoclimatology, Palaeoecology 373, 133–140.

Crippa, G., Angiolini, L., Bottini, C., Erba, E., Felletti, F., Frigerio, C., Hennissen, J.A.I., Leng, M.J., Petrizzo, M.R., Raffi, I., Raineri, G., Stephenson, M.H., 2016. Seasonality fluctuations recorded in fossil bivalves during the early Pleistocene: Implications for climate change. Palaeogeography, Palaeoclimatology, Palaeoecology 446, 234–251.

Curry, G.B., Brunton, C.H.C., 2007. Stratigraphic distribution of Brachiopods, in: Selden P.A. (Ed.): Treatise on Invertebrate Paleontology, Part H, Revised, Brachiopoda, vol. 6, Kansas: The Paleontological Institute, pp. 2396–2521.

Cusack, M., Huerta, A.P., 2012. Brachiopods recording seawater temperature—A matter of class or maturation? Chemical Geology 334, 139–143.

Garbelli, C., Angiolini, L., Shen, S.Z., 2017. Biomineralization and global change: A new perspective for understanding the end-Permian extinction. Geology 45, 19–22.

Grossman, E.L., Zhang, C., Yancey, T.E. 1991. Stable–isotope stratigraphy of brachiopods from Pennsylvanian shales in Texas. Geological Society of America Bulletin 103, 953–965.

Milner Garcia, S.A., Rollion-Bard, C., Burckel, P., Müller, T., Jurikova, H., Tomašových, A., Angiolini, L., Henkel, D., 2018. Fossil brachiopod shell calcite: How well is the oxygen isotope composition and minor element ratios preserved within the shell microstructure? 8th International Brachiopod Congress Milan, 11–14 September 2018, Permophiles 66, 78–79.

Parkinson, D., Curry, G.B., Cusack, M., Fallick, A.E. 2005. Shell structure, patterns and trends of oxygen and carbon stable isotopes in modern brachiopod shells. Chemical Geology 219, 193–235.

Peck, L.S., 2007. Brachiopods and climate change. Earth and environmental science transactions of the Royal Society of Edinburgh 98, 451–456.

Peck, L.S., Rhodes, M.C., Curry, G.B., Ansell, A.D., 1997. Physiology, in: Kaesler, R.L. (Ed.), Treatise on Invertebrate Paleontology. Part H, Revised, Brachiopoda, vol. 1. Geological Society of America Inc., and The University of Kansas, Boulder, Colorado, USA, pp. 213–242.

Popp, B.N., Anderson, T.F., Sandberg, P.A., 1986. Brachiopods as indicators of original isotopic compositions in some Paleozoic limestones. Geological Society of America Bulletin 97, 1262–1269.

Schöne, B.R., Surge, D.M., 2012. Part N, (Revised) Volume 1, Chapter 14: Bivalve sclerochronology and geochemistry. Treatise Online 46, 1–24.

Chapter 2
Brachiopod biomineralization: State of the art

Abstract

Brachiopods were very common in the geological past, even if they are not the dominant invertebrates in modern oceans. About five thousands fossil genera have been described (over 4500, Williams et al., 1996; over 4200, Curry and Brunton, 2007; over 5000, Logan, 2007; about 4800, Williams and Carlson, 2007). Due to their high biodiversity and widespread distribution in the Palaeozoic Ocean, brachiopods are very important tools for research in palaeontology and related fields in Earth Sciences. Brachiopods have complex and diverse shell chemicostructures which developed very soon during the Early Cambrian, the most striking transformation involving the replacement from organophosphatic shell to organocarbonate shell. The mechanisms of shell formation are still debated, but the innermost non specialized parts of the shell are known to be produced in equilibrium with seawater. Owing to the unique features of the biominerals forming their shells, which are capable to withstand post-depositional alteration and are generally produced near to chemical equilibrium with the seawater in which they live, organocarbonate brachiopods are considered reliable archives of climate and environmental changes in deep time.

2.1 General features of the brachiopods

Brachiopods have two mineralized valves (ventral valve and dorsal valve respectively) which protect their soft parts and the lophophore. The body occupies the posterior part of the space (body cavity) inside the shell, the rest of the mantle enclosing a mantle cavity, which is a water-filled space containing the lophophore (Fig. 1).

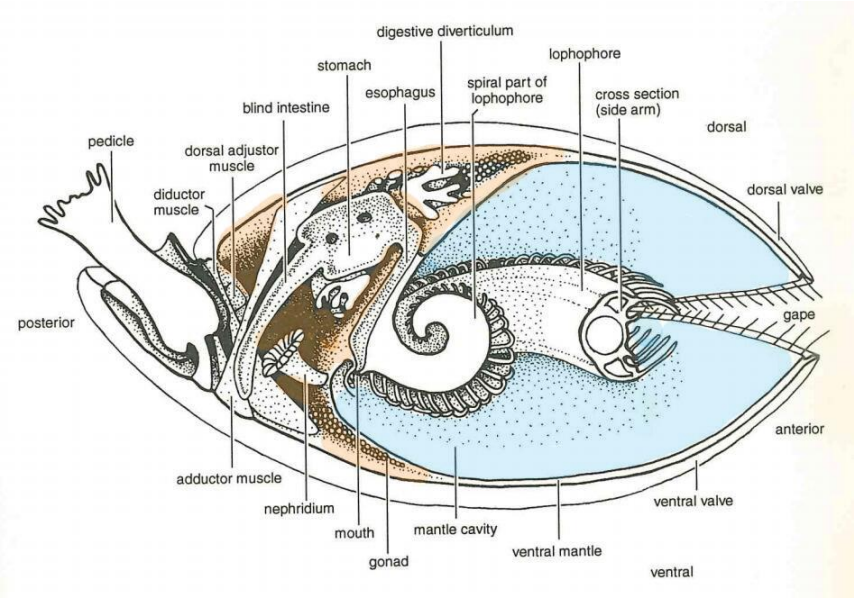

Fig. 1. Diagrammatic representation of principal organs of brachiopods as typified by *Terebratulina retusa* (Linnaeus, 1758); body cavity: orange, mantle cavity: blue; (Williams and Rowell, 1965).

The Phylum Brachiopoda comprises three subphyla: Linguliformea, Craniiformea and Rhynchonelliformea (Table 1). The name of each subphylum derives from its most ancient living order, i.e., Lingulida, Craniida, Rhynchonellida (Emig et al., 2013). Linguliformea has a shell of calcium phosphate, while Craniiformea and Rhynchonelliformea have calcite shells. Additionally, Craniiformean brachiopods have a high Mg-calcite shell, and Rhynchonelliform brachiopods have a shell of low Mg-calcite (e.g., Williams, 1970a; Cusack et al., 1997; Williams, 1997; England et al., 2007; Williams and Cusack, 2007). Rhynchonelliform brachiopods are the most widespread in the fossil record and those mostly used as archives of past climate and seawater conditions.

Table 1. The classification of brachiopods (Holmer et al., 1995; Williams et al., 1996; Cusack et al., 1997; Williams et al., 1997; Holmer and Popov, 2007)

Subphylum	Linguliformea		Craniiformea	Rhynchonelliformea				
Class	Lingulata	Paterinata	Craniata	Chileata	Kutorginata	Obolellata	Strophomenata	Rhynchonellata
Hinge	No teeth			with a strophic hinge line	the presence of paired denticles	lacking denticls	Teeth and sockets	
Pedicle	The pedicle possesses a coelomic cavity, arises and attaches from ventral valve only (living species)		Lack even a rudimentary pedicle (living species)	The pedicle develops from mantle rudiment, and continuous with body wall of both valves. Originates from the larval peduncular lobe, lacks coelomic cavity during adult stage (living species)				
	Long, burrows	Short, attached to hard surfaces	None, valve cemented to substrate	When present, variable, short or long, attached to hard surfaces or in soft substrates.				
Epithelium	It consists of an outer layer of ectodermal epithelium resting on a thin connective-tissue layer coated internally by a ciliated coelomic epithelium (Peritoneum)							
Shell	Organophosphatic shell		high Mg-calcite shells	low Mg-calcite shells				
	Calcium phosphate accounts for 74.7~93.7 %, remainder are mostly chitin and protein.		87.8~88.6 % calcium carbonate, remainders are mainly protein.	94.6~98.6 % calcium carbonate.				

2.2 Rhynchonelliformean brachiopod shell microstructure

From the external to the internal surface, the Rhynchonelliformean organocarbonate shell is generally composed of following layers (Fig. 2) (e.g., Armstrong, 1968; Williams, 1968a, 1968b; Williams, 1997; Williams and Cusack, 2007; Griesshaber et al., 2007, 2012; Goetz et al., 2009; Garbelli et al., 2012, 2014):

1) a thin organic periostracum [rarely preserved in fossils (Biernat and Balinski, 1982)]
2) a thin outer primary layer (rare in fossils except in extremely well-preserved shells);
3) a thicker inner secondary layer;
4) a tertiary layer (not always present).

The fabric of these layers is different in the various groups of Rhynchonelliformean brachiopods, especially the fabric of the secondary layer (Williams, 1997; Williams and Cusack, 2007).

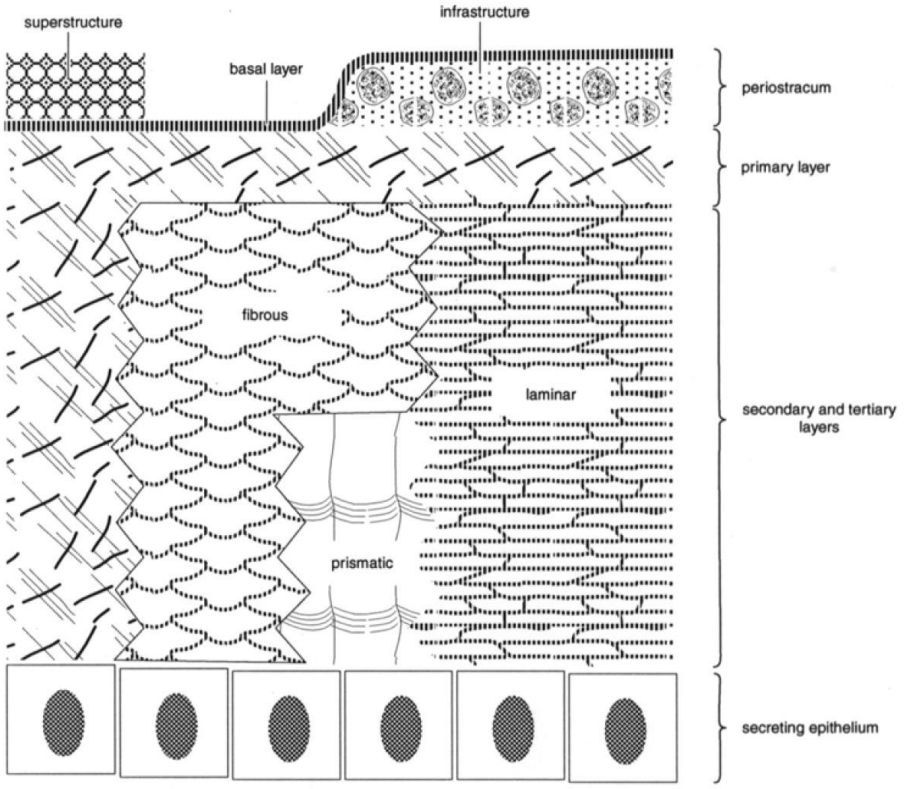

Fig. 2. Schematic representation of the main components of the calcite-shelled brachiopods (Williams, 1997).

2.2.1 Primary layer

Given relatively thin, the thickness of primary layer does not vary very much (Williams, 1966). In contrast with the variable succession and well organized fabric of the secondary layer, the primary layer lacks a notable microstructural order (Cusack et al., 2010) and its fabric is normally finely granular or acicular (Williams, 1997) (Fig. 3)

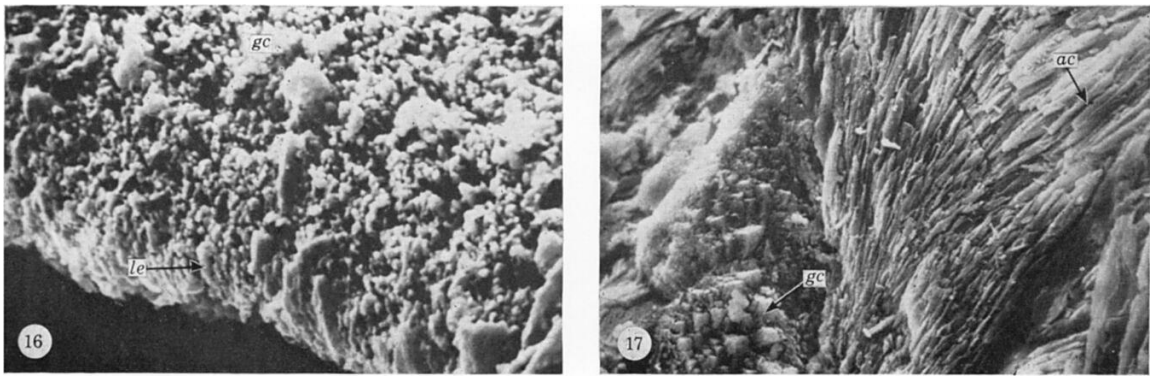

Fig. 3. Microstructure of the primary layer of *Thecidellina brarretti* (Davidson), Holocene, showing acicular crystallites and granules of calcite (gc: granules of calcite; le: lense; ac: acicular crystallites) (× 6200 and × 1400 respectively); (Williams, 1973).

2.2.2 Secondary layer

Within the layered succession of the Thynchonelliformean brachiopod shell, the secondary layer is the most variable. The fabric of the secondary layer may comprise a) calcite fibres; b) calcitic cross-bladed lamination; c) folii. In organocarbonate brachiopods, the fibrous fabric is the most widespread, except during Carboniferous and Permian times, when the cross-bladed laminar strophomenides were dominant (Williams, 1997).

a) Calcite fibres. Dominant stacking fabric structure among Rhynchonelliformean brachiopods (e.g., Rhynchonellides, Terebratulides, Pentamerides and most Orthides). Fibres appear as blades in longitudinal section, gradually widening towards the interior surface of valve. In transverse section, a typical fibre profile commonly shows a medial keel that is roundly convex inwardly, while a medial saddle that is concave outwardly (Fig. 4). Due to the overlapping growth of fibres, different sections of fibres (longitudinal, oblique, and transverse) may suddenly appear in succession (Williams, 1966, 1968a; Williams, 1997; Williams and Cusack, 2007).

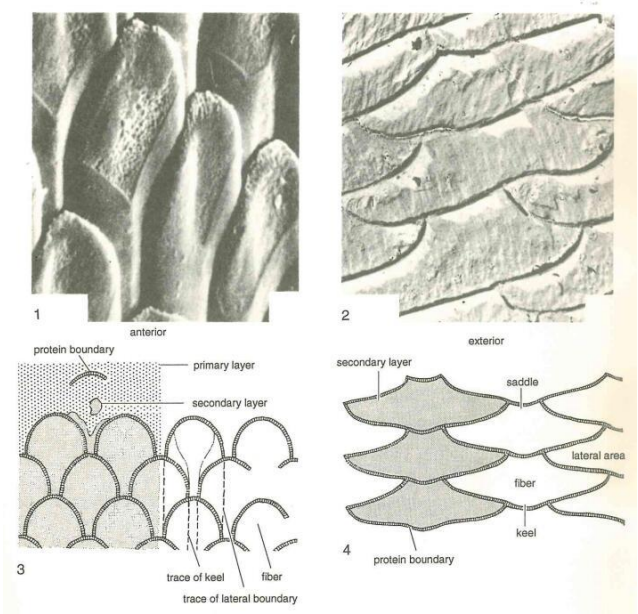

Fig. 4. Fibrous secondary layer of the Rhynchonellid *Notosaria nigricans* (Sowerby); 1, appearance of fibres on the valve floor, ×2000; 2, typical outline of the fibres in transverse section, ×4000 (Williams, 1968b); 3-4, drawing showing the morphology of the fibres and their outline in transverse section (Williams, 1966).

b) Calcite cross-bladed lamination. Most Strophomenid secondary fabric consists of a continuum of overlapping and superimposed sheets. The basic structures of each sheet are laths and blades, which show a rectangular outline in cross-section. Arranged blades may be disposed at acute angles to adjacent blades in successive sheets, distinguished as 'cross-bladed fabric'. The external surfaces of the sheets, which are normally flat, may bear sets of ridges and grooves (Armstrong, 1969; Williams, 1970b; Williams, 1997; Williams and Cusack, 2007) (Fig. 5). The cross-bladed laminar secondary layer is probably more organic rich than the fibrous fabric, and can be helpful in deep time studies (Garbelli et al., 2014, 2017).

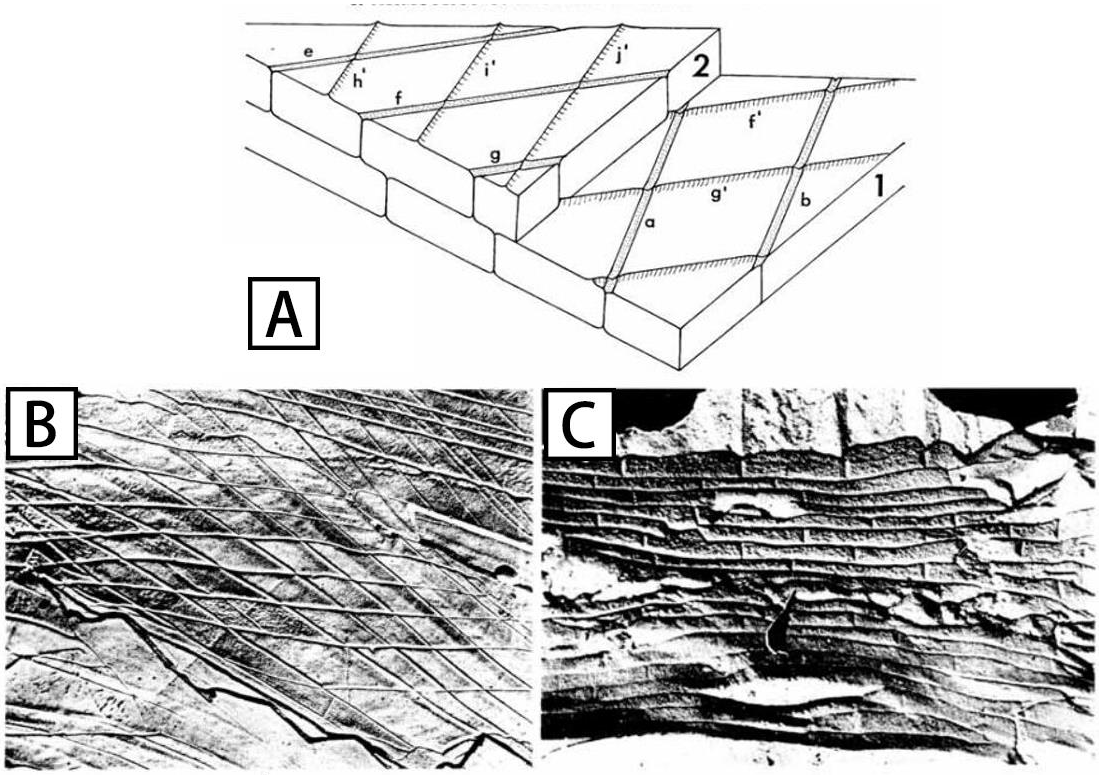

Fig. 5. Cross-bladed laminar fabric. A, Diagram showing the organization of the tabular blades which form two superimposed sheets (1 and 2); *a, b, e, f,* and *g* represent the boundaries between the blades; *f', g', h', i'* represent ridges that may form at the crossed boundaries on the underlying sheet. B, *Terrakea solida* (Etheridge and Dun), illustrating the crossing sets of grooves and ridges on the surface of a sheet ×1500; C, *Streptorhynchus pelicanensis* Fletcher, cross-bladed lamination in transverse section, ×1000 (Armstrong, 1969).

c) Foliate fabric. Typical of taxa of the Obolellata, Chileata and Kutorginata, This fabric is composed of folii which were sheathed by membranes and secreted collectively. The laminae are normally coarse and show some lenticularity in traverse section; in fact they are composed of sheets which are wrinkled into folds or are variably differentiated into lenticular tablets or laths (Williams and Cusack, 2007) (Fig. 6).

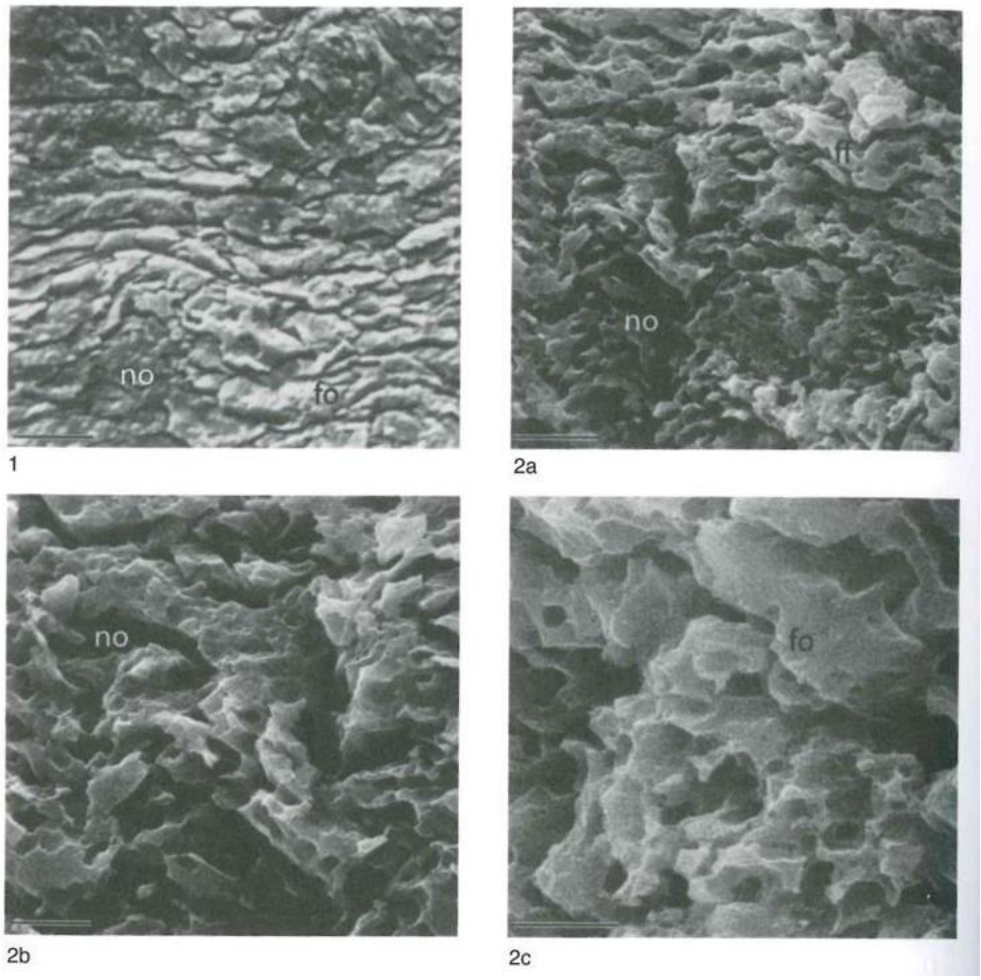

Fig. 6. Foliate fabric 1, *Trematobolus pristinus bicostatus* and 2a-c, *Obolella* sp., Lower Cambrian; (fo) folii, (no) nodules; (scale bars: 25µm, 10µm, 5µm, and 5µm respectively) (Williams and Cusack, 2007).

2.2.3 Tertiary layer

The tertiary layer has a lower organic content than the secondary layer (e.g. Goetz et al. 2009; Garbelli et al., 2014). If the secondary fibres are ensheathed in given membranes, organic membranes are instead absent in the prismatic layer. The units forming the tertiary layer are discrete prisms or better columns, which are separated by organic partitions and developed with interlocking boundaries normal to the accretionary surface. Due to the differential lateral development and reabsorption of their termination, the outlines of these columns are commonly irregular and they are always featured with clear growth lines (Mackinnon and Williams, 1974; Williams, 1997; Williams and Cusack, 2007) (Fig. 7 left). The secondary and tertiary layers may show frequent intercalations, especially in the transitional zone from the secondary to the tertiary layer and in the umbonal region (Fig. 7 right).

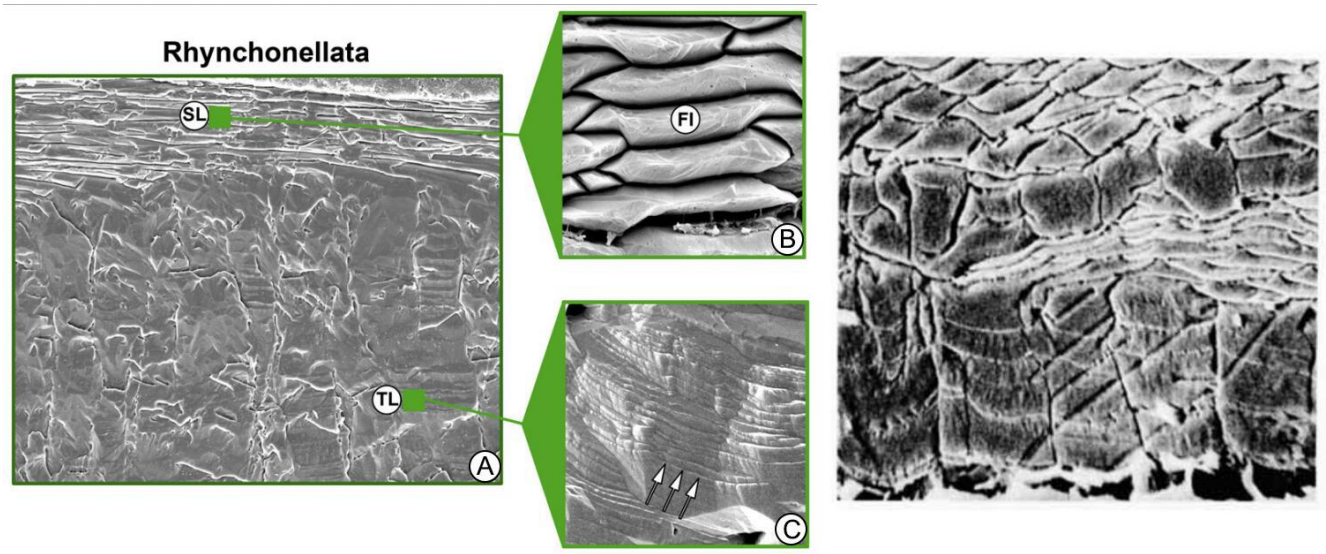

Fig. 7. Microstructure of the transition between secondary layer and tertiary layer, left, Rhynchonellata, showing details of growth steps in F (scale: A × 120, B and C × 3500) (Garbelli et al., 2014); right, *Liothyrella neozelanica* (Thomson), showing intercalations between secondary and tertiary layer (scale: × 1350) (Mackinnon and Williams, 1974).

2.2.4 Shell perforations (endopuncta and pseudopuncta)

Both in fossil and recent brachiopods, perforations are very common features (they are present in all living Rhynchonelliformean brachiopods except for the rhynchonellides) and have been developed in many different forms (Pérez-Huerta et al., 2009). Canals are slender cylindroids less than 1 μm in diameter; punctae are larger chambers up to 20 μm or more in diameter (Williams, 1997). Usually the shells permeated with canals are referred to as punctate (Williams, 1997).

Endopunctae

Endopunctation is characteristic of all terebratulides throughout their evolutional record, and permeate thecideidines with few exceptions. In longitudinal section, a typical endopuncta is funnel shaped, and ends with a perforated canopy, which is a kind of calcitic cast of microvillous plasmalemmas (Fig. 8. A, B). The diameters of endopunctae vary within wide range, from 5μm in *Terebratulina* (Owen and Williams, 1969) to 40μm in Megathyrids (Smirnova and Popiel-Barczyk, 1991). The pattern of endopunctae distribution within the shell of modern brachiopods does not change a lot; however, their densities vary greatly depending on different species (Williams, 1997).

Pseudopunctae

Pseudopunctation is the dominant feature of the strophomenate shell. A typical pseudopuncta usually consists of a slightly arcuate cylindrical structure made by deflections of the laminae of the secondary shell. Resulting from the mantle having been pushed outward radially in response to the thickening of the secondary shell and the marginal expansion of the valve, the pseudopuncta is always inclined anteriorly and emerges as a tubercle on the internal surface of the shell. Some pseudopunctae are formed exclusively of rosettes of conically disposed laminae (Fig. 8. C), but others have a distinctive rod of calcite (taleola) at the core of rosette (tubercle) (Fig. 8. D) in several groups of brachiopods (Williams, 1997).

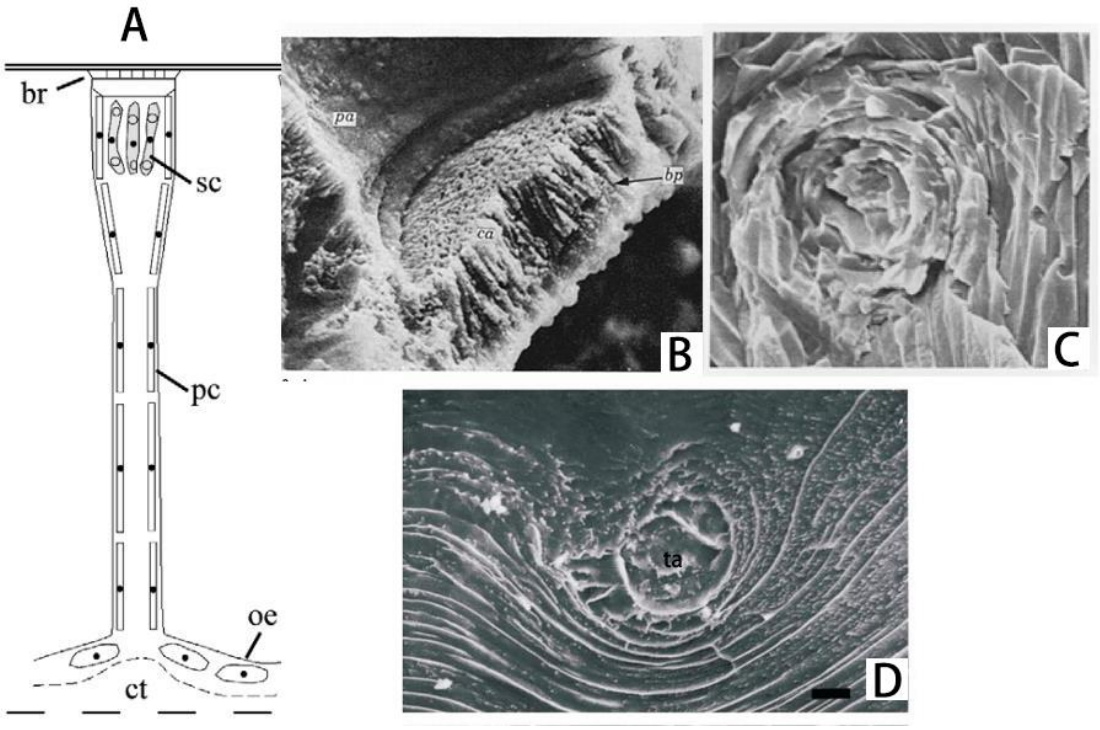

Fig. 8. A, Example of an endopuncta in a terebratulide (Williams, 1997); B, canal and canopy in *Thecidellina hedleyi* (Thomson) (× 3000) (Williams, 1973); C, *Strophomena planumbona* (Hall), detail of the core of a pseudopuncta (× 3000) (Williams and Brunton, 1993); D, *Leptaena depressa* (Sowerby), pseudopuncta with taleola (Scale bar: 10μm) (Dewing, 2004) [br, brush; sc, storage cells; pc, peripheral cells; oe, outer epithelium; ct, connective tissue; pa, endopuncta; ca, canopy; bp, brush; ta, taleola].

2.3 Basic units and hierarchical structure

Despite the distinctiveness of their fabrics, the basic biomineral unit of all three layers is structurally the same. It is an organically coated granule of calcite approximately 15-20 nm in diameter and commonly clustering into spherules approximately 50 nm in size. The granules form layers that are commonly grouped into laminae (growth bands), rarely exceeding 1 μm thick (Williams and Cusack, 2007).

The description of the hierarchical structure is very important for the understanding of their evolutionary process and biomineralization mechanisms, as shown by the overview of the hierarchical architecture of a rhynchonellid brachiopod shell (Schmahl et al., 2012) (Fig. 9).

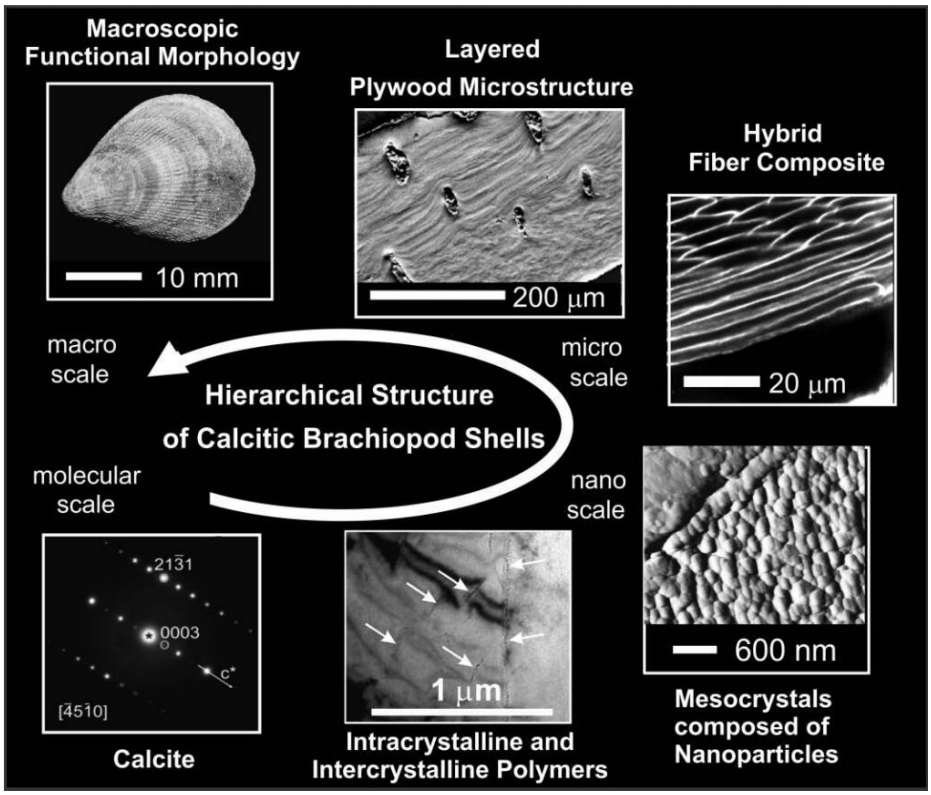

Fig. 9. Overview of the hierarchical architecture of a rhynchonelliform brachiopod shell material from the molecular scale (bottom left) to the macroscale (top left) (Schmahl et al., 2012).

2.4 Secretion of the shell

The columnar epithelial cells, which initially secreted the periostracum, are responsible for the deposition of the two/three layered calcareous shell (Williams, 1956). According to Williams (1968b), the formation of the shell is similar to a 'conveyor-belt' system with cell proliferation at the generative zone of the outer epithelium (Fig. 10).

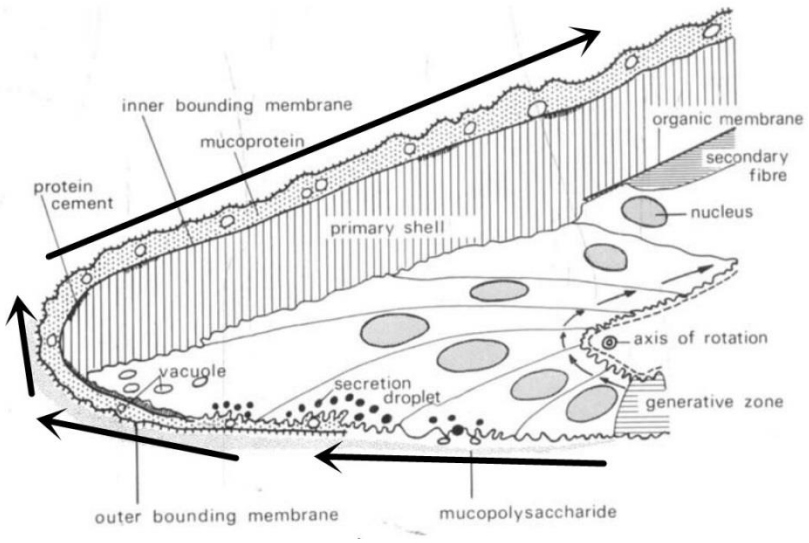

Fig. 10. Stylized longitudinal section of a valve edge of a young *Notosaria nigricans* (Sowerby) (Williams, 1968b).

A single cell performs several distinct secretory operations, and secretes the periostracum, the primary layer, the secondary layer and the tertiary layer successively (Williams, 1968b, 1997; Schmahl et al., 2004) (Fig. 11). In addition, the mantle as a whole is made up of cells simultaneously engaged in every phase of the secretory regime, which deposit different layers on a contemporaneous growth surface (Schmahl et al., 2004). One of the main outcome of the a 'conveyor-belt' model by Williams (1968b) is that each fibre of the secondary layer is produced by a single mantle cell (Fig. 11) which controls its growth during shell production, so that there is a strict relation specific fibre-cell.

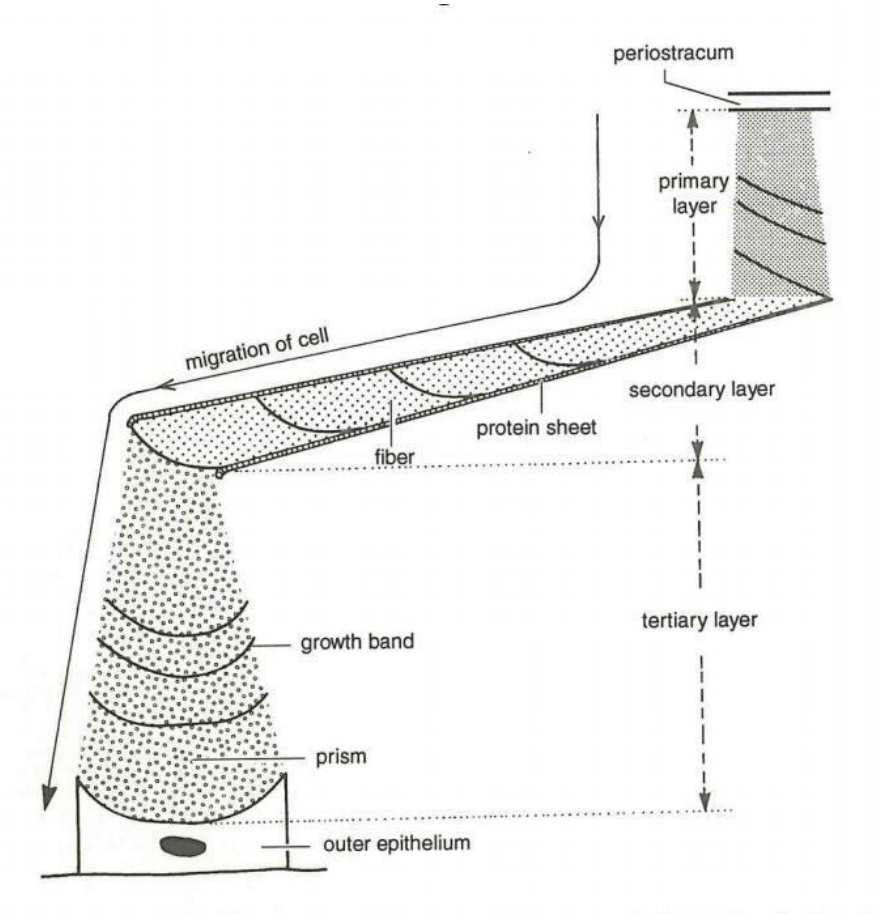

Fig. 11. Diagrammatic longitudinal section of the terebratulide *Liothyrella neozelanica* (Thomson) showing the migration of an outer epithelial cell during its secretion of succeeding layers (Mackinnon and Williams, 1974).

Very recently, during the 8th International Congress held in Milano 11-14 September 2018, new data and a new model have been presented by Ziegler et al. (2018). The authors showed that each fibre formation is not strictly related to a single mantle cell, but require communication and cooperation of neighbouring mantle cells. These findings put into discussion the bases of the conveyor-belt' model of Williams (1968b) and new discoveries and interpretations should be expected in the next years.

2.5 Early evolution of the main brachiopod fabrics

Several shell features have been used to construct the evolutionary tree of the brachiopod phylum as a whole. Among these features, the different fabrics of the secondary layer are the most identifiable characteristics, as they comprise stratiform, tabular laminar, cross-bladed laminar, foliate, and fibrous fabrics (Williams and Cusack, 2007; Garbelli et al., 2017; Garbelli, 2017).

The most significant transformation is the replacement from organophosphatic shell to organocarbonate shell that distinguished the Rhynchonelliforms (and Craniiforms) from the paterinate in the early stages of evolution. Coupled with morphological evidence, the chemicostructures of the craniiforms and the three early rhynchonelliform groups (Chileates, Kutorginates and Obolellates) may be derived from some early Rhychonelliforms (Williams and Cusack, 2007) (Fig. 12). Even if the Strophomenates and Rhynchonellates – the most successful Rhynchonelliforms – had relatively close relationships, their early development pattern remains to be further clarified, their main shell microstructure difference involving the fabric of the secondary layer, laminar in the former and fibrous in the latter.

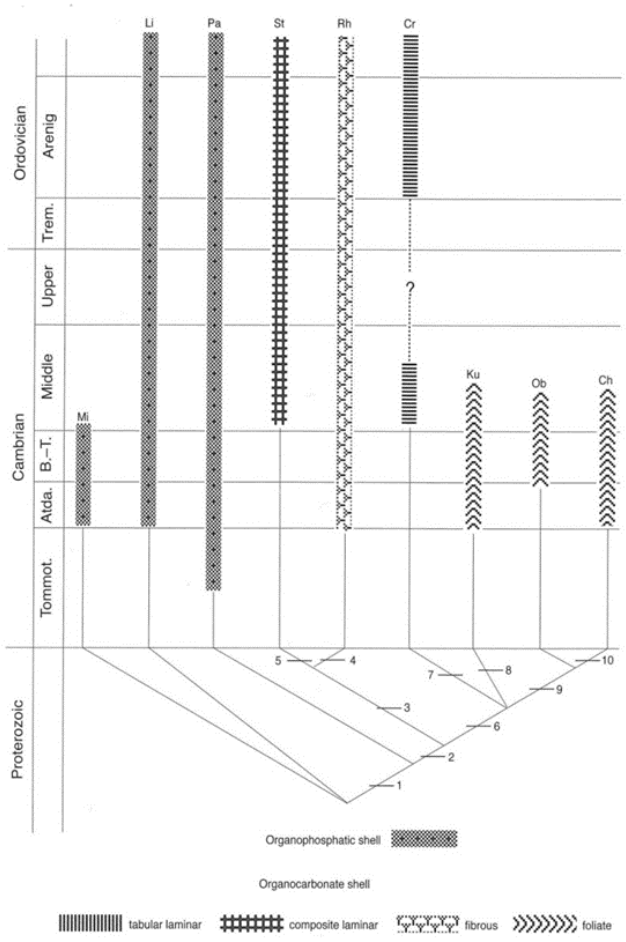

Fig. 12. Chart showing evolution of the main fabrics of the secondary shells of Cambrian-Ordovician brachiopods with halkieriide *Micrina* (*Mi*) as sister group; the eight brachiopod classes are lingulates (*Li*), paterinates (*Pa*), strophomenates (*St*), rhynchonellates (*Rh*), craniates (*Cr*), kutorginates (*Ku*), obolellates (*Ob*), and chileates (*Ch*) (Williams and Cusack, 2007). The numbered transformations are: 1: loss of canaliculate system and acquisition of basic rhynchonelliform characters including development of diductor-adductor muscle system and gonadal sacs in mantles; 2: loss of the organophosphatic, stratiform shell with GAGs and chitin and its replacement by an organocarbonate foliate shell; 3: development of articulating shells with teeth and sockets and a fibrous fabric with a discrete secretory regime; 4: differentiation of pedicles from apical rudiments; 5: development of composite lamination; 6: development of holdfasts, other than pedicles, breaching ventral valves; 7: development of straight gut and tabular lamination and loss of diductor muscles; 8: development of articulating hinge margins; 9: comparatively weak differentiation of diductor-adductor muscle system; 10: development of ventral denticles (new).

2.6 Brachiopods as biochemical archives for paleoenvironment reconstructions

There are several archives of proxies commonly used for paleoenvironment reconstructions, such as brachiopods, conodonts, and whole rocks (Brand et al., 2011). Several comparisons among different types of materials for isotopic analyses have been carried out (Qing et al., 1998; Wenzel et al., 2000; Brand, 2004, 2011). However, of all commonly occurring Paleozoic sedimentary and biogenic carbonates, the fossil brachiopod shells seem to have the highest probability of having retained their original isotopic composition (Grossman et al., 1993; Banner and Kaufman, 1994; Mii and Grossman, 1994; Mii et al., 2001; Brand et al., 2003, 2011; Garbelli et al., 2016; Brand, 2018).

According to previous studies (e.g., Popp et al., 1986a; Bates and Brand, 1991; Grossman et al., 1991; Banner and Kaufman, 1994; Azmy et al., 1998; Brand et al., 2003, 2007, 2011, 2013, 2015; Griesshaber et al., 2004; Parkinson et al., 2005; Angiolini et al., 2007), the brachiopods are the best choice for "ideal" carbonate archives of geochemical data based on the following features:

1) Brachiopods have a long geologic history and are very common in the Phanerozoic fossils record, especially so in the Palaeozoic when they were the rulers of the benthic communities (Williams et al., 1996; Curry and Brunton, 2007). Also they have modern representatives which can be tested to assess their fidelity as archives of proxies of climate and environmental conditions.

2) They have a sessile lifestyle and may tolerate difference in depth (Fürsich and Hurst, 1980; Richardson, 1997); most extant species live from the low tide to 500 m of depth (Logan, 2007) and typically in normal salinity environments (30-40 ‰) (Doyle, 1996).

3) They are low metabolic and physiologically unbuffered organisms sensitive to change in the chemico-physical composition of ambient seawater (Peck et al., 1997; Peck, 2007).

4) Shells of most brachiopods are large and thick enough to allow accurate sampling for geochemical analyses (Popp et al., 1986a).

5) Their fabric is well known both in fossil and in extant taxa (Williams, 1997; Williams and Cusack, 2007) from the nano to the macroscale.

6) Rhynchonelliformean brachiopod shells are generally resistant to diagenesis due to their mineralogy (low-Mg calcite) and compact fabric (Lowenstam, 1961; Popp et al., 1986a). However, some researchers reported differences in the magnesium content and distribution between species, and even within species through the shell layers (Cusack and Williams, 2007; England et al., 2007; Rollion-Bard et al., 2016; Romanin et al., 2018).

7) They generally produce their shell in isotopic (e.g., $\delta^{18}O$ and $\delta^{13}C$) equilibrium with the ambient environment (Brand et al., 2013, 2015). However, many recent studies questioned their supposed equilibrium: e.g. isotopic compositions varying among ventral and dorsal valves (Curry and Fallick, 2002) or within different species or various portions of the same shell (Auclair et al., 2003; Yamamoto et al., 2011, 2013); primary layer being depleted in $\delta^{18}O$ and $\delta^{13}C$ (Carpenter and Lohmann, 1995). In general, secondary and tertiary layers may be the better choice for geochemical analyses (Parkinson et al., 2005; Parkinson and Cusack, 2007; Cusack and Pérez–Huerta, 2012; Rollion-Bard et al., 2016; Romanin et al., 2018).

The latter point is very important. In fact, even if stable isotope from brachiopod shells have been used for environmental investigations since Lowenstam (1961), the assumption that brachiopod shell is precipitated in isotopic equilibrium with ambient seawater needs to be verified (Parkinson and Cusack, 2007).

There are a number of studies which support equilibrium-precipitation at least for certain parts of the brachiopod shell. Carpenter and Lohmann (1995) and Parkinson et al. (2005) investigated $\delta^{18}O$ and $\delta^{13}C$ values in a range of extant brachiopods from a variety of environments. The data from the primary layer and specialized areas of morphological structures (e.g., hinge, brachidium, foramen, interarea, muscle scars) were depleted in both $\delta^{18}O$ and $\delta^{13}C$; the nonspecialized areas of the secondary layer, however, were less fractionated and therefore closer to equilibrium. Brand et al. (2003) presented modern brachiopod isotopic data from a comprehensive set of marine environments. Their studies concluded that most modern brachiopods secondary layer incorporate oxygen isotopic in equilibrium with ambient water. At the same time, impunctate brachiopod shells are preferable in order to avoid post-depositional contamination; they also seem to produce calcite with a narrower range of oxygen isotope composition (Azmy et al., 1998; Cusack et al., 2012). Curry and Fallick (2002) reported different $\delta^{18}O$ values from ventral and dorsal valves from the same individual brachiopod. However, according to recent researches (Parkinson et al., 2005; Brand et al., 2015), no significant differences were found between dorsal and ventral valves, but primary layer and specialized areas (e.g., loop, cardinal process, muscle scars, transition zone) of the secondary shell layer are isotopically depleted relative to the non-specialised areas. The results of Milner et al. (2018) indicate that the oxygen isotopic composition and the trace element content are well preserved in the innermost part of the secondary layer and in the tertiary layer of three modern brachiopod species (*Terebratalia transversa, Magellania venosa* and *Gryphus vitreus*).

Garbelli et al. (2014) have shown that the type of shell fabric (fibrous vs. laminar secondary layer) and its relative organic matter content and the growth rates of the shell may influence the $\delta^{13}C$ record, advising caution in the reconstruction of Paleozoic global $\delta^{13}C$ brachiopod carbonate-based seawater curves. Other investigations highlighted the uncertainties of the equilibrium of the isotope values of brachiopod shells in low temperatures habitats (Marshall et al., 1996; Rahimpour-Bonab et al., 1997); brachiopod shells were enriched in $\delta^{18}O$ relative to equilibrium (Rahimpour-Bonab et al., 1997), and vital effects could not be ruled out (Marshall et al., 1996).

Moreover, recent studies also indicated various degrees of disequilibrium among conspecific individuals and shell portions (Yamamoto et al., 2011, 2013, Takayanagi et al., 2013). A recent study by Bajnai et al. (2018) has shown that clumped and oxygen isotope compositions of the shell of 16 recent brachiopod species are not in thermodynamic equilibrium due to growth rate-induced kinetic effects. However, species-specific growth rates can be taken into account when using isotope analyses to interpret of past ocean conditions as well as appropriate equations to derive palaeotemperature, as the one specific for brachiopods published by Brand et al. (2015).

In a plenary talk at the 8th International Brachiopod congress, Brand (2018) concluded that brachiopods "without reservation, but with proper screening" are the ideal archive of geochemical proxies to unravel the evolution and history of the Earth's oceans in deep time, even if they may be subject to minor vital effects, particularly in specialized areas.

2.7 Screening methods and diagenetic evaluation

Despite their resistance to diagenesis, brachiopod shells are passible to be subjected to alterations that modify the original oxygen and carbon isotope ratios. Significant $\delta^{18}O$ and $\delta^{13}C$ shifts can occur during diagenesis (Mii et al., 1997). Therefore, prior to isotopic analyses, brachiopod shells must be scrutinized carefully for preservation of their original shell structure and chemistry.

For the purpose of obtaining sound data, the samples taken for geochemical analyses should meet following requirements (e.g., Brand et al., 2011): 1) pass multiple screening tests; 2) be stratigraphically well constrained; 3) record ambient oceanographic environment.

Following the work of Williams (1968a, 1997), it became obvious that SEM is an appropriate tool to study brachiopod shell microstructure and biomineralization processes (Gaspard et al., 2007). Traditionally, microstructure preservation, cathodoluminescence and trace-element characterization are the main tools of shell-preservation evaluation (e.g., Popp et al., 1986a; Grossman et al., 1991, 1993, 1996, 2008; Banner and Kaufman, 1994; Mii and Grossman, 1994; Angiolini et al., 2007, 2009; Gaspard et al., 2007)

The main indicators to be considered during evaluation of shell preservation are the following:

1) Neat and oriented microstructure (i.e. similar to extant brachiopod one) is the first evidence of shell preservation (Popp et al., 1986a; Grossman et al., 1991). However, the type of shell fabric and its relative organic matter content can affect the shell geochemical composition (Garbelli et al., 2014)

2) Nonluminescent (NL) calcite (Grossman et al., 1993; Banner and Kaufman, 1994) is an indicator of preservation, even if some modern shells do show sign of luminescent growth banding. Isotopic values of NL shells are generally the same for the same stratigraphic interval (Mii et al., 1997). Altered fabrics revealed by SEM analyses are not always consistent with cathodoluminescence observations (Popp et al., 1986b).

3) Another common feasible measure of preservation is trace-element distribution. In particular, Fe, Mn, Sr contents of the shell are often used as indicator for diagenetical alteration. In diagenetically altered brachiopod shells, Mg and Fe concentrations are usually high, whereas Sr is relatively low (Brand and Veizer, 1980; Popp et al., 1986a, 1986b; Grossman et al., 1993). Cut-off values have been suggested, which are usually used based on contents in modern brachiopods from a variety of depositional environments: Sr of 450–1930 ppm, Mn from 1 to 199 ppm, and Fe generally lower than 140 ppm, although much higher values have also been reported (Brand et al., 2003). Similar trace-element concentrations have been recorded for Carboniferous and Permian brachiopods, and Sr contents as high as 3400 ppm and Mn contents of 250 ppm have also been measured in non-luminescent brachiopod shells (Popp et al., 1986a). Korte et al. (2003, 2005) adopted the criteria of < 250 ppm of Mn and > 400 ppm of Sr for samples to be classified as well preserved. Bruckschen et al. (1999) accepted a more conservative cut-off limit of 200 ppm for Mn, which they considered to be a more reliable indicator of diagenetic alteration than Sr content. More recently, the TE component of primary layer (3740 ppm Na, 3070 ppm Mg, 1380 ppm Sr, 48 ppm Ba, 0.8 ppm Cd) were tested mostly enriched than that of secondary layer (2300 ppm Na, 2200 ppm Mg, 1000 ppm Sr, 3-6.5 ppm Ba, 0.25 ppm Cd) (*Terebratalia transversa*, Rollion-Bard et al., 2016). Similar Mg peaks can also be found in early ontogenetic stage and primary layer (*Aerothyris kerguelenensis*, Gaspard et al., 2018).

4) Stable isotope (cf. $\delta^{18}O$ and $\delta^{13}C$) distribution may be an alternative screening test for diagenetic effects, which may lead to the enrichment in light carbon and oxygen isotopes (Brand and Veizer, 1981; Brand, 2004).

In addition, more advanced tools have been recently introduced for the analysis of the shell microstructure. Two common methods include:

5) Electron backscatter diffraction (EBSD): a microstructural-crystallographic characterisation technique. EBSD application can clarify the fabric of the brachiopod shell and the process of brachiopod shell formation (Schmahl et al., 2004; Pérez-Huerta et al., 2007a; Goetz et al., 2009; Griesshaber et al., 2012). Moreover, EBSD analysis can be a useful tool for detecting the crystallinity after diagenesis and assessing the extent of alteration (Brachiopods, Pérez-Huerta et al., 2007b; Corals, Cusack et al., 2008a; Conodonts, Pérez-Huerta et al., 2012; Casella et al., 2018).

6) Atomic force microscopy (AFM): one type of scanning probe microscopy, with a vertical resolution that can be up to 0.1 nm. Based on STM sensing technique, AFM methods can reveal the nanostructure of biominerals (e.g., proteinaceous envelopes surrounding calcite fibres, Pérez-Huerta et al., 2013), which SEM images cannot show (Cusack et al., 2008b).

To summarize, many recently published data suggest that the inner part of the fibrous secondary layer and the columnar tertiary layer are the most resistant to diagenesis, and, after proper screening, the best biogenic materials for geochemical analyses (e.g. Grossman et al., 1996; Griesshaber et al., 2004; Brand et al., 2012a; Garbelli et al., 2012; Brand, 2018).

2.8 Conclusions

Previous studies have shown that, as dominant invertebrate animals in the past oceans, brachiopods shells can be considered reliable archives for understanding the environmental and climate change in the past with implications for interpretation and prediction in recent and future times. Some unique features of their biominerals were reported: 1) they are widespread in the fossil record and can be found in various environments; 2) they well withstand post-depositional alteration; 3) they are produced in chemical equilibrium with seawater with limited vital effects.

However, there is still insufficient information on the microstructures of these biomineral archives and on the biomineralization processes that lead to their formation. To contribute to solve this issue, recently, multi-disciplinary approaches and new techniques have been applied to the modern and fossil brachiopod shells, allowing starting to describe and decipher their micro-, nano-structure, and even the biomineralization processes. Additionally, a few researches have been also devoted to unravel the shell microstructure of fossil brachiopods, as shell microstructure may be a powerful feature to construct the phylogenetic tree of the brachiopod phylum. But, two important questions remain to be resolved: 1) how does the brachiopod shell microstructure respond to the environmental change and whether is there an ontogenetic or species-specific variation? and 2) which are the main differences in the microstructure of the fossil organocarbonate shells and what are the evolutionary changes and fabric differentiations in two main classes Rhynchonellata and Strophomenata during the Palaeozoic?

The next chapters will address these issues.

References

Angiolini, L., Darbyshire, D.P.F., Stephenson, M.H., Leng, M.J., Brewer, T.S., Berra, F., Jadoul, F., 2007. Lower Permian brachiopods from Oman: their potential as climatic proxies. Earth and Environmental Science Transactions of the Royal Society of Edinburgh 98, 327–344.

Angiolini, L., Jadoul, F., Leng, M.J., Stephenson, M.H., Rushton, J., Chenery, S., Crippa, G., 2009. How cold were the Early Permian glacial tropics? Testing sea–surface temperature using the oxygen isotope composition of rigorously screened brachiopod shells. Journal of the Geological Society 166, 933–945.

Armstrong, J., 1968. Microstructure of the shell of a Permian spiriferid brachiopod. Journal of the Geological Society of Australia 15, 183–188.

Armstrong, J., 1969. The cross–bladed fabrics of the shells of *Terrakea solida* (Etheridge and Dun) and Streptorhynchus pelicanensis Fletcher. Palaeontology 12, 310–320.

Auclair, A.C., Joachimski, M.M., Lécuyer, C., 2003. Deciphering kinetic, metabolic and environmental controls on stable isotope fractionations between seawater and the shell of *Terebratalia transversa* (Brachiopoda). Chemical Geology 202, 59–78.

Azmy, K., Veizer, J., Bassett, M.G., Copper, P., 1998. Oxygen and carbon isotopic composition of Silurian brachiopods: implications for coeval seawater and glaciations. Geological Society of America Bulletin 110, 1499–1512.

Bajnai, D., Fiebig, J., Tomašových, A., Milner Garcia, S., Rollion–Bard, C., Raddatz, J., Löffler, N., Primo–Ramos, C., Brand, U., 2018. Assessing kinetic fractionation in brachiopod calcite using clumped isotopes. Scientific Reports 8, p. 533, 10.1038/s41598–017–17353–7

Banner, J.L., Kaufman, J., 1994. The isotopic record of ocean chemistry and diagenesis preserved in non–luminescent brachiopods from Mississippian carbonate rocks, Illinois and Missouri. Geological Society of America Bulletin 106, 1074–1082.

Bates, N.R., Brand. U., 1991. Environmental and physiological influences on isotopic and elemental compositions of brachiopod shell calcite: implications for the isotopic evolution of Paleozoic oceans. Chemical Geology: Isotope Geoscience section 94, 67–78.

Biernat, G., Balinski, A., 1982. Shell structure of the Devonian retziid brachiopod *Plectospira ferita*. Palaeontology 25, 857–867.

Brand, U., 2004. Carbon, oxygen and strontium isotopes in Paleozoic carbonate components: an evaluation of original seawater–chemistry proxies. Chemical Geology 204, 23–44.

Brand, U., 2018. Modern and fossil brachiopods: superheroes of archives. 8th International Brachiopod Congress Milan, 11–14 September 2018, Permophiles 66, 29.

Brand, U., Veizer, J., 1980. Chemical diagenesis of a multicomponent carbonate system 1: Trace elements. Journal of Sedimentary Petrology 50, 1219–1236.

Brand, U., Veizer, J., 1981. Chemical diagenesis of a multicomponent carbonate system 2: Stable isotopes. Journal of Sedimentary Petrology 51, 987–997.

Brand, U., Logan, A., Hiller, N., Richardson, J., 2003. Geochemistry of modern brachiopods: applications and implications for oceanography and paleoceanography. Chemical Geology 198, 305–334.

Brand, U., Webster, G.D., Azmy, K., Logan, A., 2007. Bathymetry and productivity of the southern Great Basin seaway, Nevada, USA: An evaluation of isotope and trace element chemistry in mid–

Carboniferous and modern brachiopods. Palaeogeography, Palaeoclimatology, Palaeoecology 256, 273–297.

Brand, U., Logan, A., Bitner, M.A., Griesshaber, E., Azmy, K., Buhl, D., 2011. What is the ideal proxy of Palaeozoic seawater chemistry? In: Memoirs of the Association of Australasian Palaeontologists 41, 9–24.

Brand, U., Jiang, G., Azmy, K., Bishop, J., Montañez, I.P., 2012. Diagenetic evaluation of a Pennsylvanian carbonate succession (Bird Spring Formation, Arrow Canyon, Nevada, USA)—1: Brachiopod and whole rock comparison. Chemical Geology 308, 26–39.

Brand, U., Azmy, K., Bitner, M.A., Logan, A., Zuschin, M., Came, R., Ruggiero, E., 2013. Oxygen isotopes and $MgCO_3$ in brachiopod calcite and a new paleotemperature equation. Chemical Geology 359, 23–31.

Brand, U., Azmy, K., Griesshaber, E., Bitner, M.A., Logan, A., Zuschin, M., Ruggiero, E., Colin, P.L., 2015. Carbon isotope composition in modern brachiopod calcite: A case of equilibrium with seawater? Chemical Geology 411, 81–96.

Bruckschen, P., Oesmann, S., Veizer, J., 1999. Isotope stratigraphy of the European carboniferous: proxy signals for ocean chemistry, climate and tectonics. Chemical Geology 161, 127–163.

Carpenter, S.J., Lohmann, K.C., 1995. $\delta^{18}O$ and $\delta^{13}C$ values of modern brachiopod shells. Geochimica et Cosmochimica Acta 59, 3749–3764.

Casella, L.A., Griesshaber, E., Simonet Roda, M., Ziegler, A., Mavromatis, V., Henkel, D., Laudien, J., Häussermann, V., Neuser, R., Angiolini, L., Dietzel, M., Eisenhauer, A., Immenhauser, A., Brand, U., Schmahl, W., 2018. Micro– and nanostructures reflect the degree of diagenetic alteration inmodern and fossil brachiopod shell calcite: A multi–analytical screeningapproach (CL, FE–SEM, AFM, EBSD). Palaeogeography, Palaeoclimatology, Palaeoecology 502, 13–30.

Curry, G.B., Fallick, A.E., 2002. Use of stable oxygen isotope determinations from brachiopod shells in palaeoenvironmental reconstruction. Palaeogeography, Palaeoclimatology, Palaeoecology 182, 133–143.

Curry, G.B., Brunton, H.C., 2007. Stratigraphic distribution of brachiopods. in: Selden, P.A. (Ed.), Treatise on Invertebrate Paleontology. Part H, Revised, Brachiopoda, vol. 6. Geological Society of America Inc., and The University of Kansas, Boulder, Colorado, USA, pp. 2901–3081.

Cusack, M., Pérez–Huerta, A., 2012. Brachiopods recording seawater temperature—A matter of class or maturation? Chemical Geology 334, 139–143.

Cusack, M., Walton, D., Curry, G.B., 1997. Shell biochemistry. in: Kaesler, R.L. (Ed.), Treatise on Invertebrate Paleontology. Part H, Revised, Brachiopoda, vol. 1. Geological Society of America Inc., and The University of Kansas, Boulder, Colorado, USA, pp. 243–266.

Cusack, M., England, J., Dalbeck, P., Tudhope, A.W., Fallick, A.E., Allison, N., 2008a. Electron backscatter diffraction (EBSD) as a tool for detection of coral diagenesis. Coral reefs 27, 905–911.

Cusack, M., Dauphin, Y., Chung, P., Pérez–Huerta, A., Cuif, J–P., 2008b. Multiscale structure of calcite fibres of the shell of the brachiopod *Terebratulina retusa*. Journal of structural biology 164, 96–100.

Cusack, M., Chung, P., Dauphin, Y., Pérez–Huerta, A., 2010. Brachiopod primary layer crystallography and nanostructure. Special Papers in Palaeontology 84, 99–105.

Dewing, K., 2004. Shell structure and its bearing on the phylogeny of Late Ordovician–Early Silurian strophomenoid brachiopods from Anticosti Island, Québec. Journal Information 78, 275–286.

Doyle, P., 1996. Understanding Fossils: An introduction to invertebrate palaeontology. John Wiley & Sons, New York, 1–426.

Emig, C.C., Bitner, M.A., Alvarez, F., 2013. Phylum Brachiopoda. In: Zhang, Z.–Q.(Ed.) Animal biodiversity: an outline of higher–level classification and Survey of taxonomic richness (Addenda 2013). Zootaxa 3703, 75–78.

England, J., Cusack, M., Lee, M.R., 2007. Magnesium and sulphur in the calcite shells of two brachiopods, *Terebratulina retusa* and *Novocrania anomala*. Lethaia 40, 2–10.

Fürsich, F.T., Hurst, J., 1980. Euryhalinity of Palaeozoic articulate brachiopods. Lethaia 13, 303–312.

Garbelli, C., 2017. Shell microstructures in lopingian brachiopods: implications for fabric evolution and calcification. Rivista Italiana di Paleontologia e Stratigrafia 123, 541–560.

Garbelli, C., Angiolini, L., Jadoul, F., Brand, U., 2012. Micromorphology and differential preservation of Upper Permian brachiopod low–Mg calcite. Chemical Geology 298, 1–10.

Garbelli, C., Angiolini, L., Brand, U., Jadoul, F. 2014. Brachiopod fabric, classes and biogeochemistry: Implications for the reconstruction and interpretation of seawater carbon–isotope curves and records. Chemical Geology 371, 60–67.

Garbelli, C., Angiolini L., Brand, U., Shen, S.Z., Jadoul, F., Posenato, R., Azmy, K., Cao, C.Q., 2016. Neotethys seawater chemistry and temperature at the dawn of the end Permian mass extinction. Gondwana Research 35, 272–285.

Garbelli, C., Angiolini, L., Shen, S.Z., 2017. Biomineralization and global change: A new perspective for understanding the end–Permian extinction. Geology 45, 19–22.

Gaspard, D., Marin, F., Guichard, N., Morel, S., Alcaraz, G., Luquet, G., 2007. Shell matrices of recent Rhynchonelliform Brachiopods: microstructures and glycosylation studies. Earth and Environmental Science Transactions of the Royal Society of Edinburgh 98, 415–424.

Gaspard, D., Aldridge, A.E., Boudouma, O., Fialin, M., Rividi, N., Lécuyer, C., 2018. Analysis of growth and form in *Aerothyris kerguelenensis* (Rhynchonelliform brachiopod) – Shell spiral deviations, microstructure, trace element contents and stable isotope ratios. Chemical Geology 483, 474–490.

Goetz, A.J., Griesshaber, E., Neuser, R.D., Lüter, C., Hühner, M., Harper, E., Schmahl, W.W., 2009. Calcite morphology, texture and hardness in the distinct layers of rhynchonelliform brachiopod shells. European Journal of Mineralogy 21, 303–315.

Griesshaber, E., Job, R., Pettke, T., Schmahl, W.W., 2004. Micro–scale physical and chemical heterogeneities in biogenic materials–a combined micro–Raman, chemical composition and microhardness investigation. MRS Proceedings, MRS Proceedings, Cambridge Univ Press 844, Y7.2.1–Y7.2.6.

Griesshaber, E., Schmahl, W.W., Neuser, R., Pettke, T., Blüm, M., Mutterlose, J., Brand, U., 2007. Crystallographic texture and microstructure of terebratulide brachiopod shell calcite: an optimized materials design with hierarchical architecture. American Mineralogist 92, 722–734.

Griesshaber, E., Ubhi, H.S., Schmahl, W.W., 2012. Nanometer scale microstructure and microtexture of biological materials revealed by high spatial resolution (15 to 5 kV) EBSD. Materials Science Forum 702, 924–927.

Grossman, E.L., Zhang, C., Yancey, T.E., 1991. Stable–isotope stratigraphy of brachiopods from Pennsylvanian shales in Texas. Geological Society of America Bulletin 103, 953–965.

Grossman, E.L., Mii, H.S., Yancey, T.E., 1993. Stable isotopes in Late Pennsylvanian brachiopods from the United States: Implications for Carboniferous paleoceanography. Geological Society of America Bulletin 105, 1284–1296.

Grossman, E.L., Mii, H.S., Zhang, C., Yancey, T.E., 1996. Chemical variation in Pennsylvanian brachiopod shells; diagenetic, taxonomic, microstructural, and seasonal effects. Journal of Sedimentary Research 66, 1011–1022.

Grossman, E.L., Yancey, T.E., Jones, T.E., Bruckschen, P., Chuvashov, B., Mazzullo, S.J., Mii, H.S., 2008. Glaciation, aridification, and carbon sequestration in the Permo–Carboniferous: the isotopic record from low latitudes. Palaeogeography, Palaeoclimatology, Palaeoecology 268, 222–233.

Holmer, L., Popov, L.E., Bassett, M.G., Laurie, J., 1995. Phylogenetic analysis and ordinal classification of the Brachiopoda. Palaeontology 38, 713–741.

Holmer, L.E., Popov, L,E., 2007. Incertae sedis organophosphatic bivalved stem–group brachiopods. in: Selden, P.A. (Ed.), Treatise on Invertebrate Paleontology. Part H, Revised, Brachiopoda, vol. 6. Geological Society of America Inc., and The University of Kansas, Boulder, Colorado, USA, pp. 2580–2590.

Korte, C., Kozur, H.W., Bruckschen, P., Veizer, J., 2003. Strontium isotope evolution of Late Permian and Triassic seawater. Geochimica et Cosmochimica Acta 67, 47–62.

Korte, C., Jasper, T., Kozur, H.W., Veizer, J., 2005. $\delta^{18}O$ and $\delta^{13}C$ of Permian brachiopods: a record of seawater evolution and continental glaciation. Palaeogeography, Palaeoclimatology, Palaeoecology 224, 333–351.

Logan, A., 2007. Geographic distribution of extant articulated brachiopods. in: Selden, P.A. (Ed.), Treatise on Invertebrate Paleontology. Part H, Revised, Brachiopoda, vol. 6. Geological Society of America Inc., and The University of Kansas, Boulder, Colorado, USA, pp. 3082–3115.

Lowenstam, H.A., 1961. Mineralogy, O^{18}/O^{16} ratios, and strontium and magnesium contents of recent and fossil brachiopods and their bearing on the history of the oceans. The Journal of Geology 69, 241–260.

MacKinnon, D.I., Williams, A., 1974. Shell structure of terebratulid brachiopods. Palaeontology 17, 179–202.

Marshall, J.D., Pirrie, D., Clarke, A., Nolan, C.P., Shaman, J., 1996. Stable–isotopic composition of skeletal carbonates from living Antarctic marine invertebrates. Lethaia 29, 203–212.

Mii, H–S., Grossman, E.L., 1994. Late Pennsylvanian seasonality reflected in the ^{18}O and elemental composition of a brachiopod shell. Geology 22, 661–664.

Mii, H–S., Grossman, E.L., Yancey, T.E., 1997. Stable carbon and oxygen isotope shifts in Permian seas of West Spitsbergen–Global change or diagenetic artifact? Geology 25, 227–230.

Mii, H–S., Grossman, E.L., Yancey, T.E., Chuvashov, B., Egorov, A., 2001. Isotopic records of brachiopod shells from the Russian Platform—evidence for the onset of mid–Carboniferous glaciation. Chemical Geology 175, 133–147.

Milner Garcia, S.A., Rollion–Bard, C., Burckel, P., Müller, T., Jurikova, H., Tomašových, A., Angiolini, L., Henkel, D., 2018. Fossil brachiopod shell calcite: How well is the oxygen isotope

composition and minor element ratios preserved within the shell microstructure? 8th International Brachiopod Congress Milan, 11–14 September 2018, Permophiles 66, 78–79.

Owen, G., Williams, A., 1969. The caecum of articulate Brachiopoda. Proceedings of the Royal Society of London B: Biological Sciences 172, 187–201.

Parkinson, D., Curry, G.B., Cusack, M., Fallick, A.E., 2005. Shell structure, patterns and trends of oxygen and carbon stable. Chemical Geology 219, 193–235.

Parkinson, D., Cusack, M., 2007. Stable oxygen and carbon isotopes in extant brachiopod shells: keys to deciphering ancient ocean environments. in: Selden, P.A. (Ed.), Treatise on Invertebrate Paleontology. Part H, Revised, Brachiopoda, vol. 6. Geological Society of America Inc., and The University of Kansas, Boulder, Colorado, USA, pp. 2522–2531.

Peck, L.S., 2007. Brachiopods and climate change. Earth and environmental science transactions of the Royal Society of Edinburgh 98, 451–456.

Peck, L.S., Rhodes, M.C., Curry, G.B., Ansell, A.D., 1997. Physiology. in: Kaesler, R.L. (Ed.), Treatise on Invertebrate Paleontology. Part H, Revised, Brachiopoda, vol. 1. Geological Society of America Inc., and The University of Kansas, Boulder, Colorado, USA, pp. 213–242.

Pérez–Huerta, A., Cusack, M., Zhu, W., England, J., Hughes, J., 2007a. Material properties of brachiopod shell ultrastructure by nanoindentation. Journal of The Royal Society Interface 4, 33–39.

Pérez–Huerta, A., Cusack, M., England, J., 2007b. Crystallography and diagenesis in fossil craniid brachiopods. Palaeontology 50, 757–763.

Pérez–Huerta, A., Cusack, M., McDonald, S., Marone, F., Stampanoni, M., MacKay, S., 2009. Brachiopod punctae: A complexity in shell biomineralisation. Journal of structural biology 167, 62–67.

Pérez–Huerta, A., Cusack, M., Mendez Carlos, A., 2012. Preliminary assessment of the use of electron backscatter diffraction (EBSD) in conodonts. Lethaia 45, 253–258.

Pérez–Huerta, A., Dauphin, Y., Cusack, M., 2013. Biogenic calcite granules—Are brachiopods different? Micron 44, 395–403.

Popp, B.N., Anderson, T.F., Sandberg, P.A., 1986a. Brachiopods as indicators of original isotopic compositions in some Paleozoic limestones. Geological Society of America Bulletin 97, 1262–1269.

Popp, B.N., Anderson, T.F., Sandberg, P.A., 1986b. Textural, elemental, and isotopic variations among constituents in Middle Devonian limestones, North America. Journal of Sedimentary Research 56, 715–727.

Qing, H., Barnes, C.R., Buhl, D., Veizer, J., 1998. The strontium isotopic composition of Ordovician and Silurian brachiopods and conodonts: relationships to geological events and implications for coeval seawater. Geochimica et Cosmochimica Acta 62, 1721–1733.

Rahimpour–Bonab, H., Bone, Y., Moussavi–Harami, R., 1997. Stable isotope aspects of modern molluscs, brachiopods, and marine cements from cool–water carbonates, Lacepede Shelf, South Australia. Geochimica et Cosmochimica Acta 61, 207–218.

Richardson, J.R., 1997. Ecology of articulated brachiopods. in: Kaesler, R.L. (Ed.), Treatise on Invertebrate Paleontology. Part H, Revised, Brachiopoda, vol. 1. Geological Society of America Inc., and The University of Kansas, Boulder, Colorado, USA, pp. 441–462.

Rollion–Bard, C., Saulnier, S., Vigier, N., Schumacher, A., Chaussidon, M., Lécuyer, C., 2016. Variability in magnesium, carbon and oxygen isotope compositions of brachiopod shells: Implications for paleoceanographic studies. Chemical Geology 423, 49–60.

Romanin, M., Crippa, G., Ye, F., Brand, U., Bitner, M.A., Gaspard, D., Häussermann, V., Laudien, J., 2018. A sampling strategy for recent and fossil brachiopods: selecting the optimal shell segment for geochemical analyses. Rivista Italiana di Paleontologia e Stratigrafia 124, 343–359.

Schmahl, W.W., Griesshaber, E., Kelm, K., Goetz, A., Jordan, G., Ball, A., Xu, D., Merkel, C., Brand, U., 2012. Hierarchical structure of marine shell biomaterials: biomechanical functionalization of calcite by brachiopods. Zeitschrift für Kristallographie–Crystalline Materials 227, 793–804.

Schmahl, W.W., Griesshaber, E., Neuser, R., Lenze, A., Job, R., Brand, U., 2004. The microstructure of the fibrous layer of terebratulide brachiopod shell calcite. European Journal of Mineralogy 16, 693–697.

Smirnova, T.N., Popiel–Barczyk, E., 1991. Characteristics of the shell ultrastructure in Terebratellacea. In Mackinnon D I, Lee D E, and Campbell J D, (ed), Brachiopods Through Time, Proceedings of the 2nd International Brachiopod Congress, University of Otago, Dunedin, New Zealand, 1990. Balkema. Rotterdam. 159–165.

Takayanagi, H., Asami, R., Abe, O., Miyajima, T., Kitagawa, H., Sasaki, K., Iryu, Y., 2013. Intraspecific variations in carbon–isotope and oxygen–isotope compositions of a brachiopod *Basiliola lucida* collected off Okinawa–jima, southwestern Japan. Geochimica et Cosmochimica Acta 115, 115–136.

Wenzel, B., Lécuyer, C., Joachimski, M.M. 2000. Comparing oxygen isotope records of Silurian calcite and phosphate—$\delta^{18}O$ compositions of brachiopods and conodonts. Geochimica et Cosmochimica Acta 64, 1859–1872.

Williams, A., 1956. The calcareous shell of the Brachiopoda and its importance to their classification. Biological Reviews 31, 243–287.

Williams, A., 1966. Growth and structure of the shell of living articulate bachiopods. Nature 211, 1146–1148.

Williams, A., 1968a. Evolution of the shell structure of articulate brachiopods. Special Papers in Palaeontology 2, 1–55.

Williams, A., 1968b. A history of skeletal secretion among articulate brachiopods. Lethaia 1, 268–287.

Williams, A., 1970a. Spiral growth of the laminar shell of the brachiopod Crania. Calcified tissue research 6, 11–19.

Williams, A., 1970b. Origin of laminar–shelled articulate brachiopods. Lethaia 3, 329–342.

Williams, A., 1973. The secretion and structural evolution of the shell of thecideidine brachiopods. Philosophical Transactions of the Royal Society of London. Series B, Biological Sciences 264, 439–478.

Williams, A., 1997. Shell structure. in: Kaesler, R.L. (Ed.), Treatise on Invertebrate Paleontology. Part H, Revised, Brachiopoda, vol. 1. Geological Society of America Inc., and The University of Kansas, Boulder, Colorado, USA, pp. 267–320.

Williams A., Brunton C.H.C., 1993. Role of shell structure in the classification of the orthotetidine brachiopods. Palaeontology 36, 931–966.

Williams, A., Carlson, S. J., Brunton, C.H.C., Holmer, L.E., Popov, L., 1996. A supra–ordinal classification of the Brachiopoda. Philosophical Transactions of the Royal Society B: Biological Sciences 351, 1171–1193.

Williams, A., Carlson, S.J., 2007. Affinities of Brachiopods and trends in their evolution. in: Selden, P.A. (Ed.), Treatise on Invertebrate Paleontology. Part H, Revised, Brachiopoda, vol. 6. Geological Society of America Inc., and The University of Kansas, Boulder, Colorado, USA, pp. 2822–2900.

Williams, A., Cusack, M., 2007. Chemicostructural diversity of the brachiopod shell. in: Selden, P.A. (Ed.), Treatise on Invertebrate Paleontology. Part H, Revised, Brachiopoda, vol. 6. Geological Society of America Inc., and The University of Kansas, Boulder, Colorado, USA, pp. 2396–2521.

Yamamoto, K., Asami, R., Iryu, Y., 2011. Brachiopod taxa and shell portions reliably recording past ocean environments: Toward establishing a robust paleoceanographic proxy. Geophysical Research Letters 38, L13601, doi:10.1029/2011GL047134.

Yamamoto, K., Asami, R., Iryu, Y., 2013. Correlative relationships between carbon–and oxygen–isotope records in two cool–temperate brachiopod species off Otsuchi Bay, northeastern Japan. Paleontological Research 17, 12–26.

Ziegler, A., Roda, M.S., Griesshaber, E., Henkel, D., Häusermann, V., Eisenhauer, A., Laudin, J., Schmahl, W., 2018. Mechanisms of calcite fibre formation in *Magellania venosa*. 8th International Brachiopod Congress Milan, 11–14 September 2018, Permophiles 66, 137–138.

Chapter 3
Mapping of recent brachiopod microstructure: A tool for environmental studies

*Published in Journal of Structural Biology (2018), V. 201, pp. 221-236

Facheng Ye[a], Gaia Crippa[a], Lucia Angiolini[a], Uwe Brand[b], GianCarlo Capitani[c], Maggie Cusack[d], Claudio Garbelli[e], Erika Griesshaber[f], Elizabeth Harper[g], Wolfgang Schmahl[f]

[a]Dipartimento di Scienze della Terra "A. Desio", Università degli Studi di Milano, Milan, Italy

[b]Department of Earth Sciences, Brock University, St. Catharines, Ontario L253AI, Canada

[c]Dipartimento di Scienze dell'Ambiente e di Scienze della Terra, Piazza della Scienza 4, 20126 Milano, Italy

[d]Division of Biological & Environmental Sciences, Faculty of Natural Sciences, University of Stirling, Stirling FK9 4LA, UK

[e]State Key Laboratory of Palaeobiology and Stratigraphy, Nanjing Institute of Geology and Palaeontology, Chinese Academy of Sciences, Nanjing, China

[f]Department fur Geo- und Umweltwissenschaften, Ludwig-Maximilians Universitat Munchen, Munich, Germany

[g]Department of Earth Sciences, University of Cambridge, Cambridge CB2 3EQ, UK

Abstract

Shells of brachiopods are excellent archives for environmental reconstructions in the recent and distant past as their microstructure and geochemistry respond to climate and environmental forcings. We studied the morphology and size of the basic structural unit, the secondary layer fibre, of the shells of several extant brachiopod taxa to derive a model correlating microstructural patterns to environmental conditions. Twenty-one adult specimens of six recent brachiopod species adapted to different environmental conditions, from Antarctica, to New Zealand, to the Mediterranean Sea, were chosen for microstructural analysis using SEM, TEM and EBSD. We conclude that: 1) there is no significant difference in the shape and size of the fibres between ventral and dorsal valves, 2) there is an ontogenetic trend in the shape and size of the fibres, as they become larger, wider, and flatter with increasing age. This indicates that the fibrous layer produced in the later stages of growth, which is recommended by the literature to be the best material for geochemical analyses, has a different morphostructure and probably a lower organic content than that produced earlier in life.

In two species of the same genus living in seawater with different temperature and carbonate saturation state, a relationship emerged between the microstructure and environmental conditions. Fibres of the polar *Liothyrella uva* tend to be smaller, rounder and less convex than those of the temperate *Liothyrella neozelanica*, suggesting a relationship between microstructural size, shell organic matter content, ambient seawater temperature and calcite saturation state.

3.1 Introduction

To understand climate change, it is important to estimate the longterm natural variability of environmental parameters such as seawater temperature, seasonality, pH and acidification in the recent and distant past. Biominerals, the hard parts produced by organisms for support and protection, are one of the best tools to use, as they are high-resolution archives of proxies reacting and recording environmental conditions prevailing during their growth.

Shells of marine invertebrates, such as brachiopods and bivalves, are considered excellent archives for reconstructing recent and past environmental conditions (e.g., Popp et al., 1986; Grossman et al., 1991; Parkinson et al., 2005; Angiolini et al., 2007, 2009; Brand et al., 2011; Schöne and Surge, 2012; Cusack and Huerta, 2012; Brocas et al., 2013; Crippa et al., 2016a; Garbelli et al., 2017). Brachiopod shells in particular are high resolution biomineral archives used to reconstruct global marine environments in the recent and deep past, because: 1) they record the physical and chemical composition of the seawater in which they live with no or limited vital effects (e.g., Parkinson et al., 2005; Brand et al., 2013, 2015); 2) they precipitate a low-Mg calcite shell, which is generally resistant to diagenetic alteration (Lowenstam, 1961; Brand and Veizer, 1980; Popp et al., 1986; Brand et al., 2011); 3) they are common in the Phanerozoic, especially during the Palaeozoic when they dominated benthic communities (Curry and Brunton, 2007); and, 4) they are low metabolic and physiologically unbuffered organisms sensitive to change in the physicochemical composition of the ambient seawater (Peck et al., 1997; Peck, 2007).

Fossil biominerals have considerable potential for extending climate and environmental records on a broad geographical scale and over long periods of time (Garbelli et al., 2017). Recent brachiopods are unparalleled archives on how microstructure and geochemistry may respond or adapt to general or specific environmental conditions (Watson et al., 2012; Cross et al., 2016). Also, they allow for the study of complex relationships between different shell microstructures and the oceanographic geochemical record (e.g., Immenhauser et al., 2016).

Brachiopods possess complex microstructures (e.g., Schmahl et al., 2004; Griesshaber et al., 2007; Pérez-Huerta et al., 2009; Goetz et al., 2011; Gaspard and Nouet, 2016; Garbelli, 2017), but we focus on the fibres of the secondary layer of rhynchonelliformean brachiopods. Previous studies examined the nanostructure, hardness and orientation of the fibres within the secondary layer of extant brachiopods (e.g., Griesshaber et al., 2006; Pérez-Huerta et al., 2007; Goetz et al., 2009; Schmahl et al., 2012), but not the shape and size of individual fibres in different parts of the same shell and in different taxa. Here, we analyse the microstructure of six extant rhynchonelliformean brachiopods adapted to different environmental conditions, from Signy and Trolval Islands, Antarctica, to Doubtful Sound, New Zealand to the Tuscan Archipelago, Mediterranean Sea. We relate the observed patterns to 1) ontogenetic variation, and 2) environmental variables.

3.2 Materials

Six brachiopod species were chosen for shell microstructural analysis. A total of 21 adult specimens, of similar size, were investigated, all having a secondary shell layer. Sixty samples were cut along different longitudinal and perpendicular sections to investigate the size and shape of the fibres, the structural units of the secondary layer.

The analysed specimens belong to the terebratulid species *Liothyrella neozelanica* (Thomson, 1918), *Calloria inconspicua* (Sowerby, 1846), and *Magasella sanguinea* (Leach, 1814) from Doubtful Sound, New Zealand, *Liothyrella uva* (Broderip, 1833) from Trolval Island, Ryder Bay and Signy Island, Antarctica, and *Gryphus vitreus* (Born, 1778) from the Tuscan archipelago, Italy (Table 1). The rhynchonellid species *Notosaria nigricans* (Sowerby, 1846) comes from Doubtful Sound and Kaka Point, New Zealand (Table 1). Of these, *L. uva*, *C. inconspicua*, *N. nigricans* and *M. sanguinea* possess a shell consisting of primary microgranular and secondary fibrous calcite layer, whereas *L. neozelanica* and *G. vitreus* also have an additional tertiary columnar calcite layer (Figs. 1–3).

Table 1
Brachiopods for shell microstructural analyses. Name of the species, locality and depth, corresponding geographic coordinates, water temperature and salinity, as well as the shell succession of each specimen with corresponding ID number, type of valve and the number of SEM micrographs. D: Depth, T: temperature, S: salinity.

	Species	Locality and depth	Geographic coordinate	Temperature and salinity	Shell sequence	ID number	Valve	SEM micrographs number
Terebratulida	*Liothyrella uva*	TI: Trolval Island, Ryder Bay SI: Signy Island (D: 10m), Antarctica	67 °35.44' S, 68 °12.44' W (TI) 60 °43' S, 45 °36' W (SI)	T: -2/+2 ℃, S: 34 PSU (TI & SI)	Ⅰ, Ⅱ layers	LUH1	ventral	40
						LUH2	ventral	28
						LUH3	ventral and dorsal	98
						LU	ventral	36
						LUV/LUD	ventral and dorsal	135
	Gryphus vitreus	Tuscan Archipelago (D: 140~160m between the Island of Pianosa and Montecristo), Tyrrhenian Sea, Italy	42 °26' N, 10 °04' E	T: 13~15 ℃, S: 39 PSU	Ⅰ, Ⅱ, Ⅲ layers	1D	ventral and dorsal	111
						GV	ventral and dorsal	81
						GV3	ventral and dorsal	68
						GV4	ventral and dorsal	132
						GV5	dorsal	14
	Liothyrella neozelanica	Doubtful Sound (D: 18m), New Zealand	45 °18' 00" S, 166 °58' 45" E	T: 11~17 ℃, S: 34.8 PSU	Ⅰ, Ⅱ, Ⅲ layers	1C	ventral and dorsal	144
						LZ	ventral and dorsal	288
						LN	ventral and dorsal	176
	Calloria inconspicua	Doubtful Sound (D: 18m), New Zealand	45 °18' 00" S, 166 °58' 45" E	T: 11~17 ℃, S: 34.8 PSU	Ⅰ, Ⅱ layers	1CC	ventral and dorsal	27
						CI	ventral and dorsal	43
	Magasella sanguinea	Doubtful Sound (D: 18m), New Zealand	45 °18' 00" S, 166 °58' 45" E	T: 11~17 ℃, S: 34.8 PSU	Ⅰ, Ⅱ layers	TS1	ventral and dorsal	157
Rhynchonellida	*Notosaria nigricans*	DS: Doubtful Sound (D: 18m) KP: Kaka Point (D: 2~15m), New Zealand	45 °18' 00" S, 166 °58' 45" E (DS) 46 °38' 66" S, 169 °78' 23" E (KP)	T: 11~17 ℃, S: 34.8 PSU (DS) T: 14 ℃, S: 34~35 PSU (KP)	Ⅰ, Ⅱ layers	1DC	ventral	41
						NN	ventral and dorsal	59
						NN1	ventral and dorsal	34
						NN2	ventral and dorsal	135
						NN3	ventral and dorsal	47

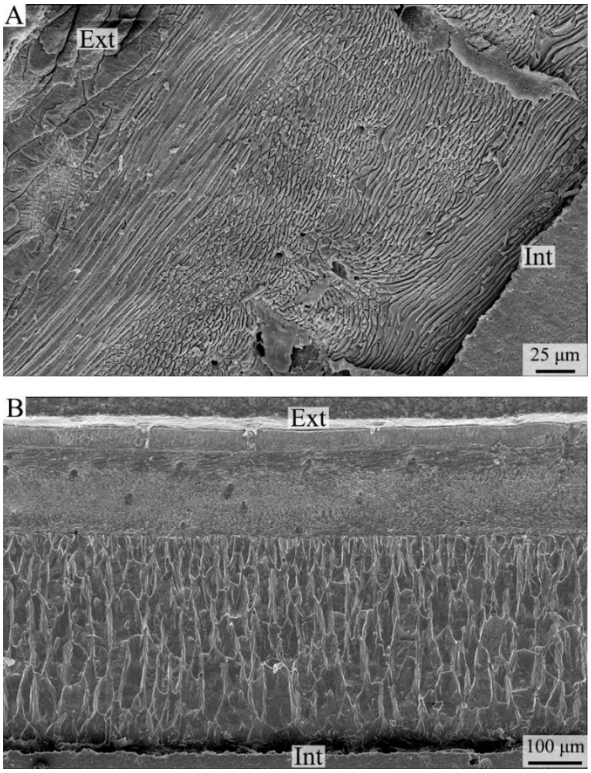

Fig. 1. A, shell structure of *L. uva*, made of primary microgranular and secondary fibrous layer; B, shell succession of *L. neozelanica* with primary microgranular layer, and secondary fibrous and tertiary columnar layers. Ext: external, Int: internal.

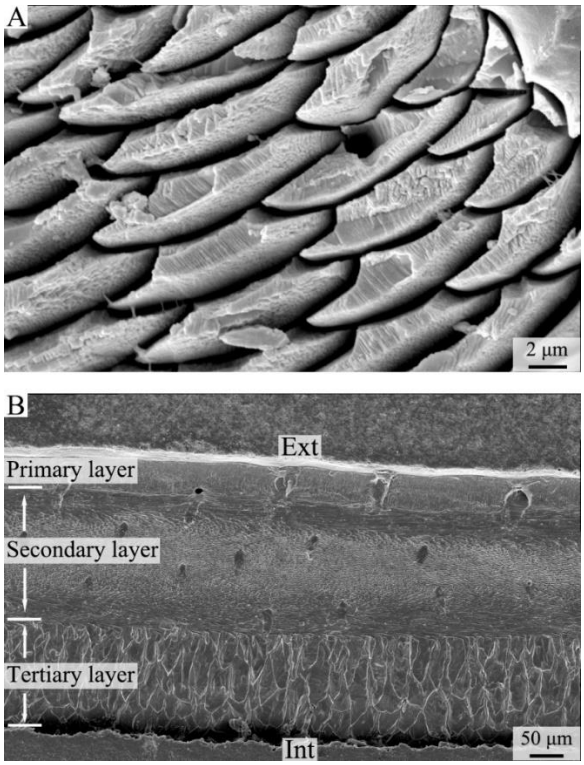

Fig. 2. *L. neozelanica*. A, enlarged photos showing fibres in transverse section (dorsal valve); B, complete shell succession showing change in the orientation of fibres from oblique to transverse from the exterior to the interior of the secondary layer (central part, ventral valve, longitudinal section). Ext: external, Int: internal.

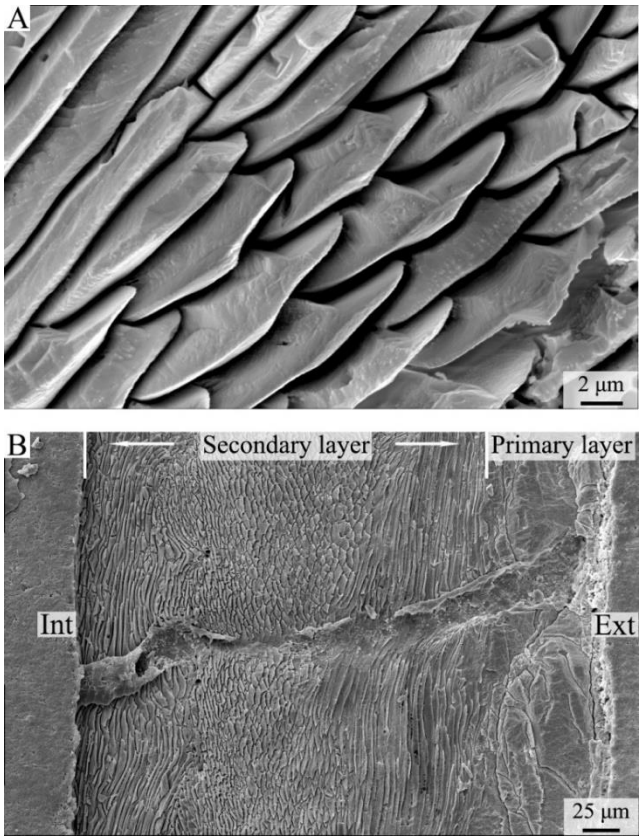

Fig. 3. A, *G. vitreus*. enlarged photo showing fibres in transverse section (ventral valve); B, *L. uva*. shell succession showing the change in the orientation of fibres from oblique to transverse to oblique from the exterior to the interior of the secondary layer (central part, ventral valve, longitudinal section). Ext: external, Int: internal.

We used an array of methods to describe the microstructure of the fibres of the secondary layer. Fibre morphology was measured in sections cut perpendicular to the fibre axis at different positions of the same shell, while considering that brachiopod shells grow from the umbo (posterior) to the anterior margin and from the exterior to the interior (Fig. 4). We also considered that the secondary layer is constructed in sublayers characterized by different orientations of the morphological axis of the fibres (cf. Schmahl et al., 2004, 2008; Griesshaber et al., 2007, 2008, 2010; Goetz et al., 2011). Orientation of the fibres is complex in the posterior part of the shell, ranging from parallel to oblique and perpendicular to the growth vector, producing many sublayers (Plates 3–5 in Ye et al., 2018, Appendix 1), but with fewer sublayers in their central and anterior regions. Specifically, *L. neozelanica* and *G. vitreus* have thin secondary and thick tertiary columnar layers, and the fibre axis in the most external and most internal sublayers is oriented obliquely to parallel to the growth vector (Griesshaber et al., 2008, 2010).

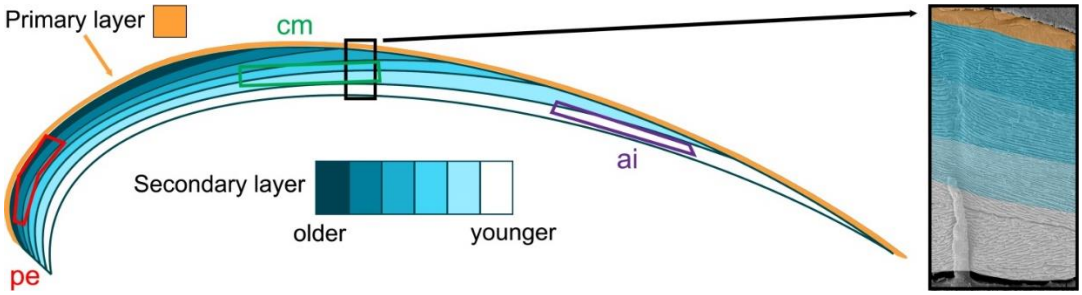

Fig. 4. Fibres were described and measured in different positions of the same shell: posterior, central and anterior from the umbo to the anterior margin and external, middle and internal along a vertical section through the secondary layer, following the direction of incremental growth of the shell. pe: posterior external; cm: central middle; ai: anterior internal (modified from Penman et al., 2013).

3.3 Methods

We used Scanning electron microscope (SEM), Electron backscatter diffraction (EBSD), and Transmission electron microscope (TEM) to measure and evaluate size and shape of the structural units (fibres) within brachiopod shells, conducted data reliability analysis, and constructed a database for statistical analyses.

3.3.1 Sample preparation

We followed the preparation method suggested by Crippa et al. (2016b) for SEM analysis of specimens. Summarized here briefly, the specimens were embedded in epoxy resin, cut along the longitudinal axis, and immersed in 36 vol hydrogen peroxide (H_2O_2) for 24 h to remove organic matter. Sectioned surfaces were smoothed with silicon carbide powder (SiC), etched with 5% hydrochloric acid (HCl) for 3 s, and then rinsed in deionised water and dried. Then, they were gold-coated and observed by a Cambridge S-360 scanning electron microscope with a lanthanum hexaboride (LaB_6) source and operating at an acceleration voltage of 20 kV (Dipartimento di Scienze della Terra "A Desio", University of Milan).

Electron Backscatter Diffraction (EBSD) measurements were performed on shells embedded in epoxy resin. The surface of the embedded specimen was subjected to several sequential mechanical grinding and polishing steps down to a grain size of 1 μm. The final step consisted of etch-polishing with colloidal alumina (particle size ~0.06 μm) in a vibratory polisher. For measurements, the samples were coated with 4–6 nm of carbon. EBSD measurements were carried out on a Hitachi SU5000 field emission SEM, equipped with a Nordlys II EBSD detector and AZTec acquisition software. The EBSD SEM was operated at 15 and 20 kV and measurements were indexed with the CHANNEL 5 HKL software (Schmidt and Olesen, 1989; Randle and Engler, 2000).

Information obtained from EBSD measurements is presented as band contrast images, and the grey scale gives the signal strength of the EBSD-Kikuchi diffraction pattern. The strength of the EBSD signal is high when a mineral is detected (bright), whereas it is weak or absent when the polymer is scanned (dark/black).

TEM mounts were prepared from epoxy embedded samples. In the first step, doubly polished petrographic thin sections (30 μm thick) were obtained by mechanical thinning. Electron transparency was then achieved by ion milling 3 mm wide discs cut out from the petrographic thin sections using a

Gatan Precision Ion Polyshing System (PIPS) (Dipartimento di Scienze della Terra "A. Desio" of Milan). TEM mounts were finally carbon coated to avoid electrostatic charging. TEM observations were performed with a Jeol JEM 2010 operating at 200 kV and equipped with an Oxford Link energy dispersive spectrometer (EDS) and with an Olympus Tengra 2.3 k × 2.3 k × 14 bit slow-scan CCD camera (Dipartimento di Scienze Fisiche, della Terra e dell'Ambiente of the University of Siena).

3.3.2 Morphometric analysis

Based on SEM micrographs of the secondary layer, fibres with regular and symmetrical cross sectional outlines were chosen for morphometric measurement. It was assumed that fibres with a symmetric outline were cut perpendicular to the plane of symmetry of the fibres (Fig. 5A). For a single fibre, symmetric profiles (section perpendicular to the fibre axis) lead to smaller/narrower values (e.g., of area, perimeter, width) than asymmetric ones (Fig. 5C and D). However, even if cut perpendicular to the morphological axis of the fibres, small tilting of the section would result in a slightly larger area or perimeter (Fig. 5B), so that the most reliable measurement was their width (= Max Feret diameter, as defined below), which did not change once the profile was deemed to be symmetrical (Fig. 5A and B).
Initially, fibres were manually outlined using Adobe Photoshop CS6, and 16 parameters were measured by Image-Pro Plus 6.0 and ImageJ (Fig. 6). Since some parameters have similar characteristics and are highly correlated, only six parameters, such as Max Feret diameter, Min Feret diameter, Area, Perimeter, Convex Area and Convex Perimeter, were measured for our morphometric analysis of fibres in brachiopods (Fig. 6; Table 2; Głąb et al., 2015; Russ and Neal, 2015). Parameter definitions were modified from those available in Image-Pro Plus and ImageJ. We decided to use the measurements of Max Feret diameter and Min Feret diameter, which represent the caliper (feret) length, instead of Max and Min diameters because, in Image-Pro Plus 6.0, the diameter passes through the centroid of the object, so it was not a suitable descriptor of the shape of the fibres. Instead, the Max Feret diameter corresponds roughly to the width of an individual fibre, whereas the Min Feret diameter corresponds to its height (Fig. 6).

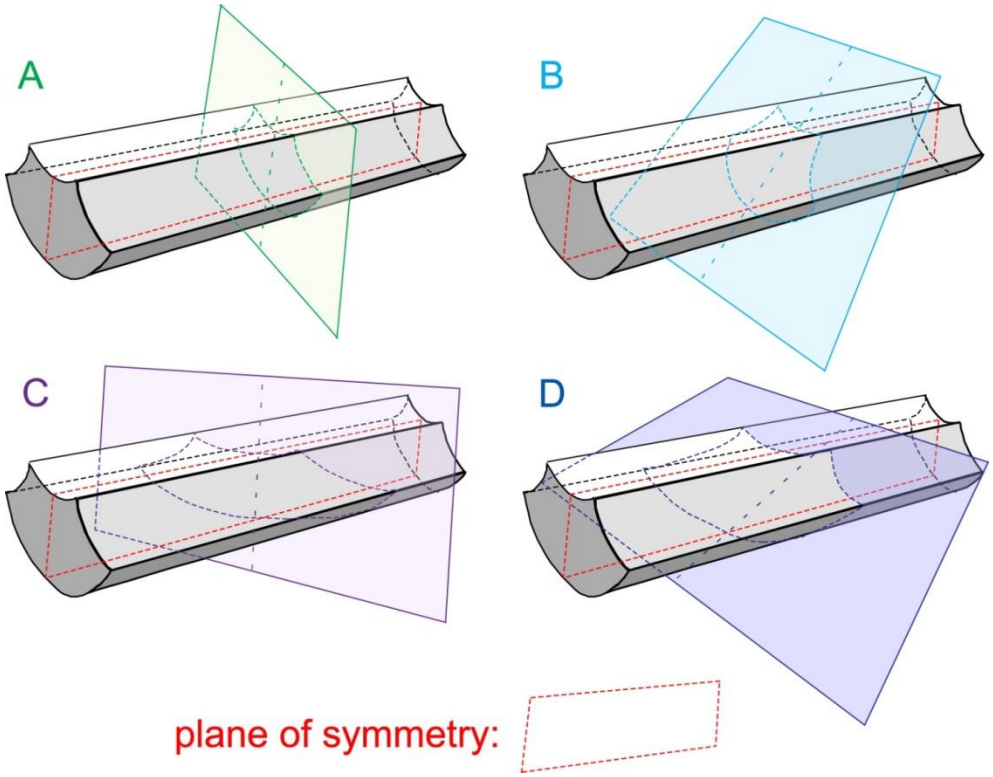

Fig. 5. Sections of fibres along different planes. A, section perpendicular to the plane of symmetry of the fibre; B, section perpendicular to the longitudinal axis of the fibre and tilted with respect to the plane of symmetry; C, section intersects obliquely the plane of symmetry; D, section is oblique and tilted with respect to the plane of symmetry.

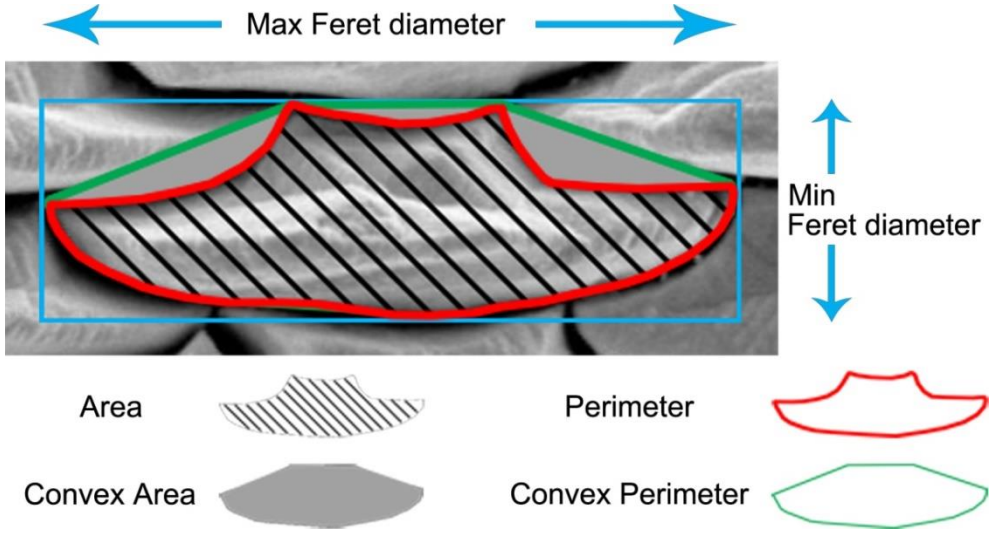

Fig. 6. Morphometric parameters used to define the size and shape of each fibre.

Table 2. Definitions of the six morphometric parameters used on the fibres of this study.

Parameters	Definitions
Max Feret diameter	Longest caliper length
Min Feret diameter	Smallest caliper length
Area	Area of the object
Perimeter	Length of the object's outline
Convex area	The area enclosed by the convex hull of the outer contour of the object
Convex perimeter	The perimeter of the convex hull of the object.

Furthermore, five shape descriptors were calculated, such as Formfactor (circularity, $4\pi \times \text{Area/Perimeter}^2$), Roundness ($4\text{Area}/\pi \times \text{Max Feret diameter}^2$), Aspect Ratio (Max Feret diameter/Min Feret diameter), Convexity (Convex Perimeter/Perimeter), and Solidity (Area/Convex Area) with the six selected and measured parameters (Russ and Neal, 2015; Ye et al., 2018, Appendix 1).

3.3.3 Data reliability analysis

To test the reliability of the visual selection process of symmetric fibres, two groups of data were compared using a geometric morphometric approach. Group 1 comprises 30 randomly selected fibres, that visually are considered symmetric, and Group 2 comprises both symmetric and asymmetric fibres (Table 3).

Table 3. Procrustes ANOVA analysis of two groups of fibres. Group 1 comprises fibres judged to be symmetric. Group 2 comprises both symmetric and asymmetric fibres. Sums of squares (SS); mean squares (MS); Fluctuating asymmetry (ind:side) is used as error effect; P: *p*-values associated with the F distribution (after 999 permutations); side: side of each fibre representing the asymmetric component; Df: degrees of freedom.

Group 1	Df	SS	MS	F	Z-score	P (999 permutation)
individuals	29	0.31945	0.0110154	69.729	0.85173	0.830
side	1	0.00064	0.0006380	0.4039	0.31761	0.846
ind:side	29	0.04581	0.0015798			
Group 2	Df	SS	MS	F	Z-score	P (999 permutation)
individuals	39	0.41058	0.0105277	49.055	0.7872	0.936
side	1	0.01301	0.0130053	60.600	37.349	0.008
ind:side	39	0.08370	0.0021461			

In cross section, 4 landmarks and 16 semi-landmarks were digitized for each fibre, following the scheme depicted in Fig. 7. The landmarks and semi-landmarks were digitized using TPSDIG 2.1. Following the procedure suggested by Mardia et al. (2000) and Klingenberg et al. (2002), pairs of landmarks were established based on geometric rules (Fig. 7). We partitioned the total shape of outlines between symmetric and asymmetric variants among fibres. Applying a two-factor ANOVA, we tested the effects of two sources of variability on the overall outline variation for the two datasets.

To perform the analyses we used the *bilat.symmetry* function, implemented in the package *geomorph* (Adams and Otarola-Castillo, 2013) for R 3.3.0 (R Core Team, 2016). Before starting the analysis of symmetry, semi-landmarks were aligned using the minimum bending energy criterion and a General Procrustes analysis to remove the effect of rotation, translation and size. Subsequently, the components of shape variation were decoupled among individuals, sides (directional asymmetry) and variation due to interaction among individual and side (fluctuating symmetry). Procrustes ANOVA was performed

to assess the significance of each component in the two datasets (for further details see Klingenberg et al., 2002).

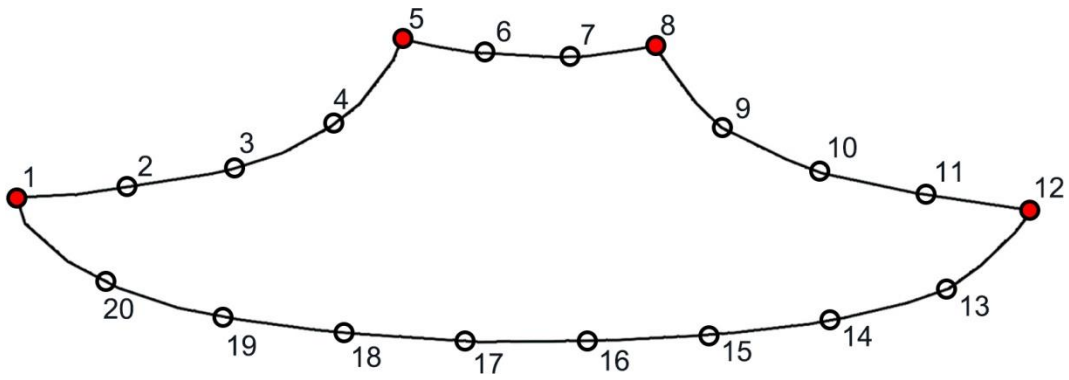

Fig. 7. Four landmarks (red circles) and sixteen semilandmarks (open circles) digitized for each fibre. The semi-landmarks (2 to 4, 6 to 7, 9 to 11, and 13 to 20) are evenly distributed between the 4 landmarks (1, 5, 8 and 12). The marks (1 and 12, 2 and 11, 3 and 10, 4 and 9, 5 and 8, 6 and 7, 17 and 16, 18 and 15, 19 and 14, 20 and 13) are set as pairs based on the hypothetical axis of bilateral symmetry.

To work out the reliability of the measurements, the most significant parameters (Area, Perimeter, Max Feret diameter, Convex Area) were tested in Excel for their probability density (cf. Duller, 2008). The assumption of normality was tested through the shapes of data distributions and the frequency distribution within the data range. Independent-sample *t*-tests were performed using SPSS Statistics (IBM Version 22.0. Armonk, NY). A p-value $\leq .05$ is considered significant and a p-value $\leq .001$ is considered highly significant.

3.4 Results

3.4.1 Data reliability and statistical analyses

For Group 1 results, the Procrustes ANOVA shows that among fibres the symmetric and asymmetric variations have similar *p*-values (.83–.85), which are not significantly different. For Group 2 results, the asymmetric component (Side) of the fibres shows a significant *p*-value (.008). Thus, in the selected fibre set, shape variability is not affected by asymmetry. In contrast, the second dataset is significantly affected by asymmetry, confirming that the visual selection process is reliable in distinguishing between types of fibres.

Six parameters: Area, Perimeter, Max Feret diameter, Min Feret diameter, Convex Perimeter, Convex Area – involving 1197 fibre measurements – were tested by Excel for their probability distribution (Figs. 1–3 in Ye et al., 2018, Appendix 1). The results show that the Max Feret diameter is the most reliable morphometric measure – supporting the assumption of the morphometric analysis (paragraph 3.2) – and Roundness and Convexity are the best morphometric descriptors of shape variation (Fig. 8).

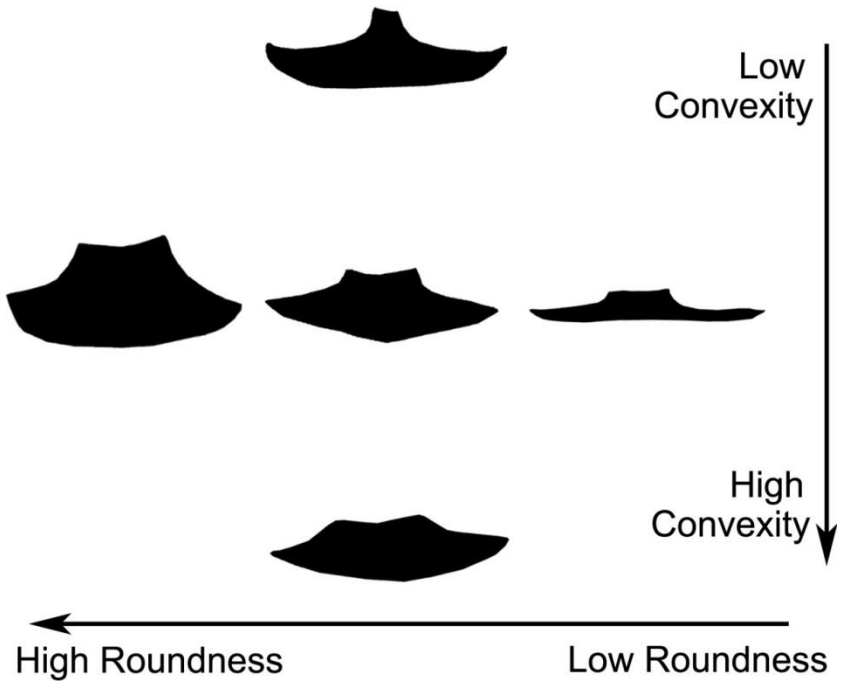

Fig. 8. Graphic visualization of the change in Roundness and Convexity of the fibres.

3.4.2 Shape and size of fibres: Dorsal vs ventral valves

For comparison of shape and size, we made 1197 measurements on six recent brachiopod species, representing 581 measurements on fibres from ventral valves and 616 measurements on fibres from dorsal valves (Table 4). In the *t*-test results for all six species, the *p*-values between dorsal and ventral fibres of Max Feret diameter (.116), Roundness (.470) and Convexity (.869) are greater than .05 and so reveal no statistically significant difference between them. The *p*-values for difference relative to Area (.019) and Perimeter (.049) are significant ($p \leq .05$), but this may be related to the fact that the distribution curves are skewed (Figs. 1–3 in Ye et al., 2018, Appendix 1). This is also evident when comparing fibres from corresponding positions in both valves measured in the anterior internal part of the dorsal valve with those measured in the anterior internal part of the ventral valve ($p > .05$). Overall, there is no significant difference in the size and shape of fibres between ventral and dorsal valves.

C. inconspicua and *G. vitreus* show a highly significant difference in Max Feret diameter ($p \leq .001$) and a significant difference in Roundness ($p \leq .05$) between dorsal and ventral valves. *L. uva* exhibits a significant difference ($p \leq .05$) in size and Roundness. *L. neozelanica* and *N. nigricans* have significant and highly significant differences only in the Roundness of the fibres of the two valves, respectively, whereas the other species show no significant difference in these morphometric parameters between the two valves.

Table 4
Average values and standard deviations (in parenthesis) of Area (µm2), Perimeter (µm), Max Feret diameter (µm), Roundness and Convexity of the fibres of ventral (V) and dorsal (D) valves. Results in bold are *p* values ranging from 0.05 to 0.001, and gray font background are *p*-values of < .001 (for more details see Ye et al., 2018).

Valve type	Number of measurements	Area	Perimeter	Max Feret diameter	Roundness	Convexity
V - *Liothyrella uva*	128	24.88 (7.95)	**24.89 (5.33)**	**10.87 (2.61)**	**0.279 (0.076)**	0.973 (0.012)
D - *Liothyrella uva*	102	26.89 (12.26)	**26.51 (6.74)**	**11.84 (3.33)**	**0.252 (0.074)**	0.975 (0.012)
V - *Gryphus vitreus*	93	*26.34 (7.33)*	*27.65 (4.41)*	*12.65 (2.26)*	0.217 (0.070)	**0.982 (0.009)**
D - *Gryphus vitreus*	184	*19.72 (6.91)*	*23.95 (5.81)*	*10.92 (2.98)*	0.226 (0.076)	**0.979 (0.010)**
V - *Liothyrella neozelanica*	134	25.04 (8.30)	26.59 (4.90)	12.07 (2.47)	**0.231 (0.083)**	0.981 (0.008)
D - *Liothyrella neozelanica*	147	24.04 (6.90)	27.28 (5.95)	12.57 (3.03)	**0.208 (0.071)**	0.982 (0.007)
V - *Calloria inconspicua*	40	**19.96 (5.08)**	**25.41 (4.40)**	**11.50 (2.24)**	**0.198 (0.046)**	0.970 (0.011)
D - *Calloria inconspicua*	30	**16.81 (5.38)**	**21.64 (4.34)**	**9.65 (2.28)**	**0.245 (0.086)**	0.973 (0.010)
V - *Magasella sanguinea*	81	29.08 (10.83)	26.65 (6.43)	11.88 (3.31)	0.279 (0.098)	0.981 (0.007)
D - *Magasella sanguinea*	54	27.67 (11.45)	25.71 (6.38)	11.46 (3.15)	0.279 (0.092)	0.981 (0.008)
V - *Notosaria nigricans*	105	35.06 (15.89)	32.53 (9.94)	15.01 (4.96)	*0.212 (0.071)*	0.982 (0.010)
D - *Notosaria nigricans*	99	39.44 (16.19)	32.45 (9.64)	14.61 (4.88)	*0.258 (0.097)*	0.980 (0.009)
Ventral - all 6 species	581	**27.29 (10.90)**	**27.42 (6.85)**	12.38 (3.47)	0.240 (0.083)	0.979 (0.011)
Dorsal - all 6 species	616	**25.66 (12.28)**	**26.78 (7.37)**	12.04 (3.66)	0.237 (0.083)	0.979 (0.010)

3.4.3 Shape and size of fibres: Ontogenetic variation

Fibres were measured at specific locations in the shell along its growth axis (Fig. 4), allowing us to check if there is an ontogenetic trend in the size and shape of the fibres. Overall, when we compare morphology and size of fibres along the growth direction from the posterior external part to the anterior internal part of each valve, the fibres become progressively larger, wider, less round (lower Roundness), and flatter (higher Aspect ratio) with age (Fig. 9; Table 5). In addition, fibres of the ventral valves become also less convex with increasing age. Significant to highly significant ($p \leq .05$ and $p \leq .001$) differences in the Perimeter, Max Feret diameter, Roundness and Convexity of the fibres from the different regions of the shell were observed along the growth transect in the dorsal valve of all species. Overall, measurements of fibres from the mid-section (vcm and dcm) of the shells (dorsal and ventral) are most consistent for Max Feret diameter and Roundness (Table 5).

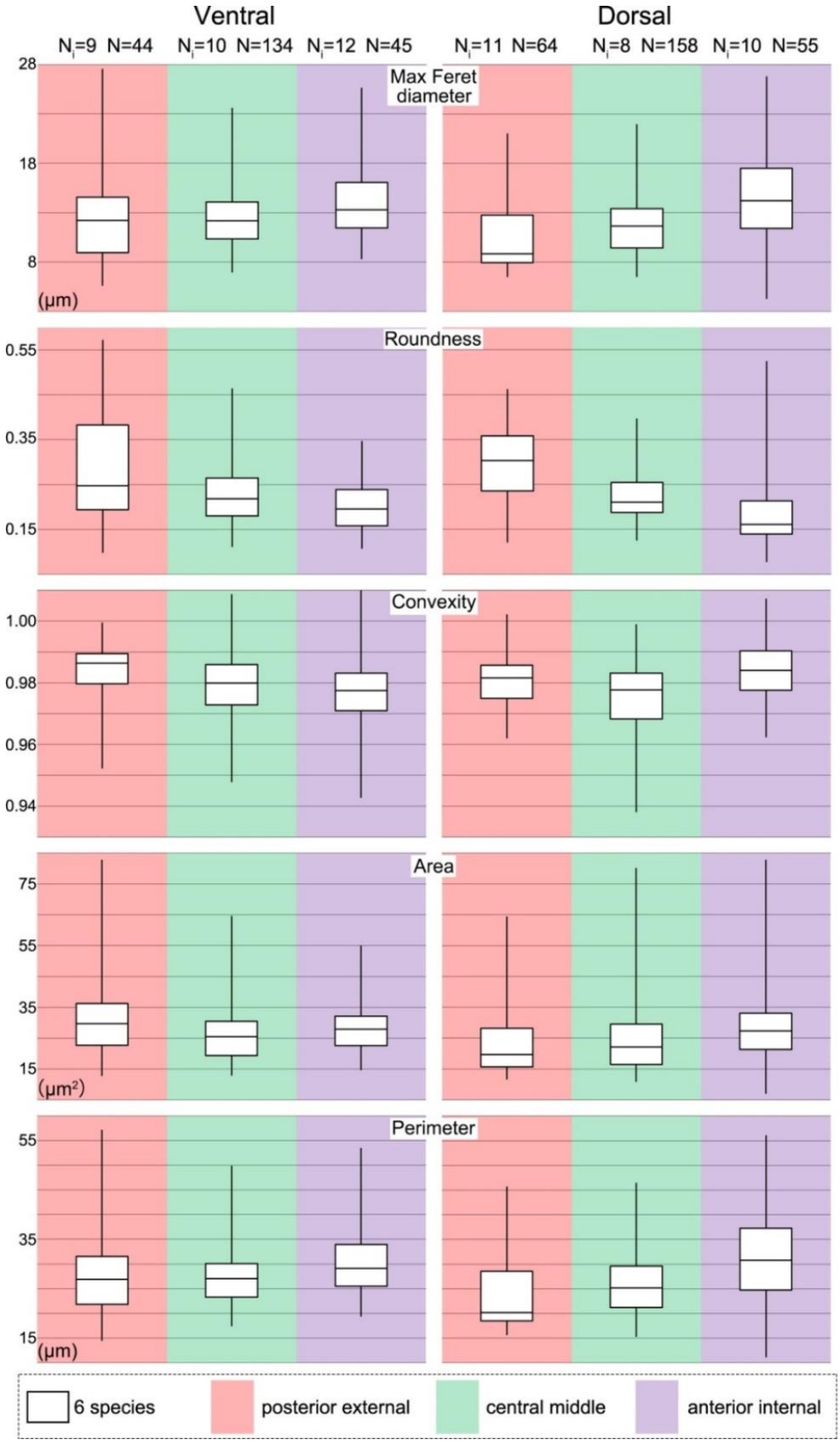

Fig. 9. Box plots showing the difference in fibre sizes and shapes of all six species at different ontogenetic stages. The bottom/top of the box and the band inside the box are the first/third quartiles and the median of the data respectively; ends of the whiskers represent the minimum and maximum of results. Ni: number of individuals; N: number of measurements.

Table 5. Measurements of the structural units (fibres) in different shell positions (v: ventral, d: dorsal; pe: posterior external, cm: central middle; ai: anterior interior). Average values and standard deviations (in parentheses) of the data for Area, Perimeter, Max Feret diameter, Roundness and Convexity. LU: *L. uva*; GV: *G. vitreus*; LN: *L. neozelanica*; NN: *N. nigricans*.

Valve and position	Number of measurements	Area	Perimeter	Max Feret diameter	Roundness	Convexity
LUvpe	11	25.02 (10.19)	23.21 (7.27)	9.97 (3.63)	0.357 (0.125)	0.979 (0.013)
LUvcm	36	22.23 (6.78)	24.58 (4.56)	10.75 (2.23)	0.249 (0.052)	0.968 (0.010)
LUvai	13	24.74 (7.39)	26.15 (5.07)	11.66 (2.41)	0.236 (0.048)	0.973 (0.010)
LUdpe	13	20.10 (3.49)	20.19 (2.35)	8.63 (1.28)	0.353 (0.073)	0.980 (0.012)
LUdcm	35	32.85 (16.42)	29.93 (7.24)	13.45 (3.60)	0.229 (0.052)	0.972 (0.013)
LUdai	7	24.86 (10.89)	26.36 (8.12)	11.99 (3.73)	0.221 (0.043)	0.980 (0.010)
GVvpe	13	34.15 (6.07)	30.06 (4.13)	13.71 (2.36)	0.249 (0.096)	0.990 (0.005)
GVvcm	22	24.37 (5.76)	27.09 (3.47)	12.45 (1.69)	0.202 (0.039)	0.979 (0.007)
GVvai	4	26.09 (3.37)	28.55 (2.79)	13.27 (1.28)	0.192 (0.037)	0.987 (0.006)
GVdpe	16	16.25 (2.79)	18.35 (1.39)	7.91 (0.74)	0.335 (0.064)	0.980 (0.006)
GVdcm	40	16.70 (3.30)	22.16 (2.79)	9.98 (1.46)	0.219 (0.049)	0.972 (0.012)
GVdai	12	31.65 (9.80)	34.32 (6.46)	16.40 (3.16)	0.150 (0.026)	0.992 (0.007)
LNvpe	9	25.04 (7.15)	23.39 (3.49)	10.15 (1.80)	0.320 (0.094)	0.980 (0.008)
LNvcm	25	23.64 (11.35)	27.00 (4.82)	12.44 (2.18)	0.194 (0.058)	0.982 (0.009)
LNvai	14	28.20 (5.56)	29.50 (4.33)	13.52 (2.26)	0.203 (0.048)	0.977 (0.007)
LNdpe	23	23.95 (9.66)	25.64 (8.23)	11.72 (4.18)	0.248 (0.086)	0.982 (0.006)
LNdcm	27	24.37 (6.34)	27.94 (5.18)	12.96 (2.53)	0.189 (0.039)	0.982 (0.006)
LNdai	24	25.91 (7.01)	30.44 (5.39)	14.19 (2.76)	0.175 (0.065)	0.982 (0.008)
NNvpe	6	55.75 (21.18)	44.74 (13.35)	21.00 (6.90)	0.181 (0.083)	0.987 (0.008)
NNvcm	22	31.50 (7.46)	30.98 (6.47)	14.35 (3.21)	0.203 (0.045)	0.985 (0.008)
NNvai	9	34.93 (12.51)	36.08 (8.91)	16.80 (4.43)	0.162 (0.045)	0.979 (0.020)
NNdpe	9	46.87 (15.32)	34.64 (6.33)	15.43 (3.11)	0.254 (0.075)	0.974 (0.009)
NNdcm	17	35.87 (11.16)	31.31 (5.40)	14.18 (2.58)	0.226 (0.035)	0.979 (0.009)
NNdai	9	43.51 (20.32)	38.23 (11.86)	17.83 (5.91)	0.189 (0.081)	0.982 (0.006)
vpe	44	31.79 (14.46)	28.22 (9.69)	12.63 (5.01)	0.292 (0.125)	0.984 (0.010)
vcm	134	26.66 (9.86)	27.44 (5.92)	12.44 (2.98)	0.227 (0.065)	0.979 (0.011)
vai	45	28.89 (9.04)	30.21 (6.71)	13.83 (3.39)	0.201 (0.052)	0.977 (0.012)
dpe	64	24.80 (12.77)	23.89 (7.67)	10.58 (3.77)	0.299 (0.089)	0.980 (0.008)
dcm	158	25.08 (12.13)	26.41 (6.41)	11.97 (3.13)	0.223 (0.056)	0.976 (0.011)
dai	43	28.22 (14.32)	30.39 (9.17)	14.10 (4.52)	0.184 (0.076)	0.984 (0.009)

The Max Feret diameter of fibres from the posterior to the anterior increased by 11% in the ventral and by 33% in the dorsal valves, and the average decrease in Roundness of the anterior internal fibres is 31% in the ventral and 39% in the dorsal valves (Table 5).

The fibres of the dorsal valve of *G. vitreus* show a highly significant change in size and shape with age, whereas those of *L. neozelanica* show a significant difference in Max Feret diameter and Roundness. In contrast, the *t*-test of the overall ventral valve data show a significant difference ($p \leq .05$) only for the Roundness and Convexity of the fibres. This result may be affected by the unusual fibre distribution in *G. vitreus* and *N. nigricans*, where they are variable in size from the posterior external part of the ventral valve. Also, posteriorly, fibres are larger than those of the central middle part and anterior internal part (Table 5), but this difference is not significant ($p > .05$). At the species level, *L. neozelanica* shows a highly significant change in fibre Perimeter, Max Feret diameter and Roundness with age.

3.4.4 Shape and size of fibres: Two-layer vs three-layer shells

The size and shape of the fibres were compared in species with different shell layer sequences, such as those with two layers (Group 1: *L. uva*, *C. inconspicua*, *M. sanguinea* and *N. nigricans*) to those with three layers (Group 2: *G. vitreus* and *L. neozelanica*) (Fig. 10). The differences in size and shape are significant to highly significant ($p \leq .05$ and $p \leq .001$) for the dorsal valve fibres of the two groups. Fibres in the three-layer brachiopods are less round and larger in the anterior internal part, but smaller in the central middle and posterior external parts with respect to those of the two-layer shells (Fig. 10). In the ventral valve, the differences in Area, Roundness and Convexity are highly significant between the two groups ($p \leq .001$); however the differences in Area should be considered with caution as they may be affected by the orientation of the section (see Fig. 5). In the central middle part of the shell, the fibres of the three-layer brachiopods are less round and more convex. Size and shape of fibres in the three-layer brachiopods are always significant to highly significantly different in the dorsal valves, but not in the ventral valves, except for the posterior external part ($p < .05$) (Table 5).

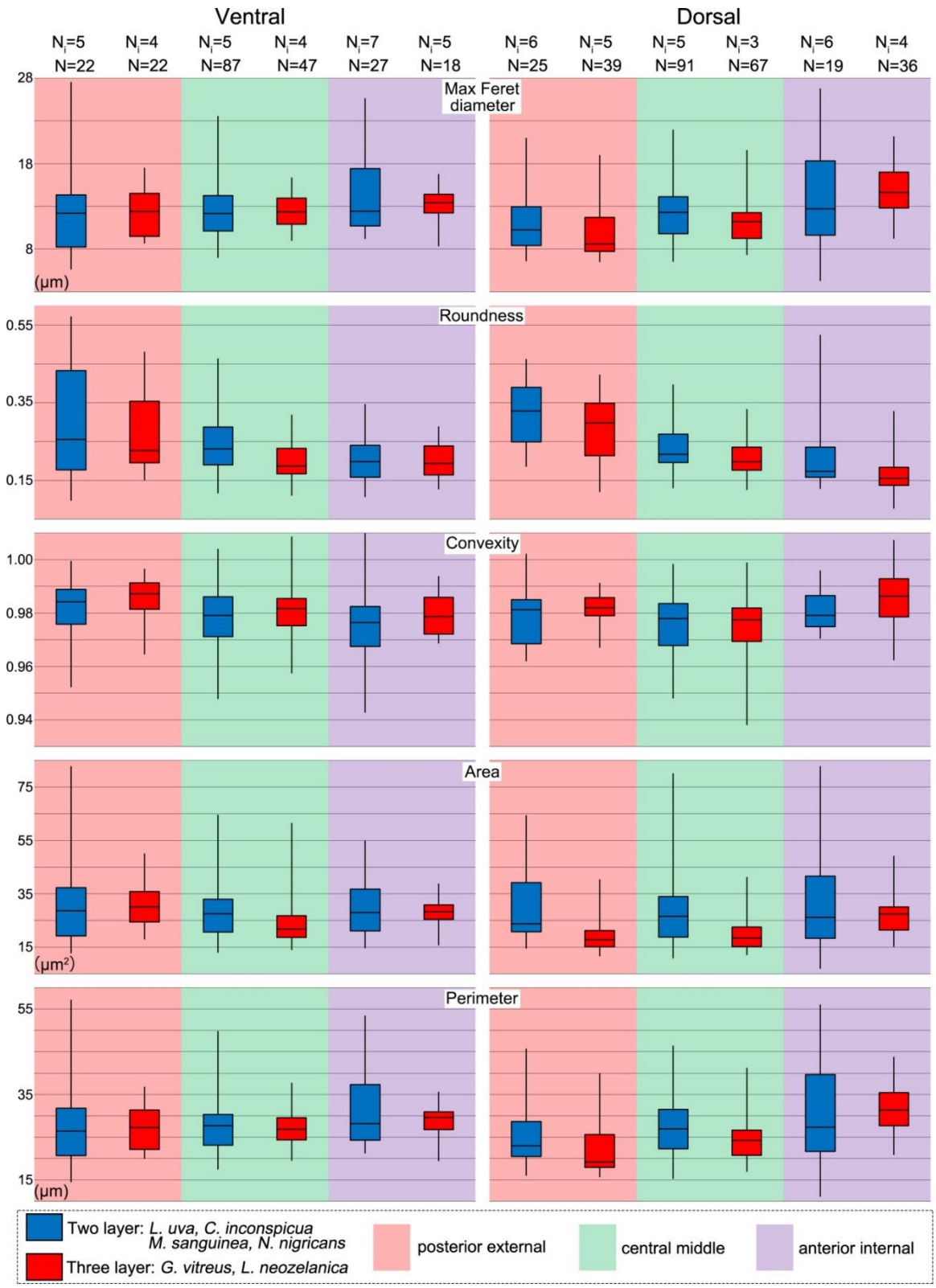

Fig. 10. Box plots showing the difference in fibre sizes and shapes of species with two-layer shells (*L. uva*, *C. inconspicua*, *M. sanguinea* and *N. nigricans*) and species with three-layer shells (*L. neozelanica* and *G. vitreus*) in different parts of the ventral and dorsal valves. The bottom/top of the box and the band inside the box are the first/third quartiles and the median of the data respectively; ends of the whiskers represent the minimum and maximum of the data. Ni: number of individuals; N: number of measurements.

EBSD band contrast images show a striking difference in fibre dimension and morphology between the three-layer shells of *G. vitreus* and *L. neozelanica*. Fibres in cross-section are large and rounded in *L. neozelanica*, whereas they are highly elongated and flat in *G. vitreus* (Fig. 11). The microstructure of *G. vitreus* is dominated by a thick columnar layer, whereas in *L. neozelanica* not only is the columnar layer thinner, but it also shows frequent intercalation with the fibrous layer.

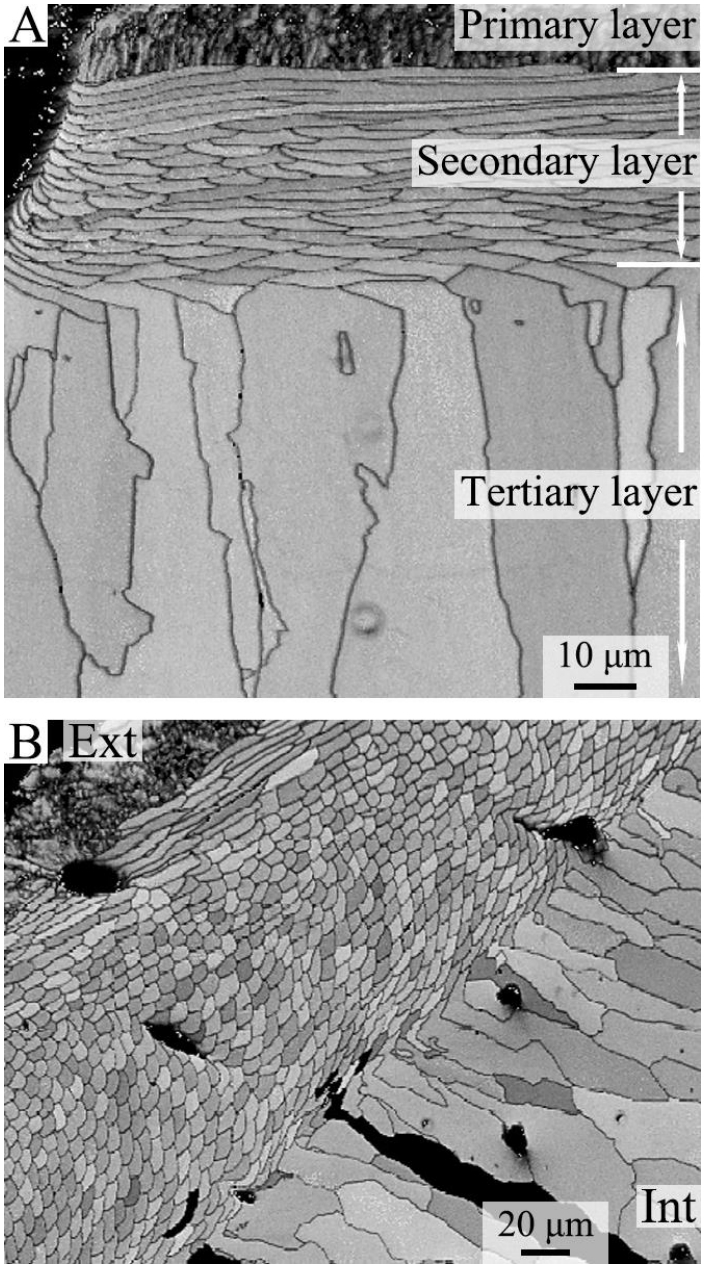

Fig. 11. EBSD band contrast images visualizing the difference in microstructure of the studied three-layer shell specimens. A, *G. vitreus*; B, *L. neozelanica*. Ext: external, Int: internal.

Comparing species with different shell layer sequences (two-layer: *N. nigricans*, *C. inconspicua*, *M. sanguinea*; three-layer: *L. neozelanica*) from the same locality (Doubtful Sound, New Zealand), the size of the ventral fibres and the Area, Roundness, and Convexity of the dorsal fibres are significant to highly significantly different ($p \leq .05$ and $p \leq .001$). Overall, the fibres of two-layer brachiopods are larger than of their three-layer counterparts.

3.4.5 Shape and size of fibres: Environment

To estimate fibre variation among different localities, we compared the New Zealand fauna (NZ) against the Mediterranean (Med) and the Antarctica ones (Ant). However, to exclude effects related to different shell sequence (see paragraph 4.4) we treated the three-layer shell of *L. neozelanica* from New Zealand as a separate unit (LN) (Fig. 12; Table 4). The three-layer brachiopod *G. vitreus* represents the Mediterranean environment. The New Zealand and Mediterranean localities are characterized by different water depths, and salinity, but similar temperatures and hydrodynamic energy (Table 1), with the first recessed into a fjord whereas the second is in relatively deep water. The Antarctic localities stand out by their lower seawater temperatures and lower carbonate saturation state (Watson et al., 2012; Takahashi et al., 2014).

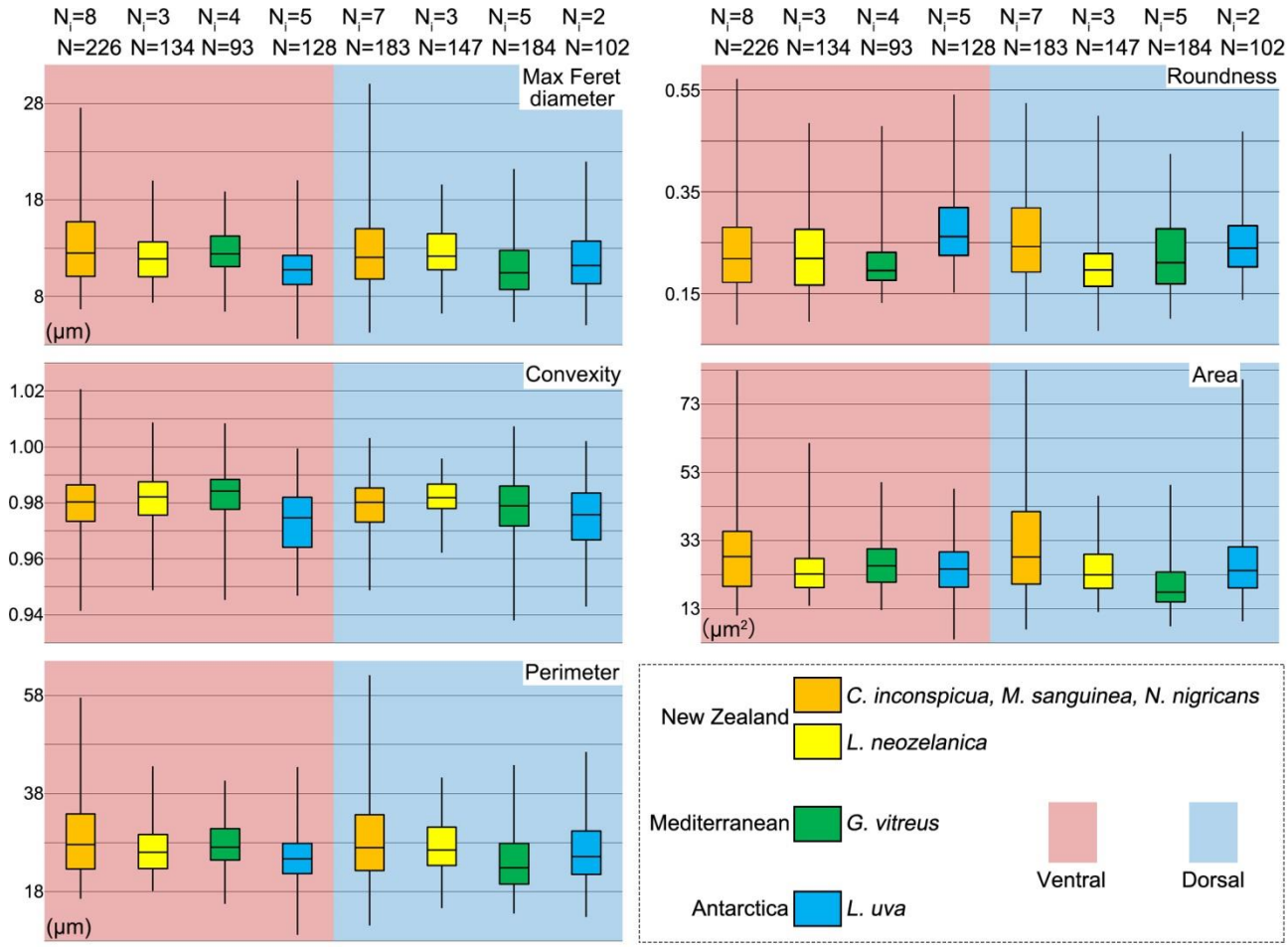

Fig. 12. Box plots showing the differences in fibre sizes and shapes among species with two-layer shells from New Zealand (*C. inconspicua*, *M. sanguinea* and *N. nigricans*), three-layer shells from New Zealand (*L. neozelanica*), three-layer shells from the Mediterranean (*G. vitreus*), and two-layer shells from Antarctica (*L. uva*), of their ventral and dorsal valves. The bottom/top of the box and the band inside the box are the first/third quartiles and the median of the data respectively; ends of the whiskers represent the minimum and maximum of the results. Ni: number of individuals; N: number of measurements.

L. uva from Antarctica differs from the other brachiopods from New Zealand and the Mediterranean by its smaller-sized, lower Convexity and higher Roundness fibres (Fig. 12). These differences are always significant to highly significant ($p \leq .05$ and $p \leq .001$) in the ventral valve. The differences in Max Feret diameter of the dorsal fibres between *L. uva* and *L. neozelanica* are not significant ($p > .05$).

Comparing the Mediterranean and New Zealand species, there is a significant difference in the Area, Perimeter and Convexity of the fibres of the ventral valves (p = .001 in Area, p = .039 in Perimeter; p = .033 in Convexity); the largest fibres are those of the New Zealand two-layer species, the smallest are those of the three-layer brachiopod *L. neozelanica* (Fig. 12). In the dorsal valve, the differences are significant to highly significant for nearly all morphometric parameters ($p \leq .05$ and $p \leq .001$) and the largest fibres are those in the New Zealand species (Fig. 12).

3.4.6 Shape and size of fibres: The *Liothyrella* species case

We analysed two species of the same genus living in different environmental conditions, to check for interspecific variability and environmental control on the size and shape of the fibres. Overall, fibres at the same ontogenetic stage of the two species are smaller, narrower, rounder, less flat and less convex in *L. uva* than those in *L. neozelanica* (Fig. 13; Table 5). However, in the central middle part of the dorsal valve only, the fibres of *L. uva* are larger in Area and have a higher Max Feret diameter than those in *L. neozelanica*. The size and shape of the fibres are highly significantly different in the ventral valves of the two species ($p \leq .001$ in Max Feret diameter, Roundness and Convexity); in the dorsal valves only the shape is highly significantly different ($p \leq .001$ in Roundness and Convexity).

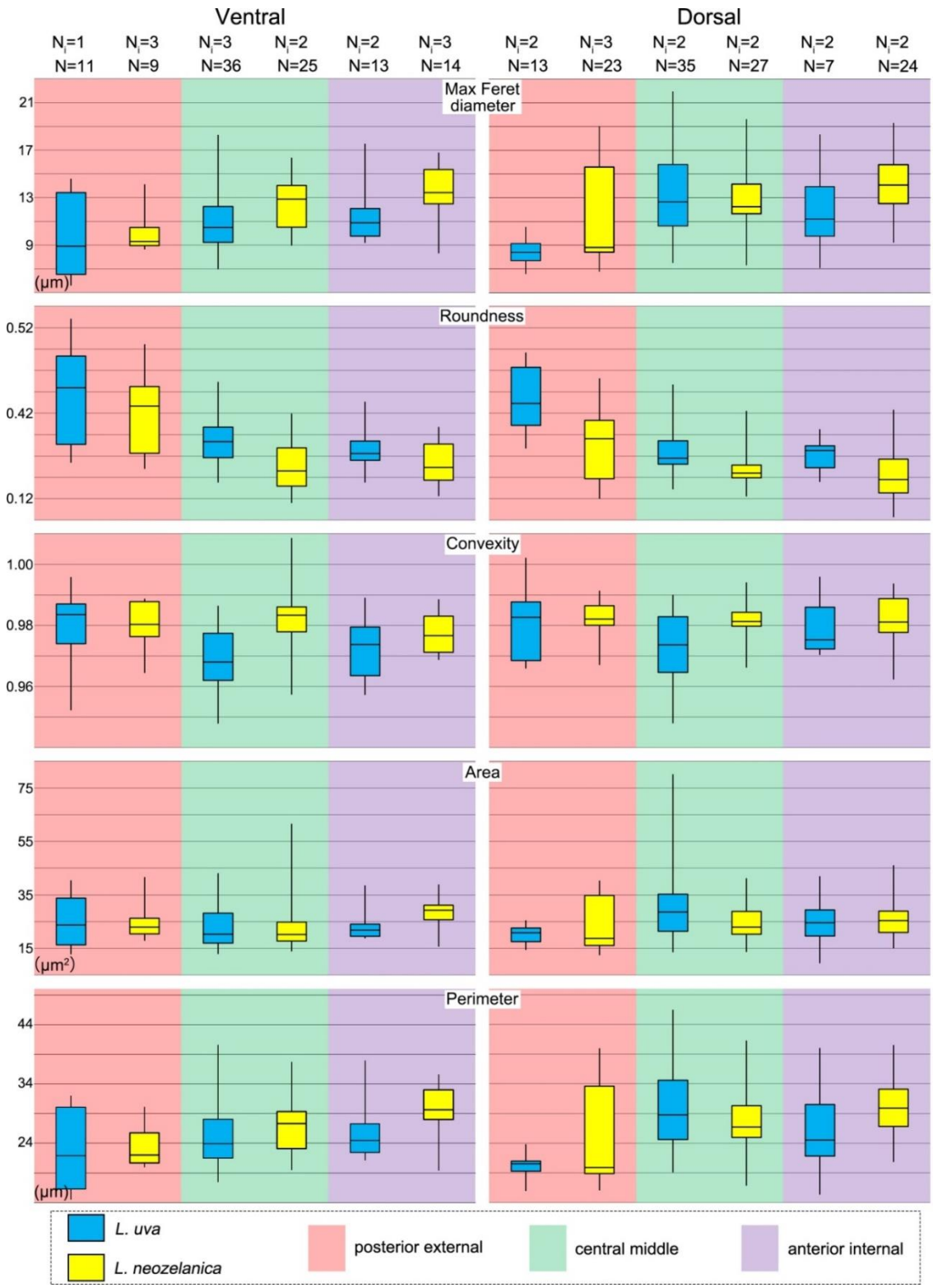

Fig. 13. Box plots showing the difference in fibre sizes and shapes of *L. uva* (blue) and *L. neozelanica* (yellow). The bottom/top of the box and the band inside the box are the first/third quartiles and the median of the data respectively; ends of the whiskers represent the minimum and maximum of the data. Ni: number of individuals; N: number of measurements.

EBSD band contrast images show that the shell of *L. uva* is formed of smaller fibres compared to the other brachiopod species.

To investigate the nanostructure of the two species at a finer scale, TEM observations were undertaken on the primary and secondary layers of *L. uva* and on secondary and tertiary layers of *L. neozelanica* (Figs. 14–16). The two species show similar secondary layer. Fibres in transverse section (Fig. 14A) appear as single crystals (Fig. 14B), are several micrometres long and 3–5 μm thick, with the c-axis approximately in the plane of the section and parallel to the shortest dimension. The most eye-catching feature is the large amount of round inclusions with dimensions up to a few hundred nanometres, containing amorphous material and in some cases a solid crystalline precipitate (Fig. 14C), locally forming ribbons (Fig. 14D) that are interconnected by dislocations (Fig. 14E). Compositional profiles of the inclusions show that they are enriched in either S or Si, with respect to the host calcite (Fig. 15). The single crystalline nature of fibres, the crystallographic c-axis orientation with respect to the external surface of the valve and to the morphology of the fibre are consistent with the results of Goetz et al. (2009).

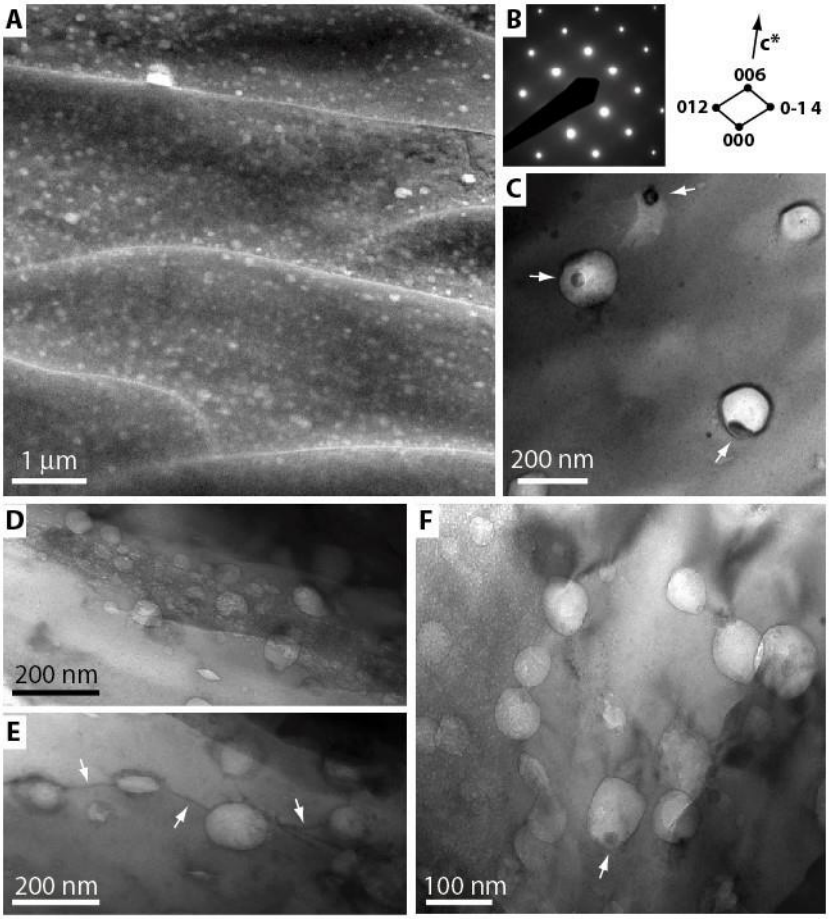

Fig. 14. TEM images of the secondary layer of *L. neozelanica* (A-E) and *L. uva* (F). A, low magnification image showing fibres in cross-section embedding numerous inclusions (brighter areas); B, diffraction pattern with spot indexing (right) showing the c-axis orientation with respect to the fibre section (beam incidence ⟨100⟩); C, bright field image showing crystalline precipitates (arrows) within the inclusions; D, concentration of round inclusions forming a ribbon; E, inclusions interconnected by dislocations (arrows); F, round inclusions similar to those observed in *L. neozelanica*; in some cases showing crystalline precipitates (arrow).

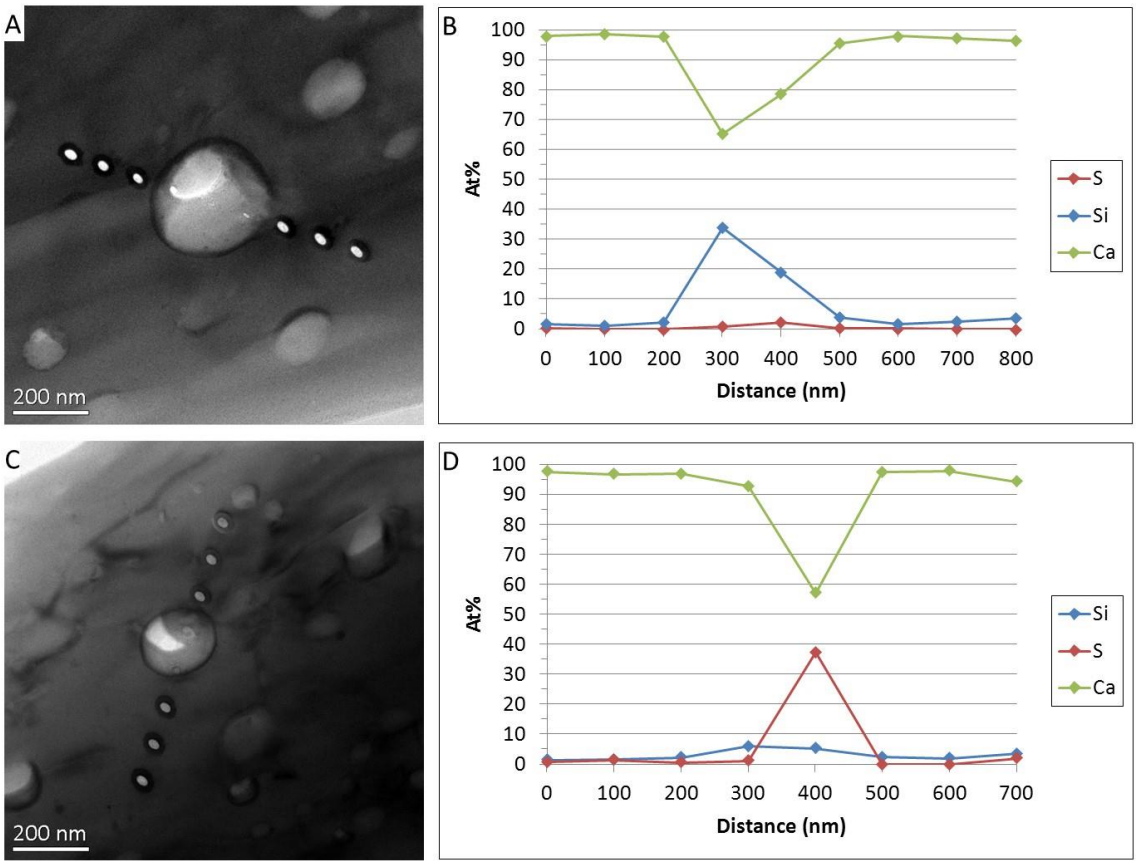

Fig. 15. Compositional profiles across round inclusions with a glassy interior (*L. neozelanica*, secondary layer) showing enrichment in silicon (A-B) and sulphur (C-D), with respect to the surrounding calcite matrix (the bright spots with dark halo in A and C correspond to the point analyses graphed in B and D, respectively).

The primary layer shows comparatively smaller single crystals (less than one micron wide and 1–2 μm long), elongated along the c-axis (Fig. 16A). Also, the primary layer crystals contain inclusions, although in smaller amount. Inclusions are smaller (tens of nanometers) than those occurring in the secondary layer, and often characterized by polygonal borders similar to the rhombohedral cleavage of calcite (Fig. 16B). Inclusions sometimes align along grain borders and do not always contain a solid crystalline precipitate. The tertiary layer of *L. neozelanica* is formed by large single crystals (several microns) (Fig. 16C) with few sporadic inclusions. Adjoining crystals seem related by a *n*60 ° rotation around the c-axis, which lies on the thin section plane (Fig. 16D–F). EBSD measurements clearly resolve the characteristics of the crystals of the tertiary layer (Fig. 11).

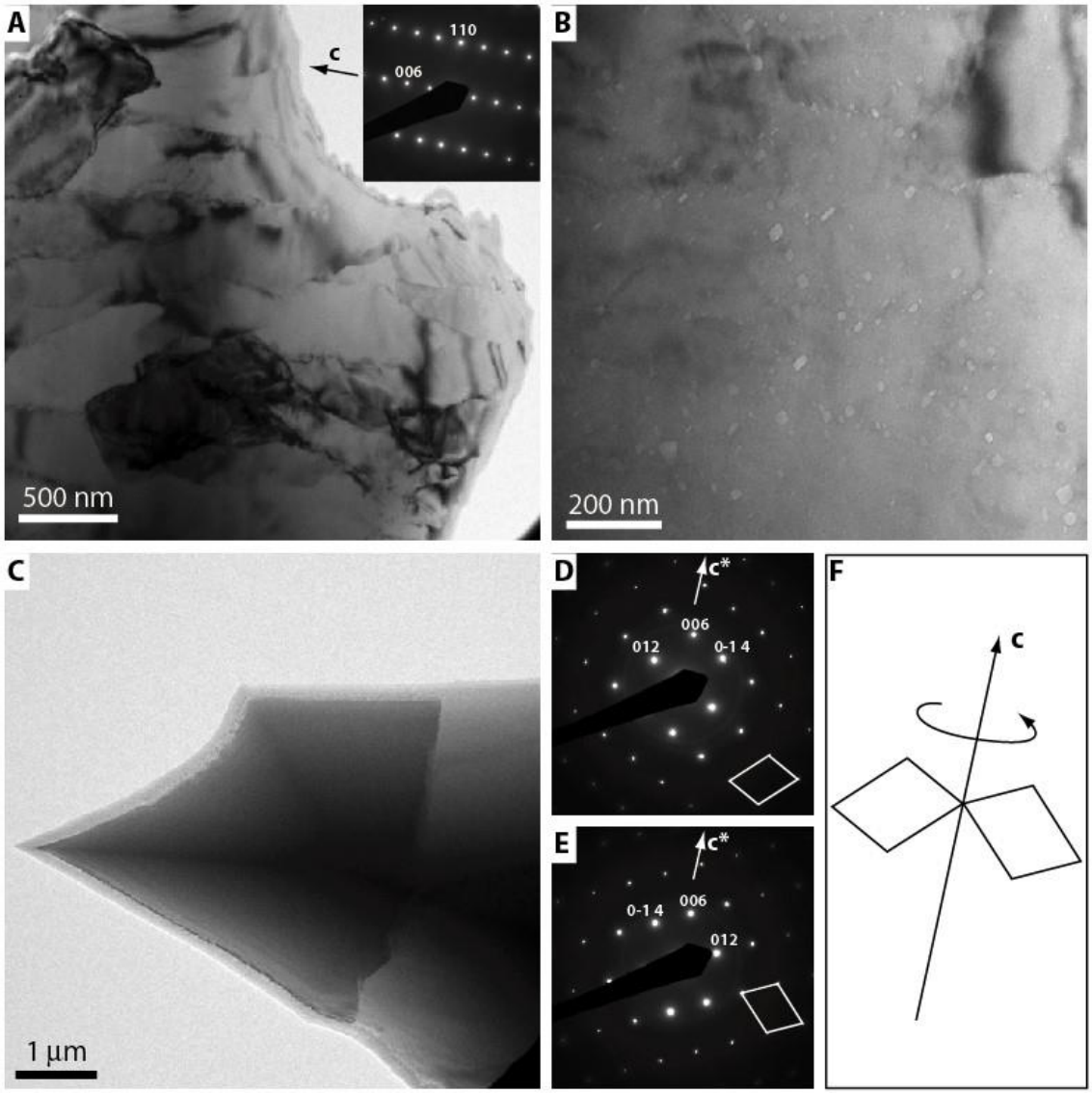

Fig. 16. A-B, Primary layer of *L. uva* and C-F, tertiary layer of *L. neozelanica*. A, TEM bright field image showing micrometre-sized calcite grains and related single crystal diffraction pattern (inset). The diffraction pattern is taken along ⟨1-1 0⟩ and the c-axis lies approximately on the thin section plane; B, bright field image with the calcite grains out of contrast to highlight the small inclusions with rhombohedral facets; C, two adjoining calcite grains (only a portion of them is shown) related by a *n* 60 ° rotation around the c-axis, as inferred from the diffraction patters in D and E (beam incidence ⟨100⟩), which refer each to individual grains, and the explaining scheme in F.

3.5 Discussion

Fibres of the secondary layer change their morphological orientation during growth, so that a single longitudinal section of a shell will not cut all fibres along the same section (Williams, 1966, 1968, 1997; Schmahl et al., 2004, 2012; Goetz et al., 2009; Gaspard and Nouet, 2016; Garbelli, 2017). The method followed in this research selected sections that represented perpendicular cuts of the fibres and recorded their actual size. It is appropriate to discuss further the fibre morphometric variation in relation to biotic factors and environmental control.

3.5.1 Fibres, ontogeny and shell fabric

Morphometric analysis of fibres in dorsal and ventral valves has important implications for the geochemical proxies and the information stored by the valves, as it is still controversial whether the two valves are formed in equilibrium with ambient seawater. Curry and Fallick (2002) reported different $\delta^{18}O$ values from ventral and dorsal valves of the same brachiopod specimen. However, recent studies found no significant difference in the geochemistry (trace chemistry and stable isotopes) between dorsal and ventral valves (Parkinson et al., 2005; Brand et al., 2015).

Based on no difference in fibre shape and size between dorsal and ventral valves, no difference in the geochemical composition of the secondary layer should be expected between the two valves. However, individually, a few species show some differences in fibre morphometrics between valves. Griesshaber et al. (2007) demonstrated that the dorsal and ventral valves of two recent species (*Terebratalia transversa* and *Megerlia truncata*) have different microstructural features. Therefore, there is a possibility in difference in fibre morphometrics at the species-specific level (i.e. in some species only)

Microstructural changes may occur within different shell layers and even in single shell layers (Grossman et al., 1996; Auclair et al., 2003; Griesshaber et al., 2005, 2007; Garbelli, 2017). Our results show that the fibres change in size and shape passing from the posterior external, to the central middle, and finally to the anterior internal part. As the posterior external part is produced first, whereas the anterior internal shell is produced last, there is an ontogenetic trend in the size and shape of the fibres, with the largest, widest and flattest fibres being produced. at the last and mature ontogenetic stages.

Variation of fibre size and shape in the growth direction may be related to the geochemical signal recorded in different parts of the shell (Griesshaber et al., 2007; Cusack et al., 2007; Garbelli et al., 2012, 2014). Yamamoto et al. (2011, 2013) reported oxygen isotope variations in different shell portions and related this to variable growth rates. Other researchers found that the inner part of the shell (inner part of secondary and tertiary layers) are in equilibrium with seawater and are the best biogenic materials for geochemical analyses (e.g., Grossman et al., 1996; Parkinson et al., 2005; Garbelli et al., 2012; Cusack and Huerta, 2012; Rollion-Bard et al., 2016). Here, we have shown that these inner (and anterior) fibres – produced at the later ontogenetic stage – are generally large, wide, and flat. Therefore, there is a relationship between the capacity to record the geochemical signal and fibre morphometrics, which may depend on ontogeny and growth rate, which in brachiopod decreases with age (Peck, 2001).

When comparing groups of species with two-layers against threelayer shells, the pattern is not straightforward. So, we conclude from this that the shell layer sequence is not the determinant factor in controlling the size and shape of the fibres of the secondary layer.

3.5.2 Shell organic content

In a previous study to assess the organic content of the shells of *L. uva* and *L. neozelanica*, using an ash free dry mass determined by ignition loss, the means were 3.38% and 1.87% respectively (Peck and Edwards, 1996). Our study explains how these differences are related to the microstructures observed because the size of fibres shows a relationship with organic matter content of the shell whereby the larger the calcite fibres, the smaller the amount of organic membrane matter coating the fibres in the same shell volume (cf. Garbelli et al., 2017). The shape of the fibres, in particular their

convexity, also plays a role, because a lower convexity means a more intricate outline allowing for enhanced development of organic membranes coating the fibres (cf. Fig. 8).
TEM observations of the secondary layer at the nanoscale show that there are no differences at this scale between the fibres of *L. uva* and those of *L. neozelanica*, both being characterized by high density of inclusions. Thus, the differential amount of organic matter stored in their respective shells should be related to the organic matter membranes among the fibres, rather than their intra-crystalline inclusions.
Our results on secondary layer fibres of generally being larger, wider, flatter and less round interiorly and anteriorly suggest that portions produced at this later ontogenetic stage must be associated with lower organic matter contents. This may be related to growth rate, but also to the energy balance of the organism (Peck, 2001). It has been suggested that the metabolic cost for precipitating $CaCO_3$ is lower than the one required for the secretion of organic membranes in the biomineral (Palmer, 1992). Thus, it may be possible that brachiopods with age shift to a slower, energy-conserving organic-poor growth process. In addition, brachiopods from cold water environments include more organic matter with their smaller fibres than counterparts from temperate regimes with larger fibres.

3.5.3 Shell hardness and predation

Fibres measured in the posterior external part of the shell of *G. vitreus* (Terebratulida) and *N. nigricans* (Rhynchonellida) are larger and less round in the ventral than in the dorsal valve.
Fibre size differences in the secondary layer may reflect changes in mechanical properties that control shell bending, attachment to hard substrate, mobility or resistance to predation. According to Pérez-Huerta et al. (2007) and Goetz et al. (2009), hardness decreases from the outside to the inside of the shell. Pérez-Huerta et al. (2007) found that the posterior part of the shell is softer and less stiff than the central and anterior regions. Goetz et al. (2009) showed that the fibrous layer is harder when the fibres are thin and randomly stacked. In the case of *G. vitreus* and *N. nigricans*, the fibres being larger and more uniformly oriented may indicate a softer and less stiff ventral posterior region. However, the larger the fibres the thicker the secondary layer produced in a certain amount of time, and shell thickness is one of the most effective defence mechanism against durophagous predation (Zuschin et al., 2003). Larger fibres allow brachiopods to increase shell thickness more rapidly, and ensure defence against predation. This may be a clear survival advantage during early stages of growth, characterized by faster, but a variable growth rate (Rosenberg et al., 1988; Curry and Fallick, 2002).
Delance and Emig (2004) showed that in the Mediterranean G. vitreus, predation drillholes are mostly located on the posterior and thickest part of the ventral valve. The same was observed by Harper et al. (2011) for *N. nigricans*. Delance and Emig (2004) concluded that *G. vitreus* does not exhibit any antipredatory adaptations and that drilling predation pressure is generally low in this species. Instead, they suggested that crushing predation would be more important, and, in their experiments, the most resistant part to this kind of predation would be the posterior and thickest region of the shell.
New Zealand *L. neozelanica*, which has a three-layer shell sequence similar to that of *G. vitreus*, does not have larger fibres in the posterior region. Interestingly, Harper and Peck (2016) have shown that *L. neozelanica* has lower rates of repair than co-occurring brachiopods as it suffers lower predation pressure. Consequently, larger fibres posteriorly may represent a survival strategy to rapidly increase shell thickness against shell-breaking predation.

3.5.4 Environmental control

It is quite reasonable to assume that environmental conditions may, in part, control the microstructural variation observed in fibres of the brachiopods from the Mediterranean Sea, a fjord of New Zealand and the bays of Antarctica. When comparing species living in different environmental settings, *L. uva*, from cold (±2 ℃) and less saturated seawater of Antarctica, faces the greatest challenge compared to the others from New Zealand and the Mediterranean. The brachiopods, particularly the two-layer species, from New Zealand have the largest and widest fibres, and they seem to be different from the Mediterranean species *G. vitreus*. However, the two settings have similar temperatures and rather low hydrodynamic energy, so other factors may control their different microstructures, such as salinity and/or carbonate saturation.

Seawater carbonate saturation for the Mediterranean Sea of 4.7 Ω (Alvarez et al., 2014) and 4.0 for New Zealand (Takahashi et al., 2014) suggests that seawater in the Mediterranean Sea with its higher saturation and salinity, may be an additional factor for the less organic rich shell microstructure of *G. vitreus*.

The effect of temperature and seawater carbonate saturation state is even more pronounced when we consider the size and shape differential of fibres in the two species of the same genus, *L. uva* and *L. neozelanica*, from different environmental settings. The Antarctic and New Zealand localities have similar salinity, but significantly different temperature and calcite saturation states (Table 1). The average calcite saturation of 4.0 Ω for New Zealand is about double the average of 2.1 for the Antarctic localities (Takahashi et al., 2014). The two species of interest have different shell successions, with *L. uva* comprising primary and secondary layers, whereas *L. neozelanica* also has an additional tertiary layer (e.g., Peck et al., 1997; Williams, 1997; Goetz et al., 2009; Gaspard and Nouet, 2016; Table 1). The smaller, narrower, and rounder fibres with lower convexity of Antarctic *L. uva* should contain more organic matter than its counterpart *L. neozelanica* from New Zealand. This conclusion, boosted by the occurrence of a tertiary layer in *L. neozelanica*, agrees well with the observations of Peck and Edwards (1996), who reported that the shell of *L. uva* has a higher overall organic matter content than *L. neozelanica*.

The differences in the shell fabric and fibre size of the two species may be best explained by the environmental context where the two species evolved, with the Antarctic *L. uva* in seawater with lower carbonate saturation state than the temperate *L. neozelanica* (Watson et al., 2012). *L. uva* has a more organic rich secondary layer to cope with carbonate deposition in less favourable carbonate saturation conditions. It may also be adaptive in retarding shell dissolution under these conditions. Therefore, we conclude that there is a correlation between the size and shape of fibres of brachiopods and their ambient environment, especially with respect to seawater carbonate saturation, and temperature (Fig. 17).

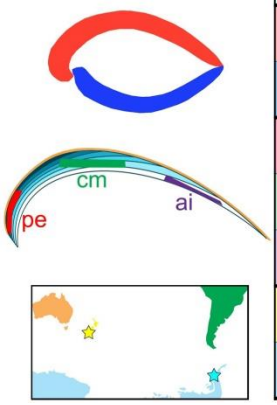

	Max Feret diameter	Roundness	Convexity
Ventral valve / Dorsal valve	Inconclusive change	Inconclusive change	Inconclusive change
Posterior external	narrow	round	Inconclusive change
Central middle	median	median	
Anterior internal	wide	flat	
Temperate: *L. neozelanica*	wide	flat	simple
Antarctica: *L. uva*	narrow	round	intricate

Fig. 17. Overview of the main results of this research showing change of fibre size and shape with age and in different environments.

3.6 Conclusions

Based on the analysis of the morphology and size of each fibre in the shells of six extant brachiopod species, we conclude that:

1) Morphometric parameters of ventral fibres are similar to those of dorsal valves when all species are considered. However, at the individual level, there are differences in morphometrics between dorsal and ventral valves that are related to a species-specific effect. In *G. vitreus* and *N. nigricans*, the fibres of the posterior external region of the ventral valve are significantly larger than those of the dorsal valve, possibly related to response to predation pressure.

2) There is an ontogenetic trend in the shape and size of the fibres: they become wider, larger, flatter, and less round with age.

3) This change in size and shape indicates that the fibrous layer produced in the late stage of growth may have a lower organic content compared to that produced first. The ontogenetic change in fibre morphometrics may be correlated to the observations that the anterior and inner parts of a shell are closer to isotopic equilibrium with seawater and are the best biogenic material for isotopic analysis.

4) An important consequence of the change in size and shape of the fibres with growth is that, in comparative studies of both recent and fossil shells, only shell portions produced at a similar ontogenetic stage should be sampled and compared.

5) The relationship between size and shape of fibres and environmental conditions is clear when comparing two species of the same genus living in seawater with different carbonate saturation state and temperature, but similar salinity. Notwithstanding their similarity at the TEM nanoscale, the fibres of *L. uva* are smaller, narrower, rounder and less convex than those of *L. neozelanica* at the microscale, contributing to the production of a more organic-rich shell, that may represent an adaptation for controlling carbonate deposition and countering shell dissolution in cold and less favourable carbonate saturation seawater conditions.

Acknowledgements

This project has received funding from the European Union's Horizon 2020 research and innovation programme under grant agreement No. 643084. We thank Curzio Malinverno and Agostino Rizzi for technical support. We thank two anonymous reviewers for their constructive comments.

References

Adams, D.C., Otarola-Castillo, E., 2013. Geomorph: an R package for the collection and analysis of geometric morphometric shape data. Methods Ecol. Evol. 4, 393–399.

Alvarez, M., Sanleón-Bartolomé, H., Tanhua, T., Mintrop, L., Luchetta, A., Cantoni, C., Schroeder, K., Civitarese, G., 2014. The CO_2 system in the Mediterranean Sea: a basin wide perspective. Ocean Sci. 10, 69–92.

Angiolini, L., Darbyshire, D.P.F., Stephenson, M.H., Leng, M.J., Brewer, T.S., Berra, F., Jadoul, F., 2007. Lower Permian brachiopods from Oman: their potential as climatic proxies. Earth. Env. Sci. T. R. So. 98, 327–344.

Angiolini, L., Jadoul, F., Leng, M.J., Stephenson, M.H., Rushton, J., Chenery, S., Crippa, G., 2009. How cold were the Early Permian glacial tropics? Testing sea-surface temperature using the oxygen isotope composition of rigorously screened brachiopod shells. J. Geol. Soc. 166, 933–945.

Auclair, A.C., Joachimski, M.M., Lécuyer, C., 2003. Deciphering kinetic, metabolic and environmental controls on stable isotope fractionations between seawater and the shell of *Terebratalia transversa* (Brachiopoda). Chem. Geol. 202, 59–78.

Brand, U., Veizer, J., 1980. Chemical diagenesis of a multicomponent carbonate system- 1: trace elements. J. Sed. Petrol, 50, 1219–1236.

Brand, U., Azmy, K., Bitner, M.A., Logan, A., Zuschin, M., Came, R., Ruggiero, E., 2013. Oxygen isotopes and $MgCO_3$ in brachiopod calcite and a new paleotemperature equation. Chem. Geol. 359, 23–31.

Brand, U., Azmy, K., Griesshaber, E., Bitner, M.A., Logan, A., Zuschin, M., Ruggiero, E., Colin, P.L., 2015. Carbon isotope composition in modern brachiopod calcite: A case of equilibrium with seawater? Chem. Geol. 411, 81–96.

Brand, U., Logan, A., Bitner, M.A., Griesshaber, E., Azmy, K., Buhl, D., 2011. What is the ideal proxy of Palaeozoic seawater chemistry? Mem. Assoc. Australas. 41, 9–24.

Brocas, W.M., Reynolds, D.J., Butler, P.G., Richardson, C.A., Scourse, J.D., Ridgway, I.D., Ramsay, K., 2013. The dog cockle, *Glycymeris glycymeris* (L.), a new annually-resolved sclerochronological archive for the Irish Sea. Palaeogeogr. Palaeoclimatol. Palaeoecol. 373, 133–140.

Crippa, G., Angiolini, L., Bottini, C., Erba, E., Felletti, F., Frigerio, C., Hennissen, J.A.I., Leng, M.J., Petrizzo, M.R., Raffi, I., Raineri, G., Stephenson, M.H., 2016a. Seasonality fluctuations recorded in fossil bivalves during the early Pleistocene: Implications for climate change. Palaeogeogr. Palaeoclimatol. Palaeoecol. 446, 234–251.

Crippa, G., Ye, F., Malinverno, C., Rizzi, A., 2016b. Which is the best method to prepare invertebrate shells for SEM analysis? Testing different techniques on recent and fossil brachiopods. Boll. Soc. Paleontol. Ital. 55, 111–125.

Cross, E.L., Peck, L.S., Lamare, M.D., Harper, E.M., 2016. No ocean acidification effects on shell growth and repair in the New Zealand brachiopod *Calloria inconspicua* (Sowerby, 1846). ICES J. Mar. Sci. 73, 920–926.

Curry, G.B., Brunton, C.H., 2007. Stratigraphic distribution of brachiopods, in: Selden, P.A. (Ed.), Treatise on Invertebrate Paleontology. Part H, Revised, Brachiopoda, vol. 6. Geological Society of America and Paleontological Institute, Boulder, Colorado, and Lawrence, Kansa, USA, pp. 2901–3081.

Curry, G.B., Fallick, A.E., 2002. Use of stable oxygen isotope determinations from brachiopod shells in palaeoenvironmental reconstruction. Palaeogeogr. Palaeoclimatol. Palaeoecol. 182, 133–143.

Cusack, M., Huerta, A.P., 2012. Brachiopods recording seawater temperature-A matter of class or maturation? Chem. Geol. 334, 139–143.

Cusack, M., Parkinson, D., Pérez-Huerta, A., England, J., Curry, G.B., Fallick, A.E., 2007. Relationship between $\delta^{18}O$ and minor element composition of *Terebratalia transversa*. Earth. Env. Sci. T. R. So. 98, 443–449.

Delance, J.H., Emig, C.C., 2004. Drilling predation on *Gryphus vitreus* (Brachiopoda) off the French Mediterranean coasts. Palaeogeogr. Palaeoclimatol. Palaeoecol. 208, 23–30.

Duller, C., 2008. Teaching statistics with excel A big challenge for students and lecturers. Austrian J. Stat. 37, 195–206.

Garbelli, C., 2017. Shell microstructures in Upper Permian brachiopods: implication for fabric evolution and calcification. Riv. It. Paleont. Strat. 123, 541–560.

Garbelli, C., Angiolini, L., Brand, U., Jadoul, F., 2014. Brachiopod fabric, classes and biogeochemistry: Implications for the reconstruction and interpretation of seawater carbon-isotope curves and records. Chem. Geol. 371, 60–67.

Garbelli, C., Angiolini, L., Jadoul, F., Brand, U., 2012. Micromorphology and differential preservation of Upper Permian brachiopod low-Mg calcite. Chem. Geol. 298, 1–10.

Garbelli, C., Angiolini, L., Shen, S.Z., 2017. Biomineralization and global change: A new perspective for understanding the end-Permian extinction. Geology 45, 19–22.

Gaspard, D., Nouet, J., 2016. Hierarchical architecture of the inner layers of selected extant rhynchonelliform. J. Struct. Biol. 196, 197–205.

Goetz, A.J., Griesshaber, E., Neuser, R.D., Lüter, C., Hühner, M., Harper, E., Schmahl, W.W., 2009. Calcite morphology, texture and hardness in the distinct layers of rhynchonelliform brachiopod shells. Eur. J. Mineral. 21, 303–315.

Goetz, A.J., Steinmetz, D.R., Griesshaber, E., Zaefferer, S., Raabe, D., Kelm, K., Irsen, S., Sehrbrock, A., Schmahl, W.W., 2011. Interdigitating biocalcite dendrites form a 3-D jigsaw structure in brachiopod shells. Acta biomater. 7, 2237–2243.

Griesshaber, E., Job, R., Pettke, T., Schmahl, W.W., 2005. Micro-scale physical and chemical heterogeneities in biogenic materials – a combined micro-Raman, chemical composition and microhardness investigation. In Katti, K., Ulm, F.J., Hellmich, C., Viney, C. (Eds.), Mechanical properties of bio-inspired and biological materials, MRS Symp. Proc. Series, Mater. Res. Soc. 844, 93–98.

Griesshaber, E., Kelm, K., Knieps, M., Schmahl, W.W., Job, R., Mader, W., 2006. The ultrastructure of brachiopod shells – a mechanically optimized material with hierarchical architecture. Mater. Res. Soc. Symp. Proc., 989E, 0898–L12–01.

Griesshaber, E., Neuser, R.D., Brand, U., Schmahl, W.W., 2008. Texture and Microstructure of Modern Rhynchonellide Brachiopod Shells – An Ontogenetic Study. Proc. ICOTOM 15 Conference. Am. Ceram. Soc., 201, 605–619.

Griesshaber, E., Neuser, R.D., Schmahl, W.W., 2010. The application of EBSD analysis to biomaterials: microstructural and crystallographic texture variations in marine carbonate shells. Semin Soc Esp Mineral. 07, 22–34.

Griesshaber, E., Schmahl, W.W., Neuser, R., Pettke, T., Blum, M., Mutterlose, J., Brand, U., 2007. Crystallographic texture and microstructure of terebratulide brachiopod shell calcite: An optimized materials design with hierarchical architecture. Am. Mineral. 92, 722–734.

Grossman, E.L., Mii, H.S., Zhang, C., Yancey, T.E., 1996. Chemical variation in Pennsylvanian brachiopod shells; diagenetic, taxonomic, microstructural, and seasonal effects. J. Sediment. Res. 66, 1011–1022.

Grossman, E.L., Zhang, C., Yancey, T.E., 1991. Stable-isotope stratigraphy of brachiopods from Pennsylvanian shales in Texas. Geol. Soc. Am. Bull. 103, 953–965.

Głąb, T., Sadowska, U., Żabiński, A., 2015. Application of image analysis for grass tillering determination. Environ. Monit. Assess. 187, 674.

Harper, E.M., Peck, L.S., 2016. Latitudinal and depth gradients in marine predation pressure. Glob. Ecol. Biogeogr. 25, 670–678.

Harper, E.M., Robinson, J.H., Lee, D.E., 2011. Drill hole analysis reveals evidence of targeted predation on modern brachiopods. Palaeogeogr. Palaeoclimatol. Palaeoecol. 305, 162–171.

Immenhauser, A., Schöne, B.R., Hoffmann, R., Niedermayr, A., 2016. Mollusc and brachiopod skeletal hard parts: Intricate archives of their marine environment. Sedimentology 63, 1–59.

Klingenberg, C.P., Barluenga, M., Meyer, A., 2002. Shape analysis of symmetric structures: quantifying variation among individuals and asymmetry. Evolution 56, 1909–1920.

Lowenstam, H.A., 1961. Mineralogy, O^{18}/O^{16} ratios, and strontium and magnesium contents of recent and fossil brachiopods and their bearing on the history of the oceans. J. Geol. 69, 241–260.

Mardia, K.V., Bookstein, F.L., Moreton, I.J., 2000. Statistical assessment of bilateral symmetry of shapes. Biometrika. 87, 285–300.

Palmer, A.R., 1992. Calcification in marine molluscs: How costly is it? Proc. Natl. Acad. Sci. U.S.A. 89, 1379–1382.

Parkinson, D., Curry, G.B., Cusack, M., Fallick, A.E., 2005. Shell structure, patterns and trends of oxygen and carbon stable isotopes in modern brachiopod shells. Chem. Geol. 219, 193–235.

Peck, L.S., Edwards, T.M., 1996. Organic contents and elemental composition of brachiopod shell and mantle tissues, in: Cooper, P., Jin, J. (Eds.), Brachiopods. Proceedings of the Third International Brachiopod Congress, Sudbury, Ontario, Canada, September 1995. Brookfield, VT: A.A. Balkema, Rotterdam, Netherlands, pp. 203–207.

Peck, L.S., 2001. Ecology (Chapter 11), in: Carlson, S., Sandy, M. (Eds.), Brachiopods ancient and modern: a tribute to G. Arthur Cooper. The Paleontology Society Papers, and the Yale University, New Haven, Connecticut, USA, pp. 171–183.

Peck, L.S., 2007. Brachiopods and climate change. Earth. Env. Sci. T. R. So. 98, 451–456.

Peck, L.S., Rhodes, M.C., Curry, G.B., Ansell, A.D., 1997. Physiology, in: Kaesler, R.L. (Ed.), Treatise on Invertebrate Paleontology. Part H, Revised, Brachiopoda, vol. 1. Geological Society of America Inc., and The University of Kansas, Boulder, Colorado, USA, pp. 213–242.

Penman, D.E., Hönisch, B., Rasbury, E.T., Hemming, N.G., Spero, H.J., 2013. Boron, carbon and oxygen isotope composition of brachiopod shells: intra-shell variability, controls, and potential as a paleo-pH recorder. Chem. Geol. 340, 32–39.

Popp, B.N., Anderson, T.F., Sandberg, P.A., 1986. Brachiopods as indicators of original isotopic compositions in some Paleozoic limestones. Geol. Soc. Am. Bull. 97, 1262–1269.

Pérez-Huerta, A., Cusack, M., McDonald, S., Marone, F., Stampanoni, M., MacKay, S., 2009. Brachiopod punctae: a complexity in shell biomineralisation. J. Struct. Biol. 167, 62–67.

Pérez-Huerta, A., Cusack, M., Zhu, W., England, J., Hughes, J., 2007. Material properties of brachiopod shell ultrastructure by nanoindentation. J. R. Soc. Interface 4, 33–39.

R Core Team, 2016. R: A language and environment for statistical computing. R Foundation for Statistical Computing, Vienna, Austria. URL https://www.R-project.org/.

Randle, V., Engler, O., 2000. Introduction to texture analysis: macrotexture, microtexture and orientation mapping. CRC Press, Amsterdam.

Rollion-Bard, C., Saulnier, S., Vigier, N., Schumacher, A., Chaussidon, M., Lécuyer, C., 2016. Variability in magnesium, carbon and oxygen isotope compositions of brachiopod shells: Implications for paleoceanographic studies. Chem. Geol. 423, 49–60.

Rosenberg, G.D., Hughes, W.W., Tkachuck, R.D., 1988. Intermediary metabolism and shell growth in the brachiopod Terebratalia transversa. Lethaia 21, 219–230.

Russ, J.C., Neal, F.B., 2015. The Image Processing Handbook (seventh edition). Boca Raton.

Schmahl, W.W., Griesshaber, E., Merkel, C., Kelm, K., Deuschle, J., Neuser, R.D., Göetz, A.J., Sehrbrock, A., Mader, W., 2008. Hierarchical fibre composite structure and micromechanical properties of phosphatic and calcitic brachiopod shell biomaterials – an overview. Mineral. Mag. 72, 541–562.

Schmahl, W.W., Griesshaber, E., Neuser, R., Lenze, A., Job, R., Brand, U., 2004. The microstructure of the fibrous layer of terebratulide brachiopod shell calcite. Eur. J. Mineral. 16, 693–697.

Schmahl, W.W., Griesshaber, E., Kelm, K., Goetz, A., Jordan, G., Ball, A., Xu, D., Merkel, C., Brand, U., 2012. Hierarchical structure of marine shell biomaterials: biomechanical functionalization of calcite by brachiopods. Z. Kristallog. – Cryst. Mater. 227, 793–804.

Schmidt, N.H., Olesen, N.O., 1989. Computer-aided determination of crystal-lattice orientation from electron channeling patterns in the SEM. Can. Mineral. 27, 15–22.

Schöne, B.R., Surge, D.M., 2012. Part N, Revised, Volume 1, Chapter 14: Bivalve sclerochronology and geochemistry. Treat. Online 46, 1–24.

Takahashi, T., Sutherland, S.C., Chipman, D.W., Goddard, J.G., Ho, C., Newberger, T., Sweeney, C., Munro, D.R., 2014. Climatological distributions of pH, pCO_2, total CO_2, alkalinity, and $CaCO_3$ saturation in the global surface ocean, and temporal changes at selected locations. Mar. Chem. 164, 95–125.

Watson, S.A., Peck, L.S., Tyler, P.A., Southgate, P.C., Tan, K.S., Day, R.W., Morley, S.S., 2012. Marine invertebrate skeleton size varies with latitude, temperature and carbonate saturation: implications for global change and ocean acidification. Glob. Chang. Biol. 18, 3026–3038.

Williams, A., 1966. Growth and structure of the shell of living articulate brachiopods. Nature 211, 1146–1148.

Williams, A., 1968. Evolution of the shell structure of articulate brachiopods. Spec. Pap. Palaeontol. 2, 1–55.

Williams, A., 1997. Shell structure, in: Kaesler, R.L. (Ed.), Treatise on Invertebrate Paleontology. Part H, Revised, Brachiopoda, vol. 1. Geological Society of America Inc., and The University of Kansas, Boulder, Colorado, USA, pp. 267–320.

Yamamoto, K., Asami, R., Iryu, Y., 2011. Brachiopod taxa and shell portions reliably recording past ocean environments: Toward establishing a robust paleoceanographic proxy. Geophys. Res. Lett. 38, L13601, doi:10.1029/2011GL047134.

Yamamoto, K., Asami, R., Iryu, Y., 2013. Correlative relationships between carbon-and oxygen-isotope records in two cool-temperate brachiopod species off Otsuchi Bay, northeastern Japan. Paleontol. Res. 17, 12–26.

Ye, F., Crippa, G., Garbelli, C., Griesshaber, E., 2017. Microstructural data of six recent brachiopod species: SEM, EBSD, morphometric and statistical analyses. Data in Brief. submitted.

Zuschin, M., Stachowitsch, M., Stanton Jr, R.J., 2003. Patterns and processes of shell fragmentation in modern and ancient marine environments. Earth. Sci. Rev. 63, 33–82.

Chapter 4

Variation in brachiopod microstructure and isotope geochemistry under low pH–ocean acidification–conditions

*Biogeosciences Discussion, https://doi.org/10.5194/bg-2018-332, in review, 2018. (interactive public discussion. Total article views: 310. Received comments: 3)

Facheng Ye[1], Hana Jurikova[2], Lucia Angiolini[1], Uwe Brand[3], Gaia Crippa[1], Daniela Henkel[2], Jürgen Laudien[4], Claas Hiebenthal[2], Danijela Šmajgl[5]

[1]Università degli Studi di Milano, Dipartimento di Scienze della Terra 'A. Desio', via Mangiagalli 34, Milano, 20133, Italy. E–mail: facheng.ye@unimi.it; lucia.angiolini@unimi.it; gaia.crippa@unimi.it

[2]GEOMAR Helmholtz-Zentrum für Ozeanforschung Kiel, Wischhofstr. 1–3, 24148 Kiel, Germany. E–mail: hjurikova@geomar.de; dhenkel@geomar.de; chiebenthal@geomar.de

[3]Department of Earth Sciences, Brock University, 1812 Sir Isaac Brock Way, St. Catharines, ON Canada L2S 3A1. E–mail: ubrand@brocku.ca

[4]Alfred-Wegener–Institut Helmholtz–Zentrum für Polar– und Meeresforschung, Bremerhaven, Germany. E–mail: juergen.laudien@awi.de

[5]ThermoFisher Scientific, Hanna–Kunath–Str. 11, Bremen, Germany. E–mail: danijela.smajgl@thermofisher.com

Abstract

Throughout the last few decades and in the near future CO_2–induced ocean acidification is potentially a big threat to marine calcite-shelled animals (e.g., brachiopods, bivalves, corals and gastropods). Despite the great number of studies focusing on the effects of acidification on shell growth, metabolism, shell dissolution and shell repair, the consequences on biomineral formation remain poorly understood, and only few studies addressed contemporarily the impact of acidification on shell microstructure and geochemistry. In this study, a detailed microstructure and stable isotope geochemistry investigation was performed on nine adult brachiopod specimens of *Magellania venosa* (Dixon, 1789), grown in the natural environment as well as in controlled culturing experiments at different pH conditions (ranging 7.35 to 8.15 ± 0.05) over different time intervals (214 to 335 days). Details of shell microstructural features, such as thickness of the primary layer, density and size of endopunctae and morphology of the basic structural unit of the secondary layer were analysed using scanning electron microscopy (SEM). Stable isotope compositions ($\delta^{13}C$ and $\delta^{18}O$) were tested from

the secondary shell layer along shell ontogenetic increments in both dorsal and ventral valves. Based on our comprehensive dataset, we observed that, under low pH conditions, *M. venosa* produced a more organic-rich shell with higher density of and larger endopunctae, and smaller secondary layer fibres, when subjected to about one year of culturing. Also, increasingly negative $\delta^{13}C$ and $\delta^{18}O$ values are recorded by the shell produced during culturing and are related to the CO_2–source in the culture setup. Both the microstructural changes and the stable isotope results are similar to observations on brachiopods from the fossil record and strongly support the value of brachiopods as robust archives of proxies for studying ocean acidification events in the geologic past.

4.1 Introduction

Since the industrial revolution the surface ocean pH has dropped by 0.1 units and will probably drop another 0.3–0.5 units by 2100 (Caldeira and Wickett, 2005; Orr et al., 2005; IPCC, 2013). This is due to the increasing amount of atmospheric carbon dioxide (CO_2) absorbed by the ocean that extensively affects sea water carbonate chemistry (e.g., Caldeira and Wickett, 2003, 2005; Feely et al., 2004). Increased concentrations of anthropogenic CO_2 are reflected in an elevated concentration of hydrogen ions, which lowers the pH and the available carbonate ions (Orr et al., 2005). Effects on marine organisms is of great scientific interest, both for understanding the geological past and for the consequences in the immediate future (e.g., Ries et al., 2009), as the decrease in calcium carbonate saturation potentially threatens marine organisms forming biogenic calcium carbonate (e.g., Orr et al., 2005; Guinott et al., 2006; Jantzen et al., 2013a, b; McCulloch et al., 2012). This applies to calcium carbonate shell–forming species, such as brachiopods and mollusks, because they are considered excellent archives documenting how changes in environmental conditions can affect marine organisms (e.g., Kurihara. 2008; Comeau et al., 2009; Watson et al., 2012, Hahn et al., 2012, 2014; Cross et al., 2015, 2016, 2018; Crippa et al., 2016a; Milano et al., 2016; Garbelli et al., 2017; Jurikova et al., in review).

Recently, several experiments were performed to investigate if a change of seawater pH may affect growth rate, shell repair and oxygen consumption of calcifying organisms, and how they respond to ocean acidification (Supplementary Table 1). However, despite the great number of studies, the consequences on biomineral formation remain not well understood, as most studies focused mainly on growth, metabolic rates, shell dissolution and shell repair (Supplementary Table 1, and references therein). Only a few studies deal with the effect of acidification on microstructure (Beniash et al., 2010; Hahn et al., 2012; Stemmer et al., 2013; Fitzer et al., 2014a, b; Milano et al., 2016), and all of them focused on bivalves and show that neither microstructure, nor shell hardness seem to be affected by seawater pH.

The few studies that examined brachiopods or brachiopod shells suggest that the latter suffered increased dissolution under lower seawater pH conditions, whereas the organism either exhibited no changes, or an increase in shell density [calculated as dry mass of the shell (g)/shell volume (cm^3)], but otherwise no changes in shell morphology and trace chemistry (Table 1). Overall, there appears to be little to no effect on brachiopod morphology or chemistry with lower seawater pH (Cross et al., 2015, 2016, 2018).

Table 1. Culturing, dissolution experiments and natural variation on several brachiopod species and shells.

Species N (number of sample)	Growth Parameters	Shell repair/Microstructure/Oxygen consumption/Dissolution of shell/Microstructure	Method & Material	Environment/conditions T=Temperature (℃) S=Salinity (PSU) pCO_2 (µatm)	Duration of experiment	Source
Calloria inconspicua (Sowerby, 1846) N = 123	1) >3 mm in length undamaged individuals were not affected by lower pH; 2) <3 mm in length undamaged individuals grew faster at pH 7.62 than the control conditions	Not affected by lower pH (>80% of all damaged individuals repaired after 12 weeks)	Culture experiment	a) pH 8.16, T 16.5, S 33.9, pCO_2 465, Ω calcite 3.5 b) pH 7.79, T 16.9, S 33.9, pCO_2 1130, Ω calcite 1.6 c) pH 7.62, T 16.6, S 33.9, pCO_2 1536, Ω calcite 1.3	12 weeks	Cross et al., 2016
Calloria inconspicua (Sowerby, 1846) N = 389 (adults)		Punctae width decreased by 8.26%, shell density increased by 3.43%, no change in shell morphology, punctae density, shell thickness, and shell elemental composition (Ca, Mg, Na, Sr and P)	Collected every decade from one locality	Last two decades pH reduced 0.1 unit Temperature varied from 10.7–13.0 ℃ pCO_2 varied from 320-400 Salinity and Ω of calcite not provided	120–year record	Cross et al., 2018
Liothyrella uva (Broderip, 1833) N = 156	Not affected by lower pH	Not affected by either low pH conditions or temperature. (>83% of individuals repaired after 7 months)	Culture experiment	a) pH 7.98, T -0.3, S 35, pCO_2 417, Ω calcite 1.20 b) pH 8.05, T 1.7, S 35, pCO_2 365, Ω calcite 1.49 c) pH 7.75, T 1.9, S 35, pCO_2 725, Ω calcite 0.78 d) pH 7.54, T 2.2, S 35, pCO_2 1221, Ω calcite 0.50	7 months	Cross et al., 2015
Liothyrella uva (Broderip, 1833) $N_{post\text{-}mortem}$ = 5	Not applicable	Higher dissolution in gastropods and brachiopods at lower pH after 14 days	Empty shells	a) pH 7.4, T 4, S 35, Ω calcite 0.74 b) pH 8.2, T 4, S 35, Ω calcite 4.22 pCO_2 Not provided	14 to 63 days	McClintock et al., 2009

Brachiopods possess a low-magnesium calcite shell, which should be more resistant to elevated pCO_2 compared to the more soluble forms of $CaCO_3$, aragonite and high-Mg calcite (Morse et al., 2007). The shell microstructure of Rhynchonelliformean brachiopods has been used as a powerful tool to understand the biomineral response to modern global acidification and similar events in the past (Payne and Clapham, 2012; Cross et al., 2015, 2016; Garbelli et al., 2017). A comprehensive study focusing on fossil brachiopods during the end-Permian extinction showed that brachiopods tend to produce shells with higher organic components during ocean acidification events (Garbelli et al., 2017). Here, the microstructure and stable isotope geochemistry are described of the shells of adult brachiopod specimens of the cold-temperate brachiopod species *M. venosa* (Dixon, 1789) are described. The organisms grew in the natural environment and in culture under different pH conditions. *M. venosa* represents the largest recent brachiopod species, and locally may be abundant (Försterra et al., 2008), and it has the highest growth rate recorded for recent brachiopods (Baumgarten et al., 2014). Its low-magnesium calcite shell consists of a microgranular primary layer and a fibrous secondary layer (Smirnova et al., 1991; Baumgarten et al., 2014; Romanin et al., 2018; Casella et al. 2018) crossed by perforations, the endopunctae.

Since little is known about morphological and geochemical responses to increased ocean acidification in brachiopods (cf, Table 1), the main goal of this study is to document any changes in this highly important archival marine organism. It will be described if and how shell microstructural features such as the primary layer thickness, density of endopunctae and fibre morphology, and their stable carbon ($\delta^{13}C$) and oxygen ($\delta^{18}O$) isotope compositions respond to low seawater pH conditions.

4.2 Materials and methods

4.2.1 Brachiopod samples and culturing set-up

A thorough description of the brachiopod sampling and culturing is provided in Jurikova et al. (in review), but an abbreviated version here is provided. Nine adult individuals of *M. venosa* (Dixon, 1789) were chosen for microstructure investigation and an evaluation of their $\delta^{13}C$ and $\delta^{18}O$ values (Table 2). All specimens were collected by scientific SCUBA divers alive from appr. 20 m water depth of Comau Fjord (Chile) at different localities (Figure 1). Specimens #158 and #223 did not experience any treatment after collection from Comau Fjord. All other specimens, #43 (pH_3), #63 (pH_4), #8004 (pH_0), #8005 (pH_0), #9004 (pH_1 and pH_2), #9005 (pH_1 and pH_2) and #9006 (pH_1 and pH_2), were cultured under different pH conditions (Table 2 and Table 3) at either AWI in Bremerhaven or GEOMAR (at KIMOCC–Kiel Marine Organisms Culture Centre) in Kiel, Germany.

Table 2. Specimens of *M. venosa* sampled from Comau Fjord, Chile, and natural and experimental culturing conditions.

Sample ID	Sample locality at Comau Fjord (Chile)[①]	Sample seawater conditions[②]	Date of collection	Length of ventral valve (mm)	Duration of experiment	Experimental conditions
#43	Lilliguapi	pH: ~7.9 T: ~13 S: ~32 D: 20	Feb. 2012	37	214 days[③]	pCO_2: 1391, pH: 7.66 ± 0.04 T: 11.62 ± 0.54, S: 32.58 Ωcal: 1.97
#63	Lilliguapi	pH: ~7.9 T: ~13 S: ~32 D: 20	Feb. 2012	23	214 days[③]	pCO_2: 2611, pH: 7.44 ± 0.08 T: 11.69 ± 0.45, S: 32.65 Ωcal: 1.37
#158	Huinay Dock	pH: ~7.9 T: ~13 S: ~32 D: 20	Dec. 2011	36	no	
#223	Cahuelmó	pH: ~7.9 T: ~13 S: ~32 D: 23	Feb. 2012	30	no	
#8004	Comau Fjord	pH: ~7.9 T: ~13 S: ~32 D: 21	Apr. 2016	31	335 days[④]	pCO_2: 600 ,pH: 8.00–8.15 ± 0.05 T: ~10, S: 30, Ωcal: 2.0–3.5
#8005	Comau Fjord	pH: ~7.9 T: ~13 S: ~32 D: 21	Apr. 2016	46	335 days[④]	pCO_2: 600, pH: 8.00–8.15 ± 0.05 T: ~10, S: 30, Ωcal: 2.0–3.5
#9004	Comau Fjord	pH: ~7.9 T: ~13 S: ~32 D: 21	Apr. 2016	41	335 days[④]	pCO_2: 2000–4000[⑤] pH: 7.60 ± 0.05 to 7.35 ± 0.054 T: ~10, S: 30, Ωcal: 0.6–1.1
#9005	Comau Fjord	pH: ~7.9 T: ~13 S: ~32 D: 21	Apr. 2016	25	335 days[④]	pCO_2: 2000–4000[⑤] pH: 7.60 ± 0.05 to 7.35 ± 0.054 T: ~10, S: 30, Ωcal: 0.6–1.1
#9006	Comau Fjord	pH: ~7.9 T: ~13 S: ~32 D: 21	Apr. 2016	43	335 days[④]	pCO_2: 2000–4000[⑤] pH: 7.60 ± 0.05 to 7.35 ± 0.054 T: ~10, S: 30, Ωcal: 0.6–1.1

Note: D: Depth (m), T: temperature (℃), S: salinity (PSU–practical salinity units), pCO_2 (µatm).

[①]Cahuelmó 42°15'23" S, 72°26'42" W, Cross–Huinay 42°23'28" S, 72°27'27" W, Jetty (Huinay Dock) 42°22'47" S, 72°24'56" W, Lilliguapy 42°9'43" S, 72°35'55" W, samples #8004, #8005, #9004, #9005, #9006 were harvested from three sites in Comau Fjord (Cross–Huinay, Jetty, and Liliguapy), Chilean Patagonia

[②]Reference: Laudien et al. (2014) and Jantzen et al. (2017)

[③]Culture experiments conducted at the Alfred–Wegener–Institut Helmholtz–Zentrum für Polar–und Meeresforschung, Bremerhaven, Germany

[④]Culture experiments conducted at GEOMAR Helmholtz–Zentrum für Ozeanforschung Kiel, Germany (Jurikova et al., in review)

[⑤]CO_2 concentration was changed during the experiment: from 4 August 2016 to 18 April 2017 at 2000 µatm and from 18 April 2017 till 5 July 2017 at 4000 µatm

Table 3. Culture and sensor systems for *M. venosa* specimens (#43, #63, #8004, #8005, #9004, #9005 and #9006). Operated under controlled experimental settings in a climate control laboratory at the Alfred–Wegener–Institut Helmholtz–Zentrum für Polar–und Meeresforschung, Bremerhaven, Germany and at GEOMAR Helmholtz–Zentrum für Ozeanforschung Kiel, Germany.

	Culture system at AWI	Automated sensor Systems at AWI	Culture system at GEOMAR	Automated sensor Systems at GEOMAR
	Aquarium (150 L/each pH treatment) Supplied from a reservoir tank (twice a week 20 % water was replaced)		Aquarium (150 L/each pH treatment) Supplied from a reservoir tank (twice a month 10 % water was replaced)	
Temperature	Controlled in temperature constant room		Controlled using heaters or coolers	Temperature Sensor Pond
pCO_2	Bubbling of CO_2 pH 7.66 ± 0.04, pH 7.44 ± 0.08	COMPORT, Dennerle, Vinningen; IKS aquastar Aquarium computer V2.xx with Aquapilot 2011	Bubbling of CO_2 enriched air	CONTROS HydroC® underwater CO_2 sensor
Salinity	Mixing Reef commercial sea–salt (until October: Aqua Medic, Bissendorf, Germany, thereafter Dupla Marin Reef Salt, Dohse Aquaristik, Grafschaft-Gelsdorf, Germany) with deionized water (Atkinson and Bingman, 1998)	Conductivity Electrode	Mixing Tropic Marin Pro–Reef commercial sea–salt with deionized water (Atkinson and Bingman, 1998)	Conductivity Electrode
Filtering	Biofilter, protein skimmer and UV sterilizer		Biofilter, protein skimmer and UV sterilizer	
Food	Regularly fed (typically 5 times per week) with Dupla Rin, Coral Food, Reef Pearls 5–200 µm, alive *Thalassiosira weissflogii*, and 1d old nauplii of *Artemia salina*		Regularly fed (typically 5 times per week) with *Rhodomonas baltica*	
Substrate	Sabia Corallina, 7–8mm, Dohse Aquaristik, Grafschaft–Gelsdorf, Germany		No	

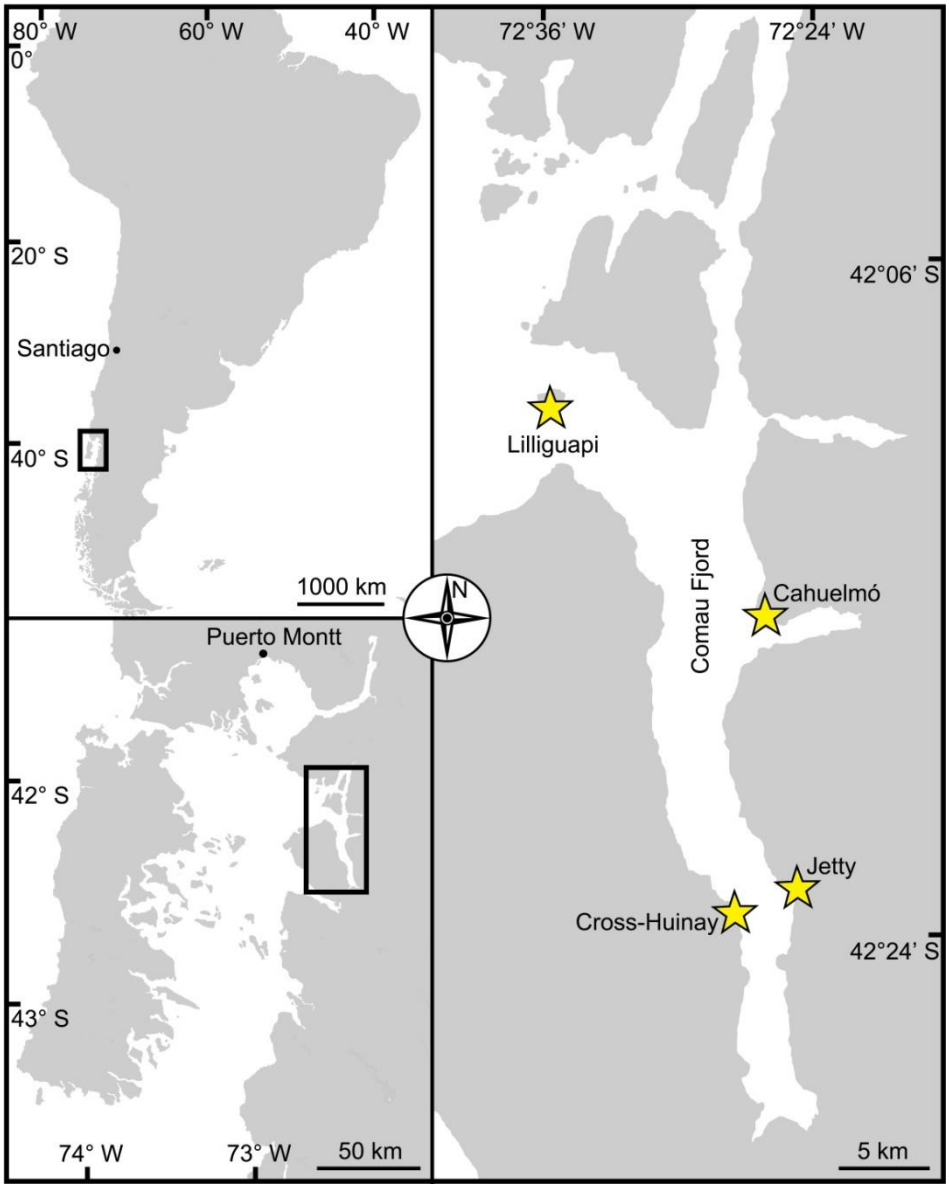

Figure 1. Map of Comau Fjord. Upper left map: Overview of Chilean Patagonia. Lower left map: Gulf of Ancud with connection in the North and South to the Pacific Ocean. Right hand map: Fjord Comau with localities of brachiopod sample collection. In both maps the rectangle marks the location of Comau Fjord.

In summary, *M. venosa* individuals sampled in Chile were transported to Germany and cultured under controlled environmental setting in a climate laboratory. As a culture medium we used artificial seawater, which was prepared by mixing a commercial salt with deionized water until the desired salinity and chemical composition was achieved. An overview of the culturing setup at both laboratories is available in Table 3. Brachiopods were first left to acclimatize, and prior to the start of experimental treatments labelled using a fluorescent dye–calcein (Sigma, CAS 1461–15–0; 50 mg/l for 3 h) (e.g., Baumgarten et al., 2013; Jurikova et al., in review). Specimens #43 and #63 were cultured at AWI at pH_3 = 7.66 (pCO_2 = 1390 µatm) and pH_4 = 7.44 (pCO_2 = 2610 µatm) from 29th August 2013 to 31th March 2014 respectively. Specimens #8004, #8005, #9004, #9005 and #9006 were cultured concurrently at GEOMAR under control or low pH conditions. Specimens #8004 and #8005 were maintained under control settings (pH_0 = 8.0/8.15) from 4th August 2016 to 5th July 2017, conditions similar to the fjord habitat. In contrast, specimens #9004, #9005 and #9006 were cultured under low–

pH artificial seawater conditions. Low–pH conditions were mediated by additional bubbling of CO_2 at AWI, and CO_2–enriched air at GEOMAR (Table 3). The acidification experiment was performed in two phases; the first one from 4th August 2016 to 18th April 2017 during which the pCO_2 was set to 2000 µatm (corresponding to a pH_1 = 7.60), and the second one during which the pCO_2 was set to 4000 µatm (corresponding to a pH_2 = 7.35) from 18th April 2017 to 5th July 2017. In order to distinguish between the shell parts participated under the specific pH conditions as well as to allow exact comparison to shells from the control treatment, calcein marking was carried out prior to the second low–pH phase (i.e. before the 4000 µatm experiment). Parts of the shell grown under specific pH conditions are indicated in Figure 2. In addition to the calcein marking, newly grown shell parts may be distinguished from visible growth lines on the surface of the shell (Figure 2). The total length (defined as maximum distance from the blue line to the anterior margin) of the curved dorsal and ventral valves grown during the 11 months of culturing (Figure 2) varied from < 5 mm to 15.6 mm (Table 4).

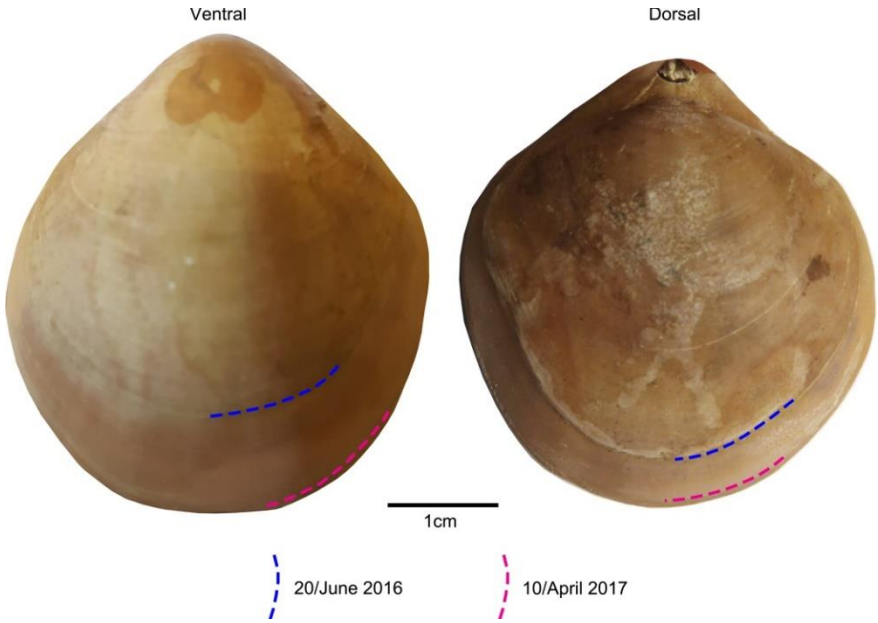

Figure 2. Growth lines marked with calcein on the surface of the brachiopod specimens (#9006).

Table 4. Total shell length of three specimens of *M. venosa* before, during and at the end of the in vitro culturing.

Sample	Initial anterior–posterior length (mm)	Length–Duration (a) 257 Days (mm)	Length–Duration (b) 78 Days (mm)
#8004 ventral	31	14 (pH_0)	1.6 (pH_0)
#8005 ventral	46	5 (pH_0)	<1 (pH_0)
#8005 dorsal	41	4 (pH_0)	<1 (pH_0)
#9004 ventral	41	13 (pH_1)	1.2 (pH_2)
#9005 ventral	25	12 (pH_1)	1.8 (pH_2)
#9006 ventral	43	9 (pH_1)	<1 (pH_2)
#9006 dorsal	38	8 (pH_1)	<1 (pH_2)

Note: (a) Culturing from 4 August 2016 to 18 April 2017; (b) Culturing from 18 April 2017 to 5 July 2017; pH_0 = 8.00–8.14, pH_1 = 7.60, pH_2 = 7.35.

4.2.2 Microstructural analysis

This study followed the sample preparation method for recent shells suggested by Crippa et al. (2016b). In order to obtain more detailed data on microstructural changes, the samples were cut with a diamond blade along different axes and directions (Figure 3A). Subsequently, the samples were immersed in 36 volume hydrogen peroxide (H_2O_2) for 24 to 48 hours to remove the organic components. The sectioned surfaces were manually smoothed with 1200 grit sandpaper, then quickly (3 seconds) cleaned with 5% hydrochloric acid (HCl), immediately washed with tap water and air-dried. Finally, the valve sections were gold–coated and analysed by a Cambridge S–360 scanning electron microscope with a lanthanum hexaboride (LaB6) source operating at an acceleration voltage of 20 kV (Dipartimento di Scienze della Terra "A. Desio", Università di Milano).

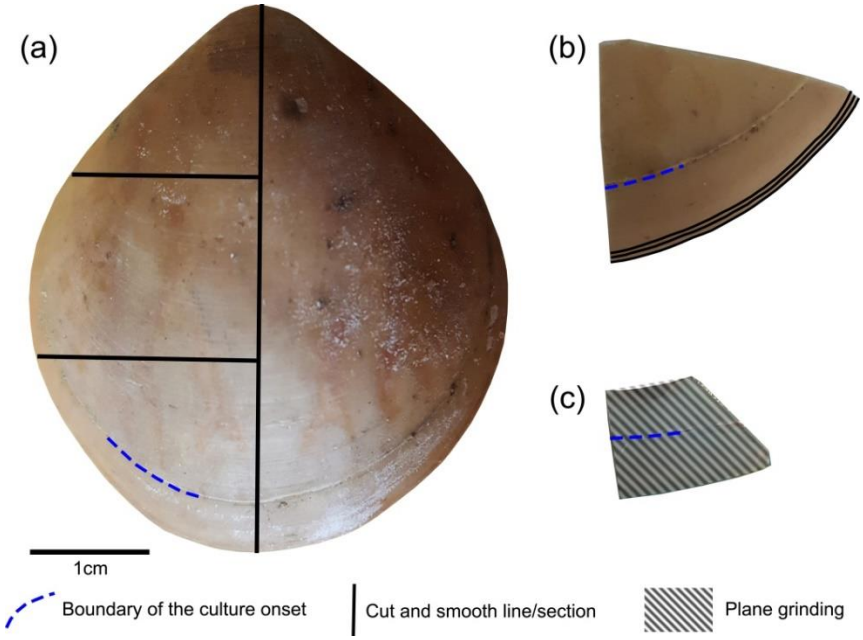

Figure 3. Brachiopod shell sample cut along different axes. A, longitudinal and transverse sections; B, transverse sections at the anterior margin of the shell; C, plane grinding of the external surface of the shell.

The methods described by Ye et al. (2018a) were followed to investigate the basic microstructural units (fibres) in SEM images. We focused primarily on the anterior margin of the valves, the part that was produced during culturing (hereinafter referred to as *during–culturing*) under different pH conditions. Therefore, additional transverse sections along the growth lines were obtained in the most anterior part (black lines in Figure 3B) by manually smoothing with 1200 grit sandpaper. Plane grinding was performed on the external surface of the shell (Figure 3) to investigate the distribution of endopunctae.

The thickness of the primary layer was measured on the SEM images of specimens #8005 and #9006 (Figure 4A) in different positions along the longitudinal growth axis (posterior, central and anterior regions). In the vicinity of the transition from natural growth to cultured growth, the region was further subdivided into four sub-zones.

To calculate and measure the density and diameter (max) of endopunctae, squares (800 μm×800 μm) were located randomly over the smoothed external surface of the anterior shell (Figure 4B). Four sub-zones (C2, A1, A2, A3) were defined according to their position along the posterior-anterior direction,

while distinguishing the part of the shell produced *before-culturing* and that produced *during–culturing*.

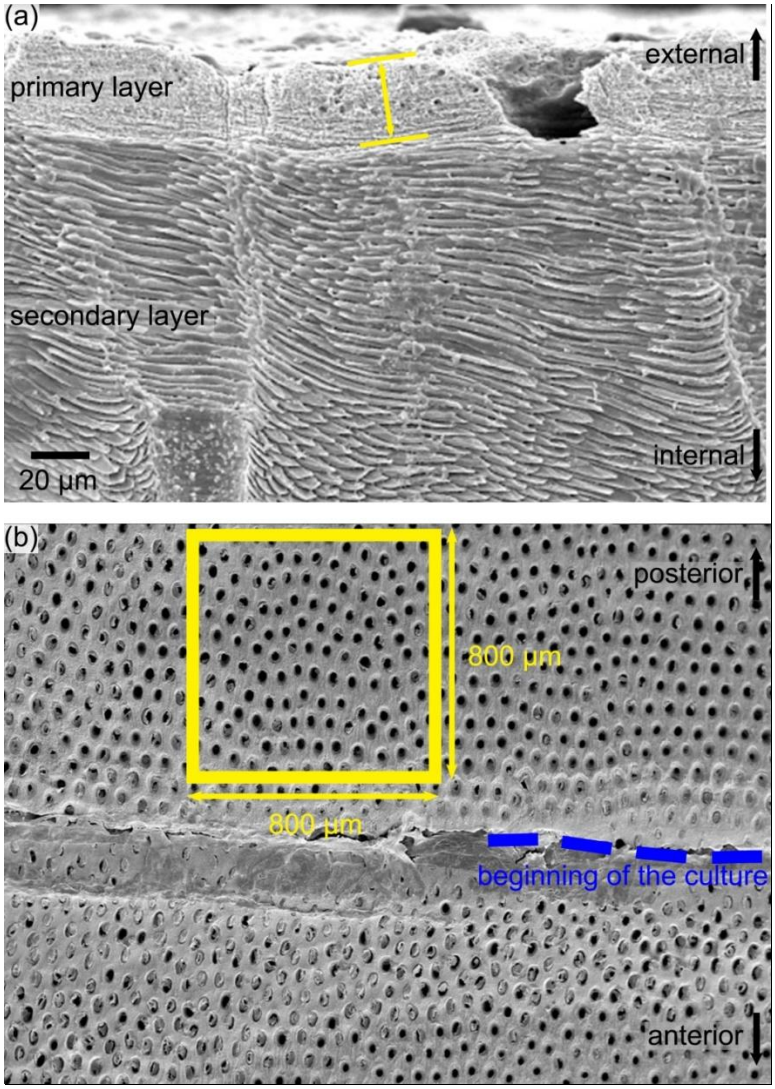

Figure 4. Measurement methods used for the thickness of primary layer and the density of the endopunctae. Note that for the latter, endopunctae were counted when included for more than their half diameter inside the square.

For morphometric analyses, fibres were manually outlined using polygonal lasso in Adobe Photoshop CS6, and size and shape parameters were measured with Image–Pro Plus 6.0 and ImageJ (for convexity). In particular, following Ye et al. (2018a, b) we measured/calculated the Feret diameter (max), Area, Roundness [4Area/π × Feret diameter (max)^2] and Convexity (Convex Perimeter/Perimeter). The width of an individual fibre roughly corresponds to the Feret diameter (max), whereas its height corresponds to the Feret diameter (min) (see Figure 6 in Ye et al., 2018a).
As individual fibres are irregular in shape in the most anterior sections of brachiopods, the morphometric measurement method proposed by Ye et al. (2018a, b) is not always suitable. Thus, modifications had to be made to Ye et al. (2018a, b) measurement method to make the comparative morphometric analysis of the fibres more robust (Figure 5A, 5B). First, all SEM images were oriented in the same direction with the base of the primary layer facing upwards. Then a uniform size zone (20 µm × 20 µm) was selected for additional measurements with the upper side of the square always placed at the boundary between the primary and the secondary layers (Figure 5C). Two new methods

were developed and were then applied: for Method 1, the width of fibres crossed by two standard lines was measured, which were always located in the same position and at the same distance in all the selected zones (yellow and orange lines in Figure 5 method 1). For Method 2, we calculated the number of boundaries based on the number of fibres crossed by the two standard lines (Figure 5 method 2). Samples were named according to the following nomenclature, the most anterior transection zone of the ventral valve was named Z1, the second most anterior transection zone of the ventral valve Z2 and so on, the most anterior transection zone of the dorsal valve was named Z4; The standard line facing towards the primary layer was named "1" and the second standard line "2" (example: "Z1–1" is the sample of the standard line facing towards the primary layer at the most anterior transection zone of the ventral valve).

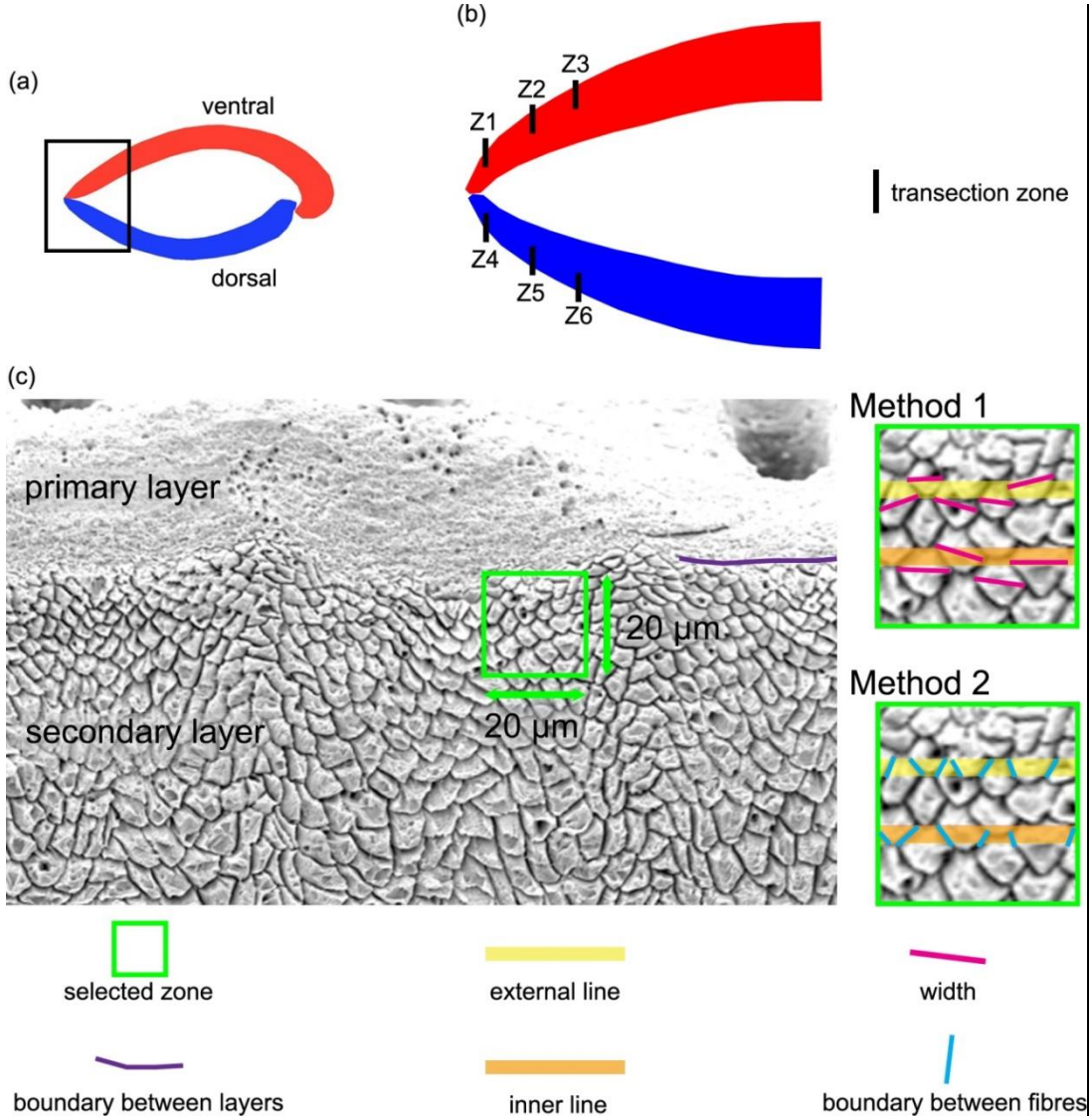

Figure 5. Methods of measurements used in the anterior transverse sections. All SEM images are oriented in the same direction: base of the primary layer facing upwards. A square (20 µm × 20 µm) with its upper side just overlapping the boundary between the primary and secondary layer was analysed. Method 1, refers to the measurement of the width of the fibres crossed by two standard lines, which were located in the same position and at the same distance in all 194 squares analysed (yellow and orange lines); Method 2, calculation of the numbers of boundaries between the fibres, which are crossed by two standard lines were carried out.

4.2.3 Carbonate stable isotopes analyses

Cleaned shells of specimens #8004, #8005, #9004, #9005 and #9006 were chosen for carbon and oxygen isotope analyses. For specimens #8005 and #9006, the primary layer and surface contaminants were manually and chemically removed by leaching with 10 % HCl, rinsed with distilled water and air–dried. Individual growth increments exclusively come from the secondary layer, and were separated from the shell in both dorsal and ventral valves using a WECHEER (WE 248) microdrill with tungsten–carbide milling bit. Shell increment fragments, of similar width, were then powdered using an agate mortar and pestle. For carbon and oxygen isotope analyses about 250 µg of powdered calcite of each sample was analysed with a Finnigan GasBench connected to a Delta V (Thermo Fisher Scientific Inc., Waltham, Massachusetts, USA) mass spectrometer at the Dipartimento di Scienze della Terra, Università degli Studi di Milano, Italy. Isotope values ($\delta^{18}O$, $\delta^{13}C$) are reported as per mil (‰) deviations of the isotopic ratios ($^{18}O/^{16}O$, $^{13}C/^{12}C$) calculated to the V-PDB scale using a within–run laboratory internal standard (MAMI) calibrated against the International Atomic Energy Agency 603 (IAEA-603; $\delta^{18}O$: -2.37 ± 0.04 ‰, $\delta^{13}C$: +2.46 ± 0.01 ‰) and NBS 18 ($\delta^{18}O$: -23.2 ± 0.1 ‰, $\delta^{13}C$: -5.014 ± 0.035 ‰) standards. Analytical reproducibility (1σ) for these analyses was better than 0.04‰ for $\delta^{13}C$ and 0.1‰ for $\delta^{18}O$ (Appendix 1). Another set of shells, #8004, #9004 and #9005, were gently rinsed with ultra pure water (Milli–Q) and dried for a few days on a hotplate at 40 °C in a clean flow hood. Targeted parts of the shell were sampled for powder under binoculars using a precision drill (Proxxon) with a mounted dental tip. Stable isotope analyses of powders of these specimens were performed at GEOMAR, Kiel on a Thermo Finnigan MAT 252 mass spectrometer coupled online to an automated Kiel carbonate preparation line. The external reproducibility (1σ) of in–house carbonate standards was better than ± 0.1 ‰ and ± 0.08 ‰ for $\delta^{13}C$ and $\delta^{18}O$, respectively (Appendix 2).

4.2.4 Stable isotopes analyses of water samples

In addition to carbon and oxygen isotope analyses of shells, analyses were also carried out on seawater samples collected from the culturing tanks. Measurements of $\delta^{13}C_{DIC}$ and $\delta^{18}O_{H2O}$ were performed using Thermo Scientific™ Delta Ray™ IRIS with URI Connect.

Isotope values ($\delta^{13}C$, $\delta^{18}O$) are reported as per mil (‰) deviations of the isotopic ratios ($^{13}C/^{12}C$, $^{18}O/^{16}O$) calculated to the VPDB scale for $\delta^{13}C$ and VSMOW scale for $\delta^{18}O$ values. Analytical reproducibility (1σ) on 3 aliquots of each water sample, was ≤ 0.03‰ for both $\delta^{13}C$ and $\delta^{18}O$ values (Appendix 3).

4.3 Results

4.3.1 Primary layer thickness

The thickness of the primary layer was measured at different positions along the shell from the posterior (umbonal) region to the *before–culturing* portion and finally to the anterior valve margin (Figure 6). Generally, in the posterior part of *M. venosa,* the primary layer is missing, or it has the lowest recorded thickness. Then the primary layer progressively thickens toward the central and anterior parts. The thickest primary layer within the same valve is always located just before the beginning of the culture (*before–culturing* portion, Table 5). During culturing the thickness of the primary layer decreases. A most distinct change was observed in specimen #9006 cultured at the lowest pH condition (pH_1: pH 7.6, and pH_2: pH 7.35) followed by another progressive increase in both

valves *during–culturing*. In contrast, the thickness of the primary layer of the control condition specimen (#8005) remained stable (dorsal valve) or slightly decreased (Figure 6, ventral valve; Table 5).

Table 5. Statistical comparison of thickness of the primary layer (µm) along the ontogenetic direction of both valves of specimens #8005 and #9006. ①: Specific positions see Figure 6. N = number of measurement. Significant values (*p*–value ≤ 0.05) are marked in bold style.

Sample	Position①	N	Mean	STD	Min	Max	*p*-values	*p*-values
#8005 dorsal	P	4	11.82	1.05	10.55	13.02	P vs C1 0.755 C1 vs C2 < **0.001** C2 vs A1 **0.033** A1 vs A2 0.726 A2 vs A3 NA	#8005DP vs #9006DP 0.120
	C1	8	11.40	2.29	8.50	15.05		#8005DC1 vs #9006DC1 < **0.001**
	C2	10	28.99	4.79	22.15	36.65		#8005DC2 vs #9006DC2 < **0.001**
	A1	8	24.36	2.52	19.80	27.06		#8005DA1 vs #9006DA1 0.088
	A2	7	24.83	2.15	21.67	27.94		#8005DA2 vs #9006DA2 0.101
	A3	1	21.77	NA	NA	NA		#8005DA3 vs #9006DA3 NA
#8005 ventral	P	2	17.64	2.36	15.28	20	P vs C1 NA C1 vs C2 < **0.001** C2 vs A1 **0.028** A1 vs A2 0.289 A2 vs A3 **0.017**	#8005VP vs #9006VP NA
	C1	6	13.68	3.96	8.50	20.52		#8005VC1 vs #9006VC1 0.123
	C2	8	47.57	2.49	42.55	50.27		#8005VC2 vs #9006VC2 0.194
	A1	8	44.18	2.68	38.33	47.98		#8005VA1 vs #9006VA1 < **0.001**
	A2	6	42.09	3.85	36.06	45.04		#8005VA2 vs #9006VA2 **0.007**
	A3	4	34.09	3.51	29.63	37.52		#8005VA3 vs #9006VA3 **0.027**
#9006 dorsal	P	7	9.08	2.77	5.56	14.64	P vs C1 < **0.001** C1 vs C2 < **0.001** C2 vs A1 < **0.001** A1 vs A2 0.779 A2 vs A3 0.096	
	C1	10	18.78	2.04	16.90	22.50		
	C2	11	46.91	5.22	35.92	55.86		
	A1	10	28.83	6.65	19.04	39.93		
	A2	8	28.06	4.03	22.50	36.69		
	A3	4	32.84	3.55	29.10	38.65		
#9006 ventral	P	7	9.78	1.72	6.07	11.79	P vs C1 < **0.001** C1 vs C2 < **0.001** C2 vs A1 < **0.001** A1 vs A2 0.102 A2 vs A3 **0.008**	
	C1	9	16.75	2.77	12.61	21.29		
	C2	12	45.16	4.34	35.09	51.40		
	A1	11	36.92	3.82	26.62	42.54		
	A2	4	32.95	2.91	30.84	37.95		
	A3	5	40.55	2.63	37.78	45.23		

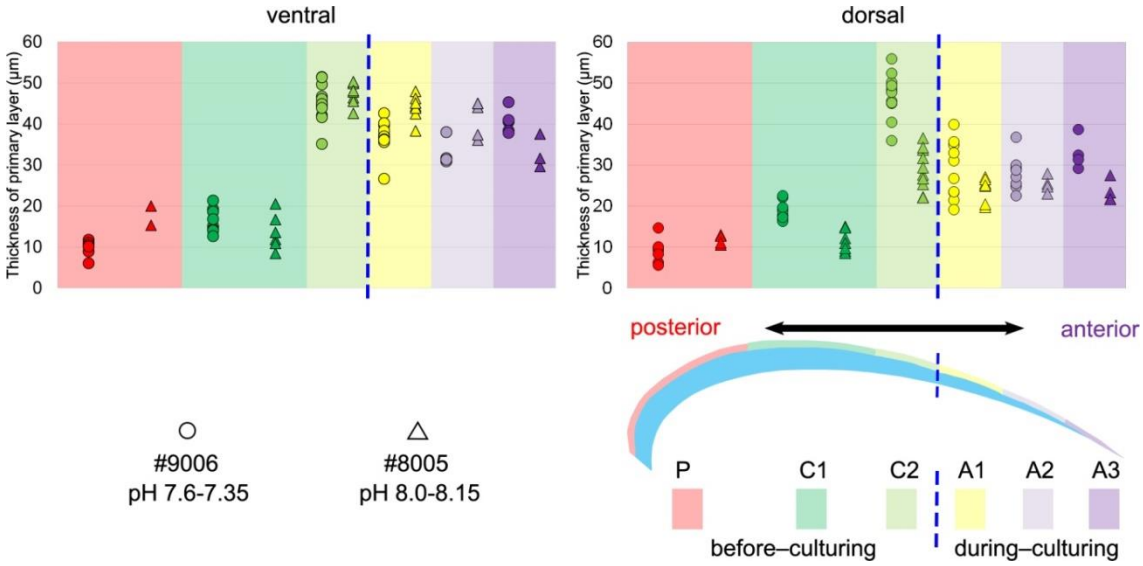

Figure 6. Variations of the thickness of the primary layer (ventral and dorsal valve) of a *M. venosa* specimen cultured at pH 7.35 and 7.6 (#9006) and a specimen cultured at pH 8.0 - 8.15 (#8005).

4.3.2 Endopunctae density and size

On the externally–ground surface of the anterior part, the total number and the diameter (max) of endopunctae in a squared frame (800 µm × 800 µm) was measured in four zones of the *before-culturing* and of the *during–culturing* parts of the shell (Figure 7). Generally, the density of endopunctae gradually increases along the selected transect (from ca. 185 /mm^2 to ca. 305 /mm^2 in ventral valve and from ca. 220 /mm^2 to ca. 280 /mm^2; Table 6). The size of endopunctae increases along the selected transect in the ventral valve (from ca. 17 µm to 33 µm; Table 7), but it slightly decreases in the dorsal valve (from ca. 36 µm to ca. 21 µm; Table 7). These trends are observed in both specimens cultured at different pH conditions. However, it is worth noting that in the most anterior part (*during–culturing*) of the ventral valve of #9006 (cultured at pH_2: pH 7.35), the density of endopunctae sharply increases and their diameter reaches the maximum recorded values (Table 6).

Table 6. Statistical comparison of the number of endopunctae (per mm^2) on both valves of #8005 and #9006. ①: Specific zones see to Figure 7. N = number of measurement.

Sample	Zone①	N	Mean	STD	Min	Max
#8005 dorsal	C2	3	236	8.6	225	250
	A1	1	280	NA	NA	NA
	A2	2	244	12.5	231	256
	A3	2	281	14	267	295
#8005 ventral	C2	2	225	1.6	223	227
	A1	1	242	NA	NA	NA
	A2	2	241	5.5	236	247
	A3	2	269	6.3	263	275
#9006 dorsal	C2	2	221	8.6	213	230
	A1	1	269	NA	NA	NA
	A2	2	250	3.1	247	253
	A3	2	266	3.1	263	269
#9006 ventral	C2	2	186	3.1	183	189
	A1	1	234	NA	NA	NA
	A2	2	230	4.7	225	234
	A3	2	308	1.6	306	309

Table 7. Statistical comparison of the diameter (max) (μm) of endopunctae on both valves of #8005 and #9006. ①: Specific zones see Figure 7. N = number of measurement. Significant values (*p*-value ≤ 0.05) are marked in bold style.

Sample	Zone①	N	Mean	STD	Min	Max	*p*-values	*p*-values
#8005D	C2	21	36.04	1.78	33.2	40.4	C2 vs A1 < **0.001**	#8005DC2 vs #9006DC2 **0.025**
	A1	10	28.36	2.33	25	32.1	A1 vs A2 < **0.001**	
	A2	15	18.77	1.10	17	21.1	A2 vs A3 **0.001**	#8005DA1 vs #9006DA1 < **0.001**
	A3	13	21.8	2.53	18.2	26.2		
#8005V	C2	11	17.07	1.42	13.6	18.9	C2 vs A1 < **0.001**	#8005DA2 vs #9006DA2 < **0.001**
	A1	13	20.88	2.22	17.1	24.3	A1 vs A2 **0.007**	
	A2	12	18.74	0.84	18	20.9	A2 vs A3 < **0.001**	#8005DA3 vs #9006DA3 < **0.001**
	A3	14	26.83	2.83	23	33.1		
#9006D	C2	12	32.54	4.39	26.2	40	C2 vs A1 0.178	#8005VC2 vs #9006VC2 < **0.001**
	A1	13	34.63	2.33	29	37.2	A1 vs A2 **0.012**	
	A2	11	32.02	2.12	27.5	36.1	A2 vs A3 **0.005**	
	A3	19	28.75	3.51	23	34.4		
#9006V	C2	13	29.98	2.04	24.3	33	C2 vs A1 < **0.001**	#8005VA1 vs #9006VA1 < **0.001**
	A1	12	38.66	2.41	35.5	42.6	A1 vs A2 < **0.001**	
	A2	14	32.51	4.08	25.3	40.3	A2 vs A3 0.516	#8005VA2 vs #9006VA2 < **0.001**
	A3	24	33.70	5.82	22	44.3		

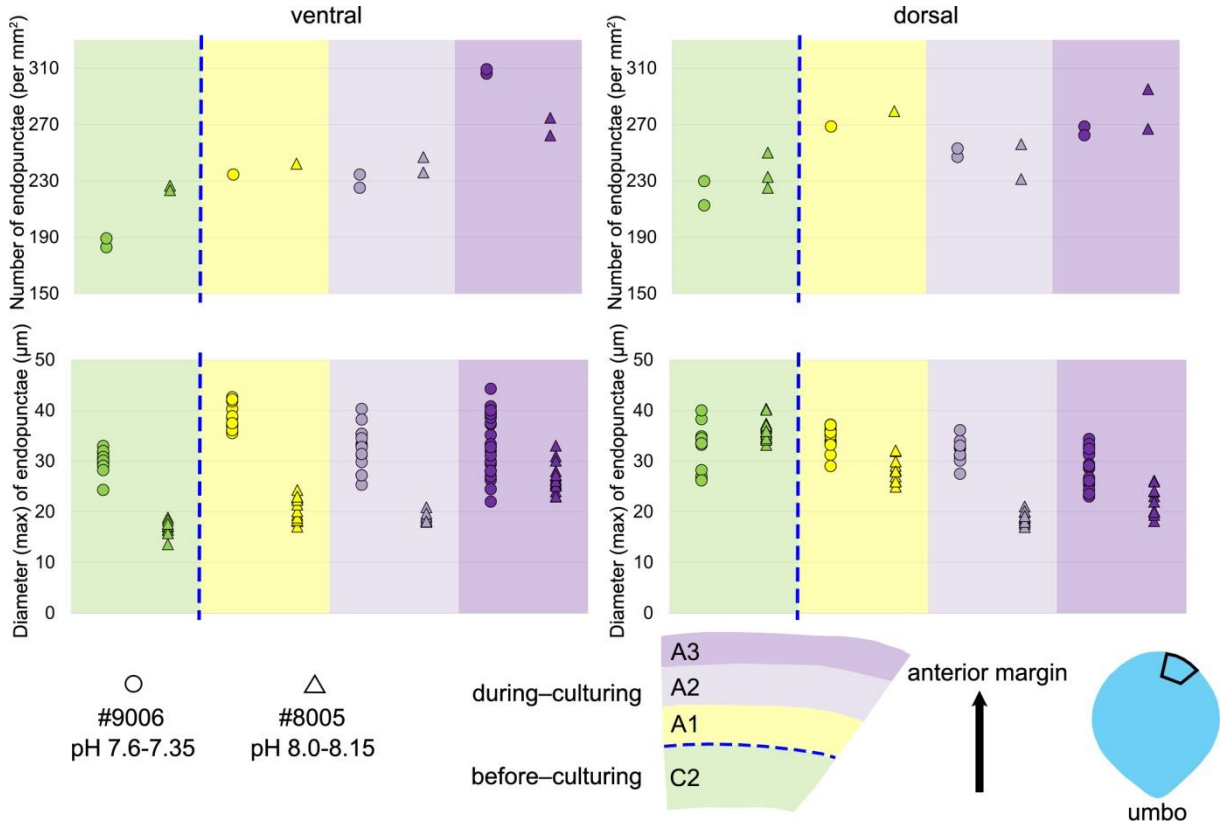

Figure 7. Variations in the number and diameter (max) of endopunctae in the ventral and dorsal valve from a specimen of *M. venosa* cultured at pH 7.35 and 7.6 (#9006) and a specimen cultured at pH 8.0–8.15 (#8005).

4.3.3 Shell morphometrics

Before–culturing

Ontogenetic variation in fibre morphometry is not obvious when all six adult specimens are considered (Table 8). However, clearer growth trends can be observed when considering the data from each single specimen separately, where *t*-tests on morphometric data from specimens #8005 and #9006 show that there are significant differences in Feret diameter (max) and Roundness between the posterior and the middle part of the shell (Table 9). Overall, in specimens #8005 and #9006 fibres become wider from the posterior to mid–shell. In contrast, #63 shows an opposite trend along the posterior to mid-shell direction (Figure 8). The fibre size and shape in the other specimens are rather constant.

Table 8. Statistical comparison of fibres size and shape data of the posterior external vs central middle parts of both the ventral valve and the dorsal valve. NC: non–cultured samples #158, #223; CU: cultured samples #43, #63, #8005, #9006; Vpe: ventral posterior external, Vcm: ventral central middle, Dpe: dorsal posterior external, Dcm: dorsal central middle, N: number of measurement. Significant values (p–value ≤ 0.05) are marked in bold style.

Sample	Position	N	Mean	STD	Min	Max	p-values
Feret diameter (max) (µm):							
NC	Vpe	7	13.79	3.22	6.97	17.33	NC Vpe vs CU Vpe 0.486 NC Vcm vs CU Vcm 0.633
CU	Vpe	26	12.47	6.58	4.59	24.78	NC Vpe vs NC Vcm 0.533 CU Vpe vs CU Vcm 0.572
NC	Vcm	32	12.98	2.91	7.09	20.61	
CU	Vcm	65	13.24	2.15	8.68	18.84	
NC	Dpe	8	18.36	4.22	13.30	24.46	NC Dpe vs CU Dpe **0.012** NC Dcm vs CU Dcm 0.373
CU	Dpe	12	10.78	6.36	4.85	22.29	NC Dpe vs NC Dcm **0.012** CU Dpe vs CU Dcm 0.391
NC	Dcm	12	12.14	1.13	9.84	14.42	
CU	Dcm	46	12.51	1.57	9.45	15.89	
Roundness:							
NC	Vpe	7	0.308	0.077	0.239	0.475	NC Vpe vs CU Vpe 0.717 NC Vcm vs CU Vcm 0.396
CU	Vpe	26	0.296	0.074	0.172	0.446	NC Vpe vs NC Vcm 0.296 CU Vpe vs CU Vcm 0.146
NC	Vcm	29	0.282	0.051	0.179	0.389	
CU	Vcm	65	0.272	0.051	0.180	0.421	
NC	Dpe	8	0.220	0.034	0.169	0.268	NC Dpe vs CU Dpe **0.003** NC Dcm vs CU Dcm **0.028**
CU	Dpe	12	0.337	0.100	0.155	0.500	NC Dpe vs NC Dcm **0.005** CU Dpe vs CU Dcm **0.048**
NC	Dcm	11	0.311	0.068	0.192	0.416	
CU	Dcm	48	0.269	0.051	0.162	0.378	
Convexity:							
NC	Vpe	7	0.985	0.004	0.979	0.991	NC Vpe vs CU Vpe 0.309 NC Vcm vs CU Vcm 0.655
CU	Vpe	26	0.982	0.008	0.968	0.999	NC Vpe vs NC Vcm 0.823 CU Vpe vs CU Vcm 0.257
NC	Vcm	32	0.984	0.005	0.975	1.000	
CU	Vcm	62	0.984	0.008	0.965	1.008	
NC	Dpe	8	0.987	0.006	0.979	0.998	NC Dpe vs CU Dpe 0.604 NC Dcm vs CU Dcm 0.273
CU	Dpe	11	0.985	0.007	0.973	0.998	NC Dpe vs NC Dcm 0.543 CU Dpe vs CU Dcm 0.207
NC	Dcm	12	0.984	0.008	0.973	1.000	
CU	Dcm	48	0.982	0.008	0.967	1.001	

Table 9. Statistical comparison of fibres size and shape data of the posterior external vs central middle area for #8005 and #9006, considering both valves together. pe: posterior external, cm: central middle, N: number of measurement. Significant values (p–value ≤ 0.05) are marked in bold style.

Sample	Position	N	Mean	STD	Min	Max	p-values
Feret diameter (max) (µm):							
#8005	pe	10	7.92	3.30	4.85	14.97	#8005 pe vs #9006 pe 0.265
#8005	cm	36	12.29	1.64	9.63	15.89	#8005 cm vs #9006 cm 0.171
#9006	pe	10	6.45	1.95	4.59	11.41	#8005 pe vs #8005 cm **0.003**
#9006	cm	25	11.73	1.39	8.68	15.24	#9006 pe vs #9006 cm < **0.001**
Roundness:							
#8005	pe	10	0.33	0.097	0.155	0.446	#8005 pe vs #9006 pe 0.547
#8005	cm	36	0.25	0.045	0.162	0.374	#8005 cm vs #9006 cm **0.012**
#9006	pe	10	0.35	0.079	0.232	0.500	#8005 pe vs #8005 cm **0.040**
#9006	cm	26	0.28	0.043	0.195	0.369	#9006 pe vs #9006 cm **0.022**
Convexity:							
#8005	pe	10	0.981	0.007	0.973	0.994	#8005 pe vs #9006 pe 0.308
#8005	cm	35	0.982	0.008	0.968	1.001	#8005 cm vs #9006 cm 0.277
#9006	pe	9	0.985	0.007	0.975	0.999	#8005 pe vs #8005 cm 0.829
#9006	cm	26	0.984	0.007	0.967	1.001	#9006 pe vs #9006 cm 0.775

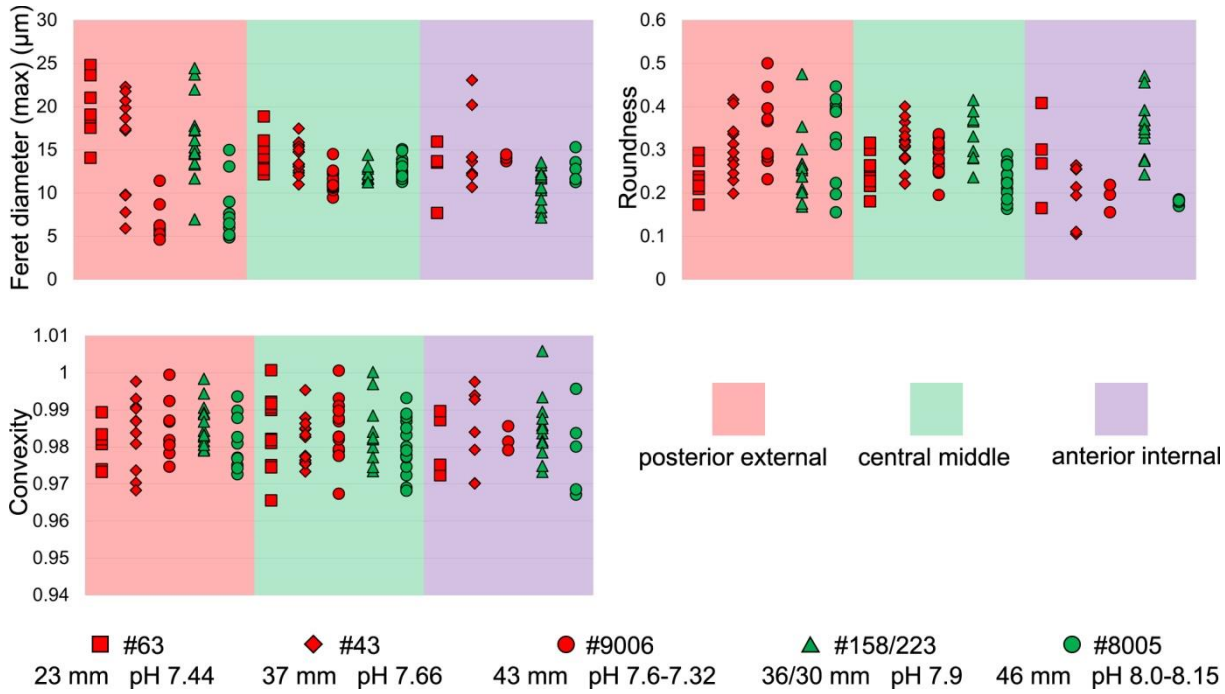

Figure 8. Comparisons of the fibre size and shape of *M. venosa* (ventral and dorsal valve) at different positions along the posterior-anterior axis; pH conditions of culturing or natural environment are reported. One circle point represents one measurement. Outliers have been removed, the latter were identified with Tukey's fences (Tukey, 1977), when falling outside the fences F1 and F2 [F1 = Q1 - 1.5IQR; F2 = Q3 + 1.5IQR; Q1/Q3 = first/third quartiles; IQR (interquartile range) = Q3 - Q1].

During–culturing

Transverse sections obtained by smoothing of the anterior part of the shell allowed to measure the width of 1392 fibres [Max Ferret diameter (max) see in Method 1], and select 388 sub–zones for fibre boundary calculation. In addition, they allowed us to focus on the parts that were produced under the different low–pH treatments (pH_1, pH_2, pH_3 and pH_4, respectively).

In all six specimens, the width of fibres increases and the number of boundaries decreases along a transect from the more external subzone to the immediately inner subzone (e.g., Z1–1 to Z1–2; Z2–1 to Z2–2; and Z3–1 to Z3–2 in Figure 9A, B, C, D). That means, even within less than 10 µm distance, the size of fibres become larger from the exterior to the interior part of the shell with growth.

Results from #9006 were compared to those of control specimen #8005 (pH_0). Specimen #9006 cultured under low–pH conditions (pH_1 and pH_2) had narrower fibres and a higher number of fibre boundaries when compared to that of control specimen #8005 (Figure 9A, C). It is worth noting that, in comparison between the two specimens, the fibres from Z1–2 and Z2–2 of #9006 are significantly smaller than those of #8005. However, there is no significant difference in the size of fibres from subzone Z3–2 between the two specimens (Table 10).

The results from specimens (#43 and #63) grown under low pH conditions (pH_3 and pH_4) for a short time interval of 214 days are difficult to interpret, as in this case, there is no direct control experiment sample to compare with the cultured specimens (Figure 9B, D). The specimens grown in the natural environment (#158, #223) have a different size and age and so different growth rates may affect the size of the fibres.

Table 10. Statistical comparison of fibres size of *M. venosa* (ventral and dorsal valve) in the anterior transverse sections. ①: specific zones see Figure 9. N: number of measurement. Significant values (p–value ≤ 0.05) are marked in bold style.

Sample	position①	N	Mean (µm)	STD	Min (µm)	Max (µm)	Difference between means (µm) and (p–values)	Difference between means (µm) and (p–values)	Difference between means (µm) and (p–values)
							#9006 vs #8005 for the same zone	Z1 vs Z2, Z2 vs Z3 for the same vertical position in the same specimen	Z1vs Z2, Z2 vs Z3 for the same transverse position in the same specimen
#9006	Z1–1	26	4.43	1.06	2.86	6.74	0.23 (0.402)		
#8005	Z1–1	49	4.66	1.13	1.89	7.37		#9006 Z1–1 vs Z2–1 **0.60 (0.013)**	
#9006	Z2–1	53	3.83	0.66	2.76	5.30	0.12 (0.419)	#9006 Z2–1 vs Z3–1 0.07 (0.650)	
#8005	Z2–1	65	3.95	1.03	2.06	6.46			
#9006	Z3–1	38	3.76	0.80	2.32	5.55	0.32 (0.134)	#8005 Z1–1 vs Z2–1 **0.71 (0.001)**	#9006 Z1 vs Z2 **0.48 (0.011)**
#8005	Z3–1	44	4.08	1.05	2.22	7.53		#8005 Z2–1 vs Z3–1 0.13 (0.554)	#9006 Z2 vs Z3 0.14 (0.323)
#9006	Z1–2	26	4.71	1.27	2.76	8.38	**0.74 (0.024)**		#8005 Z1 vs Z2 **0.59 (< 0.001)**
#8005	Z1–2	46	5.45	1.29	2.94	10.43		#9006 Z1–2 vs Z2–2 0.33 (0.200)	
#9006	Z2–2	48	4.38	0.90	2.87	7.00	**0.62 (0.001)**	#9006 Z2–2 vs Z3–2 0.30 (0.144)	#8005 Z2 vs Z3 0.09 (0.595)
#8005	Z2–2	59	5.00	0.97	2.94	7.16		#8005 Z1–2 vs Z2–2 **0.45 (0.048)**	
#9006	Z3–2	40	4.68	1.01	2.57	7.76	0.40 (0.087)	#8005 Z2–2 vs Z3–2 0.08 (0.720)	
#8005	Z3–2	38	5.08	1.00	3.02	7.78			
#9006	Z4–1	23	3.79	0.71	2.72	4.99	**0.72 (0.003)**		
#8005	Z4–1	58	4.51	1.02	2.15	7.11		#9006 Z4–1 vs Z5–1 0.11 (0.594)	
#9006	Z5–1	24	3.68	0.72	2.54	5.19	NA		#9006 Z4 vs Z5 0.09 (0.615)
#9006	Z4–2	33	4.61	0.89	3.15	6.55	0.24 (0.272)		
#8005	Z4–2	52	4.85	1.01	3.07	6.90		#9006 Z4–2 vs Z5–2 0.06 (0.811)	
#9006	Z5–2	24	4.67	1.08	2.79	7.48	NA		
							#63 vs #43 vs #158/223 for the same zone	Z1 vs Z2 for the same vertical position in the same specimen	Z1 vs Z2 for the same transverse position in the same specimen
#63	Z1–1	36	3.37	0.59	2.39	4.97			
#43	Z1–1	70	3.73	0.98	1.63	6.94	#63 vs #158/223 **0.40 (0.013)**		
#158/223	Z1–1	29	2.97	0.66	2.03	4.52	#43 vs #158/223 **0.76 (< 0.001)**	#63 Z1–1 vs Z2–1 **0.72 (< 0.001)**	
#63	Z2–1	24	4.09	0.75	2.84	5.85		#43 Z1–1 vs Z2–1 0.26 (0.109)	
#43	Z2–1	61	3.99	0.82	1.95	5.88	#63 vs #158/223 0.17 (0.404)	#158/223 Z1–1 vs Z2–1 0.95 **(< 0.001)**	
#158/223	Z2–1	56	3.92	0.83	2.17	6.14	#43 vs #158/223 0.07 (0.691)		#63 Z1 vs Z2 **0.80 (< 0.001)**
#63	Z1–2	35	4.02	0.87	2.56	6.19			#43 Z1 vs Z2 **0.40 (0.001)**
#43	Z1–2	71	4.04	0.87	2.16	7.24	#63 vs #158/223 **0.73 (0.001)**		#158/223 Z1 vs Z2 **1.2 (< 0.001)**
#158/223	Z1–2	25	3.29	0.67	2.04	4.73	#43 vs #158/223 **0.75 (< 0.001)**	#63 Z1–2 vs Z2–2 **0.95 (< 0.001)**	
#63	Z2–2	20	4.97	0.95	3.64	7.19		#43 Z1–2 vs Z2–2 **0.58 (0.001)**	
#43	Z2–2	56	4.62	1.10	2.68	7.67	#63 vs #158/223 0.28 (0.234)	#158/223 Z1–2 vs Z2–2 **1.4 (< 0.001)**	
#158/223	Z2–2	55	4.69	0.85	3.02	7.09	#43 vs #158/223 0.07 (0.688)		

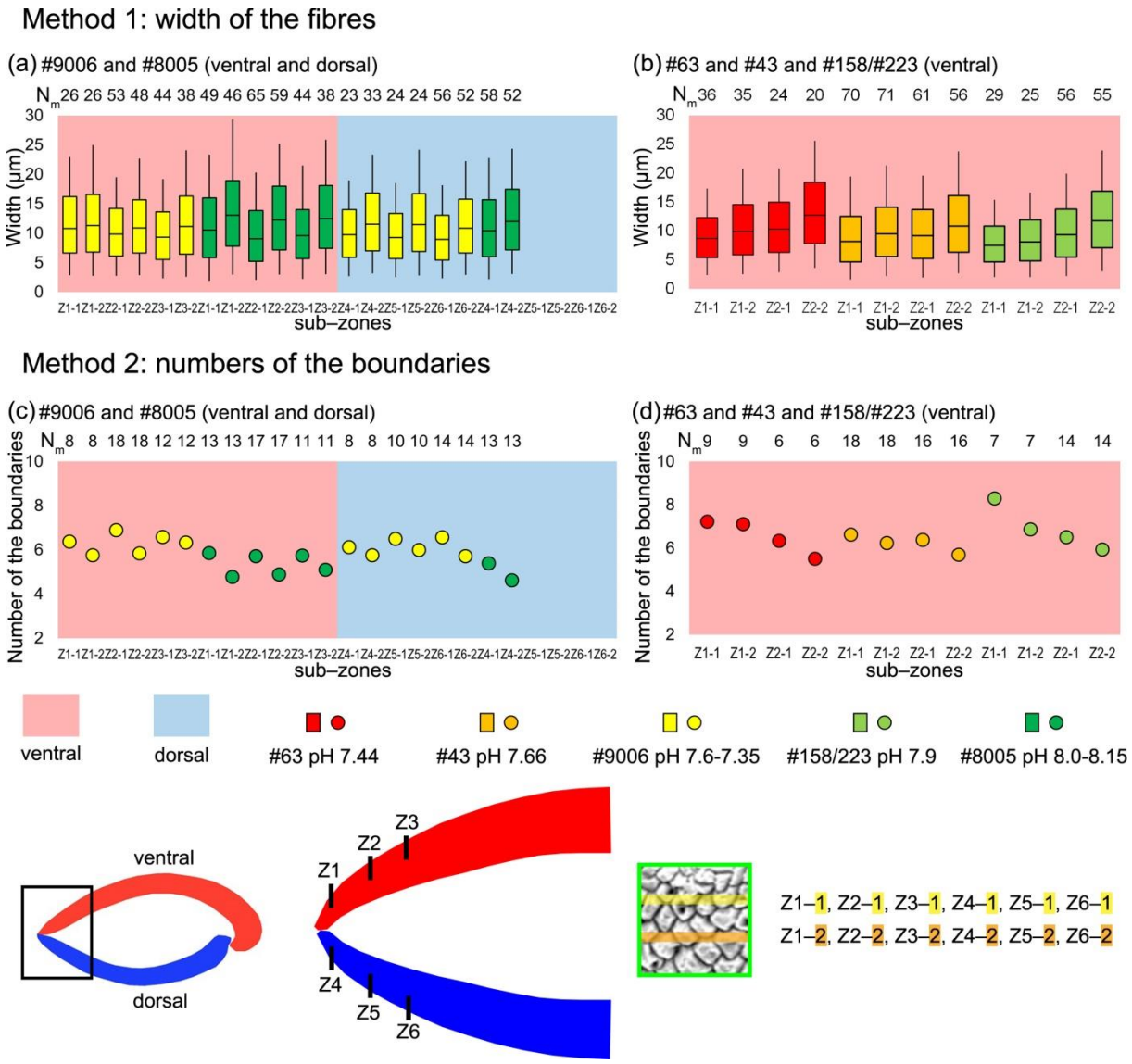

Figure 9. Differences in sizes of fibres of *M. venosa* (ventral and dorsal valve) in the anterior transverse sections of specimens cultured at different pH conditions. A, B: The bottom/top of the box and the band inside the box are the first/third quartiles and the median of the data respectively; ends of the whiskers represent the minimum and maximum of results. C, D: Circle point represents average data, N_m: number of measurement.

4.3.4 Stable isotopes

The $\delta^{13}C$ and $\delta^{18}O$ data were measured along the shell growth increments in the dorsal and ventral valves (Figure 10). In the *before–culturing* part, $\delta^{13}C$ values varied between -2.02 ‰ and +0.45 ‰ in the control group specimens #8004 and #8005, whereas they varied between -9.24 ‰ and -0.53 ‰ in the low pH group specimens #9004, #9005 and #9006. $\delta^{18}O$ values varied between -2.39 ‰ and +0.21 ‰ in the control group specimens #8004 and #8005, but varied between -4.92 ‰ and +0.05 ‰ in the low pH group specimens #9004, #9005 and #9006.

In the *during–culturing* part, $\delta^{13}C$ values varied between -6.80 ‰ and -1.34 ‰ in the control group specimens #8004 and #8005, whereas they varied between -27.09 ‰ and -9.69 ‰ in the low pH group specimens #9004, #9005 and #9006 (Figure 10). $\delta^{18}O$ values varied between -6.80 ‰ and -1.34 ‰ in the control group specimens #8004 and #8005, but varied between -6.97 ‰ and -5.29 ‰ in the low pH group specimens #9004, #9005 and #9006 (Figure 10).

A marked drop in $\delta^{13}C$ and $\delta^{18}O$ is recorded in the shell increments produced *during–culturing*, particularly so in the specimens grown under low pH conditions (pH_1 and pH_2), where $\delta^{13}C$ values decreased to -27.09 ‰ (Figure 10).

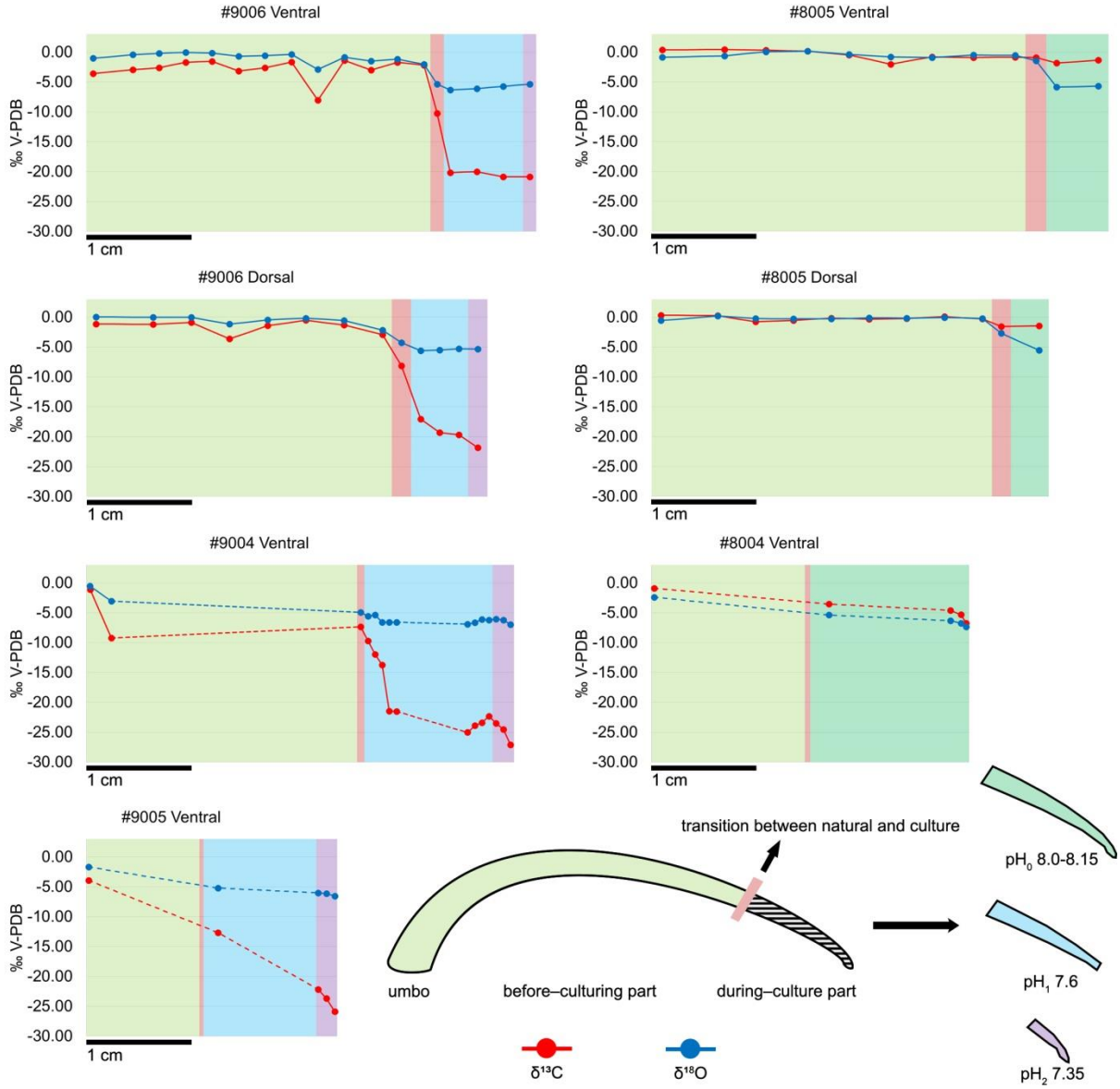

Figure 10. Plots of $\delta^{13}C$ and $\delta^{18}O$ of the ventral and dorsal valves of *M. venosa* specimens along their growth axis. Different colour backgrounds represent different pH conditions during growth. When few data were available, data-points were joined by dashed lines.

4.4 Discussion

4.4.1 Microstructure and organic components relationship

Before discussing whether and how acidification may affect the microstructure of the brachiopod shell, it is important to examine the relationship between the microstructure and the amount of organic components within the shell. It has already been stated that, in fossil and recent brachiopods, different shell microstructures have different amounts of shell organic components (Garbelli et al., 2014, 2017; Ye et al., 2018a; Casella et al., 2018).

This holds true for most rhynchonelliformean brachiopods, the primary layer of *M. venosa* consists of finely acicular and granular calcite (Williams, 1968, 1973, 1997; MacKinnon and Williams, 1974; Williams and Cusack, 2007; Casella et al., 2018). Analyses of electron back scattering diffraction show that the primary layer is produced in a thin nanocrystalline film with higher micro–hardness and smaller–sized calcite crystallites compared to those of the secondary layer (Griesshaber et al., 2004). In addition, each spherical and small unit is coated by a mixture of organics and amorphous calcium carbonate (Cusack et al., 2010). This, *per se*, may suggest a higher amount of organic components than other shell layers, but it has never been proven. In fossils, the primary layer is likely to be diagenetically altered and luminescent (Grossman et al., 1991), suggesting that higher amounts of organic components may be present. However, this has been also ascribed to the incorporation of magnesium into the lattice (Popov, et al., 2007; Cusack et al. 2008). A report of higher sulphur concentration in the primary layer of the brachiopod *Terebratulina retusa* may suggest the presence of a sulphur–rich organic components, but backscatter electron imaging revealed contradictory results (England et al., 2007). Cusack et al. (2008) showed that, in the same species, the sulphate concentration is higher in the primary layer than in the secondary layer. Depleted $\delta^{18}O$ and $\delta^{13}C$ values in the primary layer caused by kinetic effects have been reported by Carpenter and Lohmann (1995), Auclair et al. (2003), and Parkinson et al. (2005). May this indicate a greater amount of organic components in this part of the shell? Since there is no conclusive evidence for this observation, we cannot relate the increase in thickness of the primary layer to changes in organic components within the shell. With respect to previous findings (Williams, 1966; Parkinson et al., 2005), our results show that the thickness of the primary layer of *M. venosa* is much less uniform and shows an increase with growth, which is more evident during culturing at low pH conditions. However, disturbances (stress condition with handling before and at the start of the culturing) may cause an abrupt change in thickness.

Endopunctae, which in life are filled with mantle expansion, are widely distributed in the shell of *M. venosa* and show the superficial hexagonal close-packing pattern documented by Cowen (1966). The biological function of endopunctae is still controversially discussed, with some suggesting that generally, in living organism they serve as support and protection structures (Williams, 1956, 1997), as sensors, or as storage and respiration features (Pérez–Huerta et al., 2009). With more endopunctae filled by mantle expansions, the amount of organic components would increase in the same volume of shell. The density of endopunctae has been related to temperature, as species living at higher temperatures have greater endopunctae density (Campbell, 1965; Foster, 1974; Peck et al., 1987; Ackerly et al., 1993). The present analyses suggest that the increase in endopunctae density may be related in part to ontogeny; it is higher in the specimen cultured at low pH condition. This may be

expected, as specimens living under low pH conditions have to up–regulate their internal pH to be able to calcify as shown for instance in corals by McCulloch et al. (2012) and Movilla et al. (2014). This would demand a higher energetic cost and thus a larger respiration/storage surface would be favourable to cope with it.

The punctal pattern detected here is different from that observed by Cross et al. (2018), who recorded no change in the punctal density of the ventral valve of *C. inconspicua* on specimens from the last 120 years. Also different is the trend in size of the endopunctae, which measured in the dorsal valve only by Cross et al. (2018), seems to decrease in size. However, the environmental conditions of the natural ambient of 0.1 pH unit decrease and 2 ℃ increase over the last two decades (refs. in Cross et al., 2018) are very different from those of our culturing experiments. Further, the size of the endopunctae was measured from the dorsal valve only by Cross et al. (2018), whereas the increase in size we report was observed only from the ventral valve of *M. venosa*.

In addition to the thickness of the primary layer and the density of the endopunctae, the size changes of the individual fibres within the fibrous secondary layer may also contribute to the variability in organic components. Most of the recent rhynchonelliformean brachiopods, and *M. venosa* in particular, possess a shell mainly made by a fibrous secondary layer (Williams, 1997; Parkinson et al. 2005; Williams and Cusack, 2007). Each fibre of this layer is secreted by the mantle and it is ensheathed by organic membrane (e.g., Jope, 1965; Williams, 1968; MacKinnon, 1974; Williams and Cusack, 2007; Cusack et al., 2008; Casella et al., 2018; Romanin et al., 2018). Thus, with a decrease in size but within the same shell volume the surface area increases and with it the amount of organic components. Recently, the relationship between the size of fibres and the shell organic components was discussed in detail (Garbelli, 2017; Garbelli et al. 2017; Ye et al., 2018a). The main conclusion is that the smaller the calcite fibres, the higher the organic components in the shell (cf. Figure 11). Thus, smaller fibres, and a greater endopunctae density may lead to higher organic components content per shell volume (Figure 11).

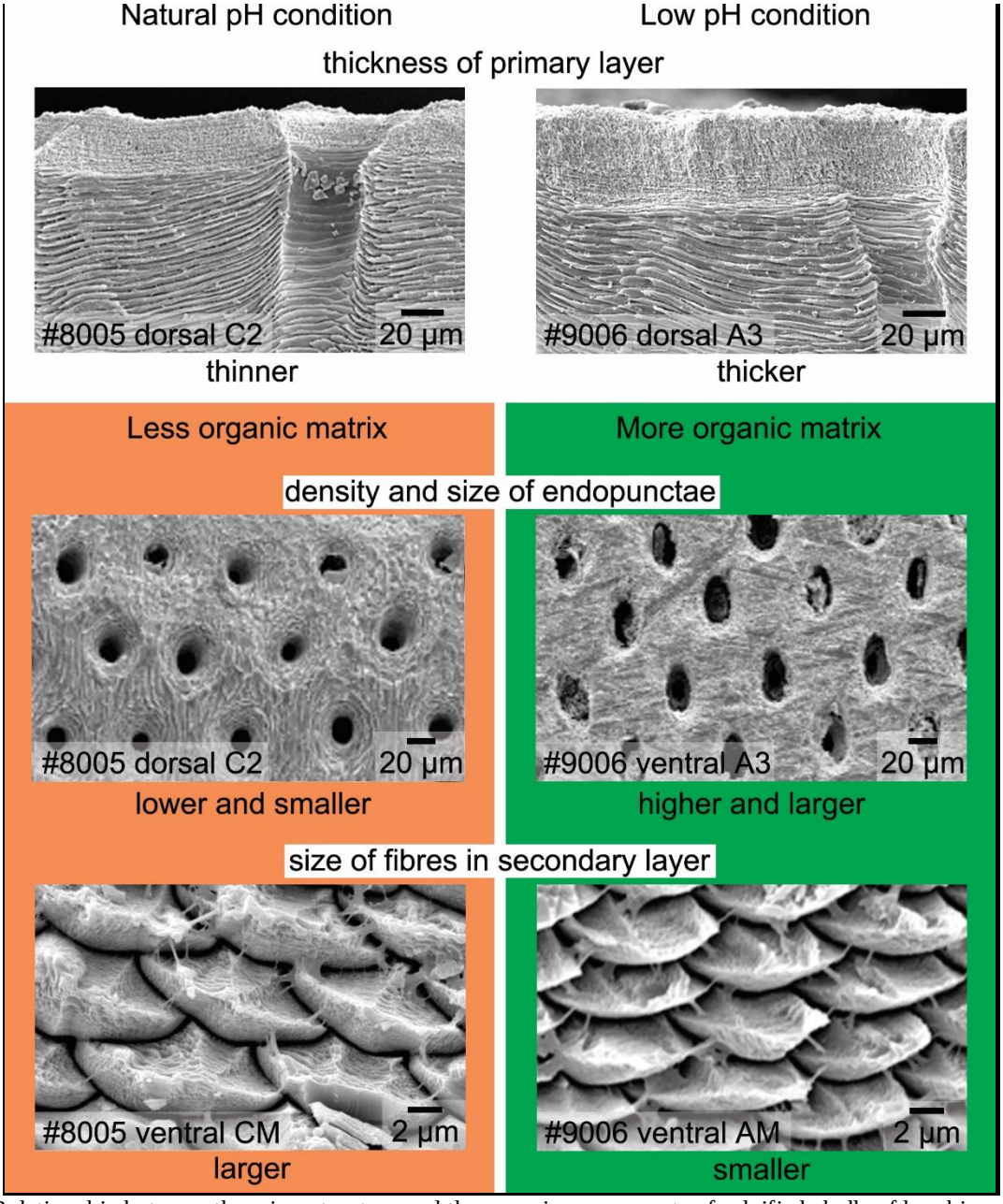

Figure 11. Relationship between the microstructure and the organic components of calcified shells of brachiopods. Position information see Figure 6 and Figure 7; CM: central middle part; AM: anterior middle part.

4.4.2 Low pH and brachiopod microstructure

Several studies tried to understand how marine carbonate shelled animals respond to ocean acidification, such as brachiopods (McClintock et al., 2009; Cross et al., 2015, 2016, 2018), bivalves (e.g., Berge et al., 2006; McClintock et al., 2009; Beniash et al., 2010; Parker et al., 2010; Melzner et al., 2011; Talmage and Gobler, 2011; Amaral et al., 2012; Hiebenthal et al., 2013; Coleman et al., 2014; Gobler et al., 2014; Milano et al., 2016), cold-water scleractinian corals (e.g., McCulloch et al., 2012; Form and Riebesell, 2012; Jantzen et al., 2013b; Büscher et al., 2017) and sea urchins (Suckling et al., 2015) (Supplementary Table 1). The results of these studies show that, in general, seawater acidification reduces the growth rates of marine calcifiers (Michaelidis et al., 2005; Shirayama and Thornton, 2005; Berge et al., 2006; Bibby et al., 2007; Beniash et al., 2010; Nienhuis et al., 2010; Thomsen and Melzner, 2010; Fernández-Reiriz et al., 2011; Melzner et al., 2011; Mingliang et al.,

2011; Talmage and Gobler, 2011; Parker et al., 2011, 2012; Liu and He, 2012; Navarro et al., 2013; Milano et al., 2016).

For the Antarctic brachiopod *Liothyrella uva* and the New Zealand brachiopod *Calloria inconspicua* no ocean acidification effects on shell growth were detected by Cross et al. (2015, 2016, 2018), although, shells of the former species may rapidly dissolve in acidified waters (McClintock et al., 2009). One response, however, appears to reinforce the shells of *C. inconspicua* by laying down a denser shell compared to specimens from New Zealand over the last 120 years while subjected to a slight decrease in pH (by 0.1) and 2 ℃ increase in temperature over the last two decades (Cross et al., 2018).

The present experiment showed that growth of specimen was not affected by the low pH conditions, instead their growth was similar of that of the specimen cultured under control conditions (#9006, ~0.9 cm in the ventral valve, ~0.8 cm in the dorsal valve; 8005, ~0.5 cm in the ventral valve, ~0.4 cm in the dorsal valve). Based on the growth von Bertalanffy growth function calculated by Baumgarten et al. (2013), the expected growth increment was calculated and compared with the measured one. Figure 12 demonstrates that the measured individual growth rates are within the range of the ones of naturally growing individuals (Fig. 12).

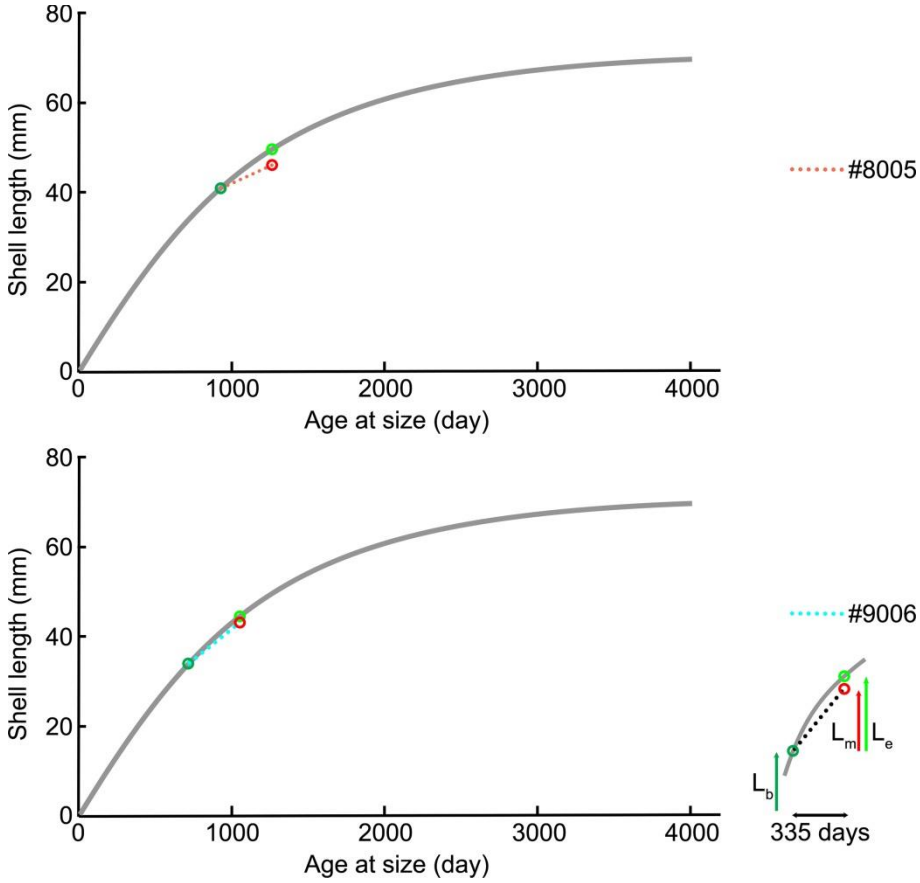

Figure 12. Projection of shell length of ventral valve on the von Bertalanffy growth function (grey line) $L_t = 71.53\ [1 - e^{-0.336(t-t0)}]$, source from Baumgarten et al. (2013), L_b: shell length at the beginning of culturing; L_m: measured shell growth at the end of culturing; Le: expected shell growth.

A limiting factor of this assessment is the limited database, but the present observations agree with studies that show no or little impact of acidification on brachiopod growth rates (Marchant et al., 2010; Thomsen et al., 2010; Talmage and Gobler, 2011; Range et al., 2011, 2012; Dickinson et al., 2012;

Fernández–Reiriz et al., 2012; Liu and He, 2012; Hiebenthal et al., 2013; Cross et al., 2015, 2016, 2018) or, even an increase in respiration, shell growth or metabolic rates after having experienced low pH condition (Wood et al., 2008; Cummings et al., 2011; Parker et al., 2012).

Therefore, the observations of marine calcifiers to seawater acidification in terms of growth rates are complex. The response of marine organisms to the interplay of several stressors such as low pH, lower dissolved oxygen and higher temperature is even more complex. Steckbauer et al. (2015) reported that hypoxia and increased pCO_2 could significantly reduce the respiration rate of marine invertebrates (Anthozoa, Gastropoda, Echinoidea and Crustacea). Highest growth rate in the bivalve *Macoma balthica* [= *Limecola balthica* (Linnaeus, 1758)] was observed in a combination of low O_2 and high pH conditions (Jansson et al., 2015). Gobler et al. (2014) reported that juveniles of the bivalves *Argopecten irradians* (Lamarck, 1819) and *Mercenaria mercenaria* (Linnaeus, 1758) are not affected when hypoxia or acidification if applied separately, but the growth rate decreases when juveniles are exposed to both conditions simultaneously.

To explore the effects of acidification on brachiopod biomineralization, the microstructures of the specimens cultured for 214 days (#43 and #63) at pH_3 and pH_4 and the other population cultured for 335 days (#8005 and #9006) at pH_0 and pH_1 to pH_2 were investigated in detail. No conclusive consideration can be carried out on the specimens cultured for 214 days, but when the culturing experiment is conducted for a time interval of 335 days, the microstructure produced by the specimen cultured at low pH conditions (pH_1 to pH_2) is different from that produced under control condition (pH_0): 1) the thickness of the primary layer increases with culturing; 2) the density and size of the endopunctae are higher; and 3) the fibres of the secondary layer are smaller. Thus, the length of culturing time–in terms of months–under low pH conditions seems to be an important control factor.

This is in line with the few data available in the literature on microstructural changes during acidification. Milano et al. (2016) reported no significant difference in the prismatic microstructure of the cockle *Cerastoderma edule* when cultured under low pH conditions for about 2 months, except for dissolution of ontogenetically younger parts of the shell. Similarly, a study by Stemmer et al. (2013) on the clam *Arctica islandica* revealed that there was no effect on the shape and size of the crystals in the homogeneous microstructure after three months of culturing at low pH (Supplementary Table 1). However, the experiments conducted by Fitzer et al. (2014a, b) for six months on the blue mussel *Mytilus edulis* showed that the animals exposed to low pH and high pCO_2 tend to produce less organised, disorientated calcite crystals and an unordered layer structure.

Thus, in bivalves, similarly to our observations, the duration of culturing may be crucial in recording significant effects. The present results lend support to the microstructure variation observed in brachiopods during the end-Permian extinction event and concomitant ocean acidification (Garbelli et al., 2017). During this event, both Strophomenata and Rhynchonellata produced more organic rich shells to cope with the long term and protracted seawater acidification effects (Garbelli et al., 2017).

4.4.3 Stable isotope variation at low pH condition

Brachiopod shells are the archives commonly used for deep–time paleoenvironmental reconstructions as they potentially record the original geochemical composition of the seawater they lived in (Grossman et al., 1993; Banner and Kaufman, 1994; Mii and Grossman, 1994; Mii et al., 2001; Brand et al., 2003, 2011, 2016; Jurikova et al., in review). Several studies suggest that oxygen and carbon

isotopic compositions of the secondary layer of brachiopod shells–especially its innermost part–tend to be in equilibrium with the seawater chemistry (e.g., Popp et al., 1986; Carpenter and Lohmann, 1995; Parkinson et al., 2005; Brand et al., 2013, 2015, 2016; Takayanagi et al., 2013; Yamamoto et al., 2013). The measured $\delta^{13}C$ and $\delta^{18}O$ values of the secondary layer produced during growth in the natural environment (Figure 10) are similar to previous results from the shells of *M. venosa* (Penman et al., 2013; Ullmann et al., 2017; Romanin et al. 2018). Furthermore, the present results show that there are no significant differences in $\delta^{13}C$ and $\delta^{18}O$ values between the dorsal and ventral valves (*p*–values in $\delta^{13}C$ and $\delta^{18}O$ of #8005 are 0.437 and 0.491 respectively, *p*–values in $\delta^{13}C$ and $\delta^{18}O$ of #9006 are 0.862 and 0.910 respectively), which are in agreement with previous findings (e.g., Parkinson et al., 2005; Brand et al., 2015; Romanin et al., 2018).

Generally, in the naturally grown shell *before–culturing*, $\delta^{13}C$ and $\delta^{18}O$ values are relatively stable along the ontogenetic direction, except for depleted values at approximately mid–shell length in both #8005 and #9006. In particular, in #9006, in this part of the shell values drop to about -6 ‰ for $\delta^{13}C$ and -2 ‰ for $\delta^{18}O$ values (Figure 10). We exclude that this drop may be produced by shell material added later, during the *during–culturing* shell thickening, as the samples were taken from the mid–shell layer and not from the shell interior. Also, negative isotope excursions of similar magnitude were recorded in *M. venosa* specimens from the South America shelf by Ullmann et al. (2017) and Romanin et al. (2018). Ullmann et al. (2017) implied that these variable $\delta^{13}C$ and $\delta^{18}O$ values indicate isotope disequilibrium with ambient waters in Terebratellids. In contrast, Romanin et al. (2018), who also analysed specimens collected from Comau Fjord, attributed the negative isotope excursion to environmental perturbations, in particular, to changes in seawater productivity and temperature, and/or to anthropogenic activities. Negative shifts in both, $\delta^{13}C$ and $\delta^{18}O$ values during ontogeny have also been observed also in in the brachiopod *Terebratella dorsata*, which co–occurs with *M. venosa* and have been explained by the effect of resorption in corresponding muscle scars (Carpenter and Lohmann, 1995). Here, we follow the interpretation of Romanin et al. (2018) to explain the mid–shell excursion observed in our specimens.

In our experiments, oxygen isotope compositions record only a minor depletion *during–culturing* at different pH conditions, a depletion which is in isotope equilibrium with $\delta^{18}O_{H2O}$ during the cultivation process [$\delta^{18}O$ (VSMOW): -6.88 ‰ for the low pH conditions and -6.69 ‰ for the control conditions].

However, a sharp drop in $\delta^{13}C$ values was observed in the secondary layer produced *during–culturing* under low pH conditions. $\delta^{13}C$ values are depleted by more than 20 ‰ in the specimens cultured at low pH conditions (pH_1 and pH_2; #9004, #9005 and #9006) (Figure 10 and Appendix), whereas the depletion is lower by just a few per mil (ca. 0.9–1.2 ‰) in the control specimens (pH_0; #8004 and #8005). Our results are comparable with those of other studies. Hahn et al. (2014) reported a decreasing trend of about 10 ‰ in $\delta^{13}C$ values in the blue mussel *Mytilus edulis* when exposed to seawater conditions of pH 8.03 (pCO_2 612 µatm) and pH of 7.21 (pCO_2 4237 µatm). In corals, a species–specific $\delta^{13}C$ response to high pCO_2 conditions was reported by Krief et al. (2010) of more negative 2.3‰ and 1.5‰ $\delta^{13}C$ values in *Porites* sp. after 14 months of culturing at low pH conditions (pH 7.49, pCO_2 1908 µatm and 7.19 pCO_2, 3976 µatm), whereas no significant difference was found in other coral species, such as *Stylophora pistillata* Esper, 1797. Given that the $\delta^{13}C_{DIC}$ in the water during the cultivation process of our specimens was low ($\delta^{13}C$ VPDB: -23.63 ‰ for the low pH conditions and -2.03 ‰ for the control conditions, which corresponds to the pH_2 phase), we can

conclude that the negative shift is probably related to the C–source in the carbon dioxide gas used in culture setup. This was also previously suggested by McConnaughey et al. (2008), Poulain et al. (2010), and Hahn et al. (2014).

The $\delta^{13}C$ and $\delta^{18}O$ composition of *M. venosa* shells produced *during-culturing* is summarized in Table 11. The fractionation of carbon and oxygen isotopes between the seawater and calcite phase, is defined as $\Delta^{13}C_{cal-DIC}$ or $\Delta^{18}O_{cal-sw} = 1000 \times \ln\alpha_{cal-DIC/sw}$, where $\alpha_{cal-DIC/sw} = [^{13}C/^{12}C]_{cal} / [^{13}C/^{12}C]_{DIC}$ or $[^{18}O/^{16}O]_{cal} / [^{18}O/^{16}O]_{sw}$, respectively.

Table 11. Carbon and oxygen fractionation in our cultured *M. venosa* specimens.

Sample #ID	Treatment	Avg. $\Delta^{13}C_{cal-DIC}$	Avg. $\Delta^{18}O_{cal-sw}$
#8004	Control	-4.06	29.99
#9005	Acidification pH_2	-1.21	30.92
#9004	Acidification pH_2	-2.23	30.70

For carbon isotopes, we observe a variability in $\Delta^{13}C_{cal-DIC}$ between the different specimens, and it is inconclusive if this is linked to an ontogenetic variations or to differences between the individuals. It appears that there is about 2 ‰ difference between the control specimen and samples from the acidification (pH_2) treatments, with the last one being, strikingly, more close to equilibrium with seawater DIC. Possibly, this illustrates the variability in kinetic effects, but may also be linked to a more changeable $\delta^{13}C_{DIC}$ in the control treatment. More measurements are however needed to fully answer this.

The $\Delta^{18}O_{cal-sw}$ values show little variability between the specimens, with similar fractionation to that of inorganically precipitated carbonates (Watkins et al., 2013; around 30 per mille at similar seawater conditions). In addition, alike in the experiment of Watkins et al. (2013), we observe a slight trend in pH, with higher $\Delta^{18}O_{cal-sw}$ at lower pH. This suggests that the $\Delta^{18}O_{cal-sw}$ behaviour of *M. venosa* is not far from that of inorganic calcite.

Thus, we think that large part of the secondary layer isotope record may reflect the environmental conditions supporting the interpretation of brachiopod shells as good archives of geochemical proxies, even when stressed by ocean acidification.

4.5 Conclusions

This study combined the analysis of shell microstructure and stable isotope geochemistry on brachiopods cultured at low pH conditions for different time intervals, and suggests the following conclusions.

In brachiopod specimens cultured for a period of 11 months, the microstructure produced by the specimen cultured at low pH is different from that produced under control conditions. In particular, the microstructure produced at low pH tends to be more organic components-rich. A result that lends strong support to the brachiopod microstructure variations observed in the fossil record and related to the effect of ocean acidification.

Low pH conditions on brachiopod shell parts precipitated during culture conditions for about one year record a change in the microstructure but not in the growth rate.

$\delta^{13}C$ and $\delta^{18}O$ values are rather constant during growth but experience a sharp drop during culturing. In particular, the $\delta^{13}C$ values of specimens cultured for one year at low pH conditions dropped abruptly. This was related to the source of carbon dioxide gas used in the culture setup

Brachiopods are thus faithful recorders of the ambient O and C isotope composition, even when stressed by environmental perturbations such as ocean acidification.

The present observations are invaluable in using specific proxies and shell morphologic features for studying ocean acidification events and changes in atmospheric CO_2 contents in the geologic past.

Acknowledgements

This project has received funding from the European Union's Horizon 2020 research and innovation programme under the Marie Skłodowska–Curie grant agreement No 643084 (BASE–LiNE Earth). We would like to express our thanks to the scientific divers and staff of the Huinay Field Station, Chile. Vreni Haussermann is thanked for logist support. We thank Nina Hörner and Ulrike Holtz for help during culturing of the brachiopods at AWI, Dirk Nürnberg at GEOMAR for assistance with isotope analyses and Curzio Malinverno and Agostino Rizzi for technical support at Università di Milano.

References

Ackerly, S., Cisne, J.L., Railsback, L.B., and Anderson, T.F.: Punctal density in the Ordovician orthide brachiopod *Paucicrura rogata*: anatomical and paleoenvironmental variation, Lethaia, 26, 17–24, 1993.

Amaral, V., Cabral, H.N., and Bishop, M.J.: Moderate acidification affects growth but not survival of 6–month–old oysters, Aquatic Ecol., 46, 119–127, 2012.

Atkinson, M.J., and Bingman, C.: Elemental composition of commercial seasalts, J. Aquaricult. Aquat. Sci., 8, 39–43, 1998.

Auclair, A.C., Joachimski, M.M., and Lécuyer, C.: Deciphering kinetic, metabolic and environmental controls on stable isotope fractionations between seawater and the shell of *Terebratalia transversa* (Brachiopoda), Chem. Geol., 202, 59–78, 2003.

Banner, J.L., and Kaufman, J.: The isotopic record of ocean chemistry and diagenesis preserved in non-luminescent brachiopods from Mississippian carbonate rocks, Illinois and Missouri, Geol. Soc. Am. Bull., 106, 1074–1082, 1994.

Baumgarten, S., Laudien, J., Jantzen, C., Häussermann, V., and Försterra, G.: Population structure, growth and production of a recent brachiopod from the Chilean fjord region, Mar. Ecol., 35, 401–413, 2013.

Beniash, E., Ivanina, A., Lieb, N.S., Kurochkin, I., and Sokolova, I.: Elevated level of carbon dioxide affects metabolism and shell formation in oysters *Crassostrea virginica*, Mar. Ecol., 419, 95–108, 2010.

Berge, J.A., Bjerkeng, B., Pettersen, O., Schaanning, M.T., and Øxnevad, S.: Effects of increased sea water concentrations of CO_2 on growth of the bivalve *Mytilus edulis* L, Chemosphere, 62, 681–687, 2006.

Bibby, R., Cleall–Harding, P., Rundle, S., Widdicombe, S., and Spicer, J.: Ocean acidification disrupts induced defences in the intertidal gastropod *Littorina littorea*, Biol. Lett., 3, 699–701, 2007.

Brand, U., Logan, A., Hiller, N., and Richardson, J.: Geochemistry of modern brachiopods: applications and implications for oceanography and paleoceanography, Chem. Geol., 198, 305–334, 2003.

Brand, U., Logan, A., Bitner, M.A., Griesshaber, E., Azmy, K., and Buhl, D.: What is the ideal proxy of Palaeozoic seawater chemistry? Mem. Assoc. Australas., 41, 9–24, 2011.

Brand, U., Azmy, K., Bitner, M.A., Logan, A., Zuschin, M., Came, R., and Ruggiero, E., Oxygen isotopes and $MgCO_3$ in brachiopod calcite and a new paleotemperature equation, Chem. Geol., 359, 23–31, 2013.

Brand, U., Azmy, K., Griesshaber, E., Bitner, M.A., Logan, A., Zuschin, M., Ruggiero, E., and Colin, P.L., Carbon isotope composition in modern brachiopod calcite: A case of equilibrium with seawater? Chem. Geol., 411, 81–96, 2015.

Brand, U., Blamey, N., Garbelli, C., Griesshaber, E., Posenato, R., Angiolini, L., Azmy, K., Farabegoli, E., and Came, R., Methane Hydrate: Killer cause of Earth's greatest mass extinction, Palaeoworld, 25, 496–507, 2016.

Büscher, J. V., Form, A. U., and Riebesell, U.: Interactive effects of ocean acidification and warming on growth, fitness and survival of the cold–water coral *Lophelia pertusa* under different food availabilities, Front. Mar. Sci., 4, 101, 2017.

Caldeira, K., and Wickett, M.E.: Anthropogenic carbon and ocean pH, Nature, 425, 365, 2003.

Caldeira, K., and Wichett, K.E.: Ocean model predictions of chemistry changes from carbon dioxide emissions to the atmosphere and ocean, J. Geophys. Res., 110, C09S04, 2005.

Campbell, K.S.W.: Australian Permian terebratuloids, Bur. Min Resour. Geol. Geophys. Aust. Bull., 68, l–113, 1965.

Carpenter S.J., and Lohmann K.C.: $\delta^{18}O$ and $\delta^{13}C$ values of modern brachiopod shells, Geochim. Cosmochim. Acta 59, 3749–3764, 1995.

Casella, L., Griesshaber, E., Simonet Roda, M., Ziegler, A., Mavromatis, V., Henkel, D., Laudien, J., Häussermann, V., Neuser, R.D., Angiolini, L., Dietzel, M., Eisenhauer, A., Immenhauser, A., Brand, U. and Schmahl, W.W.: Micro- and nanostructures reflect the degree of diagenetic alteration in modern and fossil brachiopod shell calcite: a multi–analytical screening approach (CL, FE–SEM, AFM, EBSD), Palaeogeogr. Palaeoclimatol. Palaeoecol., 502, 13–30, 2018.

Coleman, D.W., Byrne, M., and Davis, A.R.: Molluscs on acid: gastropod shell repair and strength in acidifying oceans, Mar. Ecol. Prog. Ser., 509, 203–211, 2014.

Comeau, S., Gorsky, G., Jeffree, R., Teyssie, J.L., and Gattuso, J.P.: Impact of ocean acidification on a key Arctic pelagic mollusc (*Limacina helicina*), Biogeosciences, 6, 1877–1182, 2009.

Cowen, R.: The Distribution of Punctae on the Brachiopod Shell, Geol. Mag., 103, 269–275, 1966.

Cross, E.L., Peck, L.S., and Harper, E.M.: Ocean acidification does not impact shell growth or repair of the Antarctic brachiopod *Liothyrella uva* (Broderip, 1833), J. Exp. Mar. Biol. Ecol., 462, 29–35, 2015.

Cross, E.L., Peck, L.S., Lamare, M.D., and Harper, E.M.: No ocean acidification effects on shell growth and repair in the New Zealand brachiopod *Calloria inconspicua* (Sowerby, 1846), ICES J. Mar. Sci., 73, 920–926, 2016.

Cross, E.L., Harper, E.M., and Peck, L.S.: A 120-year record of resilience to environmental change in brachiopods, Glob. Chang. Biol., https://doi.org/10.1111/gcb.14085, 2018.

Cummings, V., Hewitt, J., Rooyen, A.V., Currie, K., Beard, S., Thrush, S., Norkko, J., Barr, N., Heath, P., Halliday, N.J., Sedcole, R., Gomez, A., McGraw, C., and Metcalf, V.: Ocean acidification at high latitudes: potential effects on functioning of the Antarctic bivalve *Laternula elliptica*, PLoS ONE, 6, e16069, 2011.

Cusack, M., Dauphin Y., Cuif J.P., Salomé M., Freer A., and Yin H.: Micro–XANES mapping of sulphur and its association with magnesium and phosphorus in the shell of the brachiopod, *Terebratulina retusa*, Chem. Geol., 253, 172–179, 2008.

Cusack, M., Chung, P., Dauphin, Y., and Pérez–Huerta, A.: Brachiopod primary layer crystallography and nanostructure, in: Alvarez, F., and Curry, G.B., (Eds.): Evolution and Development of the Brachiopod Shell, Special Papers in Palaeontology, 84, Aberystwyth, Palaeontological Association, 99–105, 2010.

Crippa, G., Angiolini, L., Bottini, C., Erba, E., Felletti, F., Frigerio, C., Hennissen, J.A.I., Leng, M.J., Petrizzo, M.R., Raffi, I., Raineri, G., and Stephenson, M.H.: Seasonality fluctuations recorded in fossil bivalves during the early Pleistocene: Implications for climate change, Palaeogeogr. Palaeoclimatol. Palaeoecol., 446, 234–251, 2016a.

Crippa, G., Ye, F., Malinverno, C., and Rizzi, A.: Which is the best method to prepare invertebrate shells for SEM analysis? Testing different techniques on recent and fossil brachiopods, Boll. Soc. Paleontol. Ital., 55, 111–125, 2016b.

Dickinson, G.H., Ivanina, A.V., Matoo, O.B., Pörtner, H.O., Lannig, G., Bock, C., Beniash, E., and Sokolova, I.M.: Interactive effects of salinity and elevated CO_2 levels on juvenile Eastern oysters, *Crassostrea virginica*, J. Exp. Biol., 215, 29–43, 2012.

England, J., Cusack, M., and Lee, M.R.: Magnesium and sulphur in the calcite shells of two brachiopods, *Terebratulina retusa* and *Novocrania anomala*, Lethaia, 40, 2–10, 2007.

Feely, R.A., Sabine, C.L., Lee, K., Berelson, W., Kleypas, J., Fabry, V.J., and Millero, F.AbstractJ.: Impact of anthropogenic CO_2 on the $CaCO_3$ system in the oceans, Science, 305, 362–366, 2004.

Fernández–Reiriz, M.J., Range, P., Alvarez–Salgado, X.A., and Labarta, U.: Physiological energetics of juvenile clams *Ruditapes decussatus* in a high CO_2 coastal ocean, Mar. Ecol. Prog. Ser., 433, 97–105, 2011.

Fernández–Reiriz, M.J., Range, P., Alvarez–Salgado, X.A., Espinosa, J., and Labarta, U.: Tolerance of juvenile *Mytilus galloprovincialis* to experimental seawater acidification, Mar. Ecol. Prog. Ser., 454, 65–74, 2012.

Fitzer, S., Phoenix, V.R., Cusack, M., and Kamenos, N.A.: Ocean acidification impacts mussel control on biomineralisation, Sci. Rep., 4, doi:10.1038/srep06218, 2014a.

Fitzer, S., Cusack, M., Phoenix, V.R., and Kamenos, N.A.: Ocean acidification reduces the crystallographic control in juvenile mussel shells, J. Struct. Biol., 188, 39–45, 2014b.

Form, A.U., and Riebesell, U.: Acclimation to ocean acidification during long–term CO_2 exposure in the cold‐water coral *Lophelia pertusa*, Glob. Chang. Biol., 18, 843–3853, 2012.

Foster, M.W.: Recent Antarctic and Subantarctic brachiopods, Antarctic Research Series, 21, American Geophysical Union, Washington, D.C., pp. 183, 1974.

Försterra, G., Häussermann, V., and Lueter, C.: Mass occurrence of the recent brachiopod *Magellania venosa* (Terebratellidae) in the fjords Comau and Renihue, northern Patagonia, Chile, Mar. Ecol., 29, 342–347, 2008.

Garbelli, C., Angiolini, L., Brand, U., and Jadoul, F., Brachiopod fabric, classes and biogeochemistry: Implications for the reconstruction and interpretation of seawater carbon–isotope curves and records, Chem. Geol., 371, 60–67, 2014.

Garbelli, C.: Shell microstructures in Upper Permian brachiopods: implication for fabric evolution and calcification, Boll. Soc. Paleontol. Ital., 123, 541–560, 2017.

Garbelli, C., Angiolini, L., and Shen, S.Z.: Biomineralization and global change: A new perspective for understanding the end–Permian extinction, Geology, 45, 19–12, 2017.

Gobler, C.J., DePasquale, E.L., Griffith, A.W., and Baumann, H.: Hypoxia and acidification have additive and synergistic negative effects on the growth, survival, and metamorphosis of early life stage bivalves, PLoS ONE, 9, e83648, 2014.

Griesshaber, E., Schmahl1, W., Neuser, R., Job, R., Bluem, M., and Brand, U.: Microstructure of brachiopod shells–An inorganic/organic fibre composite with nanocrystalline protective layer, Mater. Res. Soc. Symp. Proc., 844, Y9.3.1–Y9.3.6, 2004.

Grossman, E.L., Zhang, C., and Yancey, T.E.: Stable–isotope stratigraphy of brachiopods from Pennsylvanian shales in Texas, Geol. Soc. Am. Bull., 103, 953–965, 1991.

Grossman, E.L., Mii, H., and Yancey, T.E.: Stable isotopes in Late Pennsylvanian brachiopods from the United Stated: Implications for Carboniferous paleoceanography, Geol. Soc. Am. Bull., 105, 1284–1296, 1993.

Guinotte, J.M., Orr, J., Cairns, S., Freiwald, A., Morgan, L., and George, R.: Will human–induced changes in sea water chemistry alter the distribution of deep-sea scleractinian corals? Front. Ecol. Environ., 1, 141–146, 2006.

Hahn, S., Rodolfo–Metalpa, R., Griesshaber, E., Schmahl, W.W., Buhl, D., Hall-Spencer, J.M., Baggini, C., Fehr, K.T., and Immenhauser, A.: Marine bivalve shell geochemistry and ultrastructure from modern low pH environments: environmental effect versus experimental bias, Biogeosciences, 9, 1897–1914, 2012.

Hahn, S., Griesshaber, E., Schmahl, W.W., Neuser, R.D., Ritter, A., Hoffmann, R., Buhl, D., Niedermayr, A., Geske, A., and Immenhauser, A.: Exploring aberrant bivalve shell ultrastructure and geochemistry as proxies for past sea water acidification, Sedimentology, 61, 1625–1658, 2014.

Hiebenthal, C., Philipp, E.E.R., Eisenhauer, A., and Wahl, M.: Effects of seawater pCO_2 and temperature on shell growth, shell stability, condition and cellular stress of Western Baltic Sea *Mytilus edulis* (L.) and *Arctica islandica* (L.), Mar. Biol., 160, 2073–2087, 2013.

IPCC: Climate change 2013: the physical science basis, in: Stocker, T.F., Qin, D., Plattner, G. –K., Tignor, M., Allen, S.K., Boschung, J., Nauels, A., Xia, Y., Bex, V., and Midgley, P.M. (Eds.): Contribution of working group I to the fifth assessment report of the intergovernmental panel on climate change, Cambridge University Press, Cambridge, United Kingdom and New York, NY, USA, pp. 1535, 2013.

Jansson. A., Norkko, J., Dupont, S., and Norkko, A.: Growth and survival in a changing environment: Combined effects of moderate hypoxia and low pH on juvenile bivalve *Macoma balthica*, J. Sea Res., 102, 41–47, 2015.

Jantzen, C., Laudien, J., Sokol, S., Försterra, G., Häussermann, V., Kupprat, F., and Richter, C.: In situ short-term growth rates of a cold–water coral, Mar. Freshw. Res., 64, 631–641, 2013a.

Jantzen, C., Häussermann, V., Försterra, G, Laudien, J., Ardelan, M., Maier, S., and Richter, C.: Occurrence of a cold-water coral along natural pH gradients (Patagonia, Chile), Mar. Biol., 160, 2597–2607, 2013b.

Jantzen, C., Laudien, J., Häussermann, V., Försterra, G., and Richter, C.: Seawater carbonate chemistry measured in fjord Comau, Patagonia, Chile (02-2011), Alfred Wegener Institute, Helmholtz Center for Polar and Marine Research, Bremerhaven, PANGAEA, https://doi.pangaea.de/10.1594/PANGAEA.884131, https://doi.org/10.1594/PANGAEA.884131, 2017.

Jope, H.M.: Composition of brachiopod shell, in Moore, R.C. (Ed.): Treatise on Invertebrate Paleontology. Part H, Brachiopoda, Geological society of America and University of Kansas Press, New York and Lawrence, pp. 156–164, 1965.

Jurikova, H., Liebetrau, V., Gutjahr, M., Rollion–Bard, C., Hu, M.Y., Krause, S., Henkel, D., Hiebenthal, C., Schmidt, M., Laudien, J., and Eisenhauer, A.: Boron isotope systematics of cultured brachiopod calcite: the role of vital effects, response to acidification and implications for paleo–pH reconstructions, Geochim. Cosmochim. Acta, in review.

Krief, S., Hendy, E.J., Fine, M., Yam, R., Meibom, A., Foster, G.L., and Shemesh, A.: Physiological and isotopic responses of scleractinian corals to ocean acidification, Geochim. Cosmochim. Acta, 74, 4988–5001, 2010.

Kurihara, H.: Effects of CO_2–driven ocean acidification on the early developmental stages of invertebrates, Mar. Ecol. Prog. Ser., 373, 274–284, 2008.

Lannig, G., Eilers, S., Pörtner, H.O., Sokolova, I.M., and Bock, C.: Impact of ocean acidification on energy metabolism of oyster, *Crassostrea gigas*–changes in metabolic pathways and thermal response, Mar. Drugs, 8, 2318–2339, 2010.

Laudien, J., Häussermann, V., Försterra, G., and Göhlich, H.: Physical oceanographic profiles of seven CTD casts from Gulf of Ancud into Comau Fjord in 2014, Alfred Wegener Institute, Helmholtz Center for Polar and Marine Research, Bremerhaven, PANGAEA, https://doi.org/10.1594/PANGAEA.832187, 2014.

Liu, W., and He, M.: Effects of ocean acidification on the metabolic rated of three species of bivalve from southern coast of China, Chin. J. Oceanol. Limn., 30, 206–211, 2012.

MacKinnon, D.I.: The shell structure in spiriferide brachiopoda, Bull. Br. Mus. Nat. Hist., 5, 189–258, 1974.

MacKinnon, D.I., and Williams, A.: Shell structure of terebratulid brachiopods, Palaeontology, 17, 179–202, 1974.

Marchant, H.K., Calosi, P., and Spicer, J.I.: Short–term exposure to hypercapnia does not compromise feeding, acid–base balance or respiration of *Patella vulgata* but surprisingly is accompanied by radula damage, J. Mar. Biolog. Assoc. U.K., 90, 1379–1384, 2010.

McClintock, J.B., Angus, R.A., Mcdonald, M.R., Amsler, C.D., Catledge, S.A., and Vohra, Y.K.: Rapid dissolution of shells of weakly calcified Antarctic benthic macroorganisms indicates high vulnerability to ocean acidification, Antarct. Sci., 21, 449–456, 2009.

McConnaughey, T.A., and Gillikin, D.P.: Carbon isotopes in mollusk shell carbonates, Geo–Mar. Lett., 28, 287–299, 2008.

McCulloch, M., Trotter, J., Montagna, P., Falter, J., Dunbar, R., Freiwald, A., Försterra, G., Lopez Correa, M., Maier, C., Ruggeberg, A., and Taviani, M.: Resilience of cold–water scleractinian corals to ocean acidification: Boron isotopic systematics of pH and saturation state up–regulation, Geochim. Cosmochim. Acta, 87, 21–34, 2012.

Melzner, F., Stange, P., Trübenbach, K., Thomsen, J., Casties, I., Panknin, U., Gorb, S.N., and Gutowska, M.A.: Food supply and seawater pCO_2 impact calcification and internal shell dissolution in the blue mussel *Mytilus edulis*, PLoS ONE, 6, e24223, 2011.

Michaelidis, B., Ouzounis, C., Paleras, A., and Pörtner H.O.: Effects of long-term moderate hypercapnia on acid–base balance and growth rate in marine mussels *Mytilus galloprovincialis*, Mar. Ecol. Prog. Ser., 293, 109–118, 2005.

Mii, H.S., and Grossman, E.L.: Late Pennsylvanian seasonality reflected in the ^{18}O and elemental composition of a brachiopod shell, Geology, 22, 661–664, 1994.

Mii, H.S., Grossman, E.L., Yancey, T.E., Chuvashov, B., and Egorov, A.: Isotopic records of brachiopod shells from the Russian Platform–evidence for the onset of mid–Carboniferous glaciation, Chem. Geol., 175, 133–147, 2001.

Milano, S., Schöne, B.R., Wang, S., and Müller, W.E.: Impact of high pCO_2 on shell structure of the bivalve *Cerastoderma edule*, Mar. Environ. Res., 119, 144–155, 2016.

Mingliang, Z., Jianguang, F., Jihong, Z., Bin, L., Shengmin, R., Yuze, M., and Yaping, G.: Effect of marine acidification on calcification and respiration of *Chlamys farreri*, J. Shellfish Res., 30, 267–271, 2011.

Morse, J.W., Arvidson, R.S., and Luttge, A.: Calcium carbonate formation and dissolution, Chem. Rev., 107, 342–381, 2007.

Movilla, J., Orejas, C., Calvo, E., Gori, A., López Sanz, Á., Grinyó, J., Dominguez–Carrió, C., and Pelejero, C.: Differential response of two Mediterranean cold–water coral species to ocean acidification, Coral reefs, 33, 675–686, 2014.

Navarro, J.M., Torres, R., Acuna, K., Duarte, C., Manriquez, P.H., Lardies, M., Lagos, N.A., Vargas, C., and Aguilera, V.: Impact of medium–term exposure to elevated pCO_2 levels on the physiological energetics of the mussel *Mytilus chilensis*, Chemosphere, 90, 1242–1248, 2013.

Nienhuis, S., Palmer, A.R., and Harley, C.D.G.: Elevated CO_2 affects shell dissolution rate but not calcification rate in a marine snail, Philos. Trans. R. Soc. Lond., B, Biol. Sci., 277, 2553–2558, 2010.

Orr, J.C., Fabry, V.J., Aumont, O., Bopp, L., Doney, S.C., Feely, R.A., Gnanadesikan, A., Gruber, N., Ishida, A., Joos, F., Key, R.M., Lindsay, K., Maier-Reimer, E., Matear, R., Monfray, P., Mouchet, A., Najjar, R.G., Plattner, G.K., Rodgers, K.B., Sabine, C.L., Sarmiento, J.L., Schlitzer, R., Slater, R.D., Totterdell, I.J., Weirig, M.F., Yamanaka, Y., and Yool, A.: Anthropogenic ocean acidification over the twenty–first century and its impact on calcifying organisms, Nature, 437, 681–686, 2005.

Parker, L.M., Ross, P.M., and O'Connor, W.A.: Comparing the effect of elevated pCO_2 and temperature on the fertilization and early development of two species of oysters, Mar. Biol.,157, 2435–2452, 2010.

Parker, L.M., Ross, P.M., and O'Connor, W.A.: Populations of the Sydney rock oyster, *Saccostrea glomerata*, vary in response to ocean acidification, Mar. Biol., 158, 689–697, 2011.

Parker, L.M., Ross, P.M., O'Connor, W.A., Borysko, L., Raftos, D.A., and Pörtner, H. –O.: Adult exposure influences offspring response to ocean acidification in oysters, Glob. Chang. Biol., 18, 82–92, 2012.

Parkinson, D., Curry, G.B., Cusack, M., and Fallick, A.E.: Shell structure, patterns and trends of oxygen and carbon stable isotopes in modern brachiopod shells, Chem. Geol., 219, 193–235, 2005.

Payne, J.L., and Clapham, M.E.: End–Permian mass extinction in the oceans: an ancient analog for the twenty-first century? Annu. Rev. Earth Planet. Sci., 40, 89–111, 2012.

Peck, L.S., Clarke, A., and Holmes, L.J.: Size, shape and the distribution of organic matter in the Recent Antarctic brachiopod *Liothyrella uva*, Lethaia, 20, 33–40, 1987.

Penman, D.E., Hönisch, B., Rasbury, E.T., Hemming, N.G., and Spero, H.J.: Boron, carbon, and oxygen isotopic composition of brachiopod shells: Intra–shell variability, controls, and potential as a paleo–pH recorder, Chem. Geol., 340, 32–39, 2013.

Pérez-Huerta, A., Cusack, M., McDonald, S., Marone, F., Stampanoni, M., and MacKay, S.: Brachiopod punctae: a complexity in shell biomineralisation, J. Struct. Biol., 167, 62–67, 2009.

Popp, B.N., Anderson, T.F., and Sandberg, P.A.: Brachiopods as indicators of original isotopic compositions in some Paleozoic limestones, Geol. Soc. Am. Bull., 97, 1262–1269, 1986.

Popov, L.E., Egerquist, E., and Holmer, L.E.: Earliest ontogeny of Middle Ordovician rhynchonelliform brachiopods (Clitambonitoidea and Polytoechioidea): implications for brachiopod phylogeny, Lethaia, 40, 85–96, 2007.

Poulain, C., Lorrain, A., Mas, R., Gillikin, D.P., Dehairs, F., Robert, R., and Paulet, Y.M.: Experimental shift of diet and DIC stable carbon isotopes: influence on shell $\delta^{13}C$ values in the manila clam *Ruditapes philippinarum*, Chem. Geol., 272, 75–82, 2010.

Range, P., Chícharo, M.A., Ben-Hamadou, R., Piló, D., Matias, D., Joaquim, S., Oliveira, A.P., and Chícharo, L.: Calcification, growth and mortality of juvenile clams *Ruditapes decussatus* under increased pCO_2 and reduced pH: Variable responses to ocean acidification at local scales? J. Exp. Mar. Biol. Ecol., 396, 177–184, 2011.

Range, P., Piló, D., Ben-Hamadou, R., Chícharo, M.A., Matias, D., Joaquim, S., Oliveira, A.P., and Chícharo, L.: Seawater acidification by CO_2 in a coastal lagoon environment: Effects on life history traits of juvenile mussels *Mytilus galloprovincialis*, J. Exp. Mar. Biol. Ecol., 424–425, 89–98, 2012.

Ries, J.B., Cohen, A.L., and McCorkle, D.C.: Marine calcifiers exhibit mixed responses to CO_2–induced ocean acidification, Geology, 37, 1131–1134, 2009.

Romanin, M., Crippa, G., Ye, F., Brand, U., Bitner, M.A., Gaspard, D., Häussermann, V., and Laudien J.: A sampling strategy for recent and fossil brachiopods: selecting the optimal shell segment for geochemical analyses, Riv. Ital. Paleontol. Stratigr., 124, 343–359, 2018.

Shirayama, Y., and Thornton, H.: Effect of increased atmospheric CO_2 on shallow water marine benthos, J. Geophys. Res. Oceans, 110, C09S08, doi:10.1029/2004jc002618, 2005.

Smirnova, T.N., and Popiel–Barczyk, E.: Characteristics of the shell ultrastructure in Terebratellacea, in: Brachiopods through time, MacKinnon, D. I., Lee D. E., and Campbell, J. D. (Eds.): Balkema, Rotterdam, pp. 159–165, 1991.

Steckbauer, A., Ramajo, L., Hendriks, I.R., Fernandez, M., Lagos, N.A., Prado, L., and Duarte, C.M.: Synergistic effects of hypoxia and increasing CO_2 on benthic invertebrates of the central Chilean coast, Front. Mar. Sci., 2, https://doi.org/10.3389/fmars.2015.00049, 2015.

Stemmer, K., Nehrke, G., and Brey, T.: Elevated CO_2 levels do not affect the shell structure of the bivalve *Arctica islandica* from the Western Baltic, PLoS ONE, 8, e70103, 2013.

Suckling, C.C., Clark, M.M., Richard, J., Morley, S.A., Thorne, M.A., Harper, E.M., and Peck, L.S.: Adult acclimation to combined temperature and pH stressors significantly enhances reproductive outcomes compared to short–term exposures, J. Anim. Ecol., 84, 773–784, 2015.

Takayanagi, H., Asami, R., Abe, O., and Miyajima, T.: Intraspecific variations in carbon–isotope and oxygen–isotope compositions of a brachiopod *Basiliola lucida* collected off Okinawa–jima, southwestern Japan, Geochim. Cosmochim. Acta, 115, 115–136, 2013.

Talmage, S.C., and Gobler, C.J.: Effects of elevated temperature and carbon dioxide on the growth and survival of larvae and juveniles of three species of northwest Atlantic bivalves, PLoS ONE, 6, e26941, 2011.

Thomsen, J., and Melzner, F.: Moderate seawater acidification does not elicit long-term metabolic depression in the blue mussel *Mytilus edulis*, Mar. Biol., 157, 2667–2676, 2010.

Thomsen, J., Gutowska, M.A., Saphörster, J., Heinemann, A., Trübenbach, K., Fietzke, J., Hiebenthal, C., Eisenhauer, A., Körtzinger, A., Wahl, M., and Melzner, F.: Calcifying invertebrates succeed in a naturally CO_2–rich coastal habitat but are threatened by high levels of future acidification, Biogeosciences, 7, 3879–3891, 2010.

Tukey, J.W.: Exploratory data analysis. Reading, PA: Addison–Wesley, 1977.

Ullmann, C.V., Frei, R., Korte, C., and Lüter, C.: Element/Ca, C and O isotope ratios in modern brachiopods: Species–specific signals of biomineralization, Chem. Geol., 460, 15–24, 2017.

Watkins, J.M., Nielsen, L.C., Ryerson, F.J., and DePaolo, D.J.: The influence of kinetics on the oxygen isotope composition of calcium carbonate, Earth Planet. Sci. Lett., 375, 349–360, 2013.

Watson, S., Peck, L.S., Tyler, P.A., Southgate, P.C., Tan, K.S., Day, R.W., and Morley, S.A.: Marine invertebrate skeleton size varies with latitude, temperature and carbonate saturation: implications for global change and ocean acidification, Glob. Chang. Biol., 18, 3026–3038, 2012.

Williams, A.: The calcareous shell of the Brachiopoda and its importance to their classification, Biol. Rev., 31, 243–287, 1956.

Williams, A.: Growth and structure of the shell of living articulate brachiopods, Nature, 211, 1146–1148, 1966.

Williams, A.: Evolution of the shell structure of articulate brachiopods, Spec. Pap. Palaeontol., 2, 1–55, 1968.

Williams, A.: The secretion and structural evolution of the shell of thecideidine brachiopods, Philos. Trans. R. Soc. Lond., B, Biol. Sci., 264, 439–478, 1973.

Williams, A.: Shell structure, in: Kaesler, R.L. (Ed.): Treatise on Invertebrate Paleontology, Part H, Revised, Brachiopoda, vol. 1, Geological Society of America Inc., and The University of Kansas, Boulder, Colorado, USA, pp. 267–320, 1997.

Williams, A., and Cusack, M.: Chemicostructural diversity of the brachiopod shell, in: Selden P.A. (Ed.): Treatise on Invertebrate Paleontology, Part H, Revised, Brachiopoda, vol. 6, Kansas: The Paleontological Institute, pp. 2396–2521, 2007.

Wood, H.L., Spicer, J.I., and Widdicombe, S.: Ocean acidification may increase calcification rates, but at a cost, Proc. R. Soc. Lond., B, Biol. Sci., 275, 1767–1773, 2008.

Yamamoto, K., Asami, R., and Iryu, Y.: Correlative relationships between carbon–and oxygen–isotope records in two cool-temperate brachiopod species off Otsuchi Bay, northeastern Japan, Paleontol. Res., 17, 12–26, 2013.

Ye, F., Crippa, G., Angiolini, L., Brand, U., Capitani, G., Cusack, M., Garbelli, C., Griesshaber, E., Harper, E., and Schmahl, W.: Mapping of recent brachiopod microstructure: a tool for environmental studies, J. Struct. Biol., 201, 221–236, 2018a.

Ye, F., Crippa, G., Garbelli, C., and Griesshaber, E.: Microstructural data of six recent brachiopod species: SEM, EBSD, morphometric and statistical analyses, Data in Brief, 18, 300–318, 2018b.

Chapter 5
Evolution and fabric differentiation of Palaeozoic Rhynchonelliformean brachiopod shells

Abstract

Due to the unique features of their biominerals, their high biodiversity and their dominant ecological role in Palaeozoic oceans, brachiopods are considered very robust archives to understand the evolution of marine calcifiers in changing climates and environments during the geological past. However, after the seminal works of Williams (1968, 1970, 1997), few researches have been devoted to unravel the shell microstructure of brachiopods, its evolutionary changes and fabric differentiation, in the classes Rhynchonellata and Strophomenata (Brunton, 1972; Mackinnon and Williams, 1974; Angiolini, 1993; Williams and Cusack, 2007; Garbelli et al., 2014; Garbelli, 2017). Here, a detailed study of the shell microstructure of Cambrian and Devonian brachiopods from Iran is presented. The shell microstructure of 38 brachiopod species, representatives of 22 families and 10 orders, were analysed using Scanning Electron Microscope (SEM) and a database was built, including macro- and micro-morphological features useful to characterize the shell (i.e. the size and shape of the shell, morphological measurements of structural units forming the shell layers and their organization, presence of perforations and other microstructural features). In several shells, the primary and tertiary layers were not observed. The two main microstructural variants observed are the fibrous and laminar fabrics, which constitute different types of secondary layer. Based on our data, some important considerations can be outlined: 1) Different fabrics of the secondary layer were observed in Rhynchonellata and Strophomenata; 2) the fabric of fibrous layers are comparable to the ones observed in recent brachiopods, whereas the laminar fabrics are more complex in their structural organization and they have not recent analogous; 3) brachiopods which have a fibrous secondary layer are mostly associated to biconvex shells, whereas the brachiopods which have a laminar secondary layer can be associated to a variety of shell shapes; 4) in cross section, the laminae are thinner than the fibres, which also show more variability in their thickness. Moreover, the Chonetidina, which were previously considered to bear an intermediate laminar layer composed of 'lath like-fibres', seem to have already evolved a laminar fabric during the Devonian. The number of brachiopods genera with fibrous fabric is higher than that of taxa with laminar fabric during Ordovician and Silurian, while

laminar genera began to flourish from the Devonian; this trend is consistent with the stratigraphic ranges of brachiopod groups as reported by Curry & Brunton (2007).

5.1 Materials and methods

5.1.1 Materials

A total of 95 specimens collected from different localities in Iran (Fig. 1) were selected for this study. The specimens are representative of 38 species belonging to 10 order brachiopods, spanning from Cambrian to Devonian (Table 1; Appendix 2). Most of the shells are articulated, with few of them bearing incomplete or fragmented shells, but all the specimens can be identified at generic level, and the shell orientation can still be distinguished. The material is housed in the Dipartimento di Scienze della Terra "A. Desio", Università di Milano and have been collected during several campaigns of field work in Iran. In particular, specimens labelled MRAN and NiB (Appendix 2) have been acquired based on the funded research contract "Paleontology and Biozonation of Paleozoic Sediments of Central Iran and Zagros Basins" with the Dipartimento di Scienze della Terra dell'Università di Perugia Pars Geological Reserch Center, Tehran (Angiolini, unpublished reports 2013-2016). Specimens labelled KE, have been collected during field work in the Kerman region, Central Iran in October 2016 (for details on the section see Percival et al., 2009). A few specimens (labelled LA) are from older collection housed at the Dipartimento di Scienze della Terra "A. Desio".

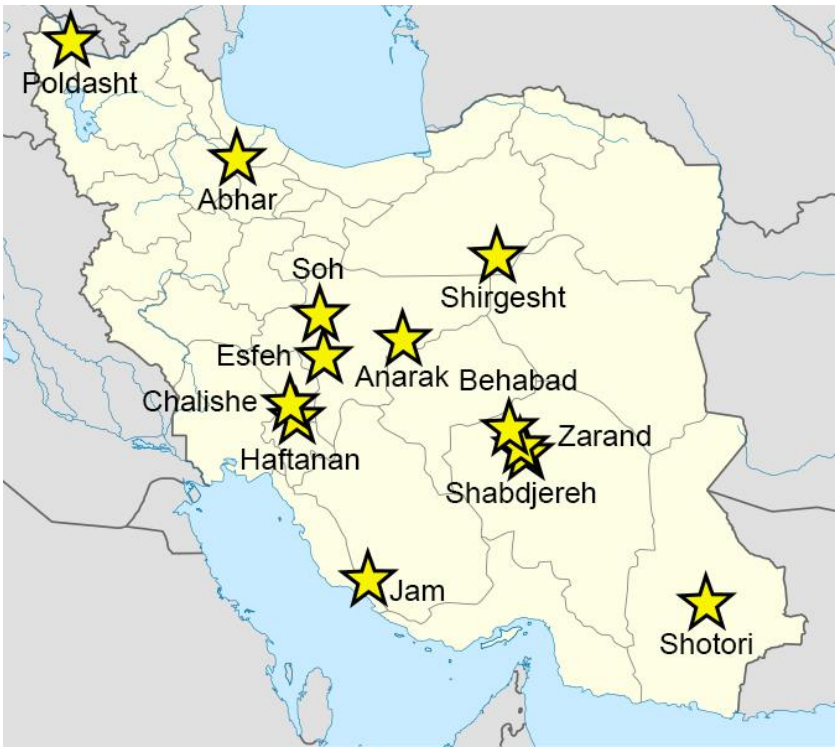

Fig. 1. Sampling localities of fossil brachiopods in Iran.

Table 1. Fossil specimens used for microstructural analysis.

Sample Name	Number of Individual	Order	Age	Sampling localities
Acrotretidae gen. et sp. ind.	1	ACROTRETIDA	Early Cambrian-Silurian	Abhar
Billingsella aff. *B. seletensis* (Nikitin, 1956)	4	BILLINGSELLIDA	Cambrian	Shirgesht
Billingsellidae gen. et sp. ind.	2	BILLINGSELLIDA	Middle Cambrian to the Lower Ordovician	Haftanan
Protambonites cf. *P. primigenius* (Havlíček, 1972)	2	BILLINGSELLIDA	Late Cambrian-Early Ordovician	Haftanan
Martellia shabdjerehensis (Percival et al., 2009)	6	BILLINGSELLIDA	Ordovician	Shabdjereh
Leptellina? sp. ind.	4	STROPHOMENIDA	Ordovician	Shabdjereh
Ingria sp. ind.	2	STROPHOMENIDA	Late Ordovician	Shirgesht
Leptaena depressa (Sowerby, 1825)	2	STROPHOMENIDA	Silurian	Shirgesht
Productella cf. *P. belanskii* (Stainbrook, 1943)	2	PRODUCTIDA	Devonian	Poldasht
Productella cf. *Productella subaculeata* (Murchison, 1840)	1	PRODUCTIDA	Devonian	Nasrolah
Productella sp. ind.	5	PRODUCTIDA	Devonian	Shishtu and Mush
Rhytialosia sp. ind.	1	PRODUCTIDA	Devonian	Nasrolah
Spinulicosta sp. ind.	2	PRODUCTIDA	Devonian	Nasrolah
Striatochonetes sp. ind.	3	PRODUCTIDA (CHONETIDA)	Devonian	Jam
Devonochonetes sp. ind.	3	PRODUCTIDA (CHONETIDA)	Devonian	Soh
Triplesia alata (Ulrich and Cooper, 1936)	1	ORTHOTETIDA (TRIPLESIIDINA)	Silurian	Shirgesht
Hesperonomiella sp. ind.	3	ORTHIDA	Middle Cambrian-Early Ordovician	Haftanan
Nicolella actoniae (Sowerby, 1839)	4	ORTHIDA	Ordovician	Shirgesht
Paralenorthis sp. ind.	9	ORTHIDA	Ordovician	Shabdjereh
Howellites ultima (Bancroft, 1945)	2	ORTHIDA	Late Ordovician	Shirgesht
Isorthis (Ovalella) inflata (Hairapetian et al., 2012)	2	ORTHIDA	Silurian	Shirgesht
Isorthis sp. ind.	2	ORTHIDA	early Silurian to Early Devonian	Zarand
Syntrophioides sp. ind.	2	PENTAMERIDA	Cambrian	Galikuh
?*Clorinda* sp. ind.	2	PENTAMERIDA	Silurian	
Clorinda molongensis (Mitchell, 1921)	3	PENTAMERIDA	Silurian	Esfeh
Spinatrypina sp. ind.	5	ATRYPIDA	Silurian, Silurian to Late Devonian	Shirgesht and Esfeh
Spinatrypina cf. *S. chitralensis* (Reed, 1922)	2	ATRYPIDA	Devonian	Nasrolah
Rhynchotrema sp. ind.	2	RHYNCHONELLIDA	Late Ordovician-Middle Silurian	Zarand
Stegocornu denisae (Hairapetian et al., 2012)	2	RHYNCHONELLIDA	Silurian	Zarand
Cyphoterorhynchus arpaensis (Abramian, 1957)	1	RHYNCHONELLIDA	Devonian	Nasrolah
Hedeinopsis hispanica hispanica (Gourvennec, 1990)	3	SPIRIFERIDA	Silurian	Shirgesht
Hedeinopsis sp. ind.	1	SPIRIFERIDA	Silurian	Zarand
Cyrtospirifer brodi (Venjukov, 1886)	1	SPIRIFERIDA	Devonian	Nasrolah
Cyrtospirifer cf. *C. kermanensis* (Brice, 1999)	5	SPIRIFERIDA	Devonian	Nasrolah
Cyrtospirifer sp. ind.	2	SPIRIFERIDA	Devonian	Behabad
Uchtospirifer aff. *Uchtospirifer nalivkini* (Lyashenko, 1957)	1	SPIRIFERIDA	Devonian	Behabad

5.1.2 Methods

All the specimens have been measured with a caliper ruler (length, width and thickness, Fig. 2). Then they were prepared following the preparation method suggested by Crippa et al. (2016). All specimens were cut into different sections along longitudinal and transverse axes; fragile specimens were embedded in epoxy resin before cutting. Sectioned surfaces were further smoothed with silicon carbide powder (SiC), etched with 5% hydrochloric acid (HCl) for 10-15 s, then rinsed under tap water and dried. The surfaces were gold-coated and then inspected with a Cambridge S-360 scanning electron microscope with a lanthanum hexaboride (LaB_6) source and operating at an acceleration voltage of 20 kV at Dipartimento di Scienze della Terra "A. Desio", Università di Milano.

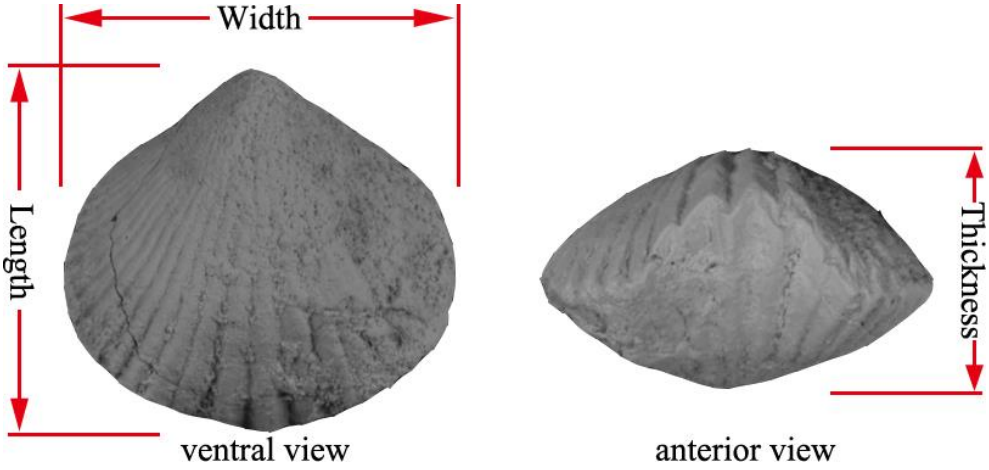

Fig. 2. Acquired measurements to estimate the size of brachiopod shell.

For the specimens showing a good preservation of the microstructure, measurements on structural units (i.e. laminae and fibres) were performed on the SEM images, using the software Photoshop. As the boundaries of each lamina and fibre are not always very clear, and the contact surfaces of each unit (fibres/laminae) are not straight, in order to reduce the error, the thickness was measured on a set of 5 laminae and longitudinal fibres. In addition, the width of fibres was also measured in case of well-preserved microstructures (Fig. 3).

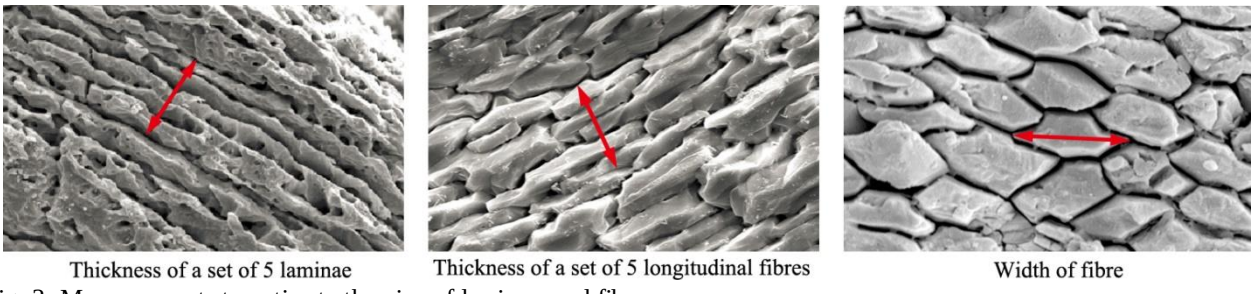

Fig. 3. Measurements to estimate the size of laminae and fibres.

5.2 Results

5.2.1 General features of the analysed shells

Table 3. Classification, age, shale and main microstructural features of the analysed fossil specimens.

Specie	Order	Age	Shape of shell	Layers	Microstructure	Others
Acrotretidae gen. et sp. ind.	ACROTRETIDA	Early Cambrian-Silurian				not good preservation
Billingsella aff. *B. seletensis*	BILLINGSELLIDA	Cambrian	Biconvex	laminar with radial folds (flat laminar)		not good preservation
Billingsellidae gen. et sp. ind.	BILLINGSELLIDA	Middle Cambrian to the Lower Ordovician	Concavo-convex	laminar with radial folds (flat laminar)		not good preservation
Protambonites cf. *P. primigenius*	BILLINGSELLIDA	Late Cambrian-Early Ordovician	Biconvex	laminar with radial folds (flat laminar)	pseudopunctae?	
Martellia shabdjerehensis	BILLINGSELLIDA	Ordovician	Biconvex	laminar with radial folds (flat laminar), columnar layer?	pseudopunctae? Spines	
Leptellina? sp. ind.	STROPHOMENIDA	Ordovician	Concavo-convex	laminar cross bladed, columnar layer?	pseudopunctae?	
Ingria sp. ind.	STROPHOMENIDA	Late Ordovician	Flat	laminar cross bladed, columnar layer?		
Leptaena depressa	STROPHOMENIDA	Silurian	Biconvex	laminar cross bladed,		
Productella cf. P. *belanskii*	PRODUCTIDA	Devonian	Concavo-convex	laminar cross bladed, columnar layer?	pseudopunctae? spines?	
Productella cf. *P. subaculeata*	PRODUCTIDA	Devonian	Concavo-convex	laminar cross bladed columnar layer?	spines?	
Productella sp. ind.	PRODUCTIDA	Devonian	Concavo-convex	laminar cross bladed	pseudopunctae? spines?	
Rhytialosia sp. ind.	PRODUCTIDA	Devonian	Concavo-convex	laminar cross bladed	pseudopunctae	
Spinulicosta sp. ind.	PRODUCTIDA	Devonian	Concavo-convex	laminar cross bladed	pseudopunctae?	
Striatochonetes sp. ind.	PRODUCTIDA	Devonian	Concavo-convex	laminar cross bladed	pseudopunctae?	
Striatochonetes sp. ind.	PRODUCTIDA (CHONETIDA)	Devonian	Concavo-convex	laminar cross bladed	pseudopunctae?	
Devonochonetes sp. ind.	PRODUCTIDA (CHONETIDA)	Devonian	Concave-convex	laminar, columnar layer?		
Triplesia alata	ORTHOTETIDA (TRIPLESIIDINA)	Silurian	Biconvex	laminar		Transverse section
Hesperonomiella sp. ind.	ORTHIDA	Middle Cambrian-Early Ordovician	Biconvex	fibrous		
Nicolella actoniae	ORTHIDA	Ordovician	Plano-convex, Concavo-convex	fibrous, columnar layer?	punctae?	
Paralenorthis sp. ind.	ORTHIDA	Ordovician	Plano-convex	fibrous, columnar layer?		
Howellites ultima	ORTHIDA	Late Ordovician	Biconvex	fibrous, columnar layer?	punctae?	
Isorthis (Ovalella) inflata	ORTHIDA	Silurian	Biconvex	fibrous, columnar layer?		
Isorthis sp. ind.	ORTHIDA	early Silurian to Early Devonian	Biconvex	fibrous		
Syntrophioides sp. ind.	PENTAMERIDA	Cambrian	Biconvex	fibrous		not good preservation
?*Clorinda* sp. ind.	PENTAMERIDA	Silurian	Biconvex	fibrous		
Clorinda molongensis	PENTAMERIDA	Silurian	Biconvex	fibrous		
Spinatrypina sp. ind.	ATRYPIDA	Silurian, Silurian to Late Devonian	Biconvex	fibrous		not good preservation
Spinatrypina cf. S. *chitralensis*	ATRYPIDA	Devonian	Biconvex	fibrous		
Rhynchotrema sp. ind.	RHYNCHONELLIDA	Late Ordovician-Middle Silurian	Biconvex	fibrous		
Stegocornu denisae	RHYNCHONELLIDA	Silurian	Biconvex	fibrous		
Cyphoterorhynchus arpaensis	RHYNCHONELLIDA	Devonian	Biconvex	fibrous		not good preservation
Hedeinopsis hispanica hispanica	SPIRIFERIDA	Silurian	Biconvex	fibrous		
Hedeinopsis sp. ind.	SPIRIFERIDA	Silurian	Biconvex	fibrous		
Cyrtospirifer brodi	SPIRIFERIDA	Devonian	Biconvex	fibrous		not good preservation
Cyrtospirifer cf. C. *kermanensis*	SPIRIFERIDA	Devonian	Biconvex	fibrous		
Cyrtospirifer sp. ind.	SPIRIFERIDA	Devonian	Biconvex	fibrous, columnar layer?		
Uchtospirifer aff. *Uchtospirifer nalivkini*	SPIRIFERIDA	Devonian	Biconvex	fibrous, columnar layer?		

5.2.2 Measurements of the microstructural units

Table 4. Measurements acquired for the laminae and fibres in the studied fossil brachiopod.

Sample Name (number of individual specimen)	Layers	Mean width of basic unit (μm) (fibre) (number of measurement)	Mean Thickness of five lines (μm) (lamina/fibre) (number of measurement)
Billingsella aff. *B. seletensis*	laminar with radial folds, columnar layer?		
Billingsellidae gen. et sp. ind. (1)	laminar with radial folds		14.01 ±2.56 (14)
Protambonites cf. *P. primigenius* (1)	laminar with radial folds		12.2 ±2.32 (15)
Martellia shabdjerehensis (3)	laminar with radial folds,		9.71 ±3.87 (67)
Leptellina? sp. ind. (2)	laminar cross bladed, columnar layer?		12.97 ±3.20 (93)
Ingria sp. ind. (2)	laminar cross bladed, columnar layer?		10.72 ±4.25 (40)
Leptaena depressa (1)	laminar cross bladed		11 ±3.18 (22)
Productella cf. P. *belanskii* (2)	laminar cross bladed, columnar layer?		6.88 ±1.06 (28)
Productella cf. *Productella subaculeata* (1)	laminar cross bladed, columnar layer?		7 ±1.18 (20)
Productella sp. ind. (3)	laminar cross bladed		6.31 ±1.30 (12)
Rhytialosia sp. ind. (1)	laminar cross bladed		8.35 ±1.74 (25)
Spinulicosta sp. ind. (2)	laminar cross bladed		6.57 ±1.98 (30)
Striatochonetes sp. ind. (3)	laminar cross bladed		7.05 ±1.38 (33)
Striatochonetes sp. ind.	laminar cross bladed		
Devonochonetes sp. ind. (1)	laminar, columnar layer?		10.38 ±0.76 (6)
Triplesia alata (1)	laminar		6.52 ±1.12 (12)
Hesperonomiella sp. ind.	fibrous		
Nicolella actoniae (4)	fibrous, columnar layer?	9.6 ±1.23 (16)	12.4 ±3.20 (64)
Paralenorthis sp. ind. (4)	fibrous, columnar layer?	13 ±2.85 (35)	12.79 ±3.45 (41)
Howellites ultima (2)	fibrous, columnar layer?	16.38 ±5.72 (15)	16.63 ±7.48 (22)
Isorthis (Ovalella) inflata (1)	fibrous, columnar layer?	16.6 ±1.41 (4)	16.15 ±3.38 (19)
Isorthis sp. ind.	fibrous		
Syntrophioides sp. ind. (1)	fibrous		23.1 ±8.66 (6)
?*Clorinda* sp. ind. (1)	fibrous	16.28 ±1.29 (4)	18.5 ±0.9 (2)
Clorinda molongensis (1)	fibrous	12.7 ±1.5 (2)	17.53 ±2.94 (4)
Spinatrypina sp. ind. (2)	fibrous	25.96 ±3.72 (5)	18.29 ±7.01 (8)
Spinatrypina cf. S. *chitralensis* (1)	fibrous		30.08 ±10.57 (6)
Rhynchotrema sp. ind. (1)	fibrous		20.39 ±8.72 (13)
Stegocornu denisae (1)	fibrous	23.02 ±2.72 (9)	24.2 ±1.95 (6)
Cyphoterorhynchus arpaensis (1)	fibrous	8.36 ±2.35 (7)	21.59 ±12.98 (35)
Hedeinopsis hispanica hispanica (1)	fibrous		19.32 ±3.97 (6)
Hedeinopsis sp. ind. (1)	fibrous	16.29 ±3.11 (14)	24.19 ±6.62 (16)
Cyrtospirifer brodi (1)	fibrous	9.474.11 (34)	16.03 ±5.49 (38)
Cyrtospirifer cf. *C. kermanensis* (4)	fibrous	22.21 ±9.11 (11)	25.37 ±13.29 (19)
Cyrtospirifer sp. ind. (2)	fibrous, columnar layer?	12.1 ±0.29 (3)	16.72 ±4.62 (2)
Uchtospirifer aff. *Uchtospirifer nalivkini* (1)	fibrous, columnar layer?		20.07 ±17.42 (20)

5.2.3 Microstructural organization of the secondary layer of the studied fossil brachiopods

5.2.3.1 Laminar fabric

Laminar with radial folds (flat laminar) – BILLINGSELLIDA

The primary layer of Billingsellida (*Billingsella* aff. *B. seletensis*, Billingsellidae gen. et sp. ind., Billingsellidae gen. indet., *Protambonites* cf. *P. primigenius*, *Martellia shabdjerehensis*, Plates 1-4) is not preserved in the specimens under investigation. The shell is composed by a laminar layer of flat-lying blades. Columnar tertiary layer was observed in *Billingsella* aff. *B. seletensis* and *Martellia shabdjerehensis*, but not evidence of its occurrence was found in Billingsellidae gen. et sp. ind. and *Protambonites* cf. *P. primigenius*. Blades usually amalgamate laterally to form a succession of sheets; in some cases, folds can be seen on the cross section (Plate 1G-H). *Protambonites* cf. *P. primigenius* and *Martellia shabdjerehensis* bear pseudopunctae crossing the laminar layer; spines are present in *Martellia shabdjerehensis* (Table 3). In the umbonal part and near the anterior edge, the orientation of laminae changes and in cross-section, they look like wedges which inter-cross each other (Plate 1E, Plate 3B).

Plate 1

A, B: laminar layer near the posterior part (*Billingsella* aff. *B. seletensis*, MRAN 898-3-4, ventral valve)

C: columnar tertiary layer? near the posterior part (*Billingsella* aff. *B. seletensis*, MRAN 898-8, ventral valve);

D: columnar tertiary layer? near the posterior part (*Billingsella* aff. *B. seletensis*, MRAN 898-3-3, ventral valve);

E, F: laminar layer near the anterior part (Billingsellidae gen. et sp. ind., MRAN 8760-2, ventral valve);

G: laminar layer near the posterior part (Billingsellidae gen. et sp. ind., MRAN 8760-2, ventral valve);

H: enlarged detail of the laminae (Billingsellidae gen. et sp. ind., MRAN 8760-2, ventral valve).

Ext: external part of the shell; Int: internal part of the shell.

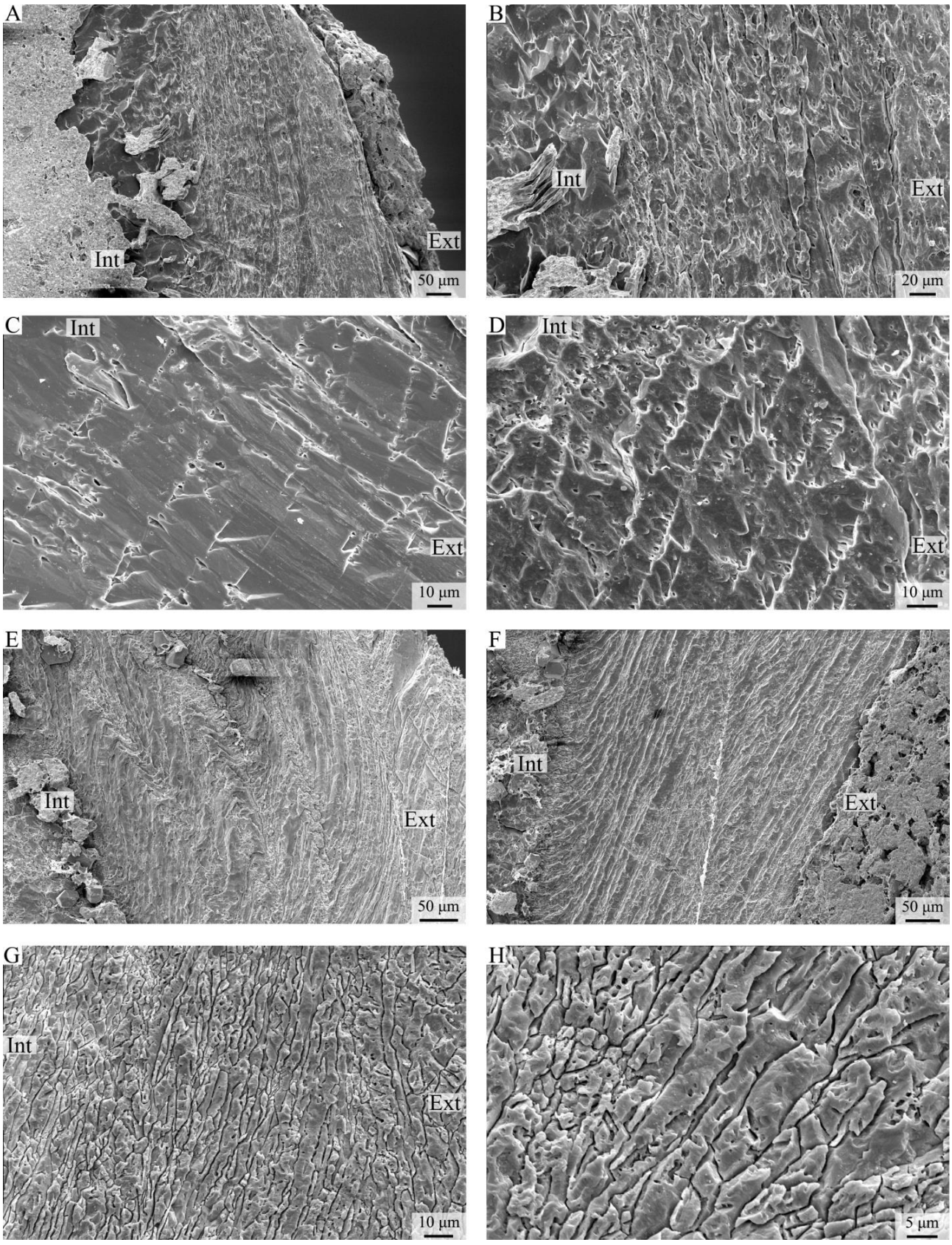
A
Int
Ext
50 µm
B
Int
Ext
20 µm
C
Int
Ext
10 µm
D
Int
Ext
10 µm
E
Int
Ext
50 µm
F
Int
Ext
50 µm
G
Int
Ext
10 µm
H
5 µm

Plate 2

A: laminar layer in the central part (Billingsellidae gen. indet., MRAN 8760-1, ventral valve);

B: enlarged detail of laminae (Billingsellidae gen. indet., MRAN 8760-1, dorsal valve);

C: laminar layer in the umbobal part (*Protambonites* cf. *P. primigenius*, MRAN 8763-2, dorsal valve);

D: laminar layer near the anterior part (*Protambonites* cf. *P. primigenius*, MRAN 8763-2, dorsal valve);

E: laminar layer near the anterior part (*Protambonites* cf. *P. primigenius*, MRAN 8763-2, ventral valve);

F: laminar layer near the posterior part (*Protambonites* cf. *P. primigenius*, MRAN 8763-2, ventral valve).

Ext: external part of the shell; Int: internal part of the shell.

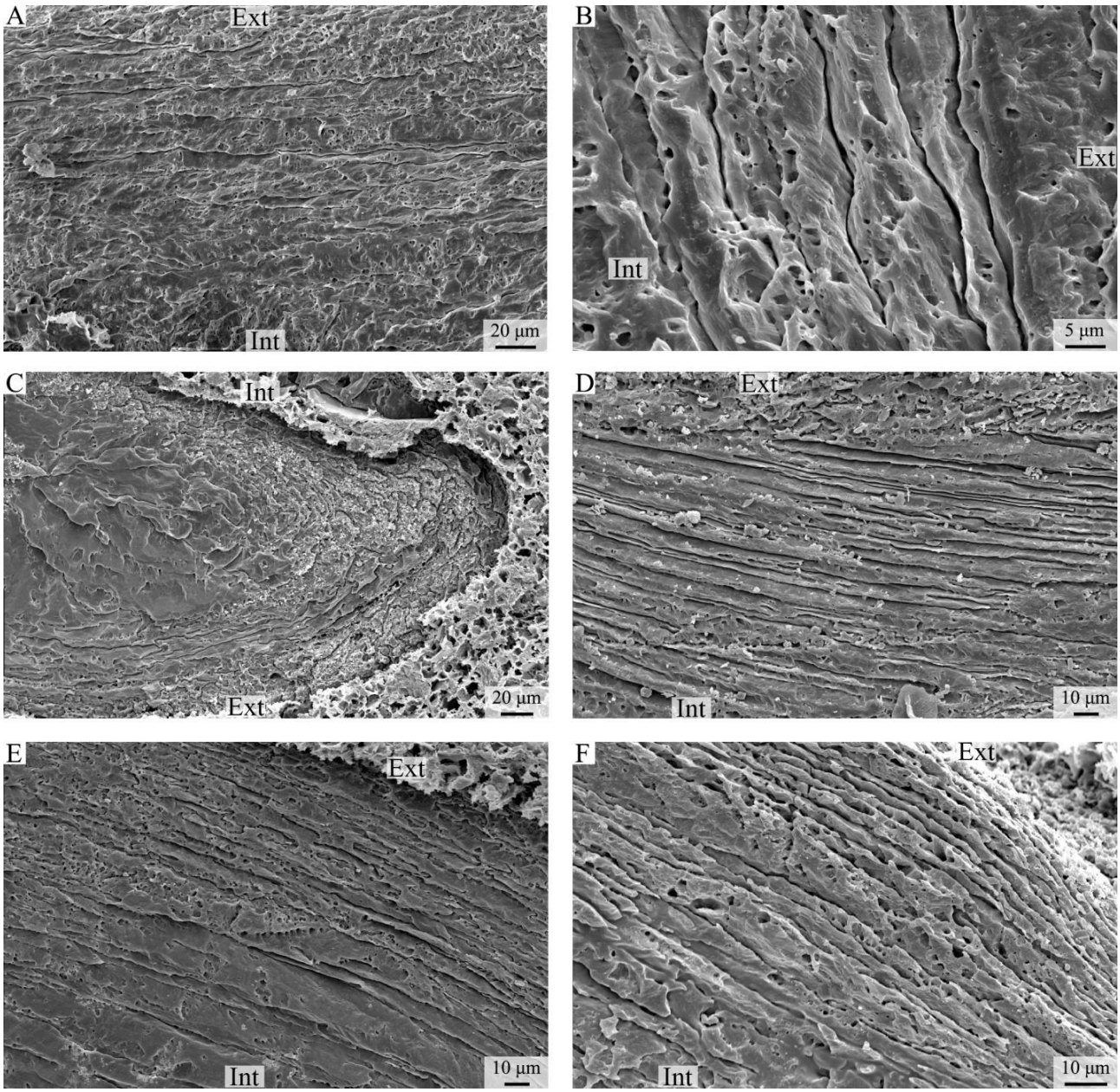
A
Ext
Int
20 µm
B
Ext
Int
5 µm
C
Int
Ext
20 µm
D
Ext
Int
10 µm
E
Ext
Int
10 µm
F
Ext
Int
10 µm

Plate 3

A: laminar layer in the umbonal part (*Martellia shabdjerehensis*, KE45-1, ventral valve);

B: laminar layer in the umbonal part (*Martellia shabdjerehensis*, KE42, dorsal valve);

C: laminar layer and tertiary layer? (*Martellia shabdjerehensis*, KE45-1, ventral valve);

D: laminar layer in the central part (*Martellia shabdjerehensis*, KE45-2, dorsal valve);

E: laminar layer in the central part (*Martellia shabdjerehensis*, KE42, ventral valve);

F: laminar layer near the anterior part (*Martellia shabdjerehensis*, KE42, dorsal valve).

Ext: external part of the shell; Int: internal part of the shell.

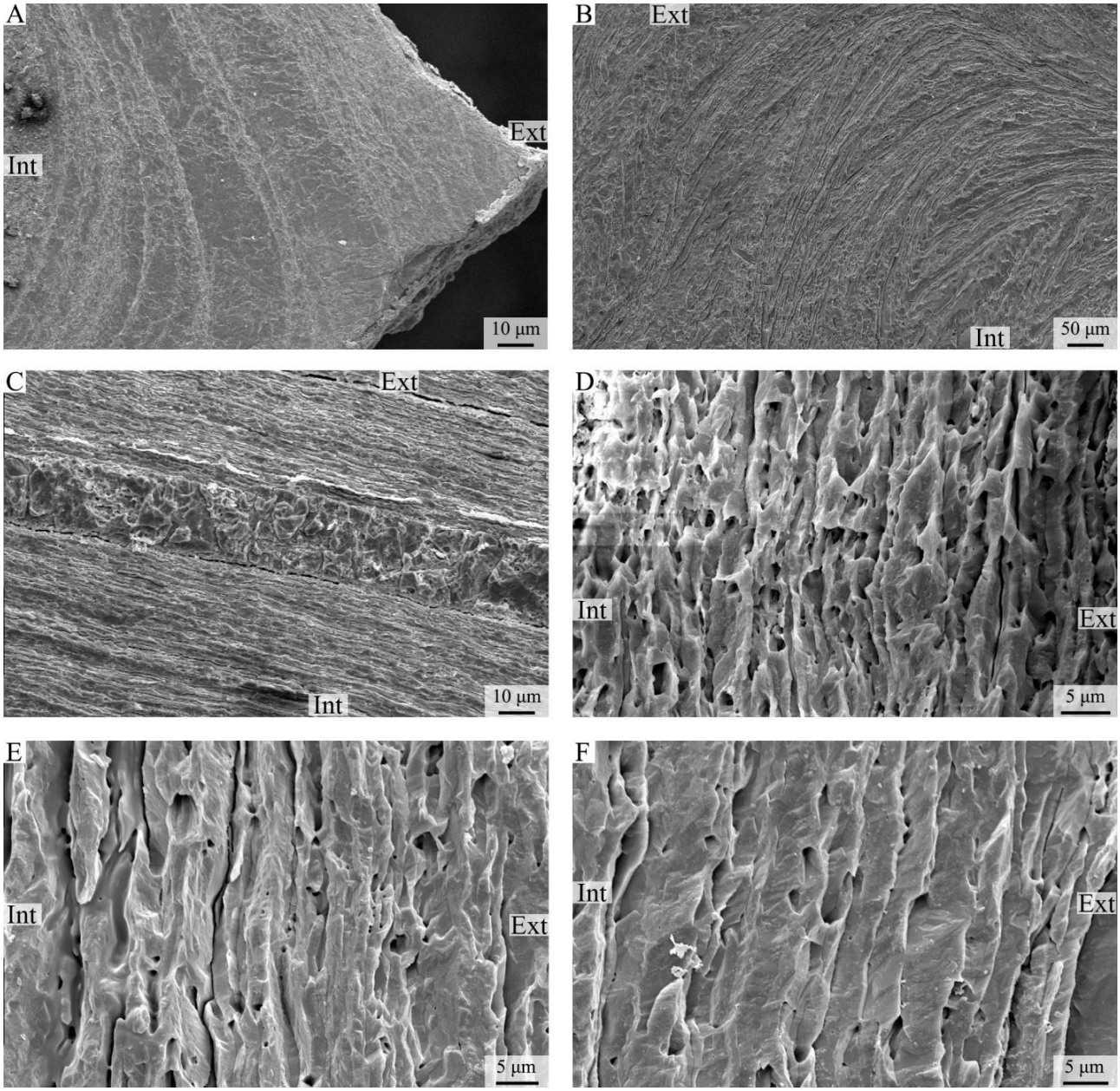
A
Int
Ext
10 µm
B
Ext
Int
50 µm
C
Ext
Int
10 µm
D
Int
Ext
5 µm
E
Int
Ext
5 µm
F
Int
Ext
5 µm

Plate 4

A: laminar layer in external view (*Martellia shabdjerehensis*, KE 42, ventral valve);

B: enlarged detail of the laminae in external view (*Martellia shabdjerehensis*, KE 42, ventral valve);

C-E: laminar layer and spines in external view (*Martellia shabdjerehensis*, KE 42, ventral valve);

F: enlarged detail of the spine in external view (*Martellia shabdjerehensis*, KE 42, ventral valve).

Ext: external part of the shell; Int: internal part of the shell.

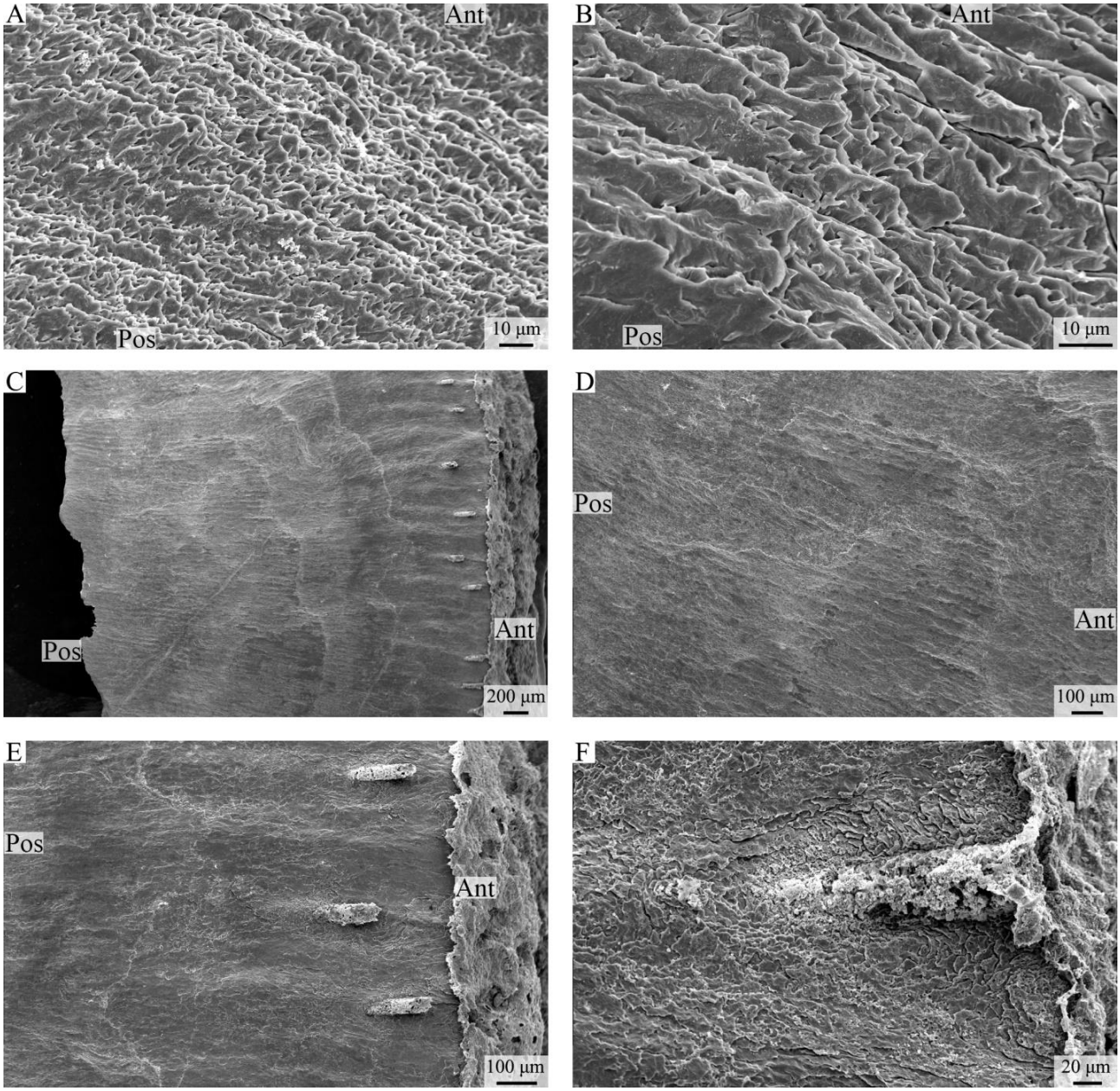
A
Ant
Pos
10 µm
B
Ant
Pos
10 µm
C
Pos
Ant
200 µm
D
Pos
Ant
100 µm
E
Pos
Ant
100 µm
F
20 µm

Laminar cross bladed – STROPHOMENIDA

The primary layer of Strophomenida (*Leptellina*? sp. ind., *Ingria* sp. ind., *Leptaena depressa*, Plates 5-7) was not observed in the specimens under investigation. The shell is composed by a laminar layer, and the basic unit of the laminae is a lath-shaped (blade) crystallite (Plate 6B, D). Laminae are grouped into packages, where the axes of blades are parallel. Packages of laminae, with blade axis orientations with different angles, alternate in the secondary layer (Plate 6B, Plate 7G). Pseudopunctae were observed in *Leptellina*? sp. ind. (Table 3, Plate 7). Typical wedges inter-cross laminar structures were found (Plate 5A). Columnar tertiary layer was found in *Leptellina*? sp. ind. and *Ingria* sp. ind., but no evidence of its presence was observed in *Leptaena depressa*.

Plate 5

A: laminar sub-layers inter-cross each other like wedges (*Ingria* sp. ind., MRAN 1108-2C, ventral valve);

B, C: laminar layer near the posterior part (*Ingria* sp. ind., MRAN 1108-4a, ventral valve);

D: enlarged detail of the laminae (*Ingria* sp. ind., MRAN 1108-4a, ventral valve);

E: transition between laminar secondary layer and tertiary layer (*Ingria* sp. ind., MRAN 1108-2C, ventral valve);

F: laminar layer near the anterior part (*Ingria* sp. ind., MRAN 1108-2C, ventral valve);

G: laminar layer in the central part (*Ingria* sp. ind., MRAN 1108-2C, ventral valve);

H: enlarged detail of the laminae (*Ingria* sp. ind., MRAN 1108-2E, ventral valve).

Ext: external part of the shell; Int: internal part of the shell.

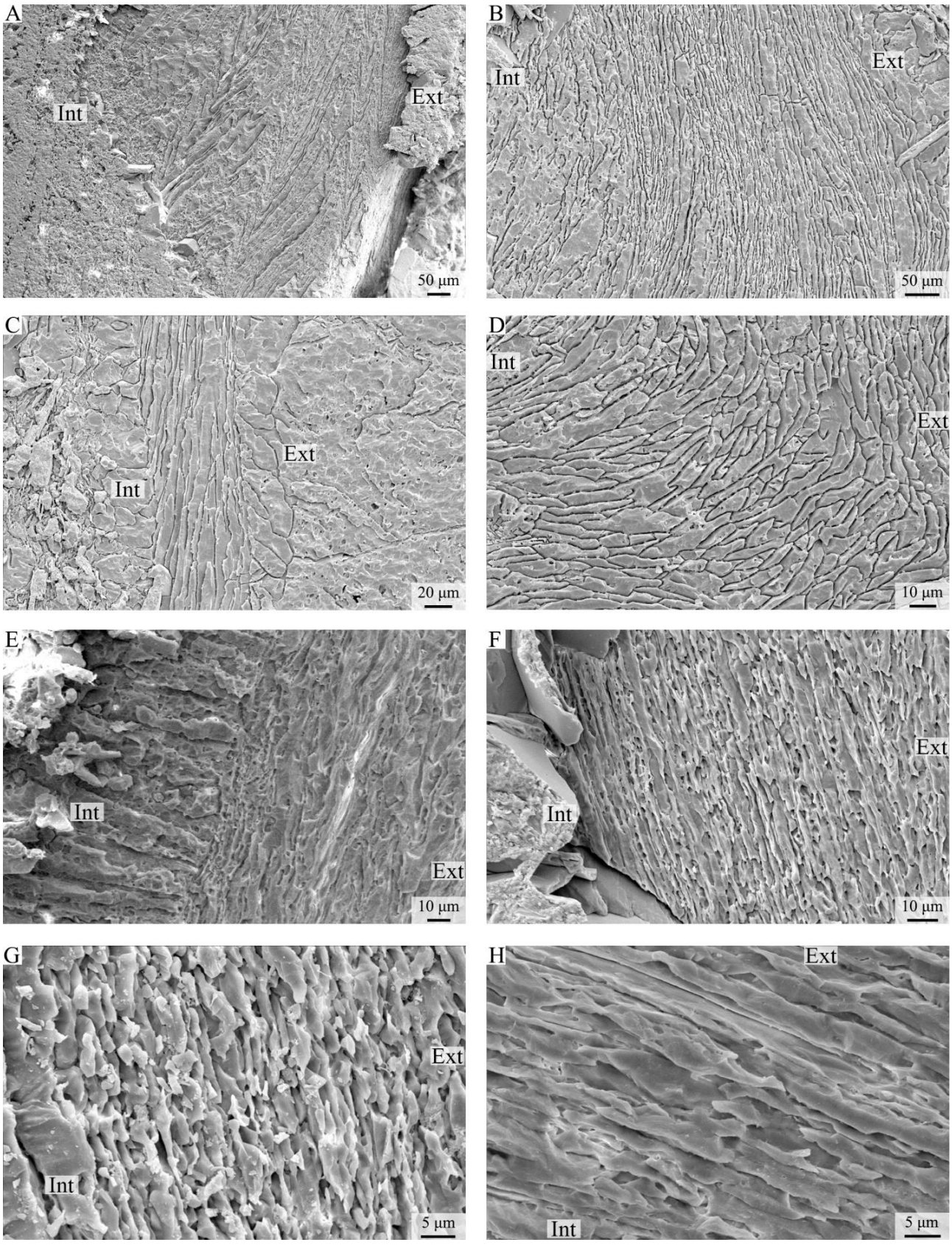
A
Int
Ext
50 µm
B
Int
Ext
50 µm
C
Ext
Int
20 µm
D
Int
Ext
10 µm
E
Int
Ext
10 µm
F
Ext
Int
10 µm
G
Ext
Int
5 µm
H
Ext
Int
5 µm

Plate 6

A: overview of laminar layer (*Leptaena depressa*, MRAN 1180-27, dorsal valve);

B: cross-bladed laminar layer in the central part (*Leptaena depressa*, MRAN 1180-27, ventral valve);

C: laminar layer near the posterior part (*Leptaena depressa*, MRAN 1180-27, ventral valve);

D: enlarged detail of the laminae (*Leptaena depressa*, MRAN 1180-27, ventral valve).

Ext: external part of the shell; Int: internal part of the shell.

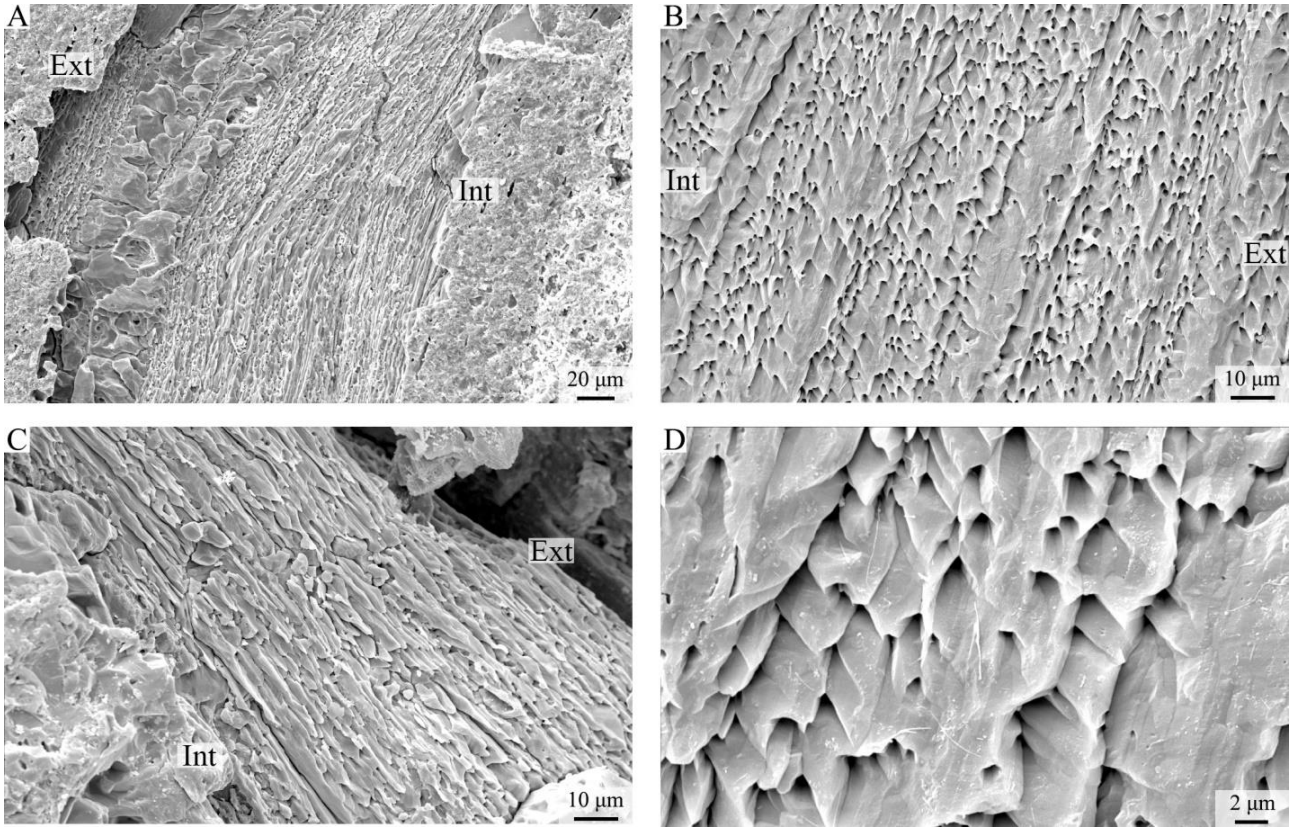
A
Ext
Int
20 µm
B
Int
Ext
10 µm
C
Ext
Int
10 µm
D
2 µm

Plate 7

A: laminar layer in the umbo part (*Leptellina* sp. ind., KE45-4, dorsal valve);

B: laminar layer with pseudopunctae near the anterior part (*Leptellina* sp. ind., KE45-4, dorsal valve);

C-E: pseudopuncta (*Leptellina* sp. ind., KE45-3, ventral valve);

F: laminar layer in the central part (*Leptellina* sp. ind., KE45-3, dorsal valve);

G: orientation change among the laminar sub-layers (*Leptellina* sp. ind., KE45-3, ventral valve);

H: enlarged detail of the laminae (*Leptellina* sp. ind., KE45-4, ventral valve).

Ext: external part of the shell; Int: internal part of the shell.

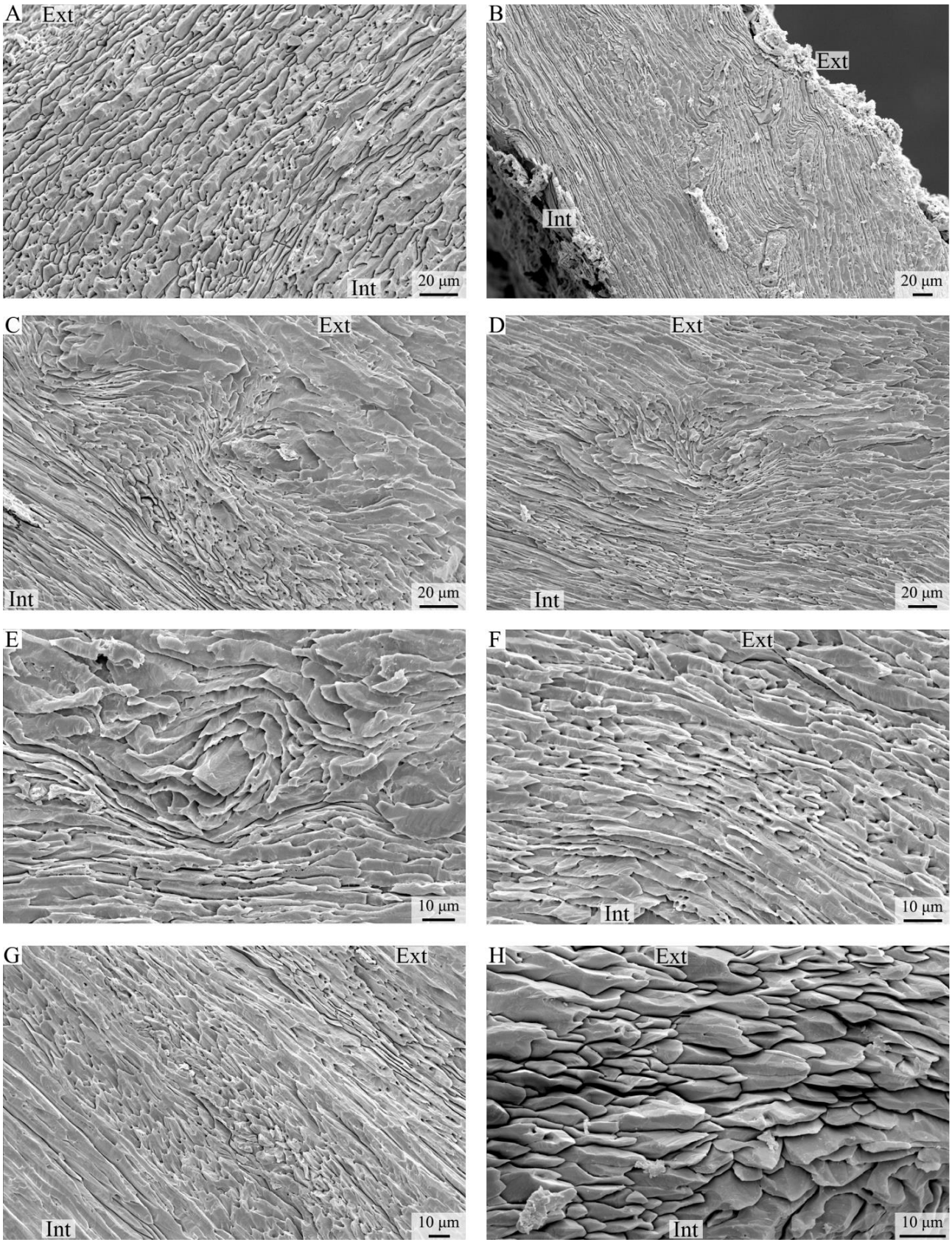
A
Ext
Int
20 µm
B
Ext
Int
20 µm
C
Ext
Int
20 µm
D
Ext
Int
20 µm
E
10 µm
F
Ext
Int
10 µm
G
Ext
Int
10 µm
H
Ext
Int
10 µm

Laminar cross bladed – PRODUCTIDA (excluding the Chonetidina)

The primary layer of Productida (*Productella* cf. *P. belanskii*, *Productella* cf. *P. subaculeata*, *Productella* sp. ind., *Rhytialosia* sp. ind., *Spinulicosta* sp. ind., *Striatochonetes* sp., Plates 8-11) (excluding the Chonetidina) is not preserved in the specimens under investigation. The shell is composed by a laminar secondary layer; the basic unit of the laminae is a lath-shaped (blade) (Plate 9H, Plate 10F, Plate 11F). Laminae are grouped into packages, where the axes of blades are parallel. Packages of laminae, with blade axis orientations with different angles, alternate in the secondary layer (Plate 8B, Plate 9F). Columnar tertiary layer was observed in *Productella* cf. *P. belanskii*, but not evidence was found in other species (Table 3). Pseudopunctae were found in *Productella* cf. *P. belanskii*, *Productella* sp. ind., *Rhytialosia* sp. ind., *Spinulicosta* sp. ind., and *Striatochonetes* sp. ind., and spines were found in *Productella* cf. *P. belanskii*, *Productella* cf. *P. subaculeata*, and *Productella* sp. ind. (Table 3).

Plate 8

A: completed laminar secondary layer in the central part (*Productella* cf. *P. belanskii*, MRAN 10810-4, ventral valve);

B: laminar layer near the anterior part (*Productella* cf. *P. belanskii*, MRAN 10810-4, ventral valve);

C: laminar secondary layer in the anterior part (*Productella* cf. *P. belanskii*, MRAN 10810-5, ventral valve);

D: spine (*Productella* cf. *P. belanskii*, MRAN 10810-5, ventral valve);

E: pseudopuncta (*Productella* cf. *P. belanskii*, MRAN 10810-5, ventral valve);

F: enlarged detail of the laminae (*Productella* cf. *P. belanskii*, MRAN 10810-4, ventral valve).

Ext: external part of the shell; Int: internal part of the shell.

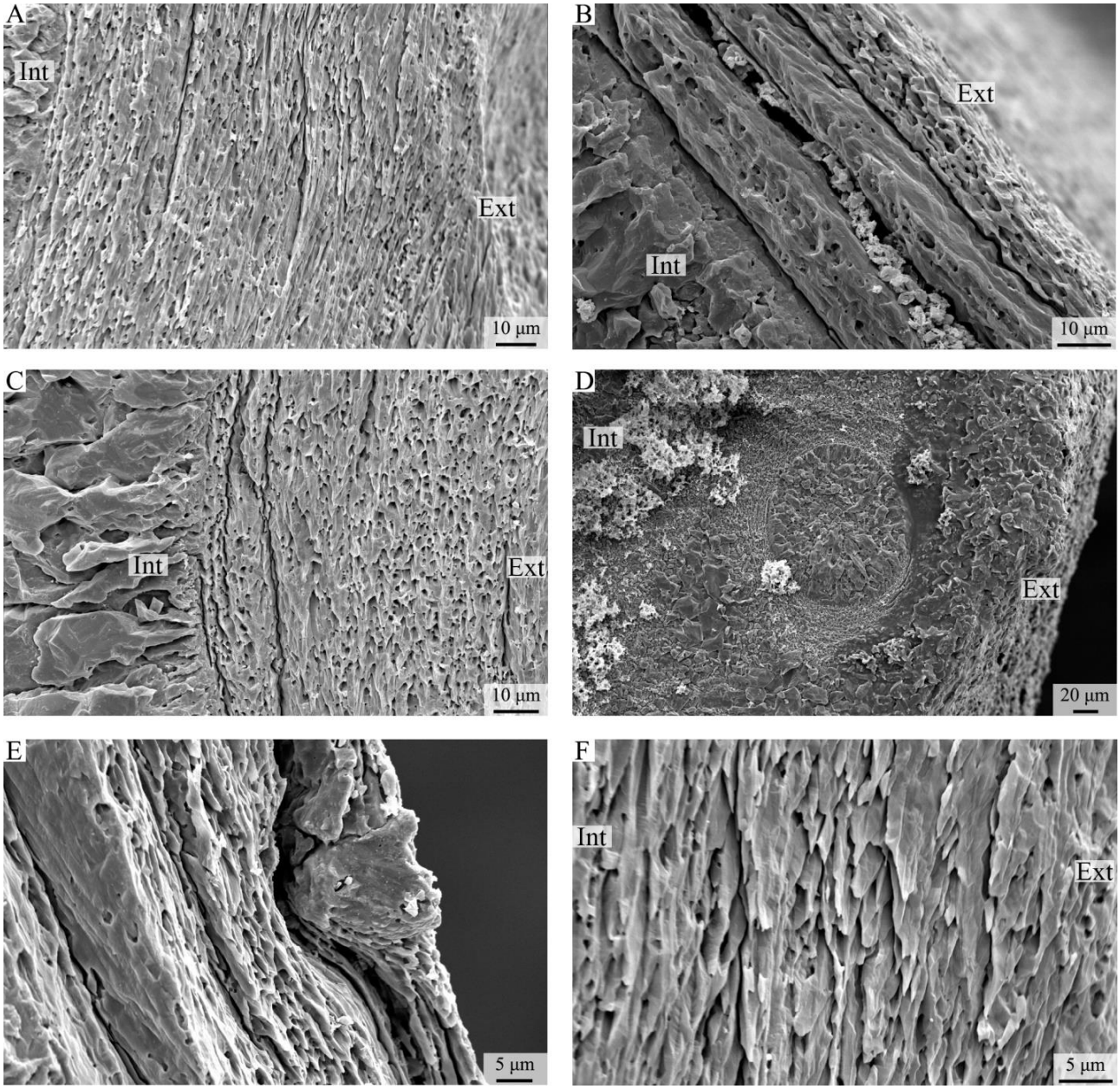
A
Int
Ext
10 µm
B
Ext
Int
10 µm
C
Int
Ext
10 µm
D
Int
Ext
20 µm
E
5 µm
F
Int
Ext
5 µm

Plate 9

A: laminar layer near the posterior part (*Productella* cf. *P. subaculeata*, MRAN 6203-3, ventral valve);

B: laminar secondary layer and tertiary layer? (*Productella* cf. *P. subaculeata*, MRAN 6203-3, ventral valve);

C-D: enlarged detail of the laminae (*Productella* cf. *P. subaculeata*, MRAN 6203-3, ventral valve);

E, F: laminar layer near the posterior part (*Spinulicosta* sp. ind., MRAN 6162-21, ventral valve);

G: pseudopuncta (*Spinulicosta* sp. ind., MRAN 6162-21, dorsal valve);

H: enlarged detail of the laminae (*Spinulicosta* sp. ind., MRAN 6162-21, ventral valve).

Ext: external part of the shell; Int: internal part of the shell.

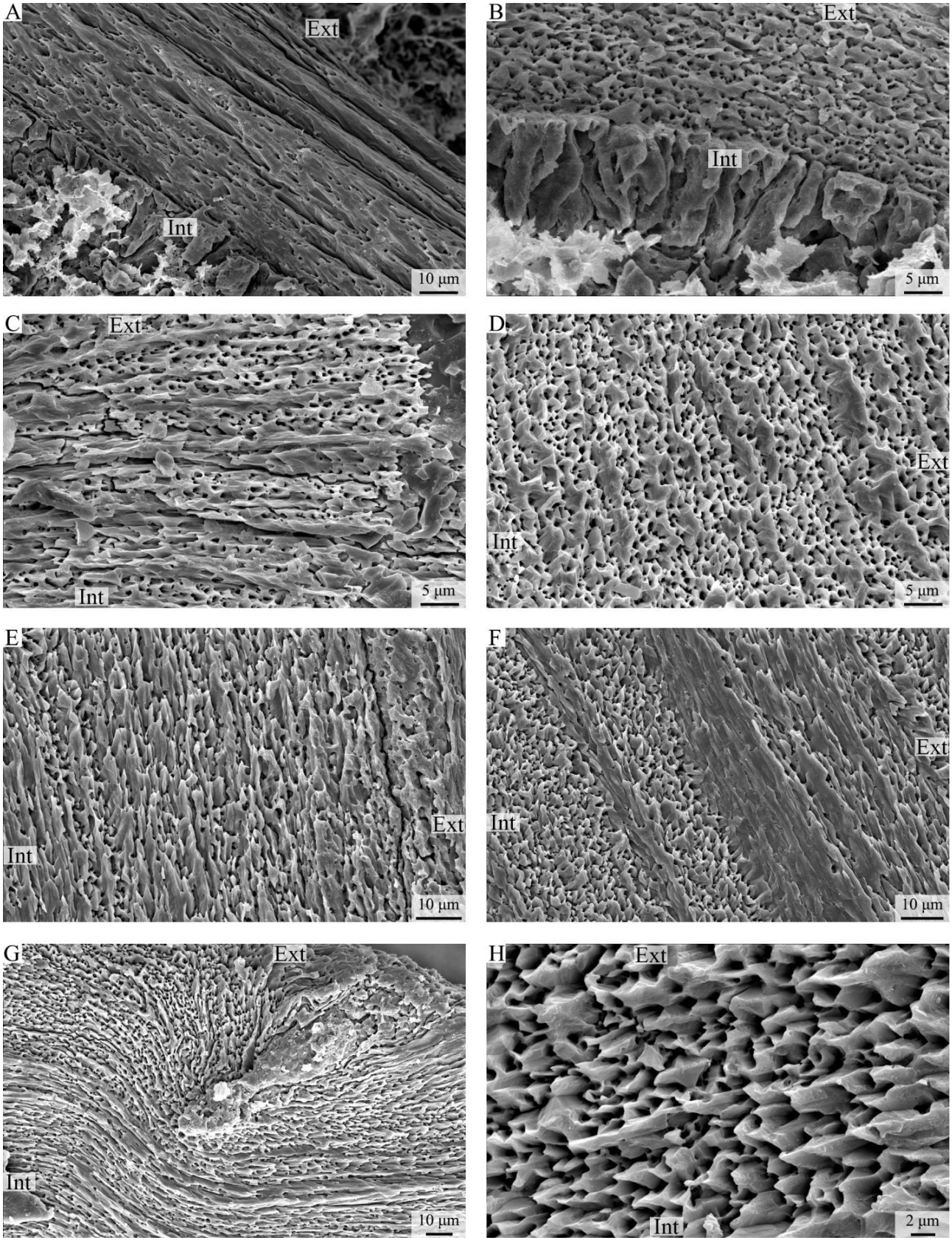
A
Ext
Int
10 µm
B
Ext
Int
5 µm
C
Ext
Int
5 µm
D
Ext
Int
5 µm
E
Ext
Int
10 µm
F
Ext
Int
10 µm
G
Ext
Int
10 µm
H
Ext
Int
2 µm

Plate 10

A: overview of the laminar layer near the posterior part (*Productella* sp. ind., MRAN 2727-2, ventral valve);

B: laminar layer in the central part (*Productella* sp. ind., MRAN 4905-2, ventral valve);

C: laminar layer and spine (*Productella* sp. ind., MRAN 4905-1, ventral valve);

D: pseudopuncta in external view (*Productella* sp. ind., MRAN 4905-2, ventral valve);

E: pseudopuncta (*Productella* sp. ind., MRAN 2727-2, ventral valve);

F: enlarged detail of the laminae (*Productella* sp. ind., MRAN 4905-1, ventral valve).

Ext: external part of the shell; Int: internal part of the shell.

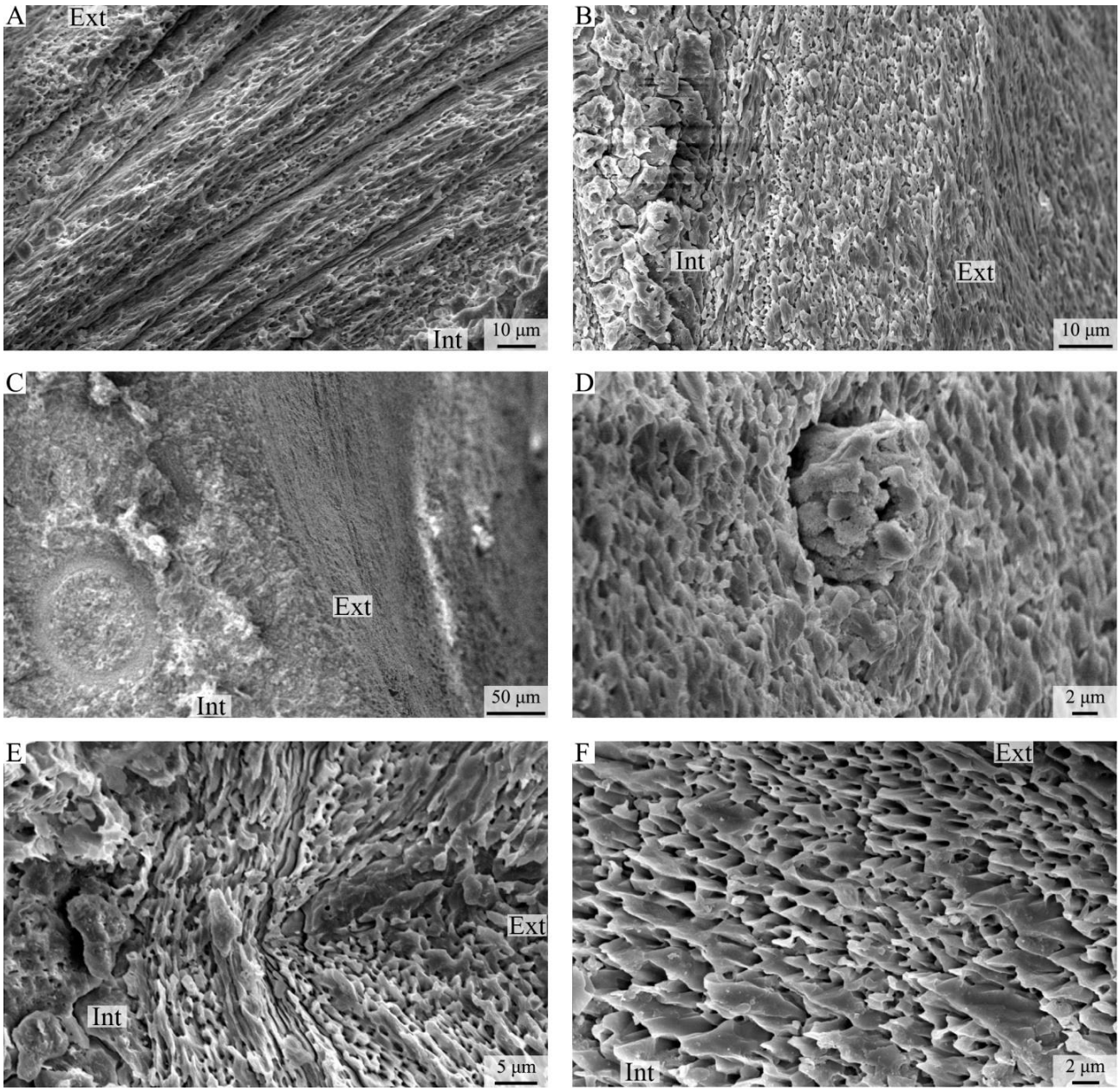
A
Ext
Int
10 µm
B
Int
Ext
10 µm
C
Ext
Int
50 µm
D
2 µm
E
Ext
Int
5 µm
F
Ext
Int
2 µm

Plate 11

A: orientation change of the laminar sub-layers (*Rhytialosia* sp. ind., MRAN 6162-2, ventral valve);

B, C: pseudopunctae (*Rhytialosia* sp. ind., MRAN 6162-2, ventral valve);

D: laminar layer near the posterior part (*Rhytialosia* sp. ind., MRAN 6162-2, ventral valve);

E: laminar layer near the anterior part (*Rhytialosia* sp. ind., MRAN 6162-2, ventral valve);

F: enlarged detail of the laminae (*Rhytialosia* sp. ind., MRAN 6162-2, ventral valve).

Ext: external part of the shell; Int: internal part of the shell.

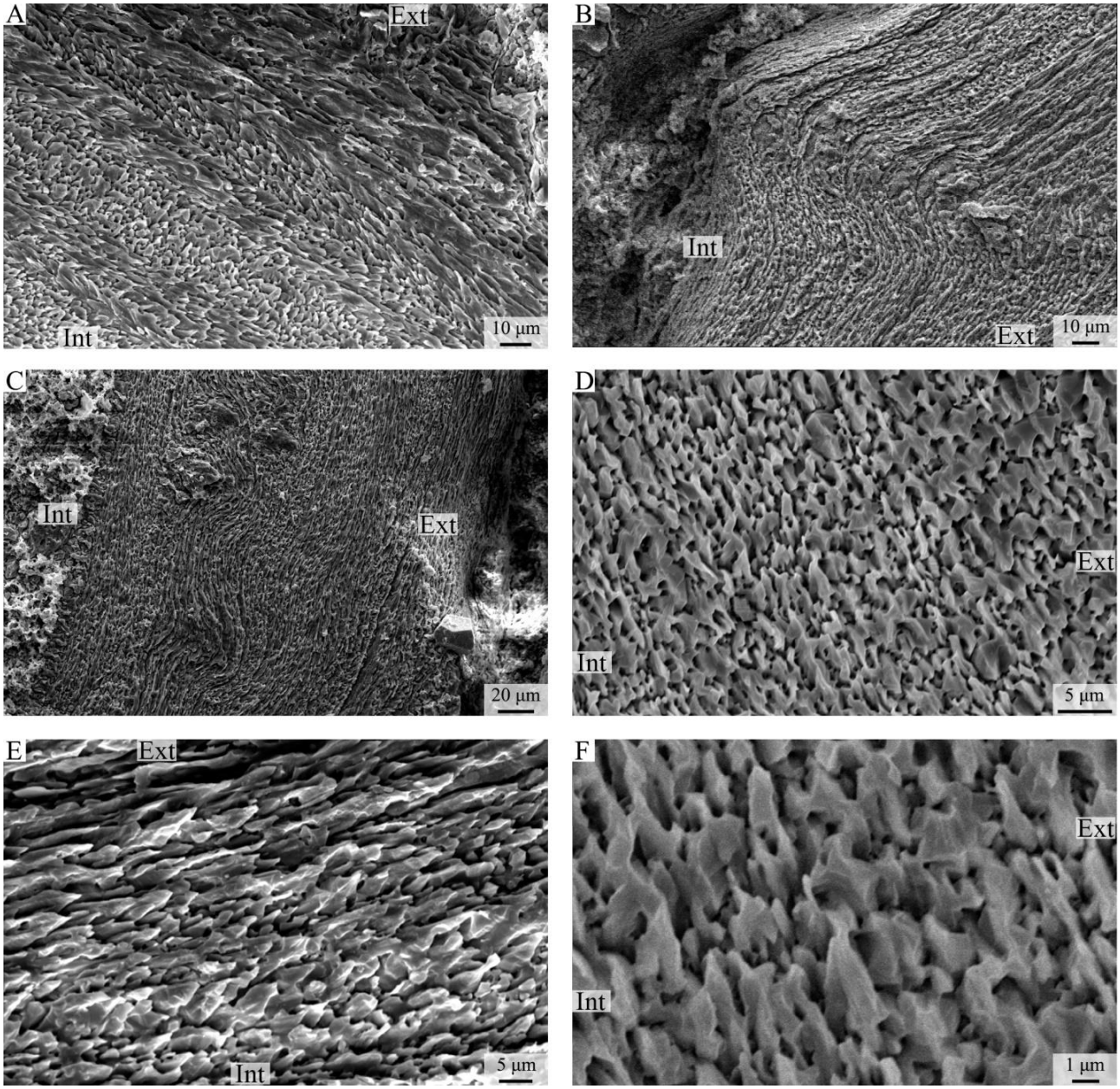
A
Ext
Int
10 µm
B
Int
Ext
10 µm
C
Int
Ext
20 µm
D
Ext
Int
5 µm
E
Ext
Int
5 µm
F
Ext
Int
1 µm

Laminar – CHONETIDINA

The primary layer of Chonetidina (*Striatochonetes* sp. ind., *Devonochonetes* sp. ind., Plate 12, 13) is not preserved in the specimens under investigation. The shell is composed by a laminar secondary layer; the basic unit of the laminae is a blade (Plate 13D-F). The evidences of a columnar tertiary layer were not found. Laminae are grouped into packages, where the axes of blades are parallel. Packages of laminae, with blade axis orientations with different angles, alternate in the secondary layer, but not typical cross-bladed fabric was found (Plate 13).

Plate 12

A: laminar layer in the central part (*Striatochonetes* sp. ind., MRAN 9136-3, ventral valve);

B: pseudopuncta crossing the laminar layer (*Striatochonetes* sp. ind., MRAN 9136-3, ventral valve);

C: laminar layer near the central internal part (*Striatochonetes* sp. ind., MRAN 9136-6, ventral valve);

D: laminar layer near the anterior part (*Striatochonetes* sp. ind., MRAN 9159-2, ventral valve);

E: enlarged detail of the laminae (*Striatochonetes* sp. ind., MRAN 9136-6, ventral valve);

F: enlarged detail of the laminae (*Striatochonetes* sp. ind., MRAN 9159-2, ventral valve).

Ext: external part of the shell; Int: internal part of the shell.

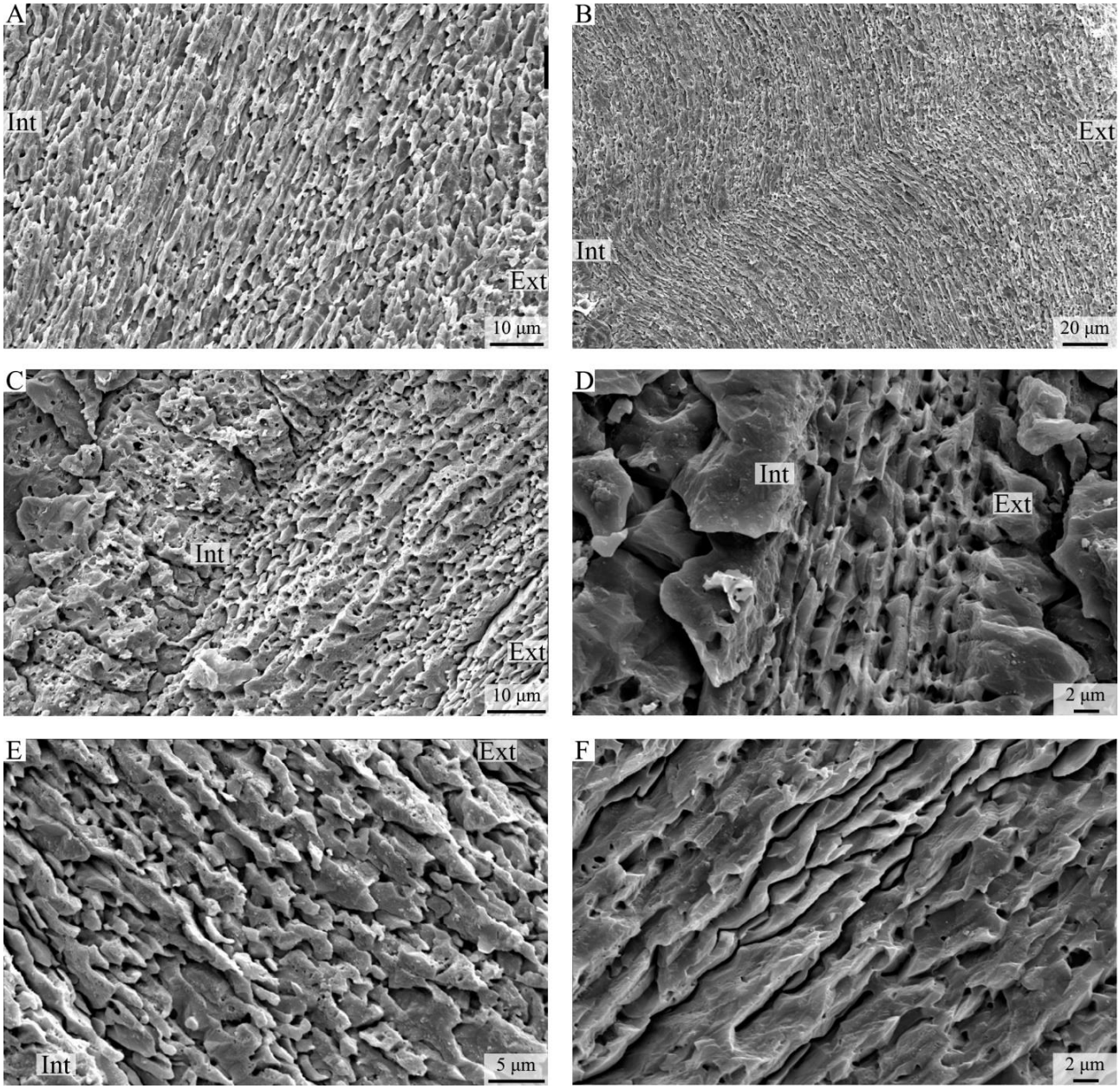
A
Int
Ext
10 µm
B
Ext
Int
20 µm
C
Int
Ext
10 µm
D
Int
Ext
2 µm
E
Ext
Int
5 µm
F
2 µm

Plate 13

A: overview of the laminar layer in the umbonal region (*Devonochonetes* sp. ind., MRAN 3648-13, ventral valve);

B: laminar layer near the posterior part (*Devonochonetes* sp. ind., MRAN 3648-4, ventral valve);

C: laminar layer in the central part (*Devonochonetes* sp. ind., MRAN 3648-2, dorsal valve);

D: enlarged detail of laminae (*Devonochonetes* sp. ind., MRAN 3648-4, ventral valve);

E, F: enlarged detail of laminae (*Devonochonetes* sp. ind., MRAN 3648-13, ventral valve).

Ext: external part of the shell; Int: internal part of the shell.

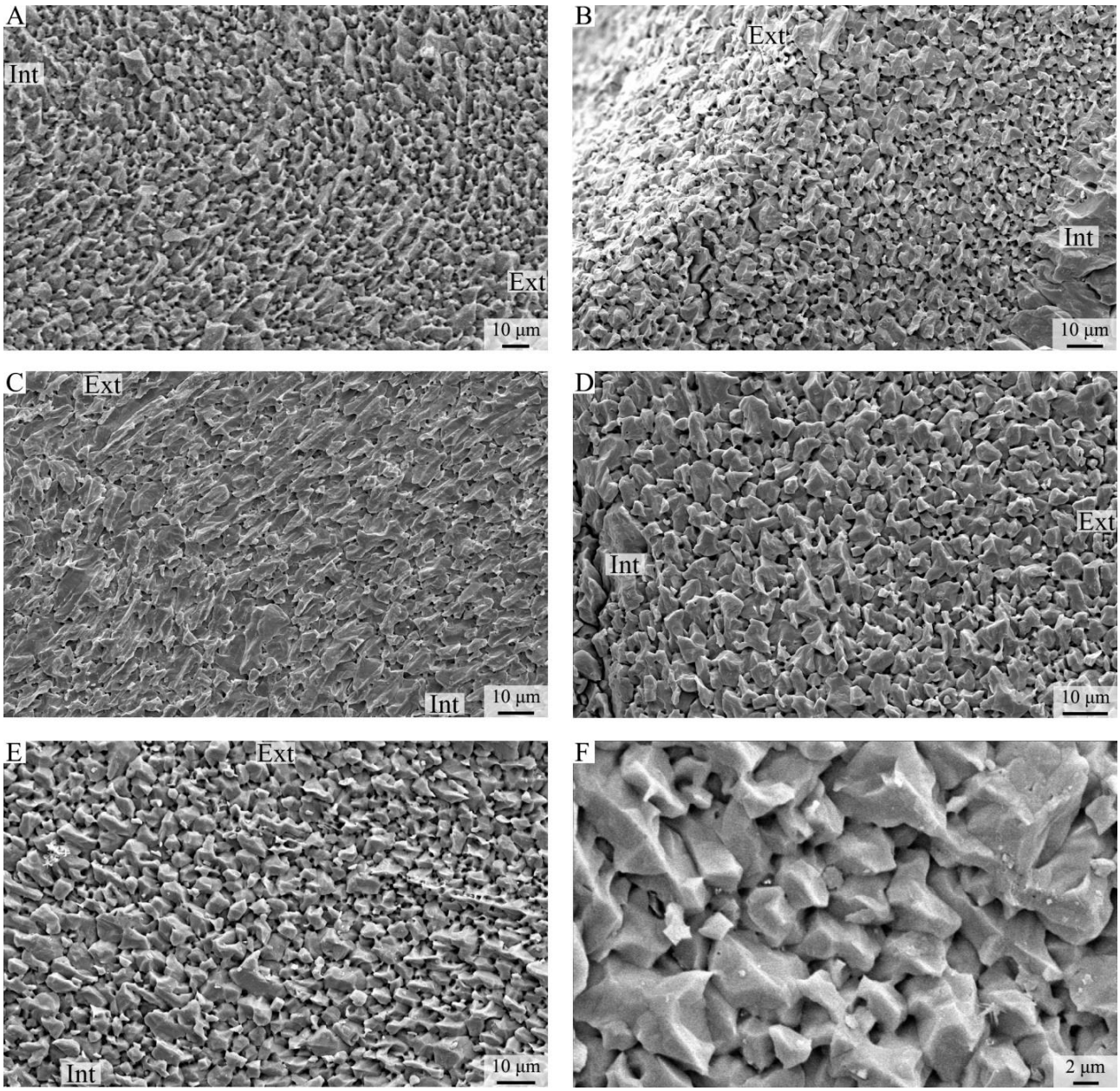
A
Int
Ext
10 µm
B
Ext
Int
10 µm
C
Ext
Int
10 µm
D
Ext
Int
10 µm
E
Ext
Int
10 µm
F
2 µm

Laminar cross bladed – TRIPLESIIDINA

The primary layer of Triplediidina (*Triplesia alata*, Plate 14) is not preserved in the specimens under investigation. The shell is composed by a laminar secondary layer, but the preservation is not good, so the basic unit of the laminae is not very clear (Plate 14B, D). The presence of columnar tertiary layer was not found. Laminae are grouped into packages, where the axes of blades are parallel. Packages of laminae, with blade axis orientations with different angles, alternate in the secondary layer, but not typical cross-bladed structure was found (Plate 14A).

Plate 14

A-D: laminar layer in cross section (*Triplesia alata*, MRAN 1181-7, dorsal valve).

Ext: external part of the shell; Int: internal part of the shell.

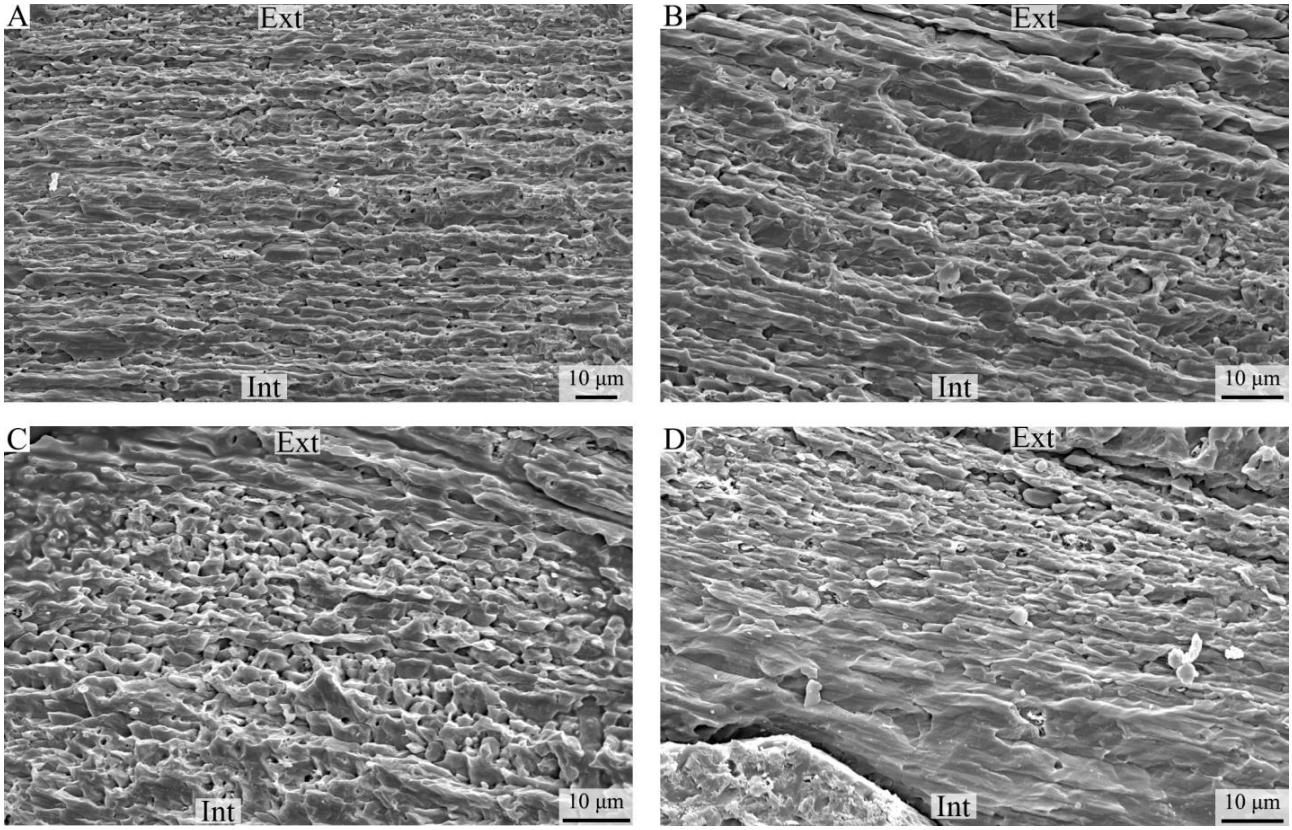
A
Ext
Int
10 µm
B
Ext
Int
10 µm
C
Ext
Int
10 µm
D
Ext
Int
10 µm

5.3.3.2 Fibrous fabric

Fibrous – ORTHIDA

The primary layer of Orthida (?*Hesperonomiella* sp. ind., *Nicolella actoniae*, *Paralenorthis* sp. ind., *Howellites ultima*, *Isorthis (Ovalella) inflata*, ?*Isorthis* sp. ind., *Isorthis* sp. ind., Plates 15-19) is not preserved in the specimens under investigation. The shell is composed by a fibrous layer: the basic structural unit is a fibre with a typical sub-diamond shape in cross section (e.g. in *Howellites ultima* Plate 16C, *Nicolella actoniae* Plate 18D). Columnar tertiary layer was observed in *Nicolella actoniae*, *Paralenorthis* sp. ind., *Howellites ultima*, *Isorthis (Ovalella) inflata*, but no evidence was found in *Hesperonomiella* sp. ind., ?*Isorthis* sp. ind., *Isorthis* sp. ind., (Table 3). Punctae were found in *Nicolella actoniae* and *Howellites ultima* (Plate 18F); wedges inter-cross structures of fibres (Plate 16A) were found in this taxon (Table 3).

Plate 15

A: fibrous layer in the central part (*Hesperonomiella* sp. ind., MRAN 8761-1, dorsal valve);

B, C: enlarged detail of the fibrous layer (*Hesperonomiella* sp. ind., MRAN 8761-1, dorsal valve);

D: fibrous layer in the central part (*Hesperonomiella* sp. ind., MRAN 8761-1, dorsal valve);

E, F: fibrous layer in the central part (*Isorthis (Ovalella) inflata*, MRAN 1189-3, dorsal valve);

G: oblique/longitudinal fibrous layer (*Isorthis (Ovalella) inflata*, MRAN 1189-3, ventral valve);

H: enlarged detail of the fibres (*Isorthis (Ovalella) inflata*, MRAN 1189-3, dorsal valve).

Ext: external part of the shell; Int: internal part of the shell.

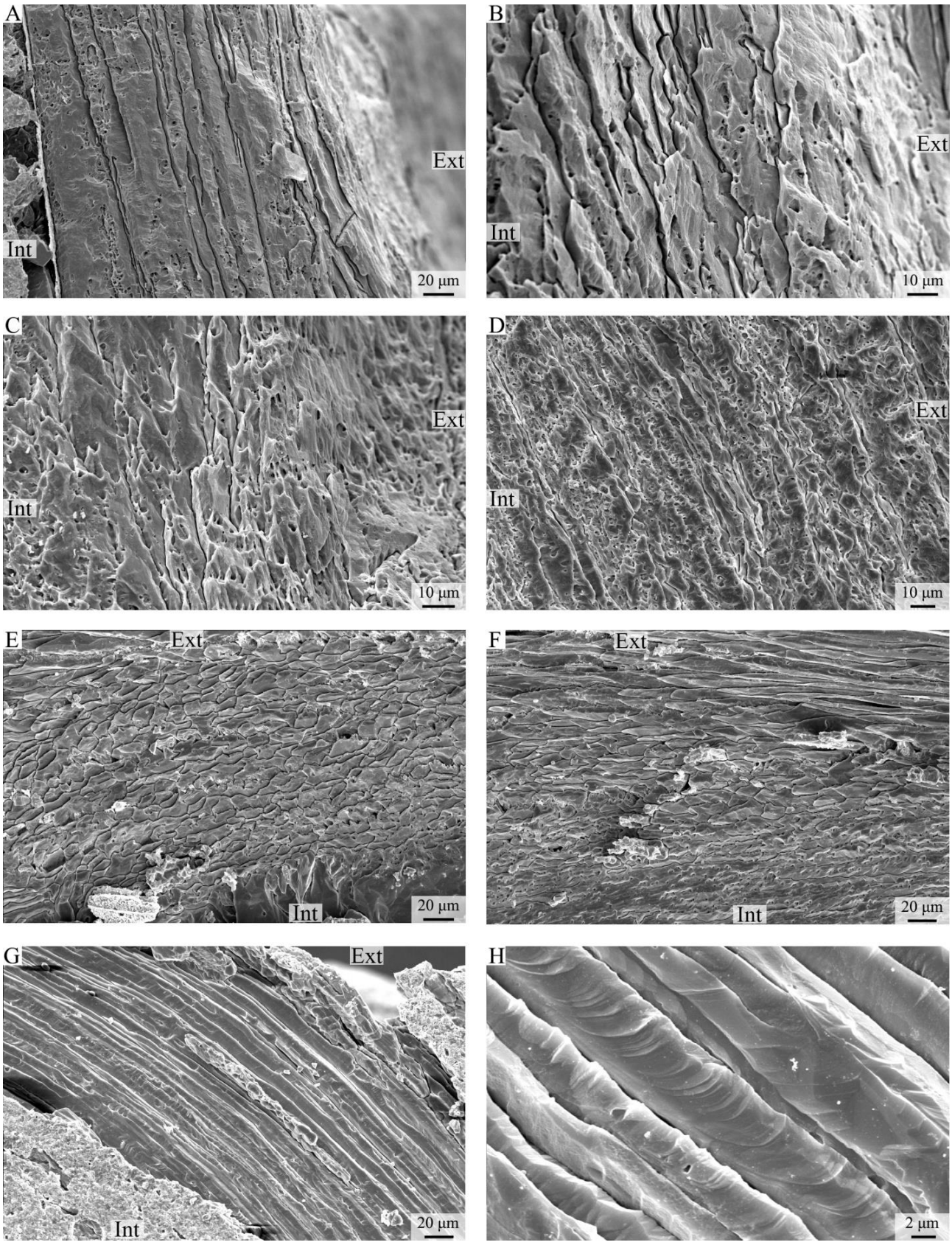
A
Ext
Int
20 µm
B
Ext
Int
10 µm
C
Ext
Int
10 µm
D
Ext
Int
10 µm
E
Ext
Int
20 µm
F
Ext
Int
20 µm
G
Ext
Int
20 µm
H
2 µm

Plate 16

A: fibrous layer inter-cross wedges in the umbonal region (*Howellites ultima*, MRAN 1125-7, ventral valve);

B: fibrous layer with punctae (*Howellites ultima*, MRAN 1108, ventral valve);

C: fibrous secondary layer and tertiary layer (*Howellites ultima*, MRAN 1108, dorsal valve);

D: fibrous layer near the anterior part (*Howellites ultima*, MRAN 1108, dorsal valve);

E, F: enlarged detail of fibrous layer (*Howellites ultima*, MRAN 1125-7, dorsal valve).

Ext: external part of the shell; Int: internal part of the shell.

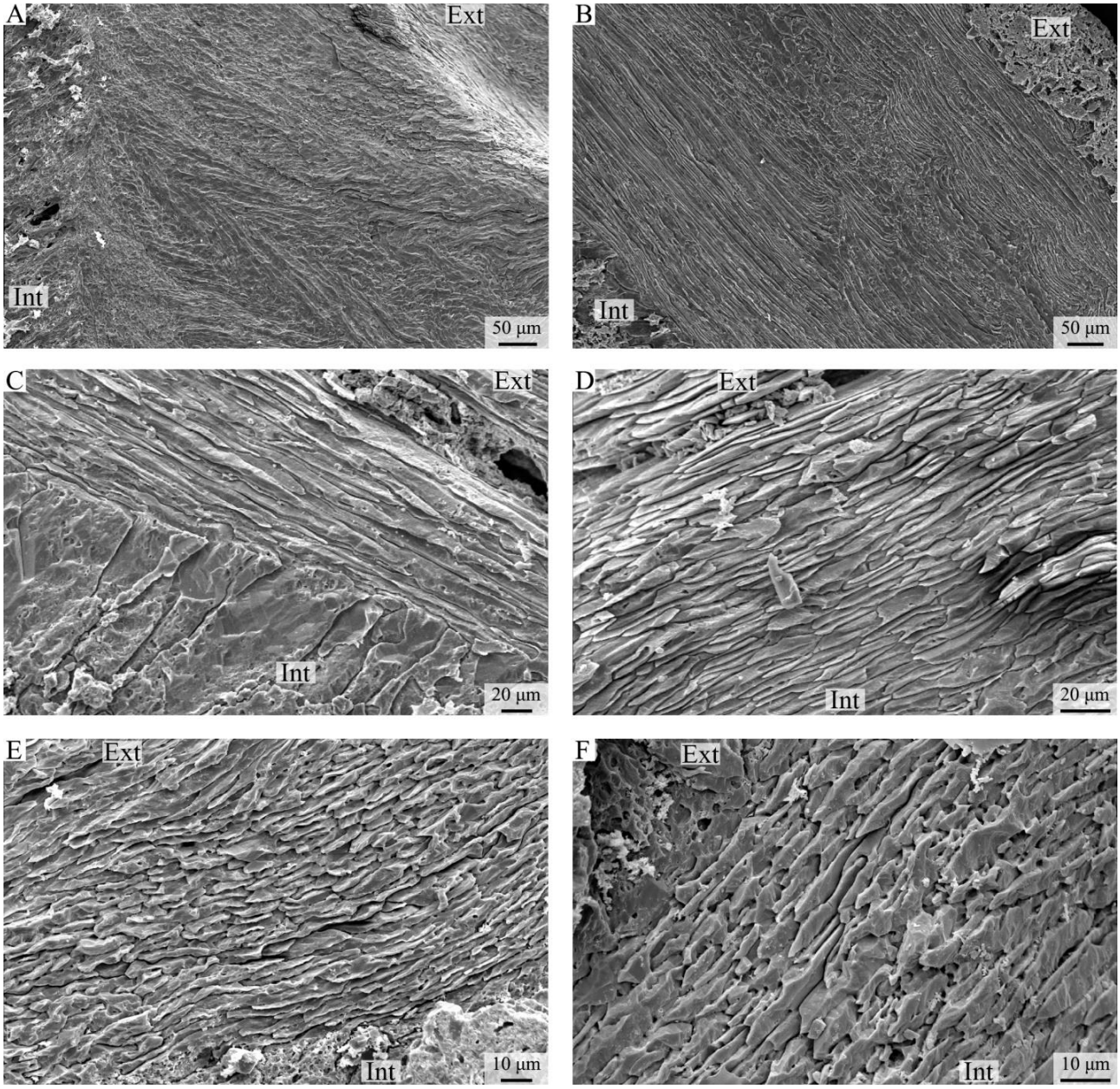
A
Ext
Int
50 µm
B
Ext
Int
50 µm
C
Ext
Int
20 µm
D
Ext
Int
20 µm
E
Ext
Int
10 µm
F
Ext
Int
10 µm

Plate 17

A: fibrous layer (*Isorthis* sp. ind., MRAN 6904-4, ventral valve);

B: fibrous layer near the anterior part (*Isorthis* sp. ind., MRAN 6903-1, ventral valve);

C: fibrous layer (*Isorthis* sp. ind., MRAN 6904-4, ventral valve);

D: enlarged detail of the fibrous layer (*Isorthis* sp. ind., MRAN 6904-4, ventral valve)

Ext: external part of the shell; Int: internal part of the shell.

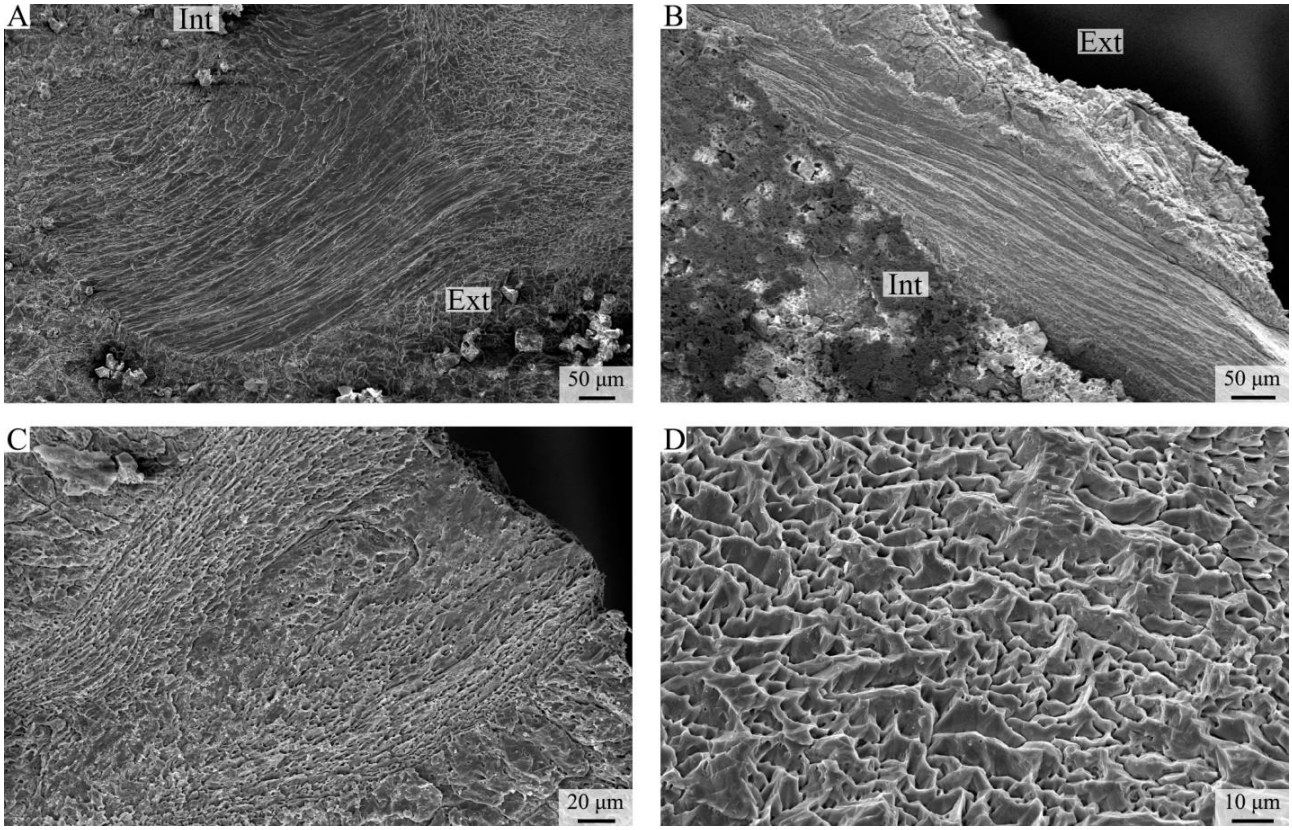
A
Int
Ext
50 µm
B
Ext
Int
50 µm
C
20 µm
D
10 µm

Plate 18

A: fibrous layer near the posterior part (*Nicolella actoniae*, MRAN 1125-6, ventral valve);

B: fibrous layer (*Nicolella actoniae*, MRAN 1130-1, ventral valve);

C, D: fibrous layer in the umbonal part (*Nicolella actoniae*, MRAN 1125-6, dorsal valve);

E: longitudinal section of the fibrous layer (*Nicolella actoniae*, MRAN 1130-1, ventral valve);

F: puncta (*Nicolella actoniae*, MRAN 1125-8, dorsal valve);

G: fibrous layer in the anterior part (*Nicolella actoniae*, MRAN 1125-11, dorsal valve);

H: oblique section of the fibrous layer in the central part (*Nicolella actoniae*, MRAN 1125-11, dorsal valve).

Ext: external part of the shell; Int: internal part of the shell.

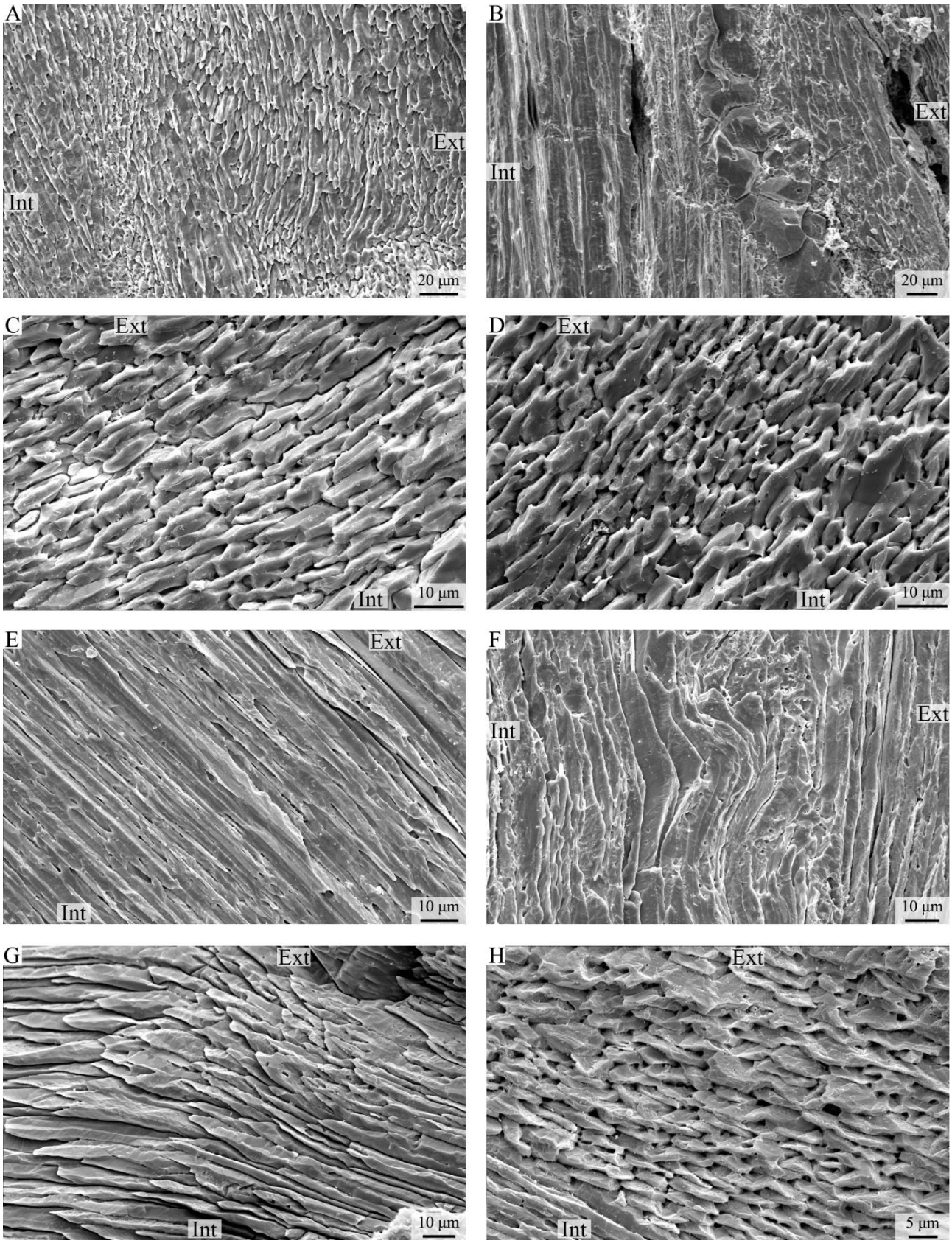
A
Ext
Int
20 µm
B
Ext
Int
20 µm
C
Ext
Int
10 µm
D
Ext
Int
10 µm
E
Ext
Int
10 µm
F
Int
Ext
10 µm
G
Ext
Int
10 µm
H
Ext
Int
5 µm

Plate 19

A: overview of the fibrous layer in the umbonal part (*Paralenorthis* sp. ind., KE41-1, ventral valve);

B: orientation change of fibrous sub-layers (*Paralenorthis* sp. ind., KE41-5, ventral valve);

C: fibrous layer in the central part (*Paralenorthis* sp. ind., KE41-1, ventral valve);

D: fibrous layer (*Paralenorthis* sp. ind., KE41-5, ventral valve);

E: longitudinal section of fibrous layer in the central part (*Paralenorthis* sp. ind., KE45-5, ventral valve);

F: longitudinal section of the fibrous layer near the anterior part (*Paralenorthis* sp. ind., KE45-5, dorsal valve);

G: enlarged detail of the fibres (*Paralenorthis* sp. ind., KE41-1, ventral valve);

H: enlarged detail of the fibres (*Paralenorthis* sp. ind., KE41-5, ventral valve).

Ext: external part of the shell; Int: internal part of the shell.

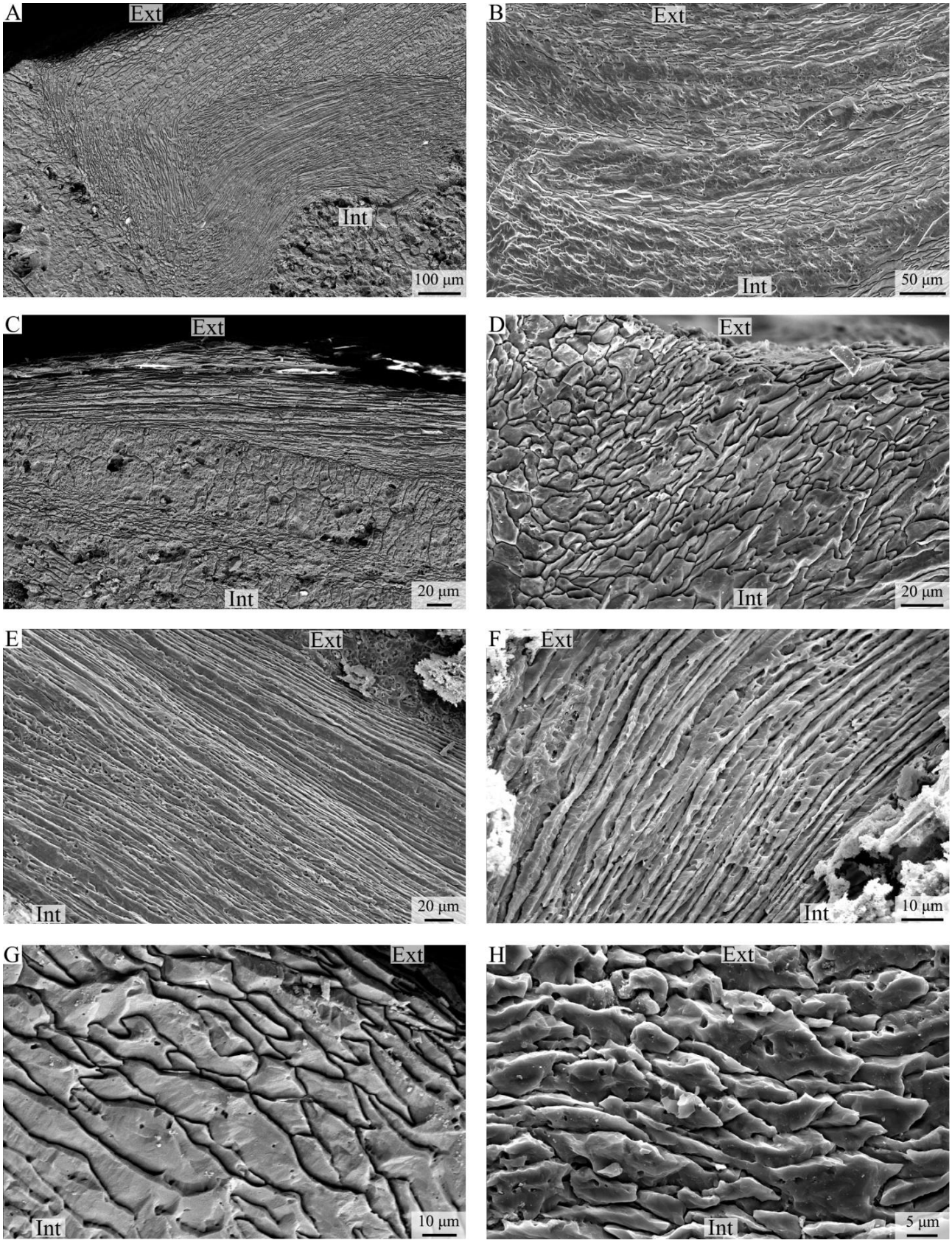
A
Ext
Int
100 µm
B
Ext
Int
50 µm
C
Ext
Int
20 µm
D
Ext
Int
20 µm
E
Ext
Int
20 µm
F
Ext
Int
10 µm
G
Ext
Int
10 µm
H
Ext
Int
5 µm

Fibrous – PENTAMERIDA

The primary layer of Pentamerida (*Syntrophioides* sp. ind., ?*Clorinda* sp. ind., *Clorinda molongensis*, Plates 20-21) is not preserved in the specimens under investigation. The shell is composed of fibrous secondary layer; the basic unit of the fibrous layer is a fibre, but not it is not well preserved (Plate 20F). Columnar tertiary layer is present in *Clorinda* sp. ind. but other microstructural features were not found in this taxon.

Plate 20

A: fibrous layer in the umbonal region (*Clorinda molongensis*, NIB5-10, dorsal valve);

B: enlarged detail of the fibres near the posterior part (*Clorinda molongensis*, MRAN 1181-13, ventral valve);

C: columnar tertiary layer near the posterior part (*Clorinda* sp. ind., LA 3, ventral valve);

D-E: enlarged detail of the columnar tertiary layer (*Clorinda* sp. ind., LA 3, ventral valve);

F: fibrous layer (*Clorinda* sp. ind., LA 3, ventral valve).

Ext: external part of the shell; Int: internal part of the shell.

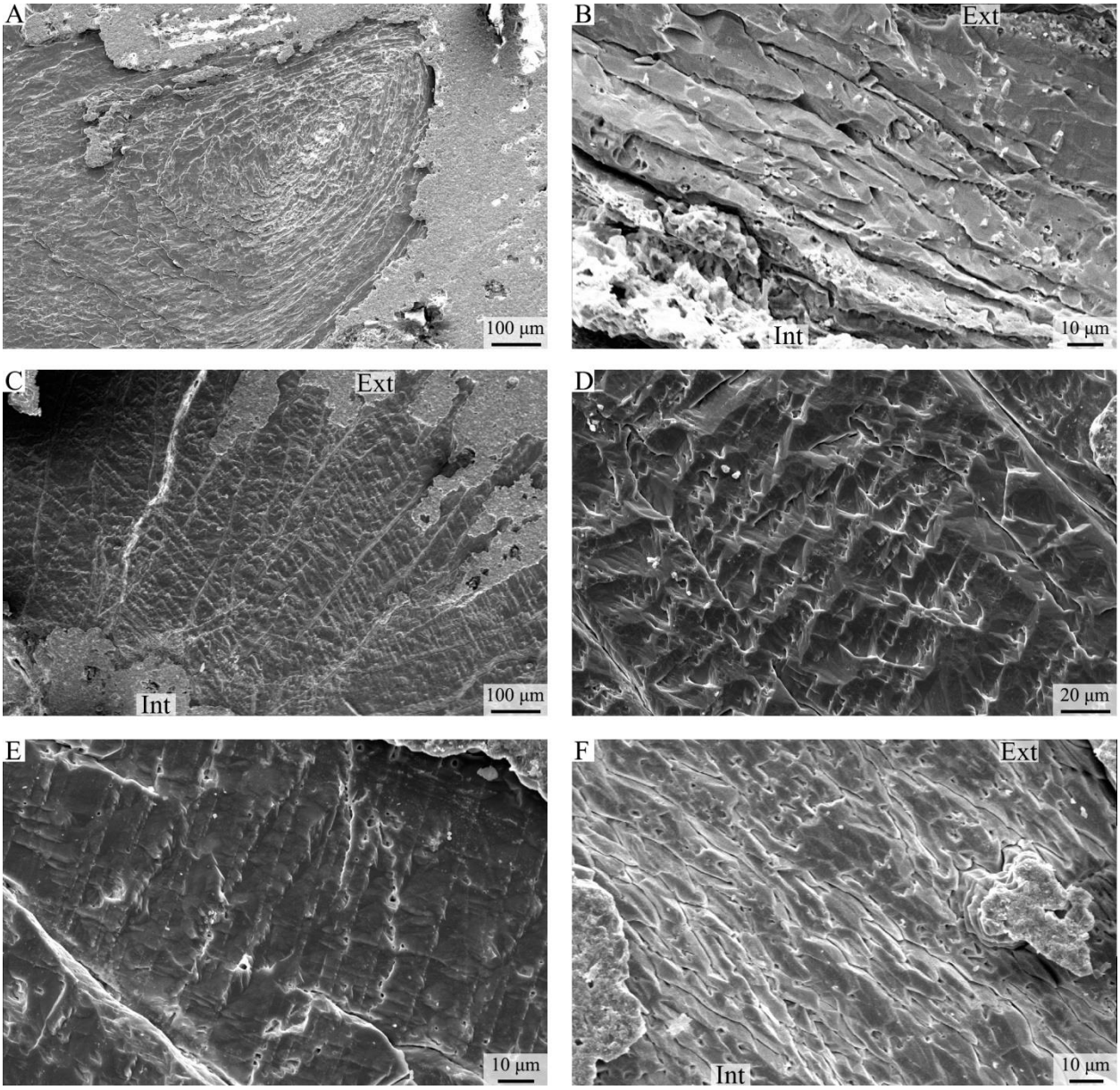
A
100 µm
B
Ext
Int
10 µm
C
Ext
Int
100 µm
D
20 µm
E
10 µm
F
Ext
Int
10 µm

Plate 21

A: fibrous layer in the central part (*Syntrophioides* sp. ind., MRAN 8291-5, dorsal valve);

B: fibrous layer in the external central part (*Syntrophioides* sp. ind., MRAN 8291-5, dorsal valve);

C: overview of the fibrous layer near the anterior part (*Syntrophioides* sp. ind., MRAN 8291-4, dorsal valve);

D: enlarged detail of the fibres (*Syntrophioides* sp. ind., MRAN 8291-5, dorsal valve).

Ext: external part of the shell; Int: internal part of the shell.

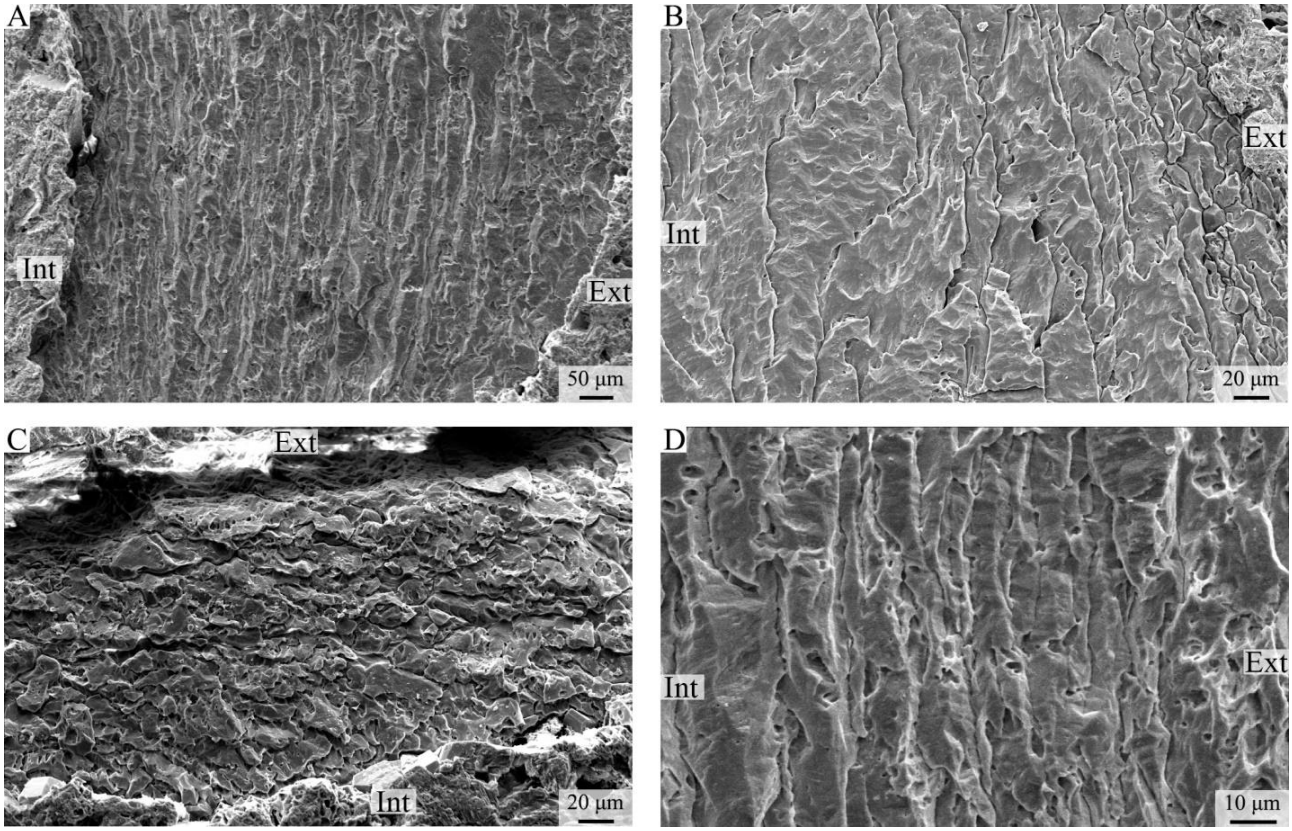
A
Int
Ext
50 µm
B
Ext
Int
20 µm
C
Ext
Int
20 µm
D
Int
Ext
10 µm

Fibrous – ATRYPIDA

The primary layer of Atrypida (*Spinatrypina* sp. ind., *Spinatrypina* cf. S. *chitralensis*, Plates 22) is not preserved in the specimens under investigation. The shell is composed by a fibrous secondary layer; the basic unit of the layer is a fibre, but it is not well preserved (Plate 22D). Columnar tertiary layer and other perforation structures were not observed in this taxon.

Plate 22

A: fibrous layer near the posterior part (*Spinatrypina* cf. S. *chitralensis*, MRAN 6162-14, dorsal valve);

B, C: fibrous layer in the central part (*Spinatrypina* cf. S. *chitralensis*, MRAN 6162-14, dorsal valve);

D: enlarged detail of the fibres near the posterior part (*Spinatrypina* cf. S. *chitralensis*, MRAN 6162-14, dorsal valve);

E: fibrous layer in the umbonal region (*Spinatrypina* sp. ind., MRAN 1180-3, ventral valve);

F: fibrous layer in the umbonal region (*Spinatrypina* sp. ind., MRAN 1180-29, dorsal valve);

G: fibrous layer in the central part (*Spinatrypina* sp. ind., MRAN 1180-3, dorsal valve);

H: fibrous layer covered by impurities cover (*Spinatrypina* sp. ind., MRAN 1180-29, ventral valve).

Ext: external part of the shell; Int: internal part of the shell.

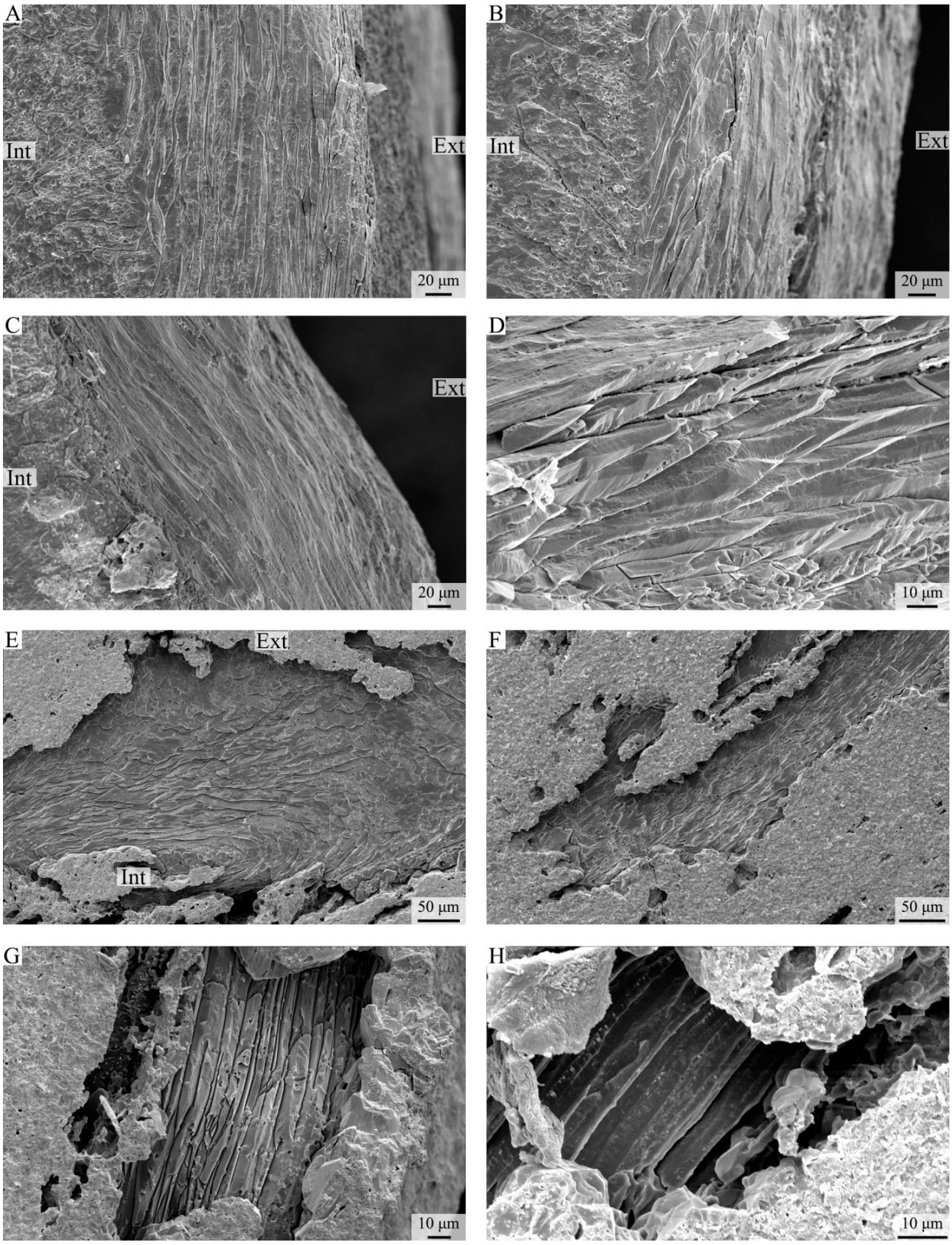
A
Int
Ext
20 µm
B
Int
Ext
20 µm
C
Ext
Int
20 µm
D
10 µm
E
Ext
Int
50 µm
F
50 µm
G
10 µm
H
10 µm

Fibrous – RHYNCHONELLIDA

The primary layer of Rhynchonellida (*Rhynchotrema* sp. ind., *Stegocornu denisae*, *Cyphoterorhynchus arpaensis*, Plates 23, 24) is not preserved in the specimens under investigation. The shell is composed by a fibrous secondary layer; the basic unit of the fibrous layer is a fibre, but not enough well preserved to assess its outline in cross section (Plate 24G, H). Columnar tertiary layer and other perforation structures were not observed in this taxon.

Plate 23

A: fibrous layer near the posterior part (*Cyphoterorhynchus arpaensis*, MRAN 6162-10, dorsal valve);

B: fibrous layer in the anterior part (*Cyphoterorhynchus arpaensis*, MRAN 6162-10, dorsal valve);

C: fibrous layer near the posterior part (*Cyphoterorhynchus arpaensis*, MRAN 6162-10, ventral valve);

D fibrous layer near the anterior part (*Cyphoterorhynchus arpaensis*, MRAN 6162-10, dorsal valve);

E: fibrous layer in the umbo part (*Cyphoterorhynchus arpaensis*, MRAN 6162-10, dorsal valve);

F: enlarged detail of the fibres in the central part (*Cyphoterorhynchus arpaensis*, MRAN 6162-10, ventral valve).

Ext: external part of the shell; Int: internal part of the shell.

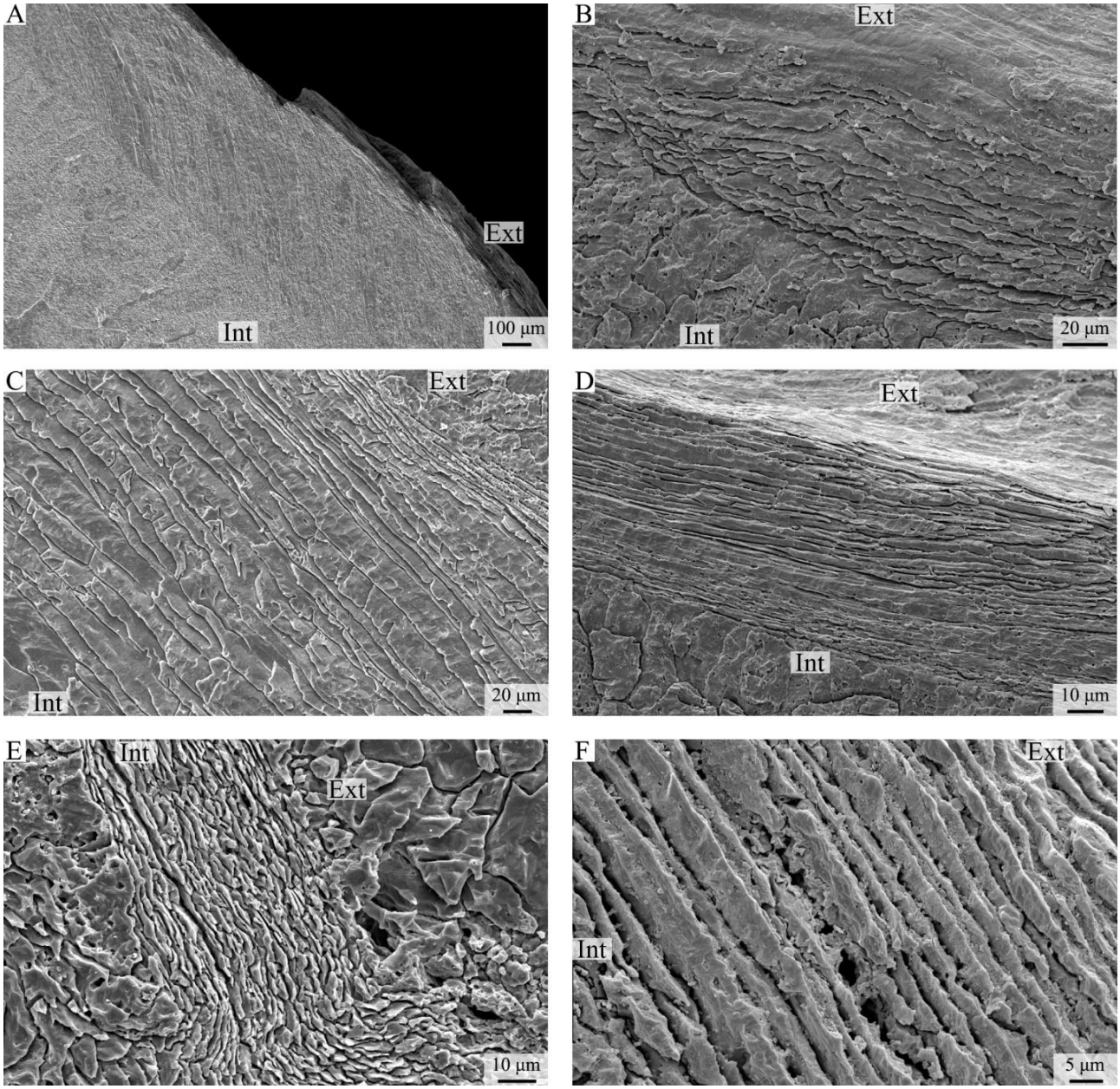
A
Ext
Int
100 µm
B
Ext
Int
20 µm
C
Ext
Int
20 µm
D
Ext
Int
10 µm
E
Int
Ext
10 µm
F
Ext
Int
5 µm

Plate 24

A: longitudinal section of fibres (*Rhynchotrema* sp. ind., MRAN 6784-1, ventral valve);

B, C: oblique/longitudinal section of fibres (*Rhynchotrema* sp. ind., MRAN 6784-1, dorsal valve);

D: fibrous layer near the umbonal region (*Rhynchotrema* sp. ind., MRAN 6784-1, dorsal valve);

E: fibrous layer in the central part (*Stegocornu denisae*, MRAN 6904-1, ventral valve);

F: longitudinal section of fibres near the posterior part (*Stegocornu denisae*, MRAN 6904-1, ventral valve);

G: fibrous layer near the posterior part (*Stegocornu denisae*, MRAN 6904-1, ventral valve);

H: enlarged detail of the fibres (*Stegocornu denisae*, MRAN 6904-1, ventral valve).

Ext: external part of the shell; Int: internal part of the shell.

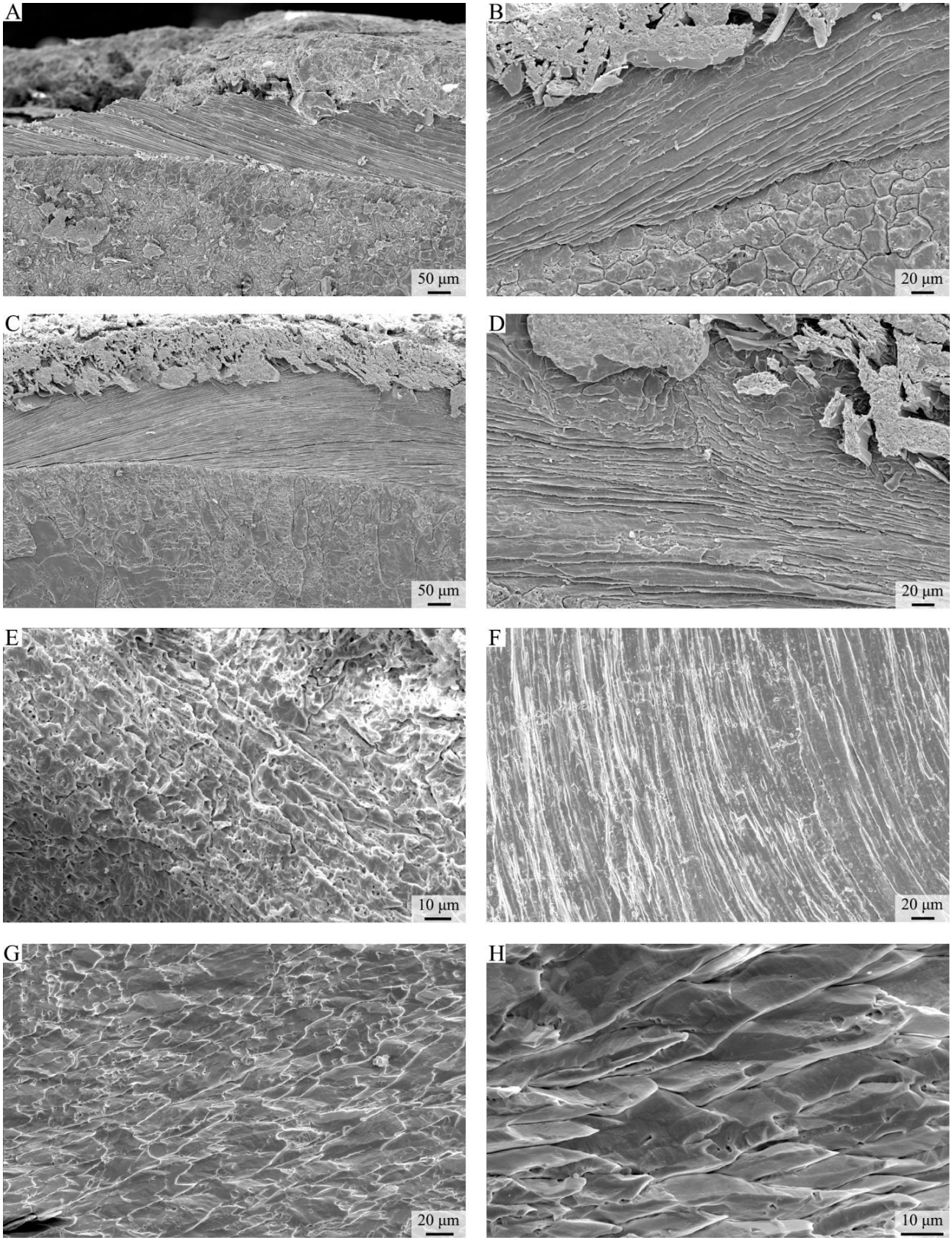
A
50 µm
B
20 µm
C
50 µm
D
20 µm
E
10 µm
F
20 µm
G
20 µm
H
10 µm

Fibrous – SPIRIFERIDA

The primary layer of Spiriferida (*Hedeinopsis hispanica hispanica*, *Hedeinopsis* sp. ind., *Cyrtospirifer brodi*, *Cyrtospirifer* cf. *C. kermanensis*, *Cyrtospirifer* sp. ind., *Uchtospirifer* aff. *Uchtospirifer nalivkini*, Plates 25-28) is not preserved in the specimens under investigation. The shell is composed by a fibrous secondary layer; the basic unit is a fibre (25C, D), with diamond- shaped to keel and saddle profile (25D, 26G). Columnar tertiary layer was observed in *Cyrtospirifer* sp., and *Uchtospirifer* aff. *Uchtospirifer nalivkini* (Table 3). Other microstructures were not found in this taxon.

Plate 25

A: fibrous layer near the anterior part (*Cyrtospirifer brodi*, MRAN 6162-12, dorsal valve);

B: fibrous layer in the anterior part in external view (*Cyrtospirifer brodi*, MRAN 6162-12, ventral valve);

C, D: enlarged detail of the fibres in cross section, fibre with a good profile was marked (*Cyrtospirifer brodi*, MRAN 6162-12, dorsal valve);

E: longitudinal section of the fibres in the central part (*Cyrtospirifer* sp. ind., MRAN 4232-1, ventral valve);

F: fibrous layer near the posterior part (*Cyrtospirifer* sp. ind., MRAN 4232-1, dorsal valve);

G, H: enlarged detail of the fibres near the posterior part (*Cyrtospirifer* sp. ind., MRAN 4232-1, dorsal valve).

Ext: external part of the shell; Int: internal part of the shell.

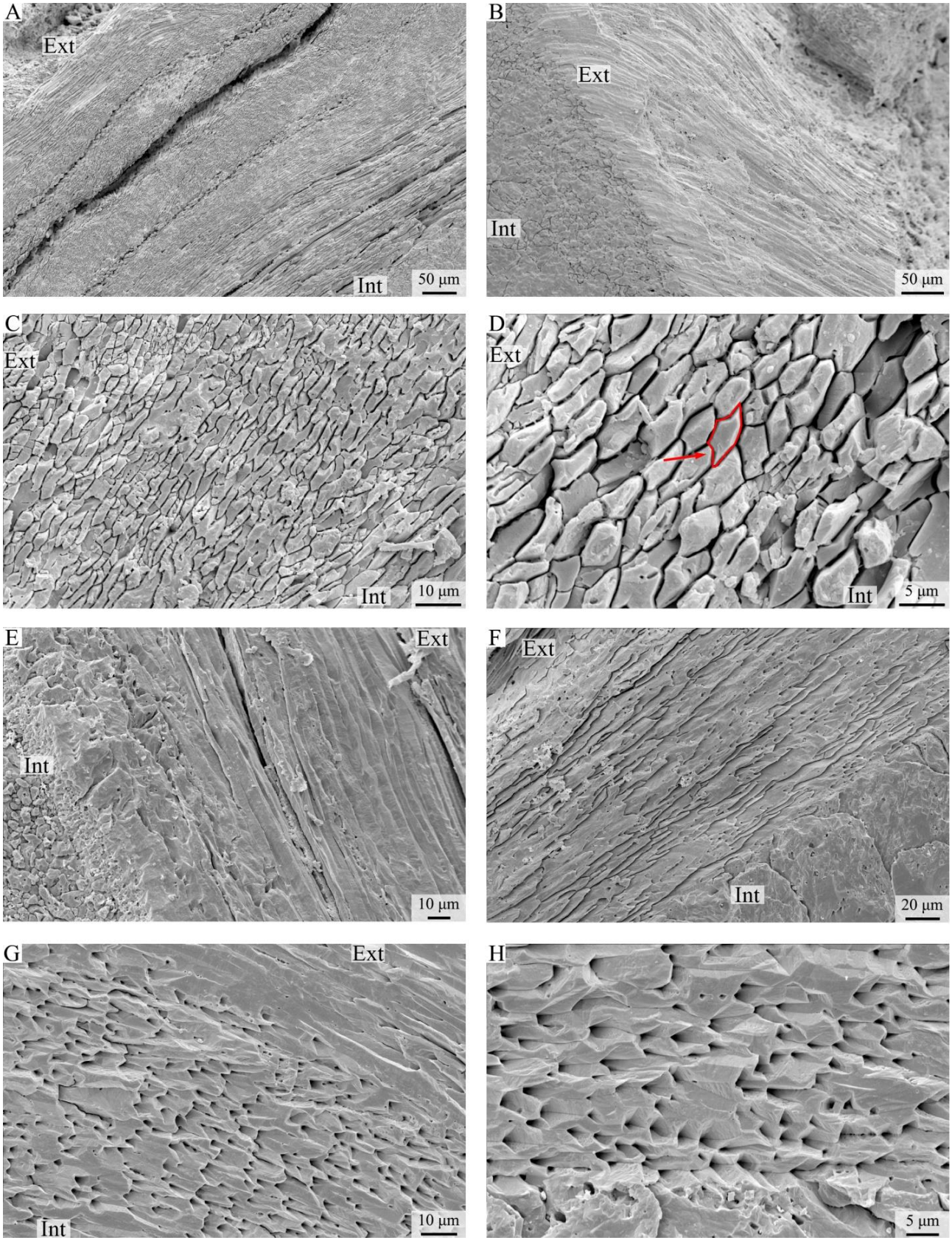
A
Ext
Int
50 µm
B
Ext
Int
50 µm
C
Ext
Int
10 µm
D
Ext
Int
5 µm
E
Ext
Int
10 µm
F
Ext
Int
20 µm
G
Ext
Int
10 µm
H
5 µm

Plate 26

A: fibrous layer near the anterior part (*Cyrtospirifer* cf. C. *kermanensis*, MRAN 4242-3, dorsal valve);

B: fibrous layer near the posterior part (*Cyrtospirifer* cf. C. *kermanensis*, MRAN 4242-3, dorsal valve);

C: fibrous layer in an external view (*Cyrtospirifer* cf. C. *kermanensis*, MRAN 6162-13, ventral valve);

D: fibrous layer in the anterior part (*Cyrtospirifer* cf. C. *kermanensis*, MRAN 6162-18, dorsal valve);

G, H: enlarged detail of the fibres, fibre with a good profile was marked (*Cyrtospirifer* cf. C. *kermanensis*, MRAN 6162-18, ventral valve);

E, F: fibrous layer in the central part (*Cyrtospirifer* cf. C. *kermanensis*, MRAN 6162-18, dorsal valve).

Ext: external part of the shell; Int: internal part of the shell.

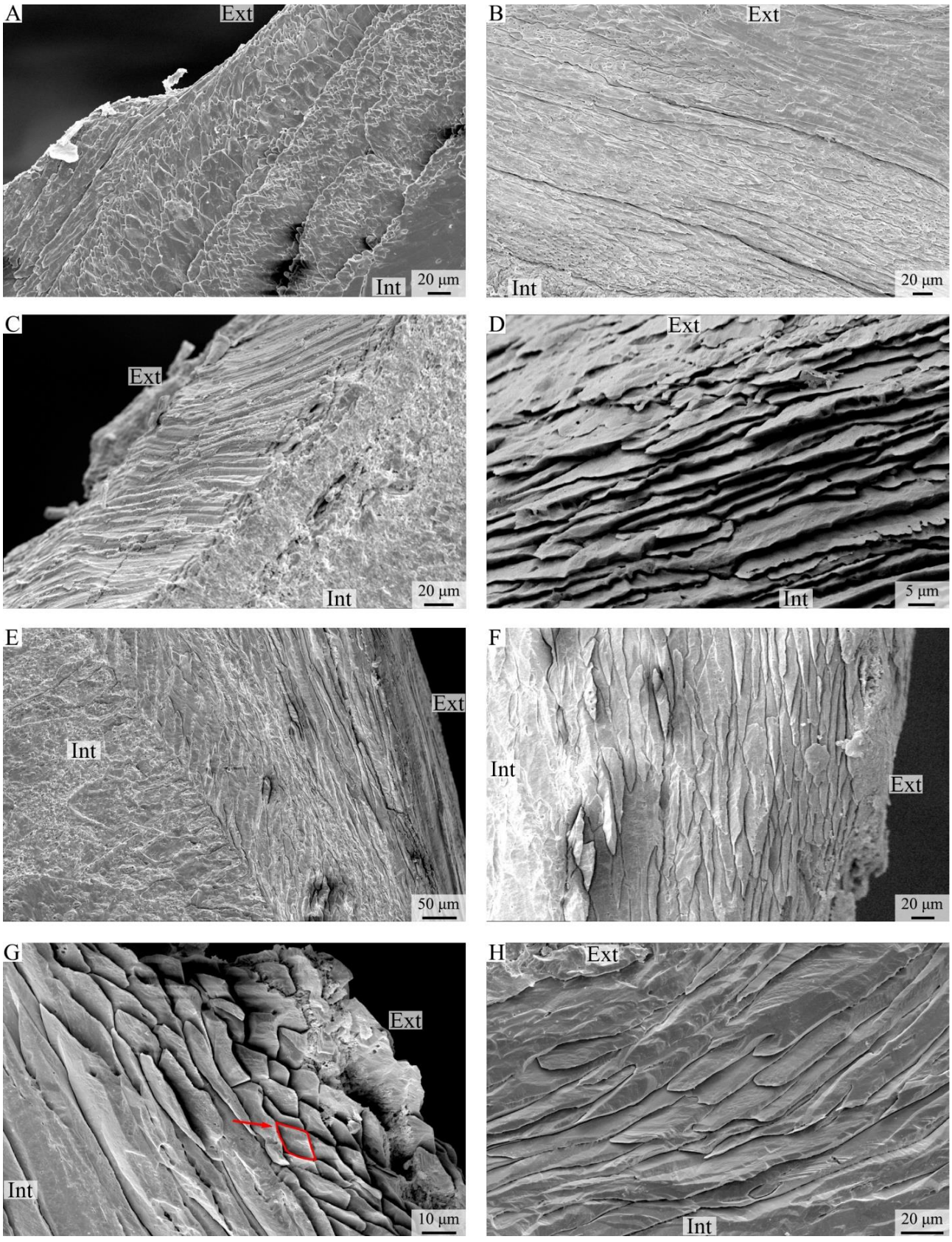
A
Ext
Int
20 µm
B
Ext
Int
20 µm
C
Ext
Int
20 µm
D
Ext
Int
5 µm
E
Int
Ext
50 µm
F
Int
Ext
20 µm
G
Ext
Int
10 µm
H
Ext
Int
20 µm

Plate 27

A-D: oblique/longitudinal section of the fibres near the posterior part (*Hedeinopsis hispanica hispanica*, MRAN 1209-2-A , ventral valve);

E: fibrous layer in the umbonal region (*Hedeinopsis* sp. ind., MRAN 6904-5, ventral valve);

F, G: fibrous layer in the central part (*Hedeinopsis* sp. ind., MRAN 6904-5, ventral valve);

H: enlarged detail of the fibres (*Hedeinopsis* sp. ind., MRAN 6904-5, ventral valve).

Ext: external part of the shell; Int: internal part of the shell.

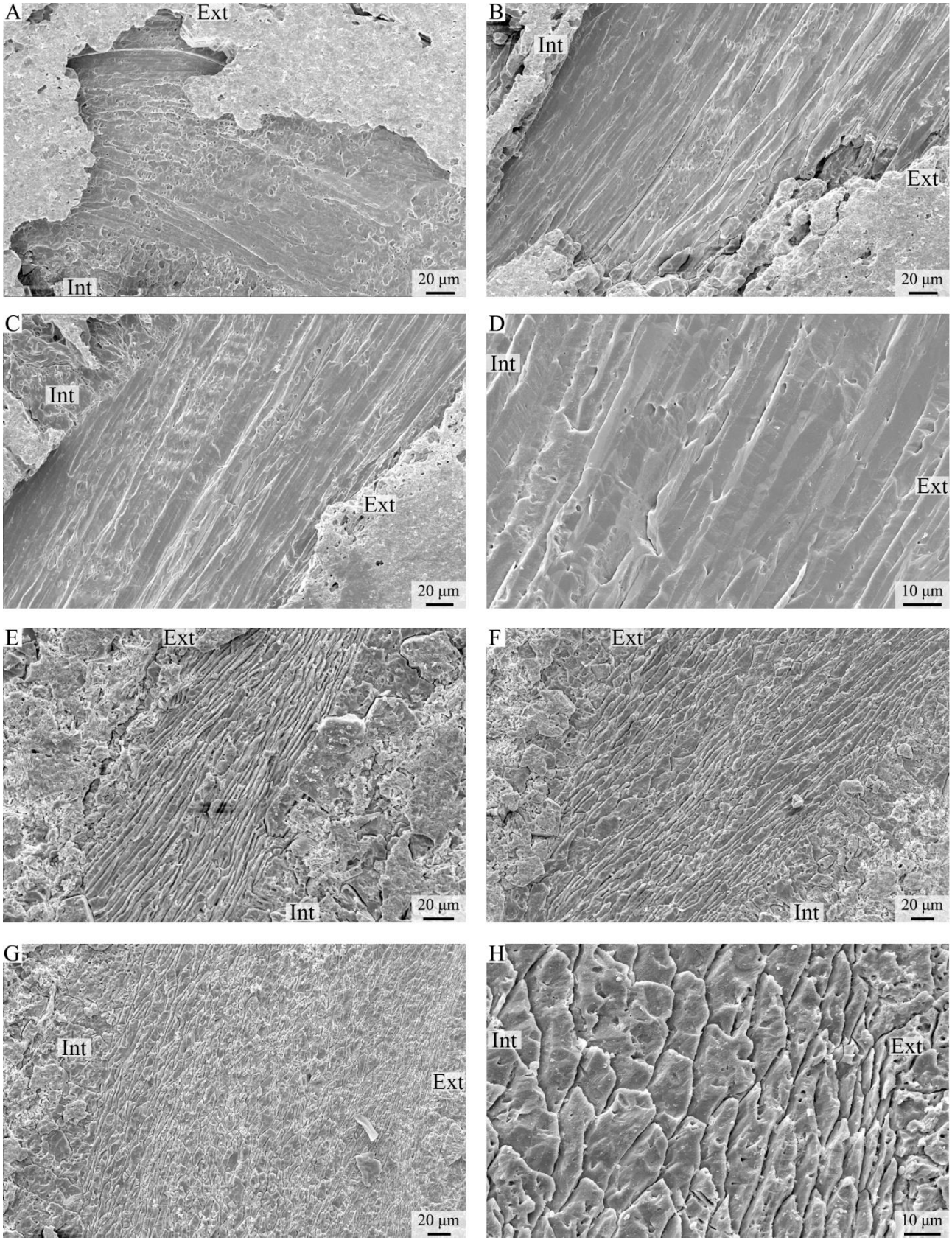
A
Ext
Int
20 µm
B
Int
Ext
20 µm
C
Int
Ext
20 µm
D
Int
Ext
10 µm
E
Ext
Int
20 µm
F
Ext
Int
20 µm
G
Int
Ext
20 µm
H
Int
Ext
10 µm

Plate 28

A: fibrous layer near the posterior part (*Uchtospirifer* aff. *Uchtospirifer nalivkini*, MRAN 4208-1, ventral valve);

B: intercalations of fibrous secondary layer and columnar tertiary layer (*Uchtospirifer* aff. *Uchtospirifer nalivkini*, MRAN 4208-1, ventral valve);

C, D: fibrous layer in the central part (*Uchtospirifer* aff. *Uchtospirifer nalivkini*, MRAN 4208-1, ventral valve).

Ext: external part of the shell; Int: internal part of the shell.

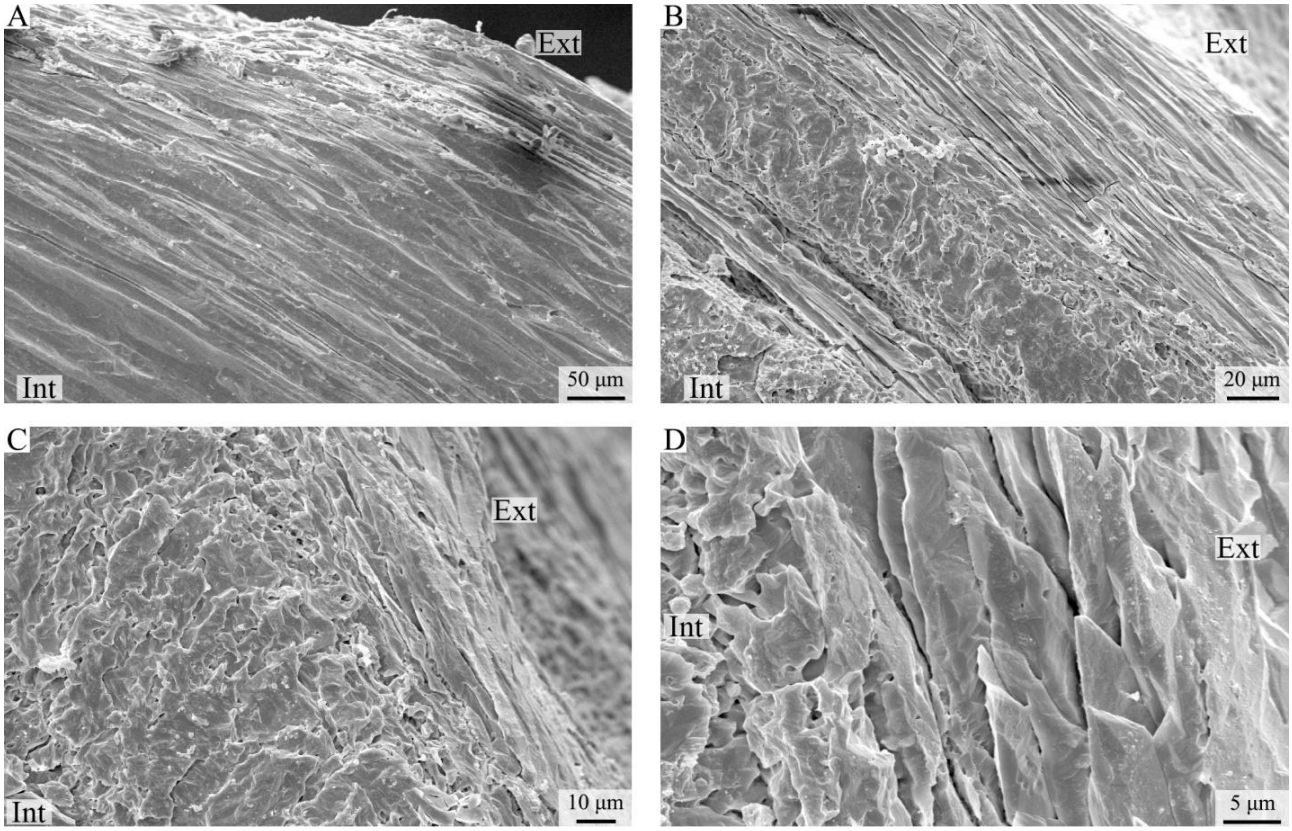
A
Ext
Int
50 µm
B
Ext
Int
20 µm
C
Ext
Int
10 µm
D
Ext
Int
5 µm

5.3 Discussion

5.3.1 Laminar microstructure organization

In Billingselloidea, the laminar secondary layer is made up by blades which are ordered and amalgamated laterally into a succession of laminar plates or sheets (Williams, 1970). Even if the specimens under investigation did not show a good preservation, laminae with radial folds, in cross-section, were observed in Billingsellidae gen. et sp. ind. (e.g. Plate 1G, H). Changes in the orientation of structural units, like those observed in the cross-bladed fabric, could not be found in the studied specimens of taxa of Billingselloidea. As suggested by Williams (1970) and Williams et al. (2000), taxa with laminar microstructure diverged from the billingselloid, but the evolutionary steps are not clear. The change of the thickness could be taken as a possible indirect evidence of this transformation: the laminae of Billingselloidea show a thickness which ranges in between the one of Productida (representative of the most derived order bearing a laminar layer) and that of the taxa bearing a fibrous fabric (Table 3). It may have happened that during the evolution from the fibrous fabric to the laminar one, the thickness of the structural unit became gradually thinner.

The basic unit of the laminar layer of the Strophomenida is a long, lath-shaped crystallite (i.e. the 'blade'; Armstrong, 1969). Unlike the flat laminar/laminar with radial folds fabrics, the cross-bladed arrangement is the most evident character of the Strophomenide secondary layer. Generally, laminae are grouped into packages, where the axes of the blades are parallel. Packages of laminae, with blade axis orientations with different angles, alternate in the secondary layer (Armstrong, 1969). According to Williams et al. (2000) and Dewing (2004), the Strophomenide laminar-shell probably represents an intermediate morphology between Billingsellida and Productida fabrics. Our data support this view because the thickness of laminae of Strophomenida (ca. 11–13 μm) ranges between that of Billingsellida (ca. 10–14 μm) and that of Productida (ca. 6–8 μm) (Fig. 4). Additionally, the shape in cross-section of the secondary layer laminae of *Ingria* sp. ind. and *Leptellina* sp. ind. from the Ordovician may appear similar to that of a fibrous fabric (Plate 5D, Plate 7H), whereas the fabric of the Silurian *Leptaena depressa* is more like a laminar fabric (Plate 6B).

In the Productida (excluding the Chonetidina), the laminar cross-bladed is the typical microstructure of the secondary layer (Brunton et al., 2000). Pseudopunctae with taleolae and spine internal cavities are frequently observed to cross this layer (Brunton et al., 2000). In the analysed Productide specimens, the laminae are the thinnest recorded and those with the most uniform thickness (Table 4, Fig. 4). The laminae are grouped into packages, where the axes of blades are parallel. Packages of laminae, with blade axis orientations at different angles, sometimes even at a right angle, alternate in the secondary layer, which is the typical character of the laminar cross-bladed fabric.

The shell microstructure of Chonetidina has been alternatively described as intermediate laminar or lath-like fibres fabric (Brunton, 1972). For example, *Strophochonetes primigenius* (Ordovician) showed transitional "fibres"; *Dawsonelloides canadensis* (Devonian) bear a lath-like fibrous fabric, where fibres are only 2–4 μm in width; also *Retichonetes vicinus* (Devonian) shows "fibres" 8-10 μm wide. On the other hand, Carboniferous species, as *Rugosochonetes silleesi,* show more distinguishable lath-like units, which are more similar to a true cross-bladed fabric. Here, in one species of Chonetidina, *Devonochonetes* sp. ind., the shape of the structural units is more similar to a blade of a lamina than to a fibre (Plate 13), and the width of the basic unit is smaller (ca. 5–10 μm)

than the one measured for the fibres (ca. 9–25 µm in this study). Therefore, at least for Devonian species, the fabric of secondary layer of Chonetidina could be considered more similar to a laminar layer.

A well-developed laminar cross-bladed fabric was previously reported in the Triplesioidea, including *Triplesia* (Williams, 1970). In the investigated species of Triplesiidina (*Triplesia alata*, Plate 14), even if the preservation is not excellent, we can detect the typical characters of this fabric, with laminae composed of well-aligned laths, but the cross-bladed organization is not very clear.

In summary, different laminar fabrics were observed: Laminae with radial folds (flat lamination) in the Billingsellida; cross-bladed lamination in the Strophomenida and Productida (excluding Chonetidina); laminar fabric, with no evidences of cross-lamination, in Chonetidina and Triplesiidina.

5.3.2 Fibrous microstructure organization

The secondary shell of Rhynchonellata brachiopods consists of a fibrous fabric, which can be crossed by perforation, being punctate, endopunctate or impuctate (Williams, 1997; Williams and Carlson, 2000). The structural units of the secondary layer are stacked fibres, which, in cross section, have an outline varying from a sub-diamond shape to a "keel and saddle" profile. Here, 21 species of five orders (Orthida, Pentamerida, Atrypida, Rhynchonellida, Spiriferida) from Cambrian to Devonian formations of Iran (Table 3) were selected for the analysis of the fibrous fabric. In general, due to diagenetic alteration processes, the sub-diamond shape in cross-section is not easy to observe, and only few cases show a good preservation of the original fibres outline (Plate 25C, D). In these cases, the shape of fibres in cross section is comparable to the modern brachiopod shell (e.g., Plate 25C, D; Plate 26F, G). The mean width of fibres ranges from 9 µm to 25 µm, thus overlapping the values recorded in several Permian genera (6–27 µm; Garbelli, 2017) and modern brachiopods (10–15 µm; Ye et al., 2018). Changes in size along the ontogenetic direction (e.g. from external to internal), with fibres becoming larger with age (Plate 19G, Plate 26F), were also observed in the fossil specimens and this could be compared to the findings in modern brachiopods (Ye et al., 2018a, 2018b).

In the Orthida, the shell structure may be impunctate and endopunctate. Here, the Orthidina *Hesperonomiella* sp. ind., *Nicolella actoniae*, *Paralenorthis* sp. ind. have an impunctate shell (Williams and Harper, 2000). Only one feature may resemble a puncta in *Nicolella actoniae* (Plate 18F, ca. 10 µm width). *Howellites ultima*, *Isorthis* (*Ovalella*) *inflata*, and *Isorthis* sp. ind., belong to the Suborder Dalmanellidina, which have a punctate (possibly endopunctate) shell (Williams and Harper, 2000). But in this study, the punctae were only found in *Howellites ultima* (Plate 16F, ca. 25 µm width); no evidence of the presence of punctae was observed in *Isorthis* (*Ovalella*) *inflata* and *Isorthis* sp. ind. The tertiary layer is not very common; it could be detected only in six species (*Nicolella actoniae*, *Paralenorthis* sp., *Howellites ultima*, *Isorthis (Ovalella) inflata*, *Cyrtospirifer* sp. ind., *Uchtospirifer* aff. *Uchtospirifer nalivkini*).

5.3.3 Morphological comparison between the laminae and the fibres

The thickness of both laminae and fibres was measured on their cross sections (a set of 5 longitudinal laminar/fibres). In summary, the thickness of the laminae (ranging from 7 to 14 µm) is thinner than the thickness of fibres (ranging from 12 to 30 µm), and the thickness of the laminae is relatively stable and uniform when compared to the variability in the thickness of the fibres (Fig. 4; Table 4). This finding

is also consistent with previous data (e.g. Williams, 1997; Garbelli et al., 2016; Garbelli, 2017), which showed that the basic unit of the fibrous layer is larger than the one of the laminar layer.

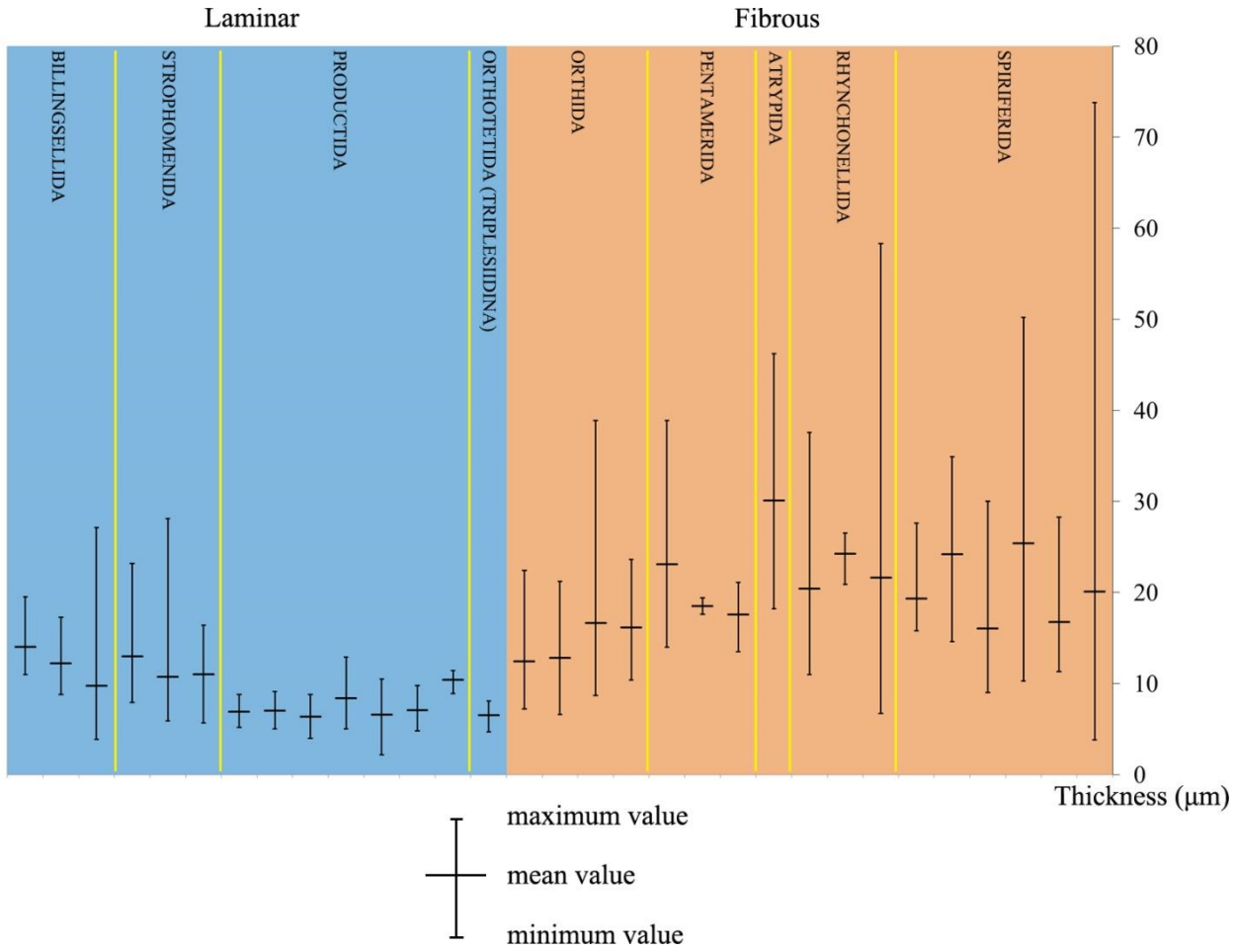

Fig. 4. Comparison of the thickness of laminae and fibres respectively in the laminar and fibrous fabric.

5.3.4 Shell shape vs laminar/fibrous fabric

The shell shape of each analysed specimen was also described and classified before sectioning. Here we try to find out if there is a relationship between the shape of the shell and its microstructure, as already suggested for some taxa (Garbelli, 2017). In this study, 86% of the species with a fibrous layer have a biconvex shell, whereas 63 % of the laminar species have a concavo-convex shell (Table 5, Fig. 5). Different shell shapes indicate different lifestyles (Harper, 1997) (Fig. 6), differences in the resistance and capacity of shell repair (Alexander, 1986) and functional constraints (Leighton, 1998), and the type of microstructure is strictly related to the performance of these functions (Perez-Huerta et al., 2007; Goetz et al., 2009; Ye et at., 2018A). The possible association between shell shape and its fabric could have some evolutionary meaning, since it is evident from the fossil record of brachiopods that most of the brachiopods bearing a laminar shell have a concavo-convex shell and sometimes evolved bizarre shapes, i.e. the coral-like form in the Richthofeniidae (Garbelli, 2017). One possible explanation maybe related to the different proportion of shell organic component in the laminar vs the fibrous fabric (Garbelli et al., 2017; Ye et al., 2018a). The laminar fabric has a higher organic component which may have conferred higher plasticity to the shell, allowing the evolution of and higher variety of shell shapes than in the fibrous groups (Garbelli, 2015; Garbelli et al., 2017).

One interesting outcome of the comparison between shell fabric and shape is that there is no correlation between the size of the shell and the size of the structural units of the fabrics (Fig. 7). In the laminar fabric shells this may be related to the limited variability in the size of the structural units, but in the fibrous fabric shells there is a very large variation, with large biconvex shells having either large sized fibres or small sized ones (see for instance the species of *Cyrtospirifer* in Fig. 7).

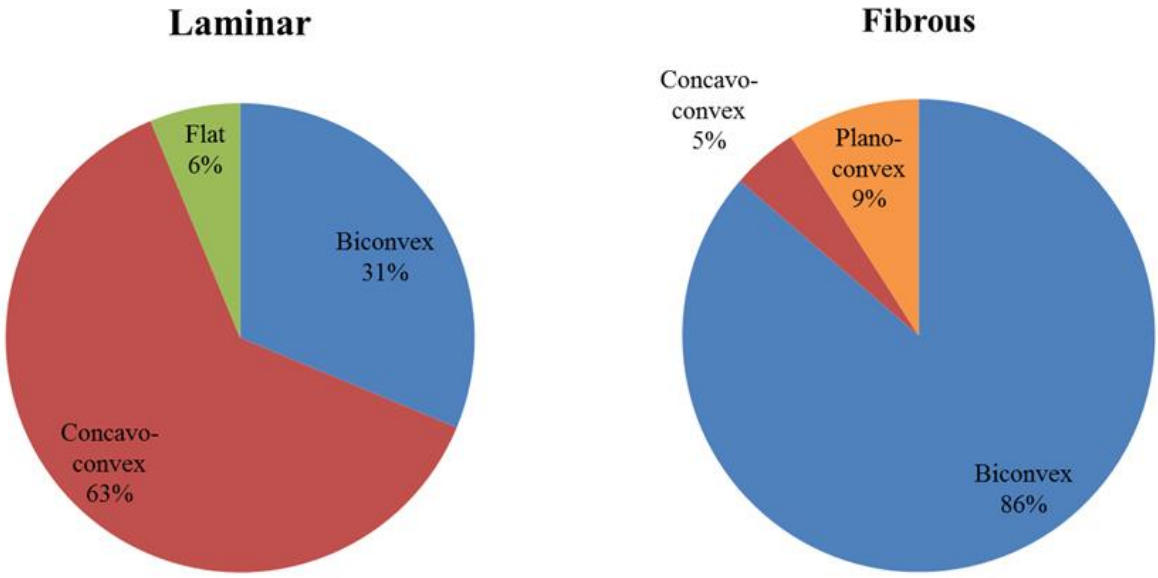

Fig. 5. Pie chart showing the relationship between shell shape and secondary layer fabric (left: laminar group, right: fibrous group)

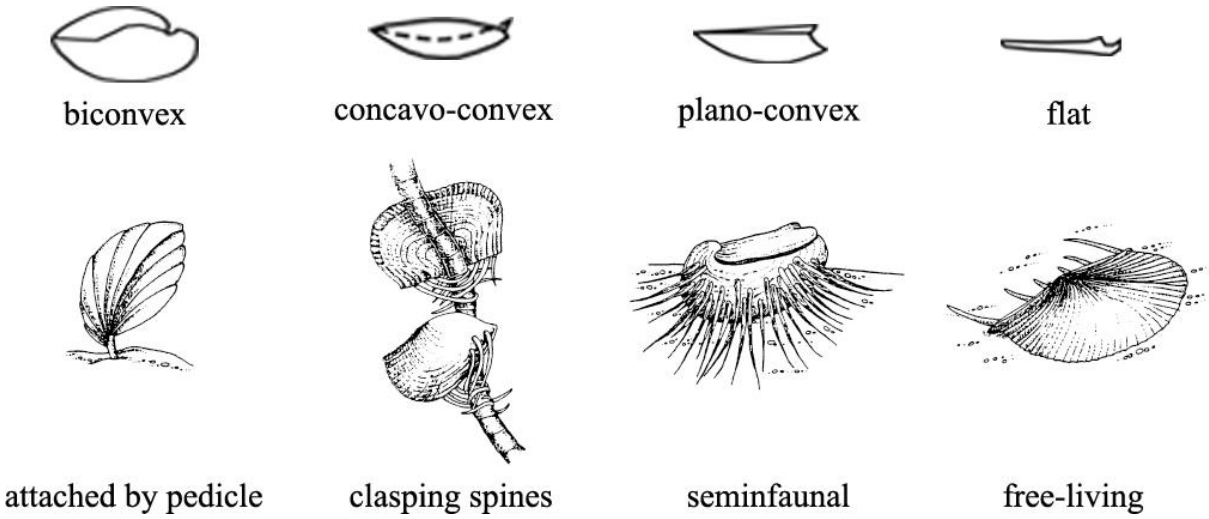

Fig. 6. Main brachiopod shell shapes and possible corresponding life styles (modified from Harper, 1997). To note that concave-convex are also seminfaunal.

Table 5. Relationship between shell shapes and secondary layer Fabric.

Laminar		Fibrous	
Biconvex	5	Biconvex	19
Concavo-convex	10	Concavo-convex	1*
Flat	1	Plano-convex	2*

*The shape of *Nicolella actoniae* can be either concavo-convex and plano-convex.

5.3.5 Variation of different fabric in time

The investigated Cambrian to Devonian taxa allows to test the change in fabric with time. Only very few Cambrian specimens were available for the analysis (three species of Billingsellida and one species of Orthida), and the preservation of these specimens was not good. The analysed Ordovician and Silurian taxa have mostly a fibrous fabric, but the examined Devonian species have a laminar fabric, which became more abundant in term of occurrences (Fig. 7). This trend is consistent with the stratigraphic ranges of brachiopod taxa as reported by Curry & Brunton (2007). Superposing the fabric type (laminar vs fibrous) to the taxa ranges (Fig. 8), it becomes evident that the laminar taxa spread during the Devonian, even if they were still less abundant than the fibrous fabric ones. However, the numbers of genera with laminar fabric exceed that of genera with fibrous fabric in the Carboniferous and Permian, until the end Permian mass extinction, when they got extinct. Their extinction may have been in part related to their microstructure (Garbelli et al., 2017) showing once again the importance of detailed microstructural studies to understand patterns of macroevolution.

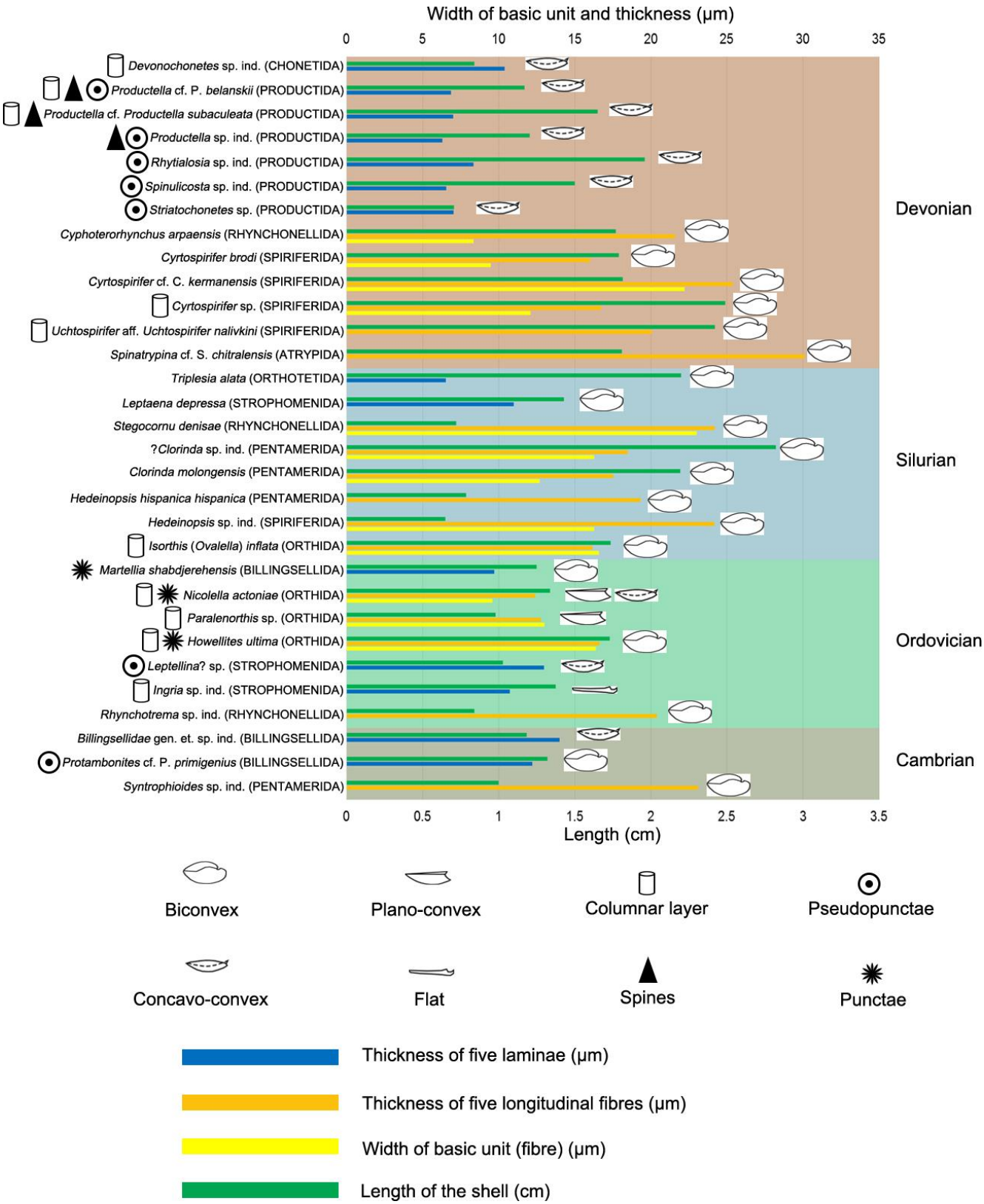

Fig. 7. Stratigraphic distribution of the main features analysed in this study, showing the variation of the size of laminae/fibres, presence/absence of perforations/other structures in different brachiopod shell shape and taxa.

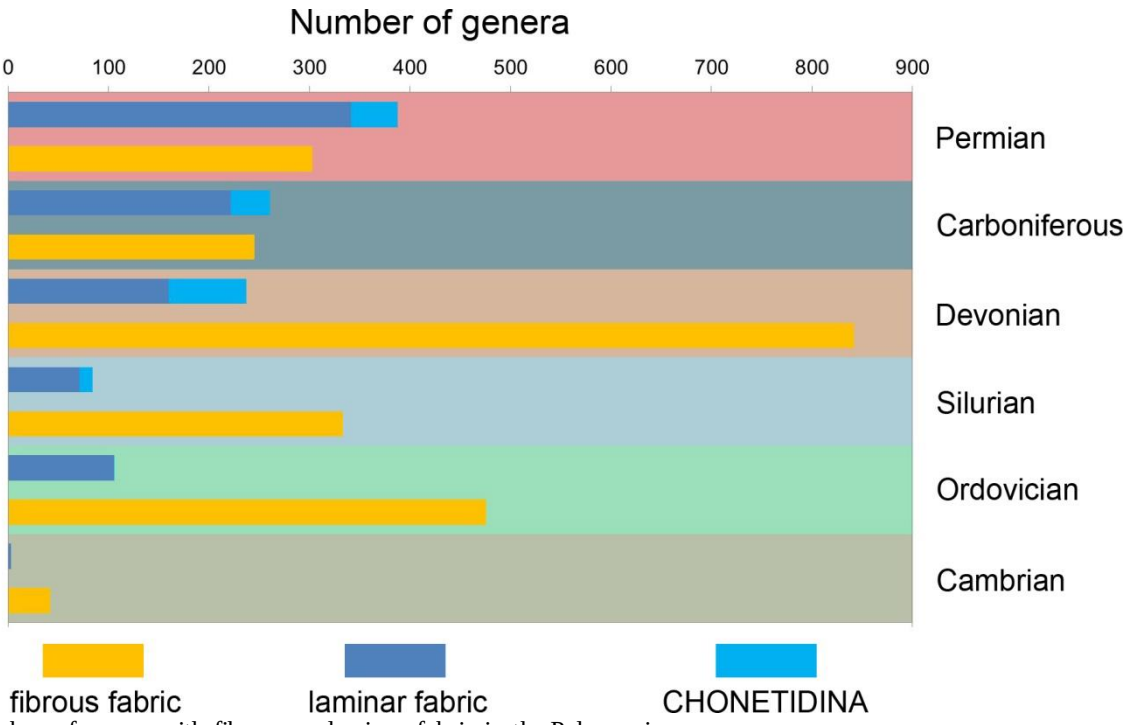

Fig. 8. Number of genera with fibrous vs laminar fabric in the Palaeozoic.

5.4 Conclusions

1. The organocarbonate Rhynchonellata and Strophomenata shells have very different secondary layer fabrics.

2. The fabric of the fibrous layer in the different analysed taxa is comparable to the one observed in modern brachiopods, whereas shells with laminar fabric are more variable and complex in their structural organization and they have no recent analogue.

3. There is a relationship between shell shape and fabric: Brachiopods with a fibrous secondary layer are mostly associated to biconvex shells, whereas brachiopods with a laminar secondary layer can be associated to a variety of shell shapes.

4. In cross section, the laminae are thinner than the fibres; the latter are also much more variable in their size, whereas laminae thickness is rather uniform.

5. The recorded gradual change in thickness of the structural units from the taxa with fibrous fabric to the Productida – the most derived taxa with laminar fabric - through the Billingselloidea could be taken as evidence to support the hypothesis (e.g. Williams et al., 2000) that taxa with laminar microstructure diverged from the Billingsellida.

6. The Chonetidina, which were previously considered to have an intermediate laminar layer composed of 'lath like-fibres', seem to have already evolved a laminar fabric during the Devonian.

7. Based on data from Iran, the number of brachiopod genera with fibrous fabric is much higher than that of laminar taxa during Ordovician and Silurian, while laminar fabric genera began to flourish in the Devonian; this trend is consistent with the stratigraphic range of brachiopod fabric types through time, as reconstructed superposing the fabric type to the known stratigraphic ranges of brachiopod taxa (Curry & Brunton, 2007).

References

Alexander, R.R., 1989. Influence of valve geometry, ornamentation, and microstructure on fractures in Late Ordovician brachiopods. Lethaia 22, 133–147.

Angiolini, L., 1993. Ultrastructure of some Permian and Triassic Spiriferida and Arthyridida (Brachiopoda). Rivista Italiana di Paleontologia e Stratigrafia, 9, 283–306.

Armstrong, J., 1969. The cross-bladed fabrics of the shells of *Terrakea solida* (Etheridge and Dun) and *Streptorhynchus pelicanensis* Fletcher. Palaeontology 12, 310–320.

Brunton, H.C., 1972. The shell structure of chonetacean brachiopods and their ancestors. Bulletin of the British Museum (Natural History) Geology 21, 1–26.

Brunton, C.H.C., Lazarev, S.S., Grant, R.E., 2000. Productida, in: Kaesler, R.L. (Ed.), Treatise on Invertebrate Paleontology. Part H, Revised, Brachiopoda, vol. 2. Geological Society of America Inc., and the University of Kansas, Boulder, Colorado, USA, pp. 350–362.

Crippa, G., Ye, F., Malinverno, C., Rizzi, A., 2016. Which is the best method to prepare invertebrate shells for SEM analysis? Testing different techniques on recent and fossil brachiopods. Bollettino della Società Paleontologica Italiana 55, 111–125.

Curry, G.B., Brunton, C.H.C., 2007. Stratigraphic distribution of Brachiopods, in: Selden P.A. (Ed.): Treatise on Invertebrate Paleontology, Part H, Revised, Brachiopoda, vol. 6, Kansas: The Paleontological Institute, pp. 2396–2521.

Dewing, K., 2004. Shell Structure and Its Bearing on the Phylogeny of Late Ordovician-Early Silurian Strophomenoid Brachiopods from Anticosti Island, Québec. Journal of Paleontology 78, 275–286.

Garbelli, C., 2015. Biomineralization and global changes: brachiopod shells as archives of the end Permian events. Milan: Università degli Studi di Milano. PhD thesis

Garbelli, C., 2017. Shell microstructures in lopingian brachiopods: implications for fabric evolution and calcification. Rivista Italiana di Paleontologia e Stratigrafia 123, 541–560.

Garbelli, C., Angiolini, L., Brand, U., Jadoul, F. 2014. Brachiopod fabric, classes and biogeochemistry: Implications for the reconstruction and interpretation of seawater carbon-isotope curves and records. Chemical Geology 371, 60–67.

Garbelli, C., Angiolini, L., Shen, S.Z., 2017. Biomineralization and global change: A new perspective for understanding the end-Permian extinction. Geology 45, 19–22.

Harper, D.A.T., Moran, R., 2003. Fossils explained 20: Brachiopod life styles. Geology Today 13, 235–238.

Leighton, L.R., 1998. Constraining functional hypotheses: Controls on the morphology of the concavo-convex brachiopod *Rafinesquina*. Lethaia 31, 293–307.

Mackinnon, D.I., Williams, A., 1974. Shell structure of Terebratulid brachiopods. Palaeontology 17, 179–202.

Percival, I.G., Wright, A.J., Nicoll, R.S., Hamedi, M.A., 2009. Martellia and associated Middle Ordovician brachiopods from the Katkoyeh Formation, east-central Iran. Memoirs of the Association of Australasian Palaeontologists 37, 315–325.

Williams, A., 1968. Evolution of the shell structure of articulate brachiopods. Special Papers in Palaeontology 2, 1–55.

Williams, A., 1970. Origin of laminar-shelled articulate brachiopods. Lethaia 3, 329–342.

Williams, A., 1997. Shell structure, in: Kaesler, R.L. (Ed.), Treatise on Invertebrate Paleontology. Part H, Revised, Brachiopoda, vol. 1. Geological Society of America Inc., and The University of Kansas, Boulder, Colorado, USA, pp. 267–320.

Williams, A., Harper, D.A., 2000. Billingsellida, in: Kaesler, R.L. (Ed.), Treatise on Invertebrate Paleontology. Part H, Revised, Brachiopoda, vol. 3. Geological Society of America Inc., and the University of Kansas, Boulder, Colorado, USA, pp. 689–790.

Williams, A., Harper, D.A.T., 2000. Orthida, in: Kaesler, R.L. (Ed.), Treatise on Invertebrate Paleontology. Part H, Revised, Brachiopoda, vol. 3. Geological Society of America Inc., and the University of Kansas, Boulder, Colorado, USA, pp. 714–723.

Williams, A., Carlson, S.J., 2000. Rhynchonellata, in: Kaesler, R.L. (Ed.), Treatise on Invertebrate Paleontology. Part H, Revised, Brachiopoda, vol. 3. Geological Society of America Inc., and the University of Kansas, Boulder, Colorado, USA, pp. 708–709.

Williams, A., Cusack, M., 2007. Chemicostructural diversity of the brachiopod shell, in: Selden P.A. (Ed.): Treatise on Invertebrate Paleontology, Part H, Revised, Brachiopoda, vol. 6, Kansas: The Paleontological Institute, pp. 2396–2521.

Ye, F., Crippa, G., Angiolini, L., Brand, U., Capitani, G., Cusack, M., Garbelli, C., Griesshaber, E., Harper, E., Schmahl, W., 2018a. Mapping of recent brachiopod microstructure: a tool for environmental studies. Journal of Structural Biology 201, 221–236.

Ye, F., Crippa, G., Garbelli, C., Griesshaber, E., 2018b. Microstructural data of six recent brachiopod species: SEM, EBSD, morphometric and statistical analyses. Data in Brief 18, 300–318.

Chapter 6

Conclusions

Brachiopod shells are considered excellent archives for understanding the environmental and climate change and reconstructing the state and composition of the oceans in recent and past times, and make reliable prediction of their evolution in the future times (e.g., Popp et al., 1986; Grossman et al., 1991; Parkinson et al., 2005; Angiolini et al., 2007, 2009; Brand et al., 2011; Cusack and Huerta, 2012; Brocas et al., 2013; Garbelli et al., 2017; Brand, 2018). However, there is still insufficient knowledge on the microstructures of these biomineral archives and their biomineralization processes during the evolutionary history. The present thesis was focused on contributing to solve these issues: examining the micro-, morpho- and chemico-structural diversity of modern and fossil brachiopods, to assess the microstructure variation in different environmental conditions and to reconstruct the evolutionary changes and fabric differentiation of the main brachiopod classes through the geological time.

A multidisciplinary approach was used for microstructural analysis [(Scanning electron microscopy (SEM), Transmission electron microscope (TEM) and Electron backscatter diffraction (EBSD)]; not only qualitative observations, but also quantitative measurements and statistical analyses on the structural units (fibres/laminae) of the secondary layer of the brachiopod shells were performed. In particular, several new methods of measuring the size of the structural units of the secondary layer in different parts of the shell were proposed for the first time for modern brachiopod taxa (paragraphs 3.3 and 4.2). These new methods to quantitatively describe the microstructure of brachiopod shells resulted to be are a very powerful tool to interpret the microstructure variation in different ontogenetic stages and environmental conditions.

As these were not always easy to apply to fossil shells, especially in the case of laminar secondary layer and/or poor preservation due to diagenetic alteration, an alternative method was suggested for the fossils (paragraph 5.2).

Through these new approaches, detail of microstructural patterns were described and compared on six modern brachiopod species from different environmental conditions, deriving the following conclusions:

1) No significant difference in the shape and size of the fibres were found between ventral and dorsal valves.

2) There is an ontogenetic trend in the morphology of the fibres, as they become larger, wider, and flatter with increasing age. This change in size and shape indicates that the animal produced a fibrous layer with a different organic content during the ontogeny.

Additionally, other microstructural features (e.g. thickness of primary layer, density and size of punctation) were measured and stable isotope geochemistry investigation were performed on the species *Magellania venosa* (Dixon, 1789), analysing different specimens, grown either in the natural environment and in controlled culturing experiments at different pH conditions. The following conclusions were reached:

1) Under low pH conditions, *M. venosa* produced a more organic-rich shell with higher density of and larger endopunctae, and smaller secondary layer fibres, when subjected to about one year of culturing.

2) Increasingly negative $\delta^{13}C$ and $\delta^{18}O$ values were recorded by the shell produced during culturing and are related to the CO_2–source in the culture setup.

3) Both the microstructural changes and the stable isotope results support the value of brachiopods as robust archives of proxies for studying ocean acidification events in the geologic past.

The measurements made on the thickness and width of structural units (laminae/fibres) of Cambrian to Devonian fossil brachiopod shells coupled with very detailed qualitative micro-scale observations lead to the following conclusions:

1) The fossil organocarbonate brachiopod shells have two main secondary layer fabrics: laminar fabric the Strophomenata; fibrous fabric the Rhynchonellata.

The Strophomenata laminar fabric shells are more variable and complex in their structural organization, but the thickness of the laminae is rather uniform and much thinner than that of the fibres; the Rhynchonellata fibrous fabric is more simple and uniform in its organization, but the size of the fibres is much more variable. It is comparable to the modern brachiopods fabric.

2) Brachiopods with a fibrous secondary layer are mostly associated to biconvex shells, whereas brachiopods with a laminar secondary layer can be associated to a variety of shell shapes.

3) Detailed microstructural studies are a very useful tool to construct the phylogenetic tree of the brachiopod phylum, e.g., the recorded gradual change in thickness of the laminae from Billingselloidea to Productida could be an important evidence to support the hypothesis that taxa with laminar microstructure diverged from the Billingsellida (Williams, 1970; Williams et al., 2000); the microstructure observation on the Chonetidina suggested that their shells had already evolved a laminar fabric during the Devonian.

This study shows that more microstructural analyses of the kind performed in this thesis are necessary in order to better constrain the evolutionary history of the phylum and to use brachiopod shells as biomineral archives to reconstruct the global change in the geological past.

Therefore, based on our new methodology and results, I believe that the morphology of the brachiopod shell basic microstructure unit is very useful and informationable feature, and could be used to reflect the different environmental conditions where they live. In addition, an ontogenetic trend in the shape and size of the basic microstructure units of the same shell could explain why a suitable sampling strategy is important for geochemical analyses. Moreover, the observations of the effects of acidification on the shell microstructure and stable isotope geochemistry of brachiopod shells offer an invaluable indication for studying ocean acidification events in the geologic past. In last, the fabric differentiation of the microstructure feature of fossil brachiopod shells is also proved can use for better understand the brachiopod evolution during the Palaeozoic. Sum up, all new methodology and results of this study could be easily use/apply by other researchers in different research fields in the future.

References

Angiolini, L., Darbyshire, D.P.F., Stephenson, M.H., Leng, M.J., Brewer, T.S., Berra, F., Jadoul, F., 2007. Lower Permian brachiopods from Oman: their potential as climatic proxies. Earth and Environmental Science Transactions of the Royal Society of Edinburgh 98, 327–344.

Angiolini, L., Jadoul, F., Leng, M.J., Stephenson, M.H., Rushton, J., Chenery, S., Crippa, G., 2009. How cold were the Early Permian glacial tropics? Testing sea-surface temperature using the oxygen isotope composition of rigorously screened brachiopod shells. Journal of the Geological Society 166, 933–945.

Brand, U., 2018. Modern and fossil brachiopods: superheroes of archives. 8th International Brachiopod Congress Milan, 11–14 September 2018, Permophiles 66, 29.

Brand, U., Logan, A., Bitner, M.A., Griesshaber, E., Azmy, K., Buhl, D., 2011. What is the ideal proxy of Palaeozoic seawater chemistry?. In: Memoirs of the Association of Australasian Palaeontologists 41, 9–24.

Brocas, W.M., Reynolds, D.J., Butler, P.G., Richardson, C.A., Scourse, J.D., Ridgway, I.D., Ramsay, K., 2013. The dog cockle, *Glycymeris glycymeris* (L.), a new annually-resolved sclerochronological archive for the Irish Sea. Palaeogeography, Palaeoclimatology, Palaeoecology 373, 133–140.

Cusack, M., Huerta, A.P., 2012. Brachiopods recording seawater temperature—A matter of class or maturation? Chemical Geology 334, 139–143.

Garbelli, C., Angiolini, L., Shen, S.Z., 2017. Biomineralization and global change: A new perspective for understanding the end-Permian extinction. Geology 45, 19–22.

Grossman, E.L., Zhang, C., Yancey, T.E., 1991. Stable-isotope stratigraphy of brachiopods from Pennsylvanian shales in Texas. Geological Society of America Bulletin 103, 953–965.

Goetz, A.J., Griesshaber, E., Neuser, R.D., Lüter, C., Hühner, M., Harper, E., Schmahl, W.W., 2009, Calcite morphology, texture and hardness in the distinct layers of rhynchonelliform brachiopod shells. European Journal of Mineralogy 21, 303–315.

Parkinson, D., Curry, G.B., Cusack, M., Fallick, A.E., 2005. Shell structure, patterns and trends of oxygen and carbon stable. Chemical Geology 219, 193–235.

Popp, B.N., Anderson, T.F., Sandberg, P.A., 1986. Brachiopods as indicators of original isotopic compositions in some Paleozoic limestones. Geological Society of America Bulletin 97, 1262–1269.

Williams, A., 1970. Origin of laminar-shelled articulate brachiopods. Lethaia 3, 329–342.

Williams, A., Harper, D.A., 2000. Billingsellida, in: Kaesler, R.L. (Ed.), Treatise on Invertebrate Paleontology. Part H, Revised, Brachiopoda, vol. 3. Geological Society of America Inc., and the University of Kansas, Boulder, Colorado, USA, pp. 689–790.

Appendix 1

Microstructural data of six recent brachiopod species: SEM, EBSD, morphometric and statistical analyses

*Published in Data in Brief (2018), v. 18, pp. 300-316

Facheng Ye[a], Gaia Crippa[a], Claudio Garbelli[b], Erika Griesshaber[c]

[a]Dipartimento di Scienze della Terra "A. Desio", Universit à degli Studi di Milano, Milan, Italy; corresponding author: facheng.ye@unimi.it

[b]State Key Laboratory of Palaeobiology and Stratigraphy, Nanjing Institute of Geology and Palaeontology, Chinese Academy of Sciences, Nanjing, China;

[c]Department fur Geo- und Umweltwissenschaften, Ludwig-Maximilians Universitat Munchen, Munich, Germany

Abstract

Here, we provide the dataset associated with the research article “Mapping of recent brachiopod microstructure: A tool for environmental studies” [1]. We present original data relative to morphometric and statistical analyses performed on the basic shell structural units (the secondary layer fibres) of brachiopod shells belonging to six extant species adapted to different environmental conditions. Based on SEM micrographs of the secondary layer, fibres from ventral and dorsal valves, and from different shell positions, showing regular and symmetrical cross sectional outlines, were chosen for morphometric measurements using Adobe Photoshop CS6, Image-Pro Plus 6.0 and ImageJ. To work out the reliability of the measurements, the most significant parameters were tested for their probability density by distribution plots; for data visualization and dimension reduction, principal component analysis (PCA) was performed using R 3.3.0 [2] and independent-samples *t*-tests were performed using SPSS Statistics (IBM Version 22.0. Armonk, NY). Besides a quantitative analysis, a qualitative description of the shell microstructure is provided by detailed SEM imaging and EBSD measurements.

Value of the data

- These data provide a quantitative and qualitative description of the microstructure of recent brachiopod shells using several tools: SEM, EBSD, morphometric and statistical analyses.
- These methods may be applied to other invertebrates and to fossil shells to objectively describe and compare their microstructures.
- These data are valuable to researchers investigating invertebrate biomineralization patterns.

1. Data

Brachiopod calcite shells are high resolution biomineral archives used to reconstruct global marine environments in the recent and deep past [4-10]. Biominerals, the hard parts produced by organisms for support and protection, are one of the best tools to use, as they are high-resolution archives of the environmental conditions prevailing during their growth. Here, we focus on the basic structural unit (fibres) of the secondary calcite layer of six recent rhynchonelliformean brachiopods. Based on SEM and EBSD analyses, 1197 morphological measurements of the fibres were performed and statistically analysed, comparing the size and shape of the fibres in different valves of the same specimen, at different positions within the valve, in different shell layer successions, in different species and in different environmental conditions.

2. Experimental Design, Materials and Methods

2.1 Sample collections

Six extant rhynchonelliformean brachiopod species (21 adult specimens) were chosen for microstructure analyses (Table 1). They have either a two-layer shell sequence or a three-layer shell sequence, both comprising a fibrous secondary layer, and are adapted to different environmental conditions, from Signy and Trolval Islands, Antarctica, to Doubtful Sound, New Zealand to the Tuscan Archipelago, Mediterranean Sea.

Table 1. Details of the studied materials for shell microstructure analyses. The name of the species, the corresponding ID and museum number, the type of valve and the number of SEM micrographs are shown. The shell succession of each species, the localities of provenance of the specimens and the corresponding geographic coordinates, Depth (D), temperature (T) and salinity (S) are also indicated.

Species		ID number		Valve	SEM micrographs number	Shell sequence	Provenance and environmental parameters
Terebratulida	*Liothyrella uva*	LUH1	LUH1 (MPUM 11565)	ventral	40	I, II layers	Trolval Island, Ryder Bay, Antarctica 67 °35.44' S, 68 °12.44' W T: -2/+2 ℃, S: 34 PSU Signy Island (D: 10m), Antarctica 60 °43' S, 45 °36' W T: -2/+2 ℃, S: 34 PSU
		LUH2	LUH2 (MPUM 11566)	ventral	28		
		LUH3	LUH3 (MPUM 11567)	ventral	34		
			LUH3A (MPUM 11591)	dorsal	21		
			LUH3C (MPUM 11591)	dorsal	27		
			LUH3P (MPUM 11591)	dorsal	16		
		LU	LUU (MPUM 11569)	ventral	17		
			LUA (MPUM 11568)	ventral	19		
		LUV/LUD	LUV (MPUM 11560)	ventral	48		
			LUVT (MPUM 11559)	ventral	42		
			LUDCA (MPUM 11592)	dorsal	26		
			LUDP (MPUM 11592)	dorsal	19		
	Gryphus vitreus	1D	1DA (MPUM 11595)	ventral	53	I, II, III layers	Tuscan Archipelago (D: 140-160m between the Island of Pianosa and Montecristo), Tyrrhenian Sea, Italy 42 °26' N, 10 °04' E T: 13-15 ℃, S: 39 PSU
			1DB (MPUM 11596)	dorsal	58		
		GV	GVV (MPUM 11597)	ventral	34		
			GVD (MPUM 11598)	dorsal	23		
			BO(GVD) (MPUM 11598)	dorsal	24		
		GV3	GV3A (MPUM 11599)	ventral	10		
			GV3C (MPUM 11599)	ventral	12		
			GV3U (MPUM 11599)	ventral	31		
			GV3 (MPUM 11600)	dorsal	15		
		GV4	GV4VA (MPUM 11601)	ventral	12		
			GV4VC1 (MPUM 11601)	ventral	8		
			GV4VC2 (MPUM 11601)	ventral	13		
			GV4VP (MPUM 11601)	ventral	10		
			GV4DA (MPUM 11602)	dorsal	20		
			GV4DC1 (MPUM 11602)	dorsal	20		
			GV4DC2 (MPUM 11602)	dorsal	27		
			GV4DP (MPUM 11602)	dorsal	22		
		GV5	GV5A1	dorsal	2		
			GV5A2	dorsal	12		

	Liothyrella neozelanica	1C	1CA (MPUM 11589)	ventral	62	I, II, III layers	Doubtful Sound (D: 18m), New Zealand 45 °18' 00" S, 166 °58' 45" E T: 11-17 °C, S: 34.8 PSU
			1CB (MPUM 11590)	dorsal	82		
		LZ	LZ (MPUM 11579)	ventral and	92		
			LZA/LZA1 (MPUM 11580)	ventral and	45		
			LZA1 (MPUM 11580)	ventral and	25		
			LZC/LZCC/LZCV (MPUM 11582)	ventral and	44		
			LZCV (MPUM 11582)	ventral	20		
			LZP/LZP1 (MPUM 11581)	ventral and	40		
			LZP1 (MPUM 11581)	ventral and	22		
		LN	LNA (MPUM 11571)	ventral	27		
			LNU (MPUM 11572)	ventral	21		
			LND1 (MPUM 11573)	dorsal	24		
			LND2 (MPUM 11574)	dorsal	28		
			LND3 (MPUM 11575)	dorsal	22		
			LND4 (MPUM 11576)	dorsal	26		
			LND5 (MPUM 11577)	dorsal	18		
			LND6 (MPUM 11578)	dorsal	10		
	Calloria inconspicua	1CC	1CC (MPUM 11593)	ventral and dorsal	27	I, II layers	Doubtful Sound (D: 18m), New Zealand 45 °18' 00" S, 166 °58' 45" E T: 11-17 ℃ , S: 34.8 PSU
		CI	CI (MPUM 11594)	ventral and dorsal	43		
	Magasella sanguinea	TS1	TS1 (MPUM 11603)	ventral and	61	I, II layers	Doubtful Sound (D: 18m), New Zealand 45 °18' 00" S, 166 °58' 45" E T: 11-17 ℃ ℃, S: 34.8 PSU
			TS1A (MPUM 11604)	ventral and	24		
			TS1C (MPUM 11604)	ventral and	32		
			TS1P (MPUM 11604)	ventral and	40		
Rhynchonellida	*Notosaria nigricans*	NN	NN (MPUM 11605)	ventral and	30	I, II layers	Doubtful Sound (D: 18m), New Zealand 45 °18' 00" S, 166 °58' 45" E T: 11-17 ℃ ℃, S: 34.8 PSU Kaka Point (D: 2-15m) New Zealand 46 °38' 66" S, 169 °78' 23" E T: 14 ℃, S: 34-35 PSU
			NN2 (MPUM 11605)	ventral and	29		
		NN1	NN1 (MPUM 11606)	ventral and	34		
		NN2	NN2VA (MPUM 11607)	ventral	20		
			NN2VB (MPUM 11607)	ventral	29		
			NN2VC (MPUM 11607)	ventral	20		
			NN2DA (MPUM 11608)	dorsal	24		
			NN2DC (MPUM 11608)	dorsal	27		
			NN2DP (MPUM 11608)	dorsal	15		
		NN3	NN3 (MPUM 11609)	ventral and	47		
		1DC	1DC (MPUM 11610)	ventral	41		

2.2 SEM

We followed SEM sample preparation as suggested by Crippa et al. [3]. The specimens were embedded in a transparent bicomponent epoxy resin and cut along the longitudinal (or transversal) axis using a low speed saw with a thin diamond blade. To remove the organic matter within the shell, samples were immersed in 36 volume hydrogen peroxide (H_2O_2) for 24 hours. Sectioned surfaces were smoothed with silicon carbide (SiC) powder of two different granulometries (400 and 1000 grit sizes), etched with 5% hydrochloric acid (HCl) for 3 seconds, and rinsed in deionised water and dried. They were gold-coated and observed by Cambridge S-360 scanning electron microscope with a lanthanum hexaboride (LaB_6) cathodes and operating at an acceleration voltage of 20 kV at Dipartimento di Scienze della Terra "A. Desio", University of Milan. Plates 1-4 show the shell microstructure of the six brachiopod species analysed: *Liothyrella uva, Gryphus vitreus, Liothyrella neozelanica, Calloria incospicua, Magasella sanguinea* and *Notosaria nigricans.*

Plate 1

A) complete shell succession from primary to tertiary layer with crossing endopunctae (*Liothyrella neozelanica*, ventral valve);

B) endopuncta crossing the primary and secondary layer (*Liothyrella neozelanica*, ventral valve);

C) transition zone between the secondary and the tertiary layers (*Liothyrella neozelanica*, dorsal valve);

D) enlarged photo showing fibres in transverse section (*Liothyrella neozelanica*, dorsal valve);

E) complete shell succession from primary to secondary layer with crossing endopunctae (*Liothyrella uva*, ventral valve);

F) change in the orientation of fibres within the fibrous secondary layer (parallel, oblique and transverse) (*Liothyrella uva*, ventral valve);

G, H) enlarged photo showing fibres in transverse section (*Liothyrella uva*, ventral valve).

Ext: external part of the shell; Int: internal part of the shell.

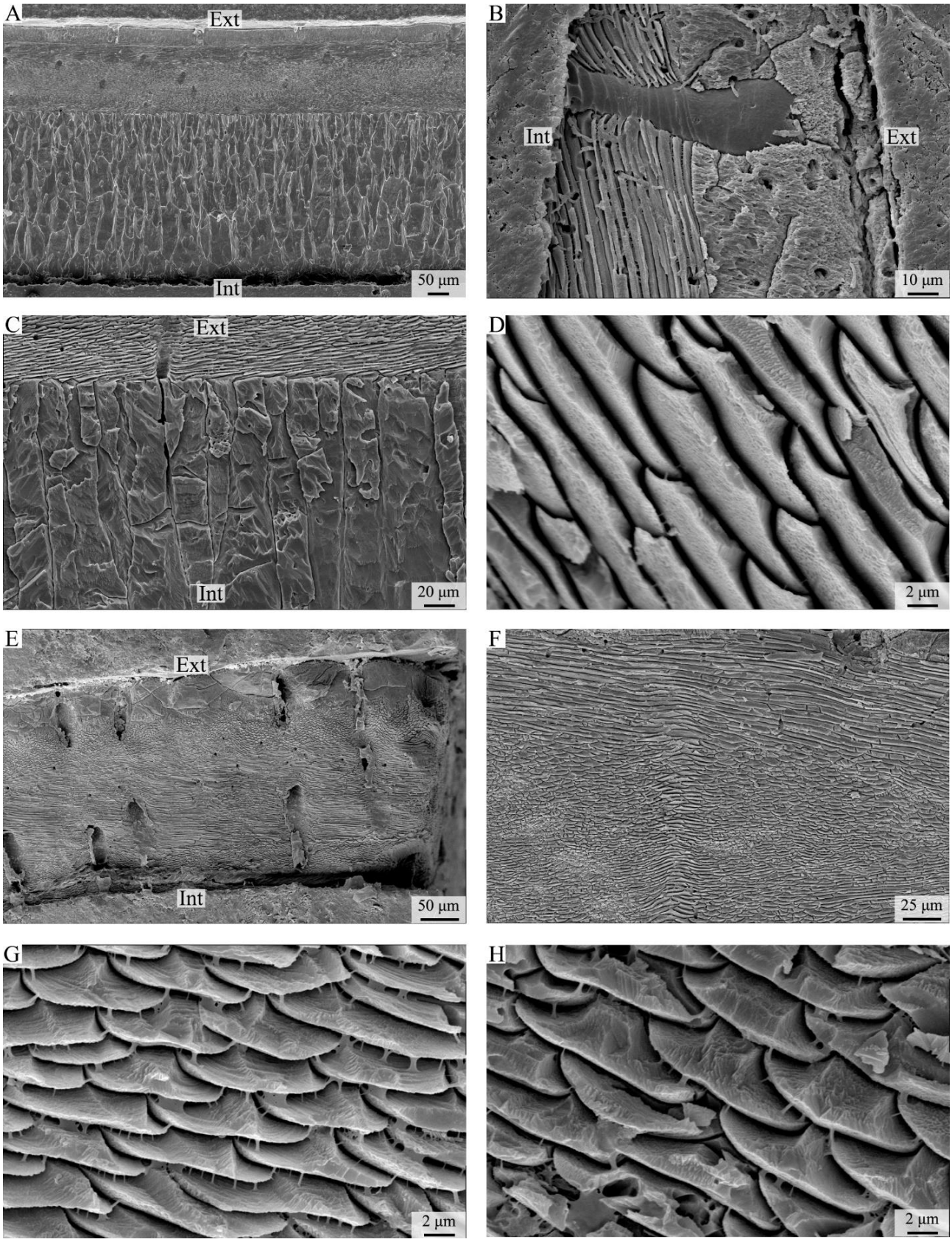
A
Ext
Int
50 µm
B
Int
Ext
10 µm
C
Ext
Int
20 µm
D
2 µm
E
Ext
Int
50 µm
F
25 µm
G
2 µm
H
2 µm

Plate 2

A) complete shell succession from primary to secondary layer with endopunctae (*Calloria inconspicua*, ventral valve);

B) fibrous secondary layer with endopuncta (*Calloria inconspicua*, ventral valve);

C) complete shell succession from primary to tertiary layer (*Gryphus vitreus*, dorsal valve);

D) enlarged photo showing fibres in transverse section (*Gryphus vitreus*, dorsal valve);

E) details of an endopuncta (*Magasella sanguinea*, dorsal valve);

F) fibrous secondary layer (*Magasella sanguinea*, dorsal valve);

G) primary layer and fibrous secondary layer (*Notosaria nigricans*, dorsal valve);

H) details of fibres in the secondary layer (*Notosaria nigricans*, ventral valve);

Ext: external part of the shell; Int: internal part of the shell.

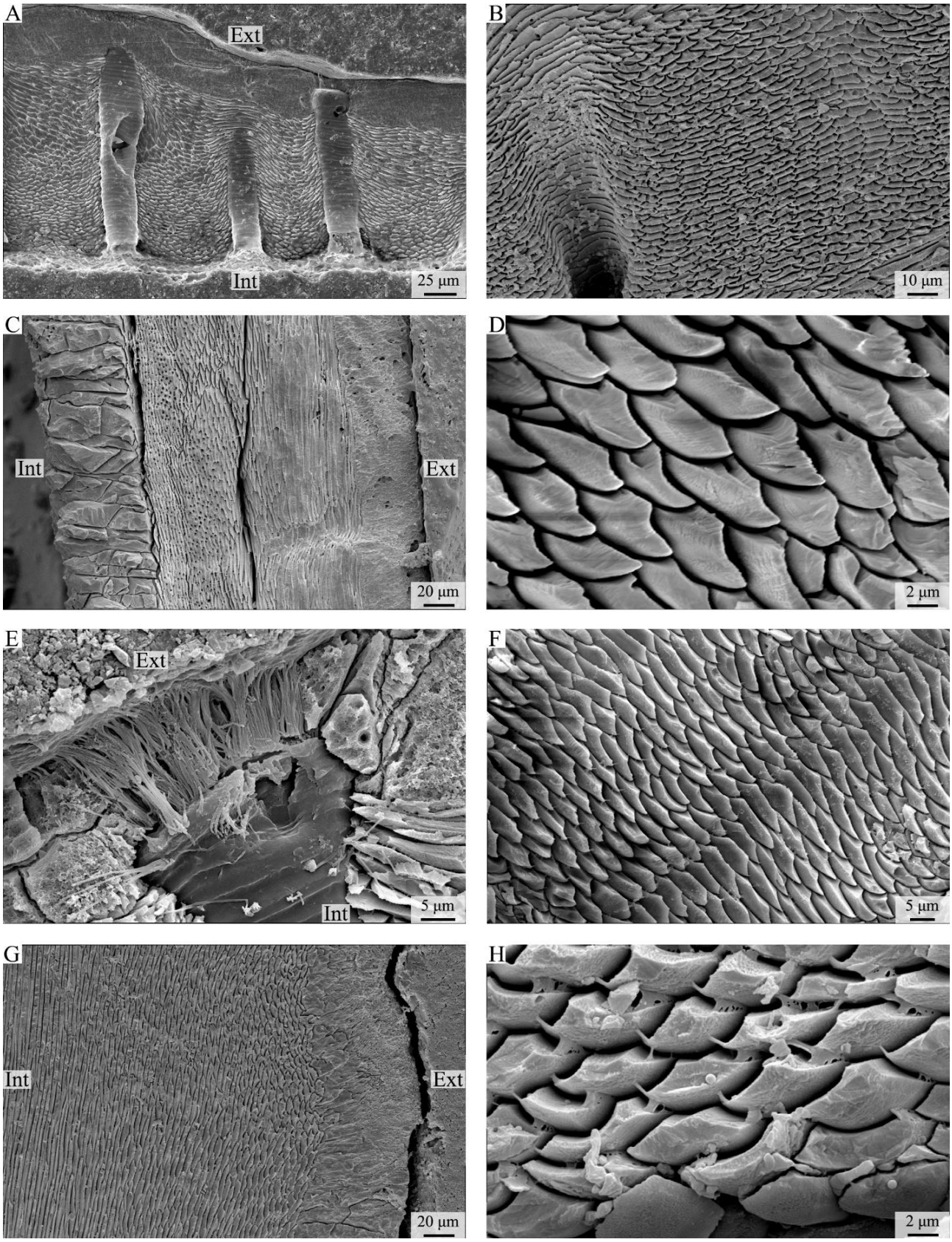
A
Ext
Int
25 µm
B
10 µm
C
Int
Ext
20 µm
D
2 µm
E
Ext
Int
5 µm
F
5 µm
G
Int
Ext
20 µm
H
2 µm

Plate 3

A) complete shell succession showing the change in the orientation of fibres from oblique to transverse from the exterior to the interior of the secondary layer (*Liothyrella neozelanica*, anterior part, ventral valve, longitudinal section);

B) complete shell succession showing the change in the orientation of fibres from oblique to transverse from the exterior to the interior of the secondary layer (*Liothyrella neozelanica*, central part, ventral valve, longitudinal section);

C) complete shell succession showing the change in the orientation of fibres from transverse to oblique from the exterior to the interior of the secondary layer, and the alternations of the secondary and tertiary layers (*Liothyrella neozelanica*, posterior part, ventral valve, longitudinal section);

D-E) complete shell succession showing the change in the orientation of fibres from oblique to transverse from the exterior to the interior of the secondary layer (*Liothyrella uva*, central part, dorsal valve, longitudinal section);

F) complete shell succession showing several sublayers with variable fibre orientation (*Liothyrella uva*, posterior part, ventral valve, longitudinal section);

G) complete shell succession showing the change in the orientation of fibres from oblique to transverse to oblique from the exterior to the interior of the secondary layer (*Calloria inconspicua*, anterior part, ventral valve, longitudinal section);

H) complete shell succession showing several sublayers with variable fibre orientation (*Calloria inconspicua*, posterior part, ventral valve, longitudinal section).

Ext: external part of the shell; Int: internal part of the shell.

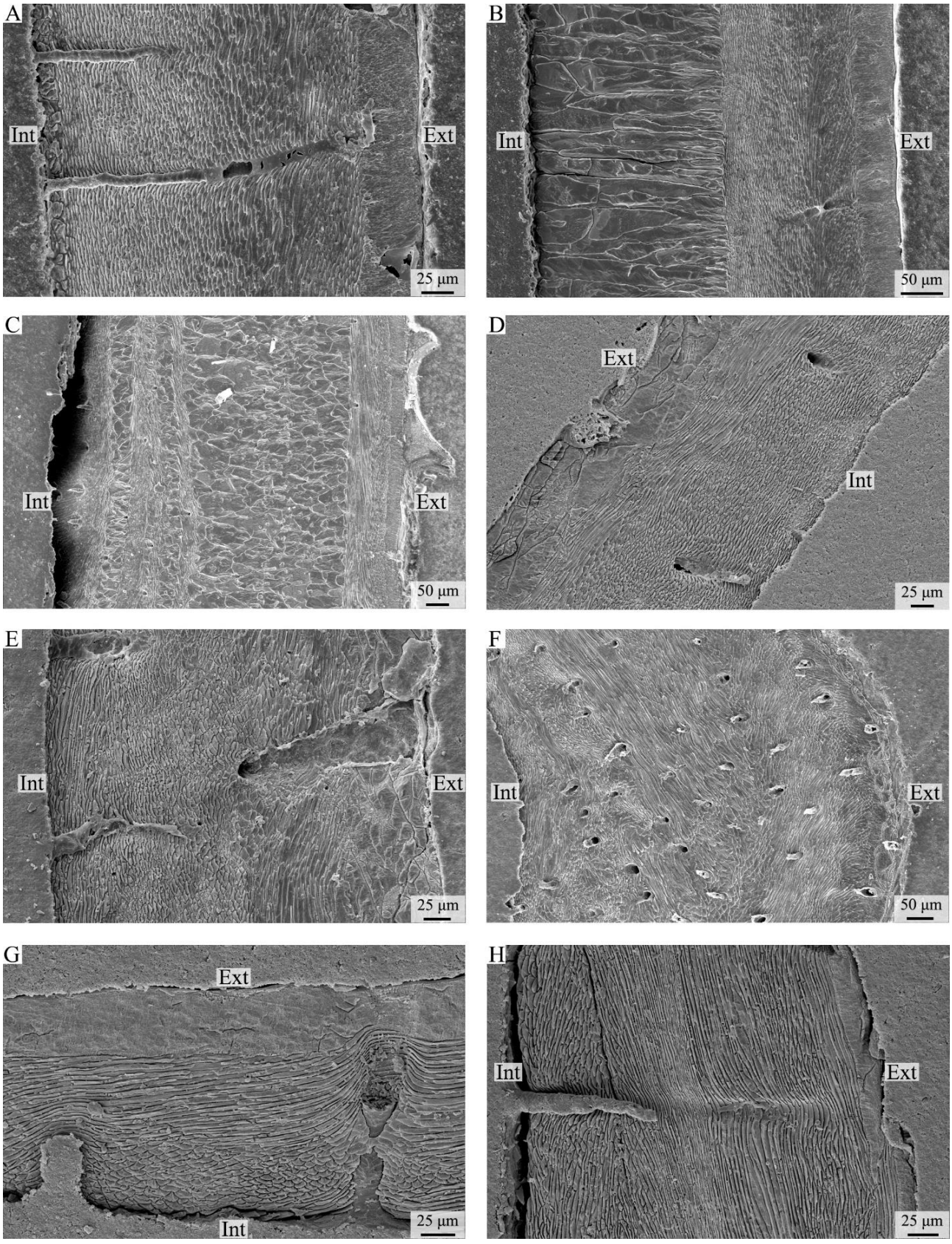
A
Int
Ext
25 µm
B
Int
Ext
50 µm
C
Int
Ext
50 µm
D
Ext
Int
25 µm
E
Int
Ext
25 µm
F
Int
Ext
50 µm
G
Ext
Int
25 µm
H
Int
Ext
25 µm

Plate 4

A-B) complete shell succession showing the change in the orientation of fibres from oblique to transverse from the exterior to the interior of the secondary layer (*Gryphus vitreus*, A: anterior part, ventral valve, longitudinal section; B: central part, dorsal valve, longitudinal section);

C) complete shell succession showing the change in the orientation of fibres from transverse to oblique from the exterior to the interior of the secondary layer, and the alternations of the secondary and tertiary layers (*Gryphus vitreus*, posterior part, ventral valve, longitudinal section);

D-F) Complete shell succession showing several sublayers with variable fibre orientation (*Magasella sanguinea*, D: anterior part, ventral valve, longitudinal section; E: central part, dorsal valve, longitudinal section; F: posterior part, ventral valve, longitudinal section);

G) secondary layer showing several sublayers with variable fibre orientation (*Notosaria nigricans*, anterior part, ventral valve, longitudinal section);

H) complete shell succession showing longitudinal to oblique fibres, except for a few transversally oriented fibres in the internal part (*Notosaria nigricans*, posterior part, ventral valve, longitudinal section).

Ext: external part of the shell; Int: internal part of the shell.

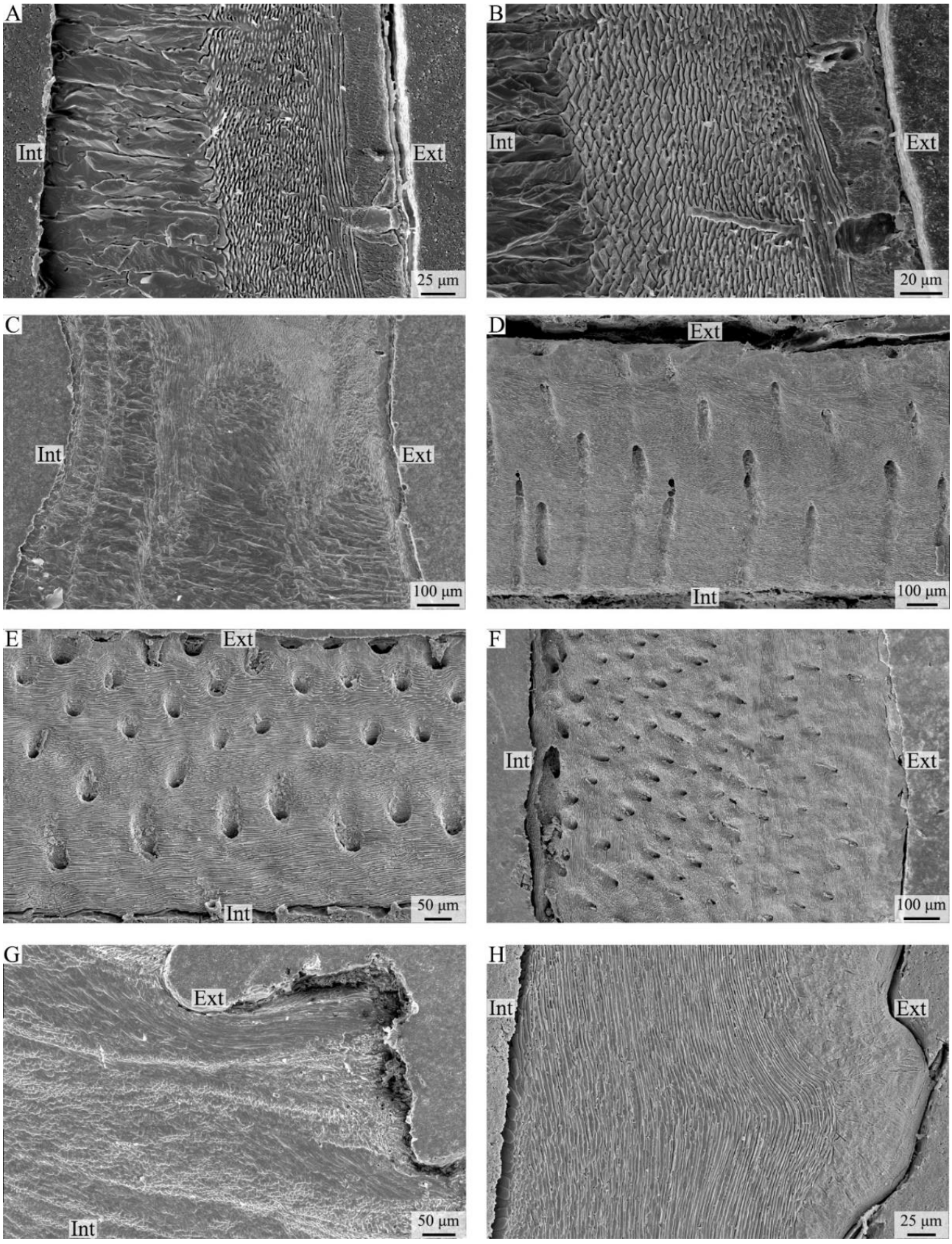
A
Int
Ext
25 µm
B
Int
Ext
20 µm
C
Int
Ext
100 µm
D
Ext
Int
100 µm
E
Ext
Int
50 µm
F
Int
Ext
100 µm
G
Ext
Int
50 µm
H
Int
Ext
25 µm

2.3 EBSD

For EBSD measurements brachiopod shells were embedded in epoxy resin and were cut along and perpendicular to the median plane of the investigated shells. Surfaces of the embedded specimens were subjected to several sequential mechanical grinding and polishing steps down to a grain size of 1 μm. The final polishing step was carried out with colloidal alumina (particle size ~ 0.06 μm) in a vibratory polisher. Sample surfaces were coated with 4-6 nm of carbon. EBSD measurements were carried out at the Department of Earth and Environmental Sciences, LMU Munich, Munich, Germany, on a Hitachi SU5000 field emission SEM, equipped with a Nordlys II EBSD detector and AZTec acquisition software. The SEM was operated at 15 and 20 kV; measurements were evaluated with CHANNEL 5 HKL software [11, 12]. EBSD data are presented as band contrast measurement images, a grey scale component that gives the signal strength of the EBSD Kikuchi diffraction pattern in each measurement point. Accordingly, the strength of the diffraction signal is high when a mineral is detected whereas it is weak or absent when a polymer is scanned. A high diffraction signal is shown with light, while a weak signal is visualized with dark grey colors in the band contrast measurement image. Plate 5 shows EBSD band contrast measurement images of two layer shells (*L. uva, C. incospicua, M. sanguinea, N. nigricans*).

Plate 5

EBSD band contrast images visualizing the difference in microstructure of two layer brachiopod shells that comprise the primary and the fibrous shell layers.

(A: *Liothyrella uva*; B: *Calloria inconspicua*; C: *Magasella sanguinea*; D: *Notosaria nigricans*)

Ext: external part of the shell; Int: internal part of the shell.

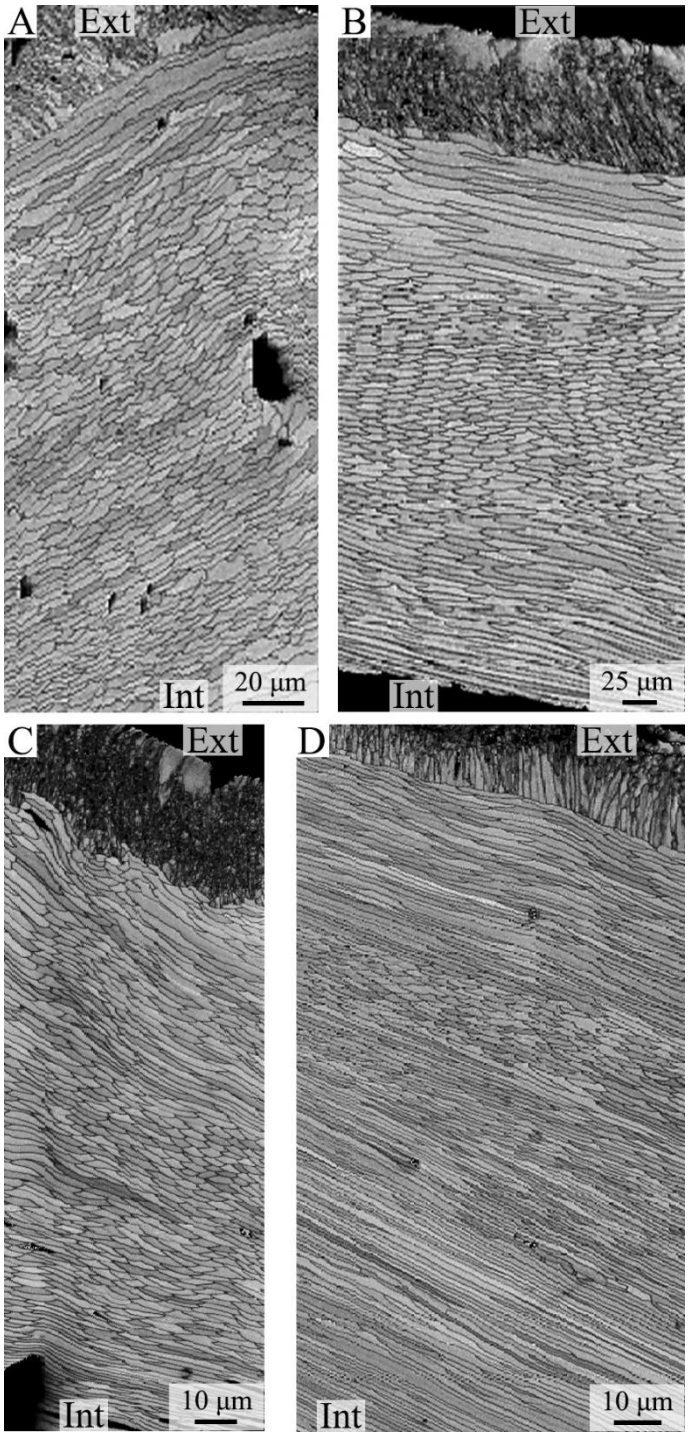
A
Ext
Int
20 µm
B
Ext
Int
25 µm
C
Ext
Int
10 µm
D
Ext
Int
10 µm

2.4 Statistical analyses

Based on SEM micrographs, each fibre, with regular and symmetrical cross sectional outline, was chosen for morphometric measurements (1197 measurements) from different ontogenetic stages; fibres were first outlined using Adobe Photoshop CS6, and then all parameters (e.g. Max Feret diameter, Min Feret diameter, Area, Perimeter, Convex area and Convex perimeter) were measured by Image-Pro Plus 6.0 and ImageJ.

The frequency distribution plots of the most significant parameters (Area, Perimeter, Max Feret diameter, Convex Area) were calculated and drawn by Excel 2013 (FREQUENCY function and NORM.DIST function) (Figs. 1-3) [cf. 13].

Based on the six measured parameters, five shape descriptors were calculated: Formfactor (circularity, $4\pi\times$Area/Perimeter^2), Roundness (4Area$/\pi\times$ Max Feret diameter^2), Aspect Ratio (Max Feret diameter/Min Feret diameter), Convexity (Convex Perimeter/Perimeter), and Solidity (Area/Convex Area) [14]. For data visualization and dimension reduction, principal component analysis (PCA) was performed on the five shape descriptors using R 3.3.0 (Figs. 4-6) [2]. We used the function *prcomp* for principal component analysis and *fviz_pca_biplot* for plot; the biplots were created using the package *factoextra* [15].

Independent-sample *t*-tests were performed using SPSS Statistics (IBM Version 22.0. Armonk, NY) (Tables 2-9). A p-value ≤ 0.05 is considered significant.

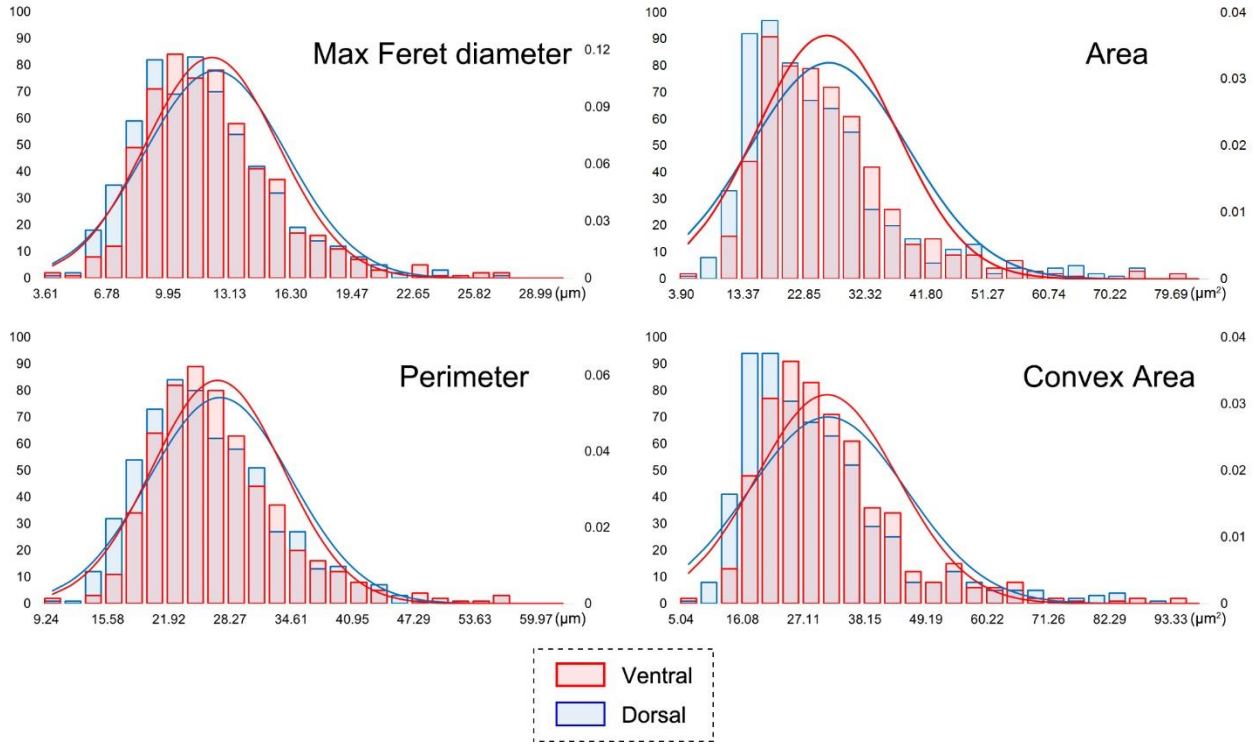

Fig. 1. Distribution plots of the original parameters of all six species in the ventral valve (red) and dorsal valve (blue).

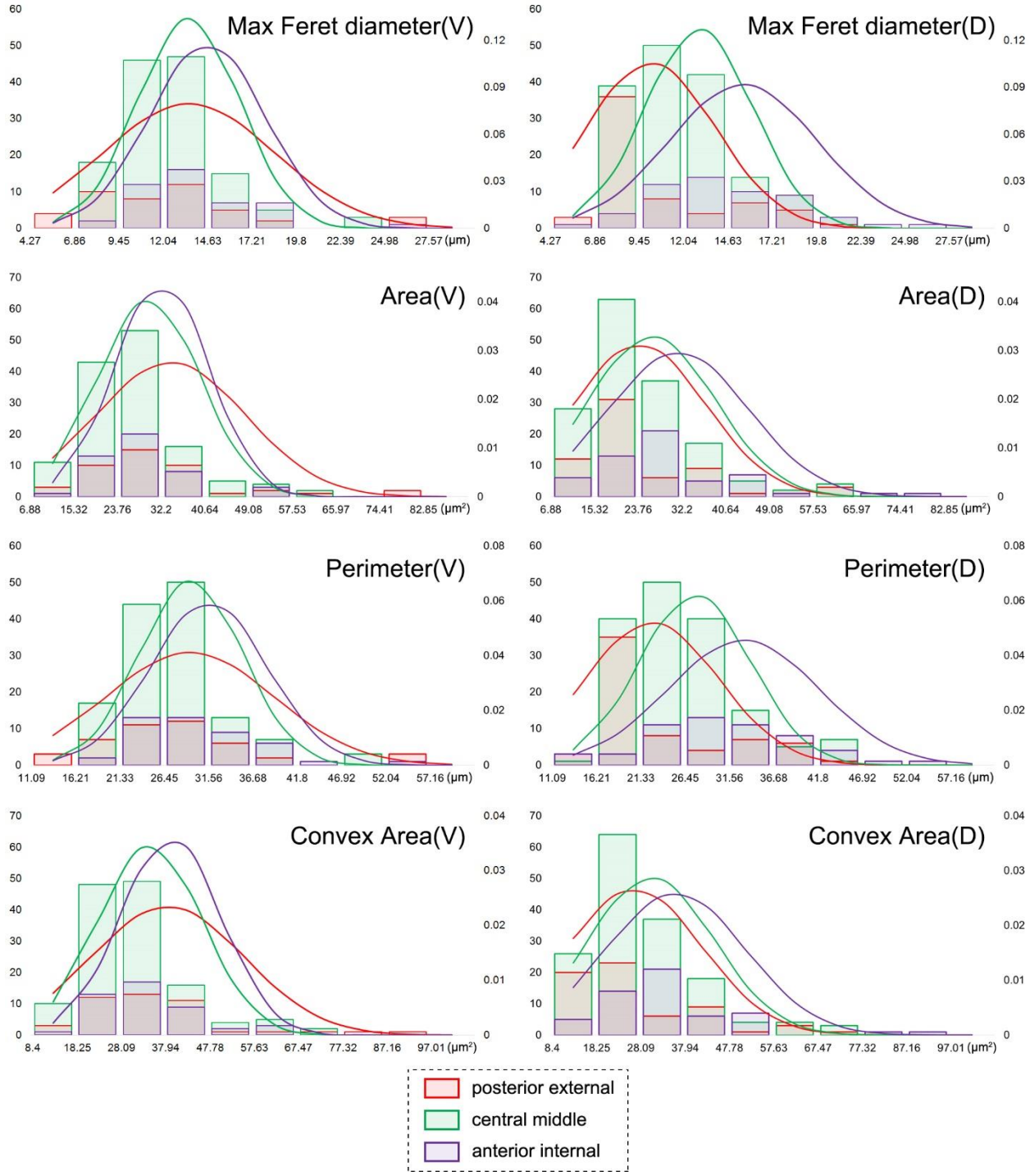

Fig. 2. Distribution plots of the original parameters from different positions in ontogenetic direction (red: posterior external; green: central middle; violet: anterior internal; V: ventral; D: dorsal).

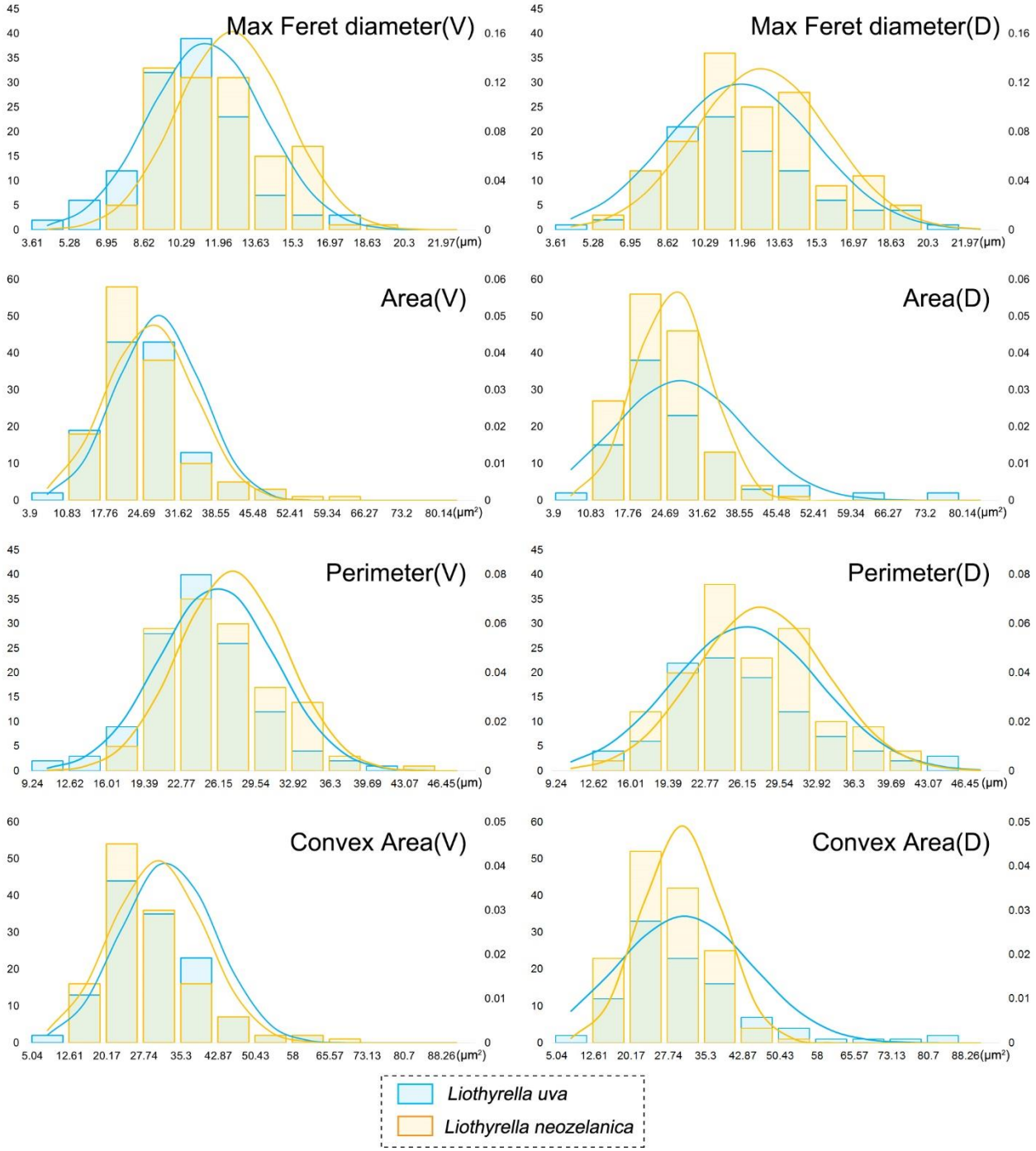

Fig. 3. Distribution plots of the original parameters of *Liothyrella uva* (light blue) and *Liothyrella neozelanica* (orange) (V: ventral; D: dorsal).

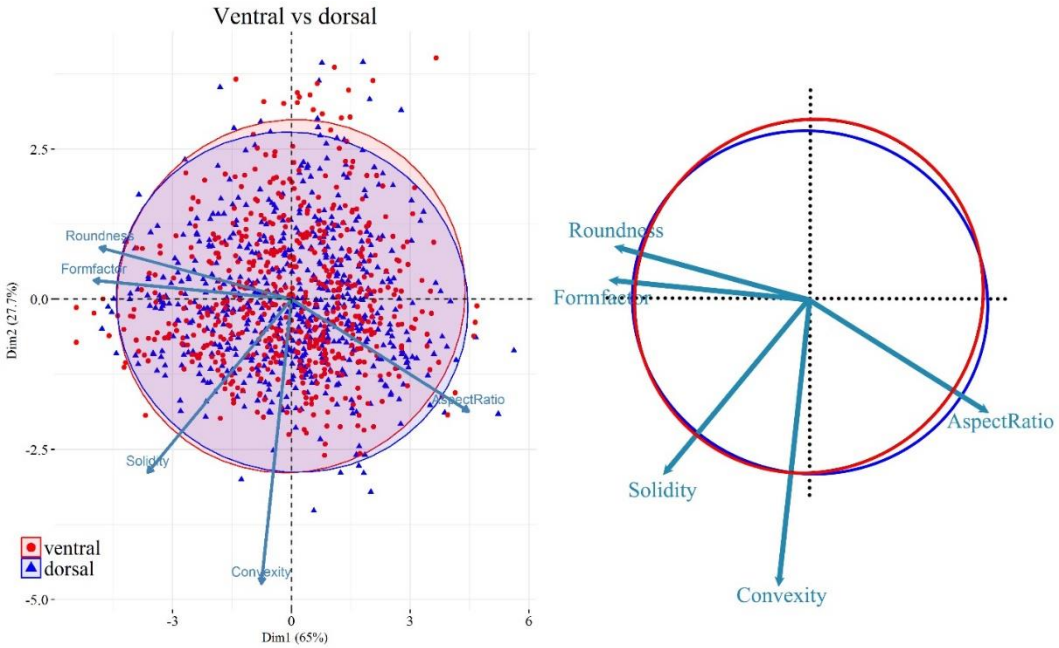

Fig. 4. PCA (Principal Component Analysis) plot of fibres from ventral (red) and dorsal (blue) valves. Five variables (Roundness, Formfactor, Solidity, Convexity, AspectRatio) are considered for the PCA; the longer the arrow, the greater the correlation between the specific factor and that direction in the PCA space. 95% confidence ellipse and centroids (larger symbols, overlapping in the central point in this case) for each data sets are also shown in the plot.

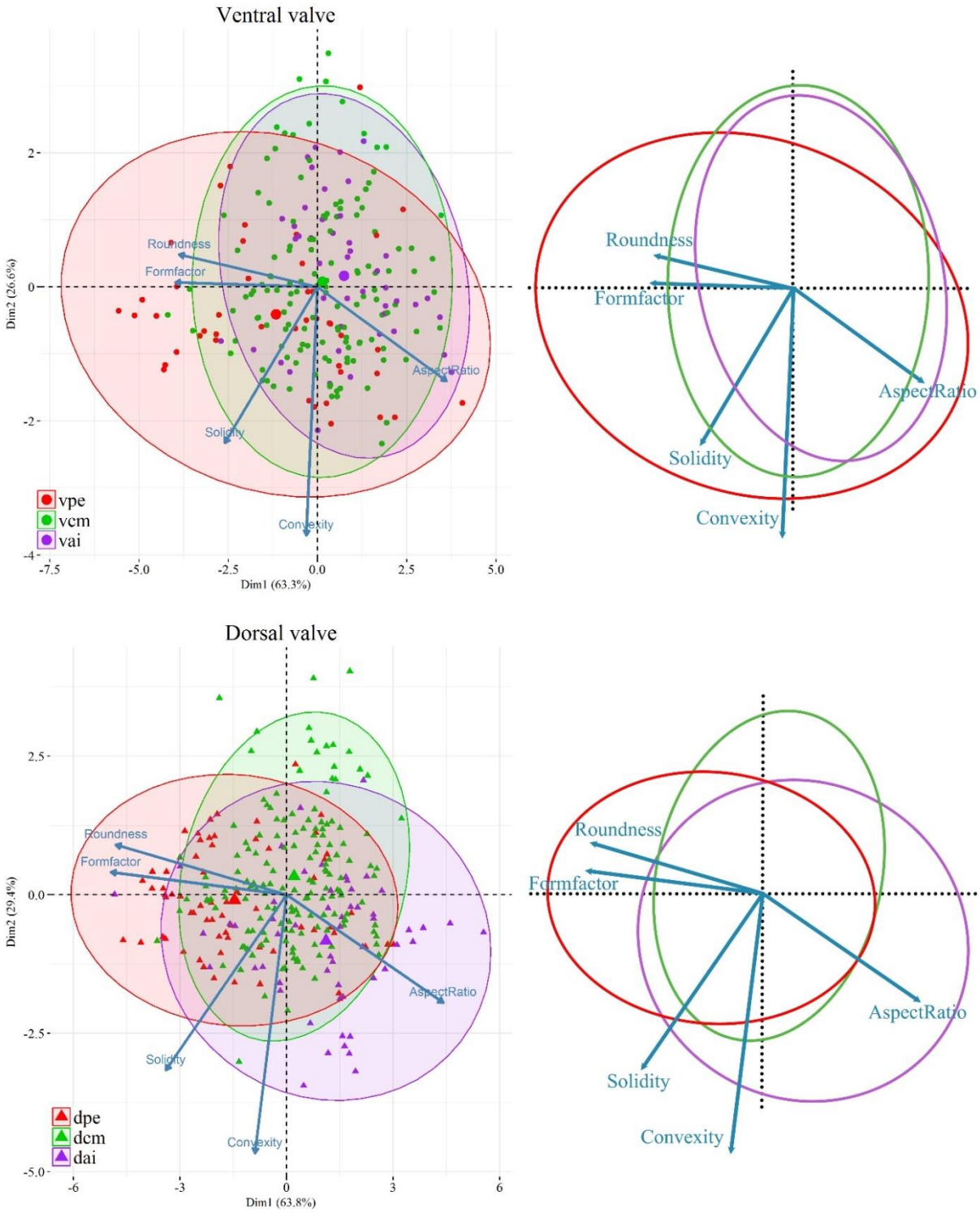

Fig. 5. PCA (Principal Component Analysis) plots showing the morphological change of the fibres in the ontogenetic direction. Five variables (Roundness, Formfactor, Solidity, Convexity, AspectRatio) are considered for the PCA; the longer the arrow, the greater the correlation between the specific factor and that direction in the PCA space (vpe: ventral posterior external; vcm: ventral central middle; vai: ventral anterior internal; dpe: dorsal posterior external; dcm: dorsal central middle; dai: dorsal anterior internal). 95% confidence ellipse and centroids (larger symbols) for each data groups are also shown in the plot.

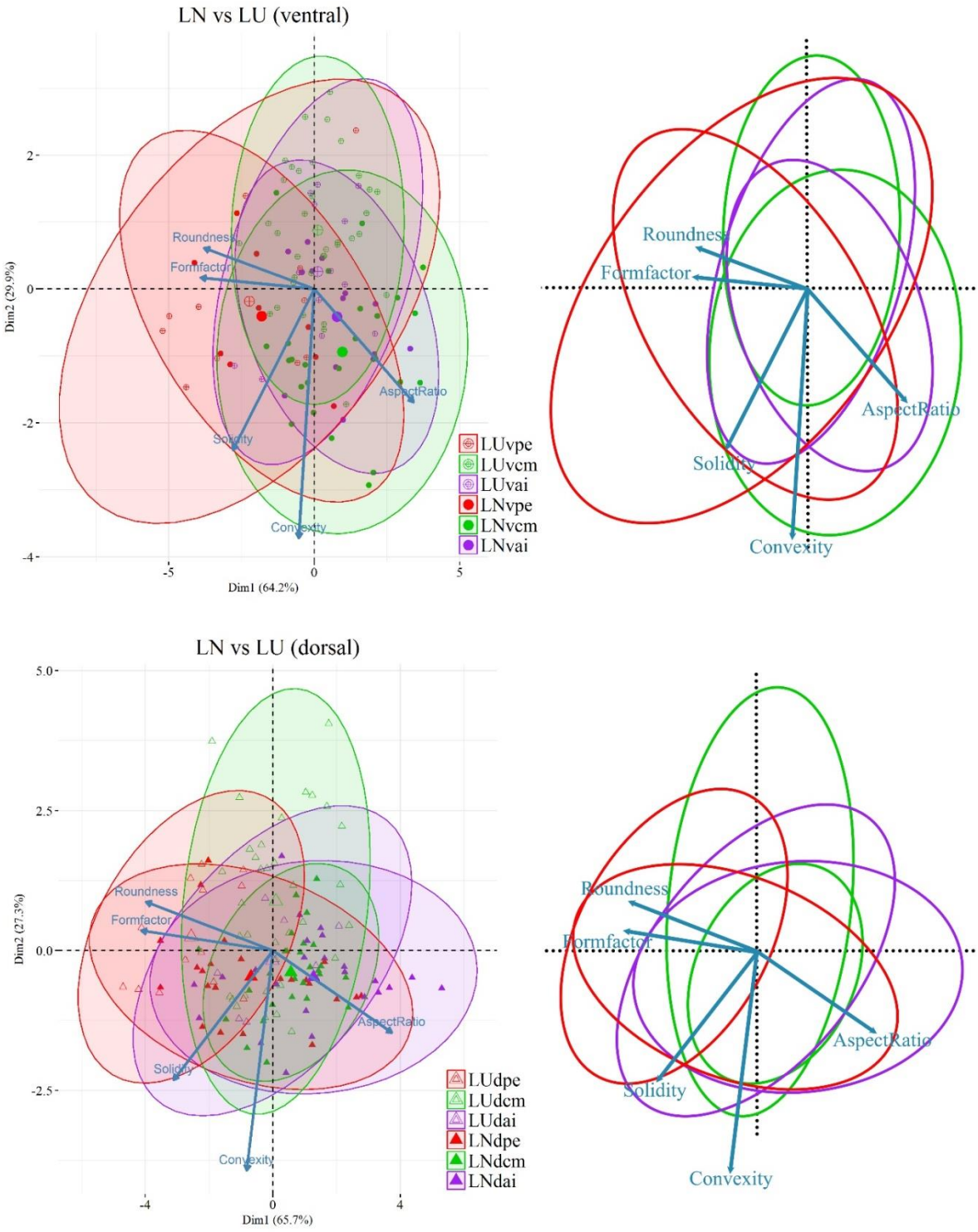

Fig. 6. PCA (Principal Component Analysis) plots showing the comparison of the fibres between *Liothyrella uva* and *Liothyrella neozelanica*. Five variables (Roundness, Formfactor, Solidity, Convexity, AspectRatio) are considered for the PCA; the longer the arrow, the greater the correlation between the specific factor and that direction in the PCA space. (LUvpe: *Liothyrella uva* ventral posterior external; LUvcm: *Liothyrella uva* ventral central middle; LUvai: *Liothyrella uva* ventral anterior internal; LNvpe: *Liothyrella neozelanica* ventral posterior external; LNvcm: *Liothyrella neozelanica* ventral central middle; LNvai: *Liothyrella neozelanica* ventral anterior internal; LUdpe: *Liothyrella uva* dorsal posterior external; LUdcm: *Liothyrella uva* dorsal central middle; LUdai: *Liothyrella uva* dorsal anterior internal; LNdpe: *Liothyrella neozelanica* dorsal posterior external; LNdcm: *Liothyrella neozelanica* dorsal central middle; LNdai: *Liothyrella neozelanica* dorsal anterior internal). 95% confidence ellipse and centroids (larger symbols) for each data sets are also shown in the plot.

Table 2

T-test of fibres size and shape data of the ventral valve vs the dorsal valve (LU: *Liothyrella uva*; GV: *Gryphus vitreus*; LN: *Liothyrella neozelanica*; CI: *Calloria incospicua*; MS: *Magasella sanguinea*; NN: *Notosaria nigricans*). Significant values (*p*-value ≤ 0.05) are marked in bold style.

	Area	Perimeter	Max Feret diameter	Roundness	Convexity
LU	t(165.165) = 1.429, *p* = 0.155	t(188.750) = 1.984, ***p* = 0.049**	t(187.755) = 2.392, ***p* = 0.018**	t(228) = -2.632, ***p* = 0.009**	t(228) = 1.130, *p* = 0.260
GV	t(275) = -7.376, ***p* < 0.001**	t(233.644) = -5.890, ***p* < 0.001**	t(234.192) = -5.414, ***p* < 0.001**	t(275) = 0.947, *p* = 0.344	t(275) = -2.784, ***p* = 0.006**
LN	t(279) = -1.099, *p* = 0.273	t(276.009) = 1.054, *p* = 0.293	t(275.477) = 1.511, *p* = 0.132	t(263.010) = -2.479, ***p* = 0.014**	t(279) = 0.120, *p* = 0.905
CI	t(68) = -2.509, ***p* = 0.015**	t(68) = -3.564, ***p* = 0.001**	t(68) = -3.394, ***p* = 0.001**	t(41.294) = 2.727, ***p* = 0.009**	t(68) = 1.412, *p* = 0.163
MS	t(133) = -0.723, *p* = 0.471	t(133) = -0.834, *p* = 0.406	t(133) = -0.737, *p* = 0.463	t(133) = -0.029, *p* = 0.977	t(133) = 0.005, *p* = 0.996
NN	t(202) = 1.951, *p* = 0.052	t(202) = -0.055, *p* = 0.956	t(202) = -0.583, *p* = 0.561	t(178.721) = 3.866, ***p* < 0.001**	t(202) = -1.506, *p* = 0.134
All 6 species	t(1195) = -2.340, ***p* = 0.019**	t(1194.446) = -1.970, ***p* =0.049**	t(1195) = -1.574, *p* = 0.116	t(1195) = -0.723, *p* = 0.470	t(1195) = -0.165, *p* = 0.869

Table 3

T-test of fibres size and shape data of the ventral valve vs the dorsal valve in different positions of the shell (pe: posterior external; cm: central middle; ai: anterior internal). Significant values (*p*-value ≤ 0.05) are marked in bold style.

Position	Area	Perimeter	Max Feret diameter	Roundness	Convexity
pe	t(106) = -2.649, ***p* = 0.009**	t(106) =-2.587, ***p* = 0.011**	t(106) = -2.423, ***p* = 0.017**	t(72.163) = 0.279, *p* = 0.781	t(106) = -1.991, ***p* = 0.049**
cm	t(290) = -1.210, *p* = 0.227	t(290) = -1.413, *p* = 0.159	t(290) = -1.312, *p* = 0.191	t(290) = -0.467, *p* = 0.641	t(290) = -2.437, ***p* = 0.015**
ai	t(98) = 0.032, *p* = 0.974	t(98) = 0.654, *p* = 0.515	t(98) = 0.970, *p* = 0.334	t(98) = -1.297, *p* = 0.198	t(98) = 3.233, ***p* = 0.002**

Table 4

T-test of fibres size and shape data of the anterior internal vs central middle vs posterior external parts of both the ventral valve (vpe, vcm, vai) and the dorsal valve (dpe, dcm, dai), considering all the six analyzed species together. See caption of Fig. 5 for the legend. Significant values (*p*-value ≤ 0.05) are marked in bold style.

Valve and position	Area	Perimeter	Max Feret diameter	Roundness	Convexity
Vpe vs Vcm	t(56.715) = -2.192, ***p* = 0.033**	t(53.925) = -0.505, *p* = 0.615	t(53.307) = -0.241, *p* = 0.811	t(50.796) = -3.335, ***p* = 0.002**	t(176) = -2.854, ***p* = 0.005**
Vpe vs Vai	t(87) = 1.136, *p* = 0.259	t(87) = -1.126, *p* = 0.263	t(87) = -1.325, *p* = 0.188	t(57.287) = 4.468, ***p* < 0.001**	t(87) = 2.884, ***p* = 0.005**
Vcm vs Vai	t(177) = -1.340, *p* = 0.182	t(177) = -2.623, ***p* = 0.009**	t(177) = -2.619, ***p* = 0.010**	t(177) = 2.394, ***p* = 0.018**	t(177) = 0.822, *p* = 0.412
Dpe vs Dcm	t(220) = -0.153, *p* = 0.878	t(100.527) = -2.322, ***p* = 0.022**	t(99.878) = -2.598, ***p* = 0.011**	t(83.739) = 6.264, ***p* < 0.001**	t(152.038) = 3.566, ***p* < 0.001**
Dpe vs Dai	t(117) = -1.733, *p* = 0.086	t(117) = -4.889, ***p* < 0.001**	t(117) = -5.402, ***p* < 0.001**	t(116.994) = 7.581, ***p* < 0.001**	t(117) = -2.241, ***p* = 0.027**
Dcm vs Dai	t(211) = -1.992, ***p* = 0.048**	t(75.180) = -3.762, ***p* < 0.001**	t(74.481) = -4.138, ***p* < 0.001**	t(211) = 4.108, ***p* < 0.001**	t(211) = -5.119, ***p* < 0.001**

Table 5

T-test of fibres size and shape data in different positions of the ventral valve. See captions of Fig. 5 and Table 2 for the legend. Significant values (*p*-value ≤ 0.05) are marked in bold style.

Species and position	Area	Perimeter	Max Feret diameter	Roundness	Convexity
LUvpe vs LUvai	t(22) = 0.079, *p* = 0.938	t(17.461) = -1.132, *p* = 0.273	t(16.910) = -1.314, *p* = 0.206	t(12.538) = 3.013, ***p* = 0.010**	t(22) = 1.284, *p* = 0.213
GVvpe vs GVvai	t(15) = 2.502, ***p* = 0.024**	t(15) = 0.680, *p* = 0.507	t(15) = 0.355, *p* = 0.727	t(15) = 1.158, *p* = 0.265	t(15) = 0.779, *p* = 0.448
LNvpe vs LNvai	t(21) = 1.193, *p* = 0.246	t(21) = 3.551, ***p* = 0.002**	t(21) = 3.758, ***p* = 0.001**	t(21) = -3.726, ***p* = 0.001**	t(21) = -0.715, *p* = 0.482
CIvpe vs CIvai	-	-	t(1.293) = 0.657, *p* = 0.609	t(1.087) = -5.131, *p* = 0.108	t(1.481) = 2.815, *p* = 0.147
MSvpe vs MSvai	t(2.081) = -1.538, *p* = 0.259	t(4) = -16.618, ***p* < 0.001**	t(4) = -15.308, ***p* < 0.001**	t(4) = 6.087, ***p* = 0.002**	t(4) = 1.527, *p* = 0.202
NNvpe vs NNvai	t(13) = 2.409, ***p* = 0.032**	t(13) =1.517, *p* = 0.153	t(13) = 1.445, *p* = 0.172	t(13) = 0.561, *p* = 0.574	t(13) = 0.877, *p* = 0.396

Table 6

T-test of fibres size and shape data in different positions of the dorsal valve. See caption of Fig. 5 and Table 2 for the legend. Significant values (*p*-value ≤ 0.05) are marked in bold style.

Species and position	Area	Perimeter	Max Feret diameter	Roundness	Convexity
LUdpe vs LUdai	t(6.673) = -1.127, *p* = 0.299	t(6.548) = -1.966, *p* = 0.093	t(6.766) = -2.314, *p* = 0.055	t(18) = 4.340, ***p* < 0.001**	t(18) = 0.100, *p* = 0.921
GVdpe vs GVdai	t(12.345) = 5.286, ***p* < 0.001**	t(11.772) = -8.424, ***p* < 0.001**	t(11.897) = -9.113, ***p* < 0.001**	t(21.023) = 10.459, ***p* < 0.001**	t(26) = -4.931, ***p* < 0.001**
LNdpe vs LNdai	t(40.052) = -0.794, *p* = 0.432	t(37.697) = -2.353, ***p* = 0.024**	t(37.929) = -2.384, ***p* = 0.022**	t(40.869) = 3.232, ***p* = 0.002**	t(45) = 0.208, *p* = 0.836
NNdpe vs NNdai	t(16) = 0.396, *p* = 0.697	t(16) = -0.801, *p* = 0.435	t(16) = -1.075, *p* = 0.298	t(16) = 1.773, *p* = 0.088	t(16) = -2.280, ***p* = 0.037**

Table 7

T-test of fibres size and shape data of Group1-three layer shells (*Gryphus vitreus* and *Liothyrella neozelanica*) vs Group 2-two layer shells (*Liothyrella uva, Calloria inconspicua, Magasella sanguinea* and *Notosaria nigricans*) for different positions of the ventral valve and dorsal valve. See caption of Fig. 5 for the legend. Significant values (*p*-value ≤ 0.05) are marked in bold style.

Group and position	Area	Perimeter	Max Feret diameter	Roundness	Convexity
Gr.1vpe vs Gr.2vpe	t(27.938) = -0.622, *p* = 0.539	t(27.378) = -0.605, *p* = 0.549	t(28.153) = -0.493, *p* = 0.626	t(36.757) = -0.748, *p* = 0.460	t(42) = 1.136, *p* = 0.262
Gr.1vcm vs Gr.2vcm	t(132) = -2.350, ***p* = 0.020**	t(128.900) = -0.653, *p* = 0.515	t(131.623) = 0.032, *p* = 0.975	t(119.932) = -4.417, ***p* < 0.001**	t(118.499) = 1.586, *p* = 0.115
Gr.1vai vs Gr.2vai	t(39.475) = -0.795, *p* = 0.432	t(40.287) = -0.848, *p* = 0.402	t(40.571) = -0.667, *p* = 0.509	t(43) = -0.033, *p* = 0.974	t(43) = 1.136, *p* = 0.262
Gr.1dpe vs Gr.2dpe	t(33.052) = -2.994, ***p* = 0.005**	t(62) = -1.644, *p* = 0.105	t(62) = -1.130, *p* = 0.263	t(62) = -1.702, *p* = 0.094	t(34.514) = 1.292, *p* = 0.205
Gr.1dcm vs Gr.2dcm	t(130.484) = -5.613, ***p* < 0.001**	t(155.250) = -3.537, ***p* = 0.001**	t(155.766) = -2.897, ***p* = 0.004**	t(156) = -3.230, ***p* = 0.002**	t(156) = -0.066, *p* = 0.947
Gr.1dai vs Gr.2dai	t(21.387) = -0.692, *p* = 0.496	t(22.352) = 0.456, *p* = 0.653	t(22.757) = 0.631, *p* = 0.534	t(53) = -2.341, ***p* = 0.023**	t(53) = 1.833, *p* = 0.072
Gr.1v vs Gr.2v	t(578.998) = -3.254, ***p* = 0.001**	t(576.984) = -1.133, *p* = 0.258	t(577.130) = -0.334, *p* = 0.738	t(579) = -3.475, ***p* = 0.001**	t(567.776) = 5.464, ***p* < 0.001**
Gr.1d vs Gr.2d	t(395.017) = -8.935, ***p* < 0.001**	t(509.357) = -4.129, ***p* < 0.001**	t(519.510) = -2.881, ***p* = 0.004**	t(560.685) = -6.134, ***p* < 0.001**	t(571.282) = 2.838, ***p* = 0.005**

Table 8

T-test of fibres size and shape data of *Liothyrella neozelanica* vs *Gryphus vitreus* (both three-layer shells) for different positions in the ventral valve and dorsal valve. See captions of Fig. 5 and Table 2 for the legend. Significant values (*p*-value ≤ 0.05) are marked in bold style.

Species and position	Area	Perimeter	Max Feret diameter	Roundness	Convexity
LNvpe vs GVvpe	t(20) = 3.222, ***p* = 0.004**	t(20) = 3.961, ***p* = 0.001**	t(20) = 3.806, ***p* = 0.001**	t(20) = -1.727, *p* = 0.100	t(20) = 3.586, ***p* = 0.002**
LNvcm vs GVvcm	t(45) = 0.273, *p* = 0.786	t(45) = 0.069, *p* = 0.945	t(45) = 0.018, *p* = 0.986	t(42.265) = 0.529, *p* = 0.600	t(45) = -1.375, *p* = 0.176
LNvai vs GVvai	t(16) = -0.714, *p* = 0.486	t(16) = -0.412, *p* = 0.686	t(16) = -0.211, *p* = 0.836	t(16) = -0.456, *p* = 0.654	t(16) = 2.580, ***p* = 0.020**
LNdpe vs GVdpe	t(27.016) = -3.609, ***p* = 0.001**	t(23.790) = -4.157, ***p* < 0.001**	t(23.940) = -4.275, ***p* < 0.001**	t(37) = 3.441, ***p* = 0.001**	t(37) = -0.939, *p* = 0.354
LNdcm vs GVdcm	t(35.615) = -5.782, ***p* < 0.001**	t(36.280) = -5.303, ***p* < 0.001**	t(37.699) = -5.524, ***p* < 0.001**	t(65) = 2.686, ***p* = 0.009**	t(62.375) = -4.495, ***p* < 0.001**
LNdai vs GVdai	t(34) = 2.023, *p* = 0.051	t(34) = 1.910, *p* = 0.065	t(34) = 2.160, ***p* = 0.038**	t(33.054) = -1.639, *p* = 0.111	t(34) = 3.929, ***p* < 0.001**
LNv vs GVv	t(225) = 1.215, *p* = 0.225	t(225) = 1.657, *p* = 0.099	t(225) = 1.804, *p* = 0.073	t(217.032) = -1.385, *p* = 0.167	t(225) = 0.634, *p* = 0.527
LNd vs GVd	t(329) = -5.660, ***p* < 0.001**	t(329) = -5.107, ***p* < 0.001**	t(329) = -4.979, ***p* < 0.001**	t(329) = 2.180, ***p* = 0.030**	t(323.389) = -2.998, ***p* = 0.003**

Table 9
T-test of fibres size and shape data of Group NZ New Zealand (*Calloria inconspicua*, *Magasella sanguinea* and *Notosaria nigricans*) vs Group LN New Zealand (*Liothyrella neozelanica*) vs Group MED Mediterranean (*Gryphus vitreus*) vs Group ANT Antarctica (*Liothyrella uva*); (v: ventral valve; d: dorsal valve). Significant values (*p*-value ≤ 0.05) are marked in bold style.

Group and position	Area	Perimeter	Max Feret diameter	Roundness	Convexity
Gr.NZv vs Gr.LNv	t(357.973) = 4.452, ***p* < 0.001**	t(357.548) = 3.611, ***p* < 0.001**	t(357.515) = 3.327, ***p* = 0.001**	t(358) = 0.237, *p* = 0.814	t(330.310) = -1.943, *p* = 0.053
Gr.NZv vs Gr.MEDv	t(298.514) = 3.268, ***p* = 0.001**	t(302.183) = 2.070, ***p* = 0.039**	t(300.104) = 1.647, *p* = 0.101	t(207.223) = 1.775, *p* = 0.077	t(317) = -2.147, ***p* = 0.033**
Gr.NZv vs Gr.ANTv	t(351.958) = 4.620, ***p* < 0.001**	t(349.047) = 5.771, ***p* < 0.001**	t(350.600) = 6.487, ***p* < 0.001**	t(352) = -4.981, ***p* < 0.001**	t(233.672) = 5.068, ***p* < 0.001**
Gr.LNv vs Gr.MEDv	t(225) = -1.215, *p* = 0.215	t(225) = -1.657, *p* = 0.099	t(225) = -1.804, *p* = 0.073	t(217.032) = 1.385, *p* = 0.167	t(225) = -0.634, *p* = 0.527
Gr.LNv vs Gr.ANTv	t(260) = 0.154, *p* = 0.878	t(260) = 2.699, ***p* = 0.007**	t(260) = 3.833, ***p* < 0.001**	t(260) = -4.797, ***p* < 0.001**	t(22.742) = 6.538, ***p* < 0.001**
Gr.MEDv vs Gr.ANTv	t(219) = 1.387, *p* = 0.167	t(219) = 4.077, ***p* < 0.001**	t(219) = 5.299, ***p* < 0.001**	t(219) = -6.141, ***p* < 0.001**	t(218.557) = 6.382, ***p* < 0.001**
Gr.NZd vs Gr.LNd	t(258.275) = 6.246, ***p* < 0.001**	t(315.809) = 1.691, *p* = 0.092	t(318.466) = 0.705, *p* = 0.481	t(326.954) = 5.898, ***p* < 0.001**	t(327.455) = -2.565, ***p* = 0.011**
Gr.NZd vs Gr.MEDd	t(246.940) = 9.713, ***p* < 0.001**	t(308.306) = 5.924, ***p* < 0.001**	t(314.858) = 4.873, ***p* < 0.001**	t(348.395) = 4.027, ***p* < 0.001**	t(365) = 0.543, *p* = 0.587
Gr.NZd vs Gr.ANTd	t(256.290) = 3.165, ***p* = 0.002**	t(260.731) = 2.287, ***p* = 0.023**	t(261.222) = 2.186, ***p* = 0.030**	t(252.246) = 0.944, *p* = 0.346	t(174.498) = 3.192, ***p* = 0.002**
Gr.LNd vs Gr.MEDd	t(329) = 5.660, ***p* < 0.001**	t(329) = 5.107, ***p* < 0.001**	t(329) = 4.979, ***p* < 0.001**	t(329) = -2.180, ***p* = 0.030**	t(323.389) = 2.998, ***p* = 0.003**
Gr.LNd vs Gr.ANTd	t(145.357) = -2.122, ***p* = 0.035**	t(247) = 0.939, *p* = 0.349	t(247) = 1.800, *p* = 0.073	t(247) = -4.743, ***p* < 0.001**	t(154.474) = 5.114, ***p* < 0.001**
Gr.MEDd vs Gr.ANTd	t(137.337) = -5.444, ***p* < 0.001**	t(284) = -3.360, ***p* = 0.001**	t(284) = -2.395, ***p* = 0.017**	t(284) = -2.849, ***p* = 0.005**	t(284) = 2.792, ***p* = 0.006**

References

[1] F. Ye, G. Crippa, L. Angiolini, U. Brand, G. Capitani, M. Cusack, C. Garbelli, E. Griesshaber, E. Harper, W. Schmahl, Mapping of recent brachiopod microstructure: a tool for environmental studies, J. Struct. Biol. (2018) in press.

[2] R Core Team, R: A language and environment for statistical computing. R Foundation for Statistical Computing, Vienna, Austria, 2016. https://www.R-project.org/

[3] G. Crippa, F. Ye, C. Malinverno, A. Rizzi, Which is the best method to prepare invertebrate shells for SEM analysis? Testing different techniques on recent and fossil brachiopods, Boll. Soc. Paleontol. Ital. 55 (2016) 111–125.

[4] B.N. Popp, T.F. Anderson, P.A. Sandberg, Brachiopods as indicators of original isotopic compositions in some Paleozoic limestones, Geol. Soc. Am. Bull. 97 (1986) 1262–1269.
[5] D. Parkinson, G.B. Curry, M. Cusack, A.E. Fallick, Shell structure, patterns and trends of oxygen and carbon stable isotopes in modern brachiopod shells, Chem. Geol. 219 (2005) 193–235.
[6] L. Angiolini, D.P.F. Darbyshire, M.H. Stephenson, M.J. Leng, T.S. Brewer, F. Berra, F. Jadoul, Lower Permian brachiopods from Oman: their potential as climatic proxies, Earth. Env. Sci. T. R. So. 98 (2007) 327–344.
[7] L. Angiolini, F. Jadoul, M.J. Leng, M.H. Stephenson, J. Rushton, S. Chenery, G. Crippa, How cold were the Early Permian glacial tropics? Testing sea-surface temperature using the oxygen isotope composition of rigorously screened brachiopod shells, J. Geol. Soc. 166 (2009) 933–945.
[8] U. Brand, A. Logan, M.A. Bitner, E. Griesshaber, K. Azmy, D. Buhl, What is the ideal proxy of Palaeozoic seawater chemistry?, Mem. Assoc. Australas. 41 (2011) 9–24.
[9] M. Cusack, A.P. Huerta, Brachiopods recording seawater temperature–A matter of class or maturation?, Chem. Geol. 334 (2012) 139–143.
[10] C. Garbelli, L. Angiolini, S.Z. Shen, Biomineralization and global change: A new perspective for understanding the end-Permian extinction, Geology 45 (2017) 19–12.
[11] N.H. Schmidt, N.O. Olesen, Computer-aided determination of crystal-lattice orientation from electron channeling patterns in the SEM, Canad. Mineral. 27 (1989) 15-22.
[12] V. Randle, O. Engler, Introduction to texture analysis, CRC Press, 408 p., Amsterdam, 2000.
[13] C. Duller, Teaching statistics with excel a big challenge for students and lecturers, Austrian J. Stat. 37 (2008) 195–206.
[14] J.C. Russ, F.B. Neal, The Image Processing Handbook, seventh ed., Boca Raton, 2015.
[15] A. Kassambara, Factoextra: Extract and Visualize the Results of Multivariate Data Analyses. R package version 1.0.4. (2017) Retrieved from https://www.rdocumentation.org/packages/factoextra/versions/1.0.4.

Appendix 2

Table 1. Morphological measurement data on the brachiopod shell

Sample Name	Shape of shell	Length(cm) (f: fragment)	Width(cm) (f: fragment)	High(cm) (V: ventral valve, D: dorsal valve)
Billingsella aff. *B. seletensis*	Biconvex			
MRAN 898-8		2.03	1.64	0.30 V
MRAN 898-11		1.72	1.76	0.40 D
MRAN 898-3-3		1.66	2.05	
MRAN 898-3-4		2.21	2.12	
Billingsellidae gen. et sp. ind.	Concavo-convex			
MRAN 8760-1		1.15	1.20	0.20
MRAN 8760-2		1.22	1.37	
Protambonites cf. *P. primigenius*	Biconvex			
MRAN 8763-2		1.32	1.40	0.24
Martellia shabdjerehensis	Biconvex			
KE43-7		1.25	1.16	0.55
KE43-8		1.05	1.44	0.5
KE45-1		1.59	1.76	0.61
KE42-2a		1.29	1.55	0.68
KE42-2b		1.03	1.2	0.54
KE45-2		1.29	1.29	0.65
Leptellina? sp. ind.	Concavo-convex			
KE43-1		1.19	1.50	0.57
KE43-2		1.01	1.54	0.21
KE45-4		1	1.46	0.22
KE45-3		0.91	1.3	0.22
Ingria sp. ind.	Flat			
MRAN 1108-2C		1.64	1.54	0.17 V
MRAN 1108-2E		1.61	1.86	0.1 V
MRAN 1108-4A		1.13	1.36	0.1 V
MRAN 1108-4B		1.12	1.3	0.1 V
Leptaena depressa	Biconvex			
MRAN 1180-27		1.39	2.42	0.66
MRAN 1180-23		1.47	2.06	0.45
Productella cf. *P. belanskii*	Concavo-convex			
MRAN 10810-4		1.16	1.54	0.38
MRAN 10810-5		1.18 f	1.31 f	0.43
Productella cf. *P. subaculeata*	Concavo-convex			
MRAN 6203-3		1.65	2.1	1.17
Productella sp. ind.	Concavo-convex			
MRAN 10771-5		1.11	1.22	0.52
MRAN 2727-2		1.67	1.7	

MRAN 4905-2		1.18	1.1	
MRAN 4905-1		0.95	1.06	
MRAN 2727-1		1.11	1.12	
Rhytialosia sp. ind.	Concavo-convex			
MRAN 6162-2		1.96	2.26	0.80 V
Spinulicosta sp. ind.	Concavo-convex			
MRAN 6162-21		1.73	1.72	0.38
MRAN 6203-1		1.27	1.28	
Striatochonetes sp. ind.	Concavo-convex			
MRAN 9159-2		0.77	0.98	0.27 D
Striatochonetes sp. ind.	Concavo-convex			
MRAN 9136-3		0.68	0.85	
MRAN 9136-6		0.67	1.03	
Devonochonetes sp. ind.	Concave-convex			
MRAN 3648-2		0.75	1.15	
MRAN 3648-4		0.93	1.3	
MRAN 3648-13		0.84	1.04	0.11 V D
Triplesia alata	Biconvex			
MRAN 1181-7		2.20	2.70	1.36
Hesperonomiella sp. ind.	Convex dorsal			
MRAN 8761-1		1.97	1.64	0.41 D
MRAN 8761-2		1.57	1.70	
MRAN 8761-3		1.55	1.5	
Nicolella actoniae	Plano-convex, Concavo-convex			
MRAN 1125-6		1.2	1.48	0.43
MRAN 1125-11		1.26	1.44	0.3
MRAN 1125-8		1.25	1.38	0.6
MRAN 1130-1		1.64	2.04	0.81
Paralenorthis sp. ind.	Plano-convex			
KE41-1		0.92	1.32	0.19 V
KE41-1-2		1.11	1.36	0.30 V
KE41-5		0.77	0.66	0.18
KE43-3		1.13	1.73	0.42
KE43-4		0.75	0.86	0.4
KE41-7		1.19	1.20	0.36
KE45-5		0.6	0.72	0.35
KE42-1		1.44 f	1.88	0.75 V
KE41-7A		0.91	1.06	0.23 V
Howellites ultima	Biconvex			
MRAN 1108		1.51	1.88	0.77
MRAN 1125-7		1.95	2.03	0.94
Isorthis (Ovalella) inflata	Biconvex			
MRAN 1189-3		1.37	1.70	0.6
MRAN 1189-3a		2.10 f	2.32 f	0.74
?*Isorthis* sp. ind.	Biconvex			
MRAN 6904-4		1.32	1.14	0.16 V
Isorthis sp. ind.	Biconvex			
MRAN 6903-1		1.33	1.45	

Syntrophioides sp. ind.	Biconvex			
MRAN 8291-4		1.05		0.21 D
MRAN 8291-5		0.95	0.76	0.13 D
?*Clorinda* sp. ind.	Biconvex			
LA 2		2.62 f	2.22	0.72
LA 3		3.02	3.00	1.20 V
Clorinda molongensis	Biconvex			
NiB5-9		2.55 f	2.66	1.01 f
MRAN 1181-13		1.82 f	2.37 f	0.71 D
NiB5-10A		2.21 f	2.88 f	1.59
Spinatrypina sp. ind.	Biconvex			
MRAN 1181-8		1.27	1.72	0.72
NiB5-2-S		1.74	2.06	0.87
LA 1		1.23	1.54	1.34
MRAN 1180-3		1.96	2.33	0.75
MRAN 1180-29		1.4	1.65	0.7
Spinatrypina cf. *S. chitralensis*	Biconvex			
MRAN 6162-4		2.24	2.34	1.53
MRAN 6162-14		1.38	1.47	0.66
Rhynchotrema sp. ind.	Biconvex			
MRAN 6784-1		0.84	0.96	0.65
Stegocornu denisae	Biconvex			
MRAN 6904-3		0.72	0.94	0.26 V
Cyphoterorhynchus arpaensis	Biconvex			
MRAN 6162-10		1.77	1.50	1.22
Hedeinopsis hispanica hispanica	Biconvex			
MRAN 1209-1A		0.74	0.94	
MRAN 1209-1C		0.78	1	
MRAN 1209-2-A		0.84	1.13	
Hedeinopsis sp. ind.	Biconvex			
MRAN 6904-5		0.65	0.62	0.16 V
Cyrtospirifer brodi	Biconvex			
MRAN 6162-12		1.79	2.02	1.23
Cyrtospirifer cf. *C. kermanensis*	Biconvex			
MRAN 6162-13		1.44	1.66	0.86
MRAN 4232-7		1.89	1.96	1.25
MRAN 6162-1		1.62	1.73	1.28
MRAN 6162-18		1.5	1.63	1.07
MRAN 4242-3		2.63	3.15	1.82
Cyrtospirifer sp. ind.	Biconvex			
MRAN 4232-6 (4232-10)		2.5	3.02	2.08
MRAN 4232-1		2.48	2.64	2
Uchtospirifer aff. *Uchtospirifer nalivkini*	Biconvex			
MRAN 4208-1		2.42	2.77	2.33

Table 2. Geological information of fossil brachiopod specimens

Sample Name	Formation	Section	Age
Acrotretidae gen. et sp. ind.			
MRAN 7885	Soltanieh, lower Shl. Mb.	Abhar	early Cambrian-Silurian
Billingsella aff. *B. seletensis*			
MRAN 898-8	Derinjal	Shirgesht	late Cambrian
MRAN 898-11	Derinjal	Shirgesht	late Cambrian
MRAN 898-3-3	Derinjal	Shirgesht	Cambrian
MRAN 898-3-4	Derinjal	Shirgesht	Cambrian
Billingsellidae gen. et sp. ind.			
MRAN 8760-1	Ilbeyk	Haftanan	middle Cambrian-early Ordovician
MRAN 8760-2	Ilbeyk	Haftanan	middle Cambrian-early Ordovician
Protambonites cf. *P. primigenius*			
MRAN 8763-2	Ilbeyk	Haftanan	late Cambrian-early Ordovician
Martellia shabdjerehensis			
KE43-7	Natkoyeh	Shabdjereh (central Iran)	Ordovician
KE43-8	Natkoyeh	Shabdjereh (central Iran)	Ordovician
KE45-1	Natkoyeh	Shabdjereh (central Iran)	Ordovician
KE42-2a	Natkoyeh	Shabdjereh (central Iran)	Ordovician
KE42-2b	Natkoyeh	Shabdjereh (central Iran)	Ordovician
KE45-2	Natkoyeh	Shabdjereh (central Iran)	Ordovician
Leptellina? sp. ind.			
KE43-1	Natkoyeh	Shabdjereh (central Iran)	Ordovician
KE43-2	Natkoyeh	Shabdjereh (central Iran)	Ordovician
KE45-4	Natkoyeh	Shabdjereh (central Iran)	Ordovician
KE45-3	Natkoyeh	Shabdjereh (central Iran)	Ordovician
Ingria sp. ind.			
MRAN 1108-2C	Shirgesht	Shirgesht	late Ordovician
MRAN 1108-2E	Shirgesht	Shirgesht	late Ordovician
MRAN 1108-4A	Shirgesht	Shirgesht	late Ordovician
MRAN 1108-4B	Shirgesht	Shirgesht	late Ordovician
Leptaena depressa			
MRAN 1180-27	Niur	Shirgesht	early-middle Silurian
MRAN 1180-23	Niur	Shirgesht	Silurian
Productella cf. *P. belanskii*			
MRAN 10810-4	Shishtu	Poldasht (ilanlou)	Famennian
MRAN 10810-5	Shishtu	Poldasht (ilanlou)	Famennian
Productella cf. *P. subaculeata*			
MRAN 6203-3	Bahram 2	Nasrolah 2	Frasnian-Fammenian
Productella sp. ind.			
MRAN 10771-5	Shishtu	Poldasht (ilanlou)	Frasnian
MRAN 2727-2	Shishtu 1	Shotori	Famennian
MRAN 4905-2	Mush	Anarak	Frasnian-Famennian
MRAN 4905-1	Mush	Anarak	Devonian
MRAN 2727-1	Shishtu 1	Shotori	Devonian
Rhytialosia sp. ind.			

MRAN 6162-2	Bahram 1	Nasrolah 2	Frasnian
Spinulicosta sp. ind.			
MRAN 6162-21	Bahram 1	Nasrolah 2	Frasnian
MRAN 6203-1	Bahram	Nasrolah 2	Devonian
Striatochonetes sp. ind.			
MRAN 9159-2	Bahram	Jam	middle Devonian
Striatochonetes sp. ind.			
MRAN 9136-3	Bahram	Jam	Devonian
MRAN 9136-6	Bahram	Jam	Devonian
Devonochonetes sp. ind.			
MRAN 3648-2	Bahram	Soh	Givetian-Frasnian
MRAN 3648-4	Bahram	Soh	Givetian-Frasnian
MRAN 3648-13	Bahram	Soh	Givetian-Frasnian
Triplesia alata			
MRAN 1181-7	Niur	Shirgesht	early Silurian
Hesperonomiella sp. ind.			
MRAN 8761-1	Ilbeyk	Haftanan	middle Cambrian-early Ordovician
MRAN 8761-2	Ilbeyk	Haftanan	middle Cambrian-early Ordovician
MRAN 8761-3	Ilbeyk	Haftanan	middle Cambrian-early Ordovician
Nicolella actoniae			
MRAN 1125-6	Shirgesht	Shirgesht	late Ordovician
MRAN 1125-11	Shirgesht	Shirgesht	late Ordovician
MRAN 1125-8	Shirgesht	Shirgesht	late Ordovician
MRAN 1130-1	Shirgesht	Shirgesht	Ordovician
Paralenorthis sp. ind.			
KE41-1	Natkoyeh	Shabdjereh (central Iran)	Ordovician
KE41-1-2	Natkoyeh	Shabdjereh (central Iran)	Ordovician
KE41-5	Natkoyeh	Shabdjereh (central Iran)	Ordovician
KE43-3	Natkoyeh	Shabdjereh (central Iran)	Ordovician
KE43-4	Natkoyeh	Shabdjereh (central Iran)	Ordovician
KE41-7	Natkoyeh	Shabdjereh (central Iran)	Ordovician
KE45-5	Natkoyeh	Shabdjereh (central Iran)	Ordovician
KE42-1	Natkoyeh	Shabdjereh (central Iran)	Ordovician
KE41-7A	Natkoyeh	Shabdjereh (central Iran)	Ordovician
Howellites ultima			
MRAN 1108	Shirgesht	Shirgesht	late Ordovician
MRAN 1125-7	Shirgesht	Shirgesht	late Ordovician
Isorthis (Ovalella) inflata			
MRAN 1189-3	Niur	Shirgesht	early Silurian
MRAN 1189-3a	Niur	Shirgesht	early Silurian
?*Isorthis* sp. ind.			
MRAN 6904-4	Baharam	Zarand	Silurian
Isorthis sp. ind.			
MRAN 6903-1	Baharam	Zarand	early Silurian-early Devonian
Syntrophioides sp. ind.			
MRAN 8291-4	Ilbeyk	Galikuh	late Cambrian
MRAN 8291-5	Ilbeyk	Galikuh	late Cambrian
?*Clorinda* sp. ind.			

LA 2	Niur		Silurian
LA 3	Niur		Silurian
Clorinda molongensis			
NiB5-9		Esfeh	Silurian
MRAN 1181-13	Niur	Shirgesht	Silurian
NiB5-10A		Esfeh	Silurian
Spinatrypina sp. ind.			
MRAN 1181-8	Niur	Shirgesht	early Silurian
NiB5-2-S		Esfeh	Silurian
LA 1	Niur		Silurian
MRAN 1180-3	Niur	Shirgesht	Silurian to late Devonian
MRAN 1180-29	Niur	Shirgesht	Silurian to late Devonian
Spinatrypina cf. *S. chitralensis*			
MRAN 6162-4	Bahram	Nasrolah 2	Frasnian
MRAN 6162-14	Bahram	Nasrolah 2	Frasnian
Rhynchotrema sp. ind.			
MRAN 6784-1	Kuhbanan	Zarand	Late Ordovician-Middle Silurian
Stegocornu denisae			
MRAN 6904-3	Baharam	Zarand	Silurian
Cyphoterorhynchus arpaensis			
MRAN 6162-10	Bahram	Nasrolah 2	Devonian
Hedeinopsis hispanica hispanica			
MRAN 1209-1A	Niur	Shirgesht	Silurian
MRAN 1209-1C	Niur	Shirgesht	Silurian
MRAN 1209-2-A	Niur	Shirgesht	Silurian
Hedeinopsis sp. ind.			
MRAN 6904-5	Baharam	Zarand	Silurian
Cyrtospirifer brodi			
MRAN 6162-12	Bahram	Nasrolah 2	Devonian
Cyrtospirifer cf. *C. kermanensis*			
MRAN 6162-13	Bahram	Nasrolah 2	Devonian
MRAN 4232-7	Shishtu 2	Behabad	Devonian
MRAN 6162-1	Bahram	Nasrolah 2	Frasnian
MRAN 6162-18	Bahram	Nasrolah 2	Frasnian
MRAN 4242-3	Shishtu 2	Behabad	Frasnian
Cyrtospirifer sp. ind.			
MRAN 4232-6 (4232-10)	Shishtu 2	Behabad	Devonian
MRAN 4232-1	Shishtu 2	Behabad	Devonian
Uchtospirifer aff. *Uchtospirifer nalivkini*			
MRAN 4208-1	Shishtu 2	Behabad	late Givetian-Frasnian

Acknowledgments

Upon the completion of this thesis, I am grateful to those people who have offered me encouragement and support during these three years. First, I would like to express my sincere gratitude to my supervisor Prof. Lucia Angiolini for the constant support in my Ph.D. study and related research, as well as for her many many helps for my stay in Italy. Your patient guidance, valuable suggestions, and immense knowledge helped me a lot in these three years of research and in writing this thesis. I could not have imagined having a better supervisor for my Ph.D.

Besides my supervisor, I would like to deeply thank the co-tutors of this thesis: Prof. Uwe Brand, thanks for your insightful comments and language helps for my manuscripts and thesis; Prof. Shuzhong Shen, thanks so much for your recommendation and samples supply. Yours advices and helps lead to widen my research from various perspectives.

Super thanks to Dr. Gaia Crippa, I truly appreciate your very kindness heart, your big patience, not only for my academical study, but also for my daily life in Italy. Without your precious support it would have not been possible to accomplish my manuscripts and my thesis. My gratitude to you for all you have done during my last three years.

A great thank goes to Dr. Claudio Garbelli, thanks for your methodological support and important help for my thesis writing. Many thanks to Curzio Malinverno and Agostino Rizzi for your technical support and numerous hours of hard work in the laboratory.

Also, I would like to express my sincere gratitude to Dr. Daniela Henkel, Prof. Anton Eisenhauer, and the BASE-LiNE Earth program, for providing me the opportunity to continue my academical career. This project has received funding from the European Union's Horizon 2020 research and innovation programme under the Marie Skłodowska–Curie grant agreement No 643084 (BASE–LiNE Earth).

Big thanks to Prof. Erika Griesshaber and Prof. Wolfgang Schmahl, for providing very useful technical skills and trainings in Munich, besides constructive suggestions in my paper writing.

Many thanks to Prof. GianCarlo Capitani, Prof. Maggie Cusack, Prof. Elizabeth Harper, Prof. Jürgen Laudien, Hana Jurikova, Claas Hiebenthal, and Danijela Šmajgl for culturing and providing brachiopod specimens, isotope analyses and constructive suggestions in my paper writing.

Prof. Mike Stephenson, Dr. Maryamnaz Bahrammanesh Tehrani, Prof. Mohammad Reza Ghotbi and Dr. Gianluca Raineri are thanked for geological field trip support in England, Iran and Italy.

I extend my thanks to my friends in the Dipartimento di Scienze della Terra "A. Desio", Università degli Studi di Milano, as well as my friends in BASE-LiNE group. Also I thank my former supervisor Prof. Wei Wang for my master thesis and continuous support. The same thank goes to those who helped me during the last three years, if I did not mentioned here.

Last but not least, this thesis is dedicated to my parents, for your love and encouragement, you raise me up to more than I can be. In particular, I would like to thank my father, even if you can no longer hear it: I miss you, too much.